Modeling and Managing Separation for Noise Abatement Arrival Procedures

by

Liling Ren

M.S. Aerospace Engineering
Beijing University of Aeronautics and Astronautics, P. R. China, 1988

B.S. Aerospace Engineering
Beijing Institute of Aeronautics and Astronautics, P. R. China, 1985

SUBMITTED TO THE DEPARTMENT OF AERONAUTICS AND ASTRONAUTICS
IN PARTIAL FULFILLMENT OF THE REQUIREMENTS FOR THE DEGREE OF

DOCTOR OF SCIENCE IN AEROSPACE SYSTEMS
AT THE
MASSACHUSETTS INSTITUTE OF TECHNOLOGY

February 2007

Signature of Author: _____
Liling Ren, Department of Aeronautics and Astronautics
September 27, 2006

Certified by: _____
John-Paul B. Clarke, Principal Research Scientist
Thesis Supervisor

Certified by: _____
Charles M. Oman, Senior Lecturer
Committee Chair

Certified by: _____
Eric Feron, Professor, School of Aerospace Engineering
Georgia Institute of Technology

Certified by: _____
Frank M. Cardullo, Professor, Department of Mechanical Engineering
State University of New York at Binghamton

Accepted by: _____
Jaime Peraire, Professor of Aeronautics and Astronautics
Chair, Committee on Graduate Students

Modeling and Managing Separation for Noise Abatement Arrival Procedures

by

Liling Ren

Submitted to the Department of Aeronautics and Astronautics in Partial Fulfillment of the Requirements for the Degree of Doctor of Science in Aerospace Systems

Abstract

Aircraft noise is a significant concern to communities near airports, and therefore a constraint to the growth of aviation. Advanced noise abatement approach and arrival procedures have been shown in previous studies and in limited implementation to be a cost effective means of achieving near- and medium-term noise reductions. Additionally, these procedures can be employed to reduce fuel burn, emissions, and flight time. However, because of aircraft trajectory variations due to operational uncertainties, it is difficult for air traffic controllers to predict and maintain separation between aircraft. Thus, without proper decision support tools, controllers need to add arbitrarily large buffers, thereby reducing airport throughput.

A design and operational framework is proposed to advance the implementation of noise abatement arrival procedures. Under this framework, a target separation is given at an intermediate metering point to ensure with a certain (limited) level of confidence that the remainder of the noise abatement arrival procedure may be completed without further controller intervention. Small probability exceptions are handled by alternative plans. A design methodology is presented, along with the details of a unique Monte Carlo simulation-based Tool for Analysis of Separation And Throughput (TASAT) that is used to determine the minimum possible target separation between aircraft at the metering point. Hence, a smaller separation buffer can be used and traffic throughput can be maintained at a relatively high level.

The Monte Carlo simulation-based design tool accounts for operational uncertainties such as differences in aircraft performance, Flight Management System logic, aircraft weight, pilot response, and winds. A mode-decomposition and autoregressive approach was developed to model the stochastic wind variations between flights. Aircraft trajectories from the Monte Carlo simulations (or from radar tracks if they are available) are used within the context of the design methodology to determine target separations for given desired level of confidence.

The utility of the design framework, methodology, and tools was illustrated through simulation analysis and a Area Navigation (RNAV) Continuous Descent Arrival (CDA) flight test at Louisville International Airport. The flight test results were consistent with the model prediction. The research demonstrated that with the developed tools, noise abatement arrival procedures can be implemented to achieve noise reductions and other economic and environmental benefits while maintaining a relatively high level of traffic throughput. Suggestions for the selection of target separations and the location of the intermediate metering point were provided based on the analysis.

Thesis Supervisor: John-Paul B. Clarke
Title: Principal Research Scientist

ACKNOWLEDGMENTS

I would like to thank my advisor and friend, Prof. John-Paul Clarke, for giving me the opportunity to work on this wonderful project and to learn from him over the last four years, as well as for his advice, guidance, encouragement, and patience. Thanks also go to other committee members for their tremendous help and immeasurable guidance; to Dr. Charles Oman for going extra miles serving as my committee chair; to Prof. Eric Feron for his encouragement, especially during those times when it was needed; and to Prof. Frank Cardullo for his continuous support since I first met him ten years ago. I am also grateful to Prof. R. John Hansman for his mentoring; to Prof. Amedeo Odoni for serving as my minor advisor, to Prof. Charles Coleman for reviewing my thesis. I am appreciative of Dr. Jim Kuchar for giving me initial guidance and support at MIT.

I would also like to thank Carl Burleson, Lourdes Maurice, and Sandy Liu of the FAA, Len Tobias and Tom Davis of NASA Ames. Without their support, financial and technical, this work would not have been possible.

This work would not have been possible without the support of many other people. I would like to thank Kevin Elmer and Kwok-On Tong of The Boeing Company, Tom Staigle of Delta Air Lines, Dannie Bennett, Sarah Johnson, David Senechal, Walter White, and Andrew Willgruber of the FAA, Jim Brooks of Georgia Tech, Robert Slattery of Louisville RAA, David Williams of the NASA, Jeffery Firth, Robert Hilb, Stuart Lau, James Walton of UPS for providing various data and sharing their valuable expertise. I am also grateful to Prof. Nhut Tan Ho of California State University Northridge for his early work at MIT in developing the initial version of the fast-time aircraft simulator and the pilot response delay model. I am appreciative of: Peter-john Passingham of Airbus Industrie for providing A319 performance data; Tom G. Reynolds of the University of Cambridge for providing sample MST data and reference materials on the historical development of CDA in UK; Eric Parks of the US Airways for sharing his experience with A320 FMS; Gregg Fleming of Volpe National Transportation System Center for providing ETMS data; Joosung Lee and Daniel King of MIT for their help on implementing the BM2 in the fast-time simulator; Ryan Tam of MIT for his help on the INM software; and Patricia A. Miller of NOAA for providing access to the ACARS data. I would also like to thank Robert Doherty of the MIT Writing Center for his help on editing the final version of this thesis.

All my friends at International Center for Air Transportation and the extended community of MIT deserve my gratitude for making my graduate life an enriching experience. Especially, my thanks go to: Antonio Abad, Yiannis Anagnostakis, Philippe Bonnefoy, Francis Carr, Emmanuel Carrier, Nathan Doble, Diana Dorinson, Yasmine El Alj, Antony Evans, Terence Fan, Flora Garicia, Thomas Gorin, Xiaowei He, Jonathan Histon, Jerome Huber, Masha Ishutkina, Kip Johnson, Laura Kang, Michelle Karow, Alf Kohler, Alex Lee, Wenyu Luo, Laura Major, Terran Melconian, Alan Midkiff, Bruno Miller, Miguel Molina, Alex Mozdzanowska, Fabio Rabbani, Hayley Reynolds, Robin Riedel, Sepehr Sarmadi,

Natalia Sizov, Lixia Song, Georg Theis, Adeem Usman, Laurence Vigeant-Langlois, Roland Weibel, Lee Winder, Shiro Yamanaka, and Katherine Zou.

My special appreciation goes to Prof. D. C. Sun of Binghamton University, who has always been a source of encouragement and guidance to my graduate life at MIT.

Greatest thanks of all go to my family: to my mom and my dad for their unconditional support; to my siblings: Xiaohui, Lihua, and Libin for everything they have done to support my study; to my wife Helen and my son Marty for accompanying me through one of the most exciting and challenging adventures of my life.

TABLE OF CONTENTS

LIST OF FIGURES

LIST OF TABLES

LIST OF ACRONYMS

ACARS	Aircraft Communications Addressing and Reporting System
ADC	Air Data Computer
ANCA	Airport Noise and Capacity Act
AR	autoregressive
ARINC	Aeronautical Radio Inc.
ARTS	Automated Radar Terminal System
ATA	Air Transport Association
ATC	Air Traffic Control
Body	Aircraft body fixed frame
CAEP	Committee on Aviation Environmental Protection
CAS	Calibrated Airspeed
CDA	Continuous Descent Arrival or Continuous Descent Approach
cdf	cumulative distribution function
Center	Air Route Traffic Control Center
CFR	Code of Federal Regulations
CG	Center of Gravity
DC	Direct Current
DNL	day-night average sound level
EAS	Equivalent Airspeed
EPNL	effective perceived noise level
ESRL	Earth System Research Laboratory
ETMS	Enhanced Traffic Management System
FAA	Federal Aviation Administration
FDR	Flight Data Recorder
FIR	Finite Impulse Response
FMS	Flight Management System
FPA	Flight Path Angle
GAO	United States General Accounting Office
GPS	Global Positioning System
GSD	Global Systems Division
IAS	Indicated Airspeed
ICAO	International Civil Aviation Organization
IFR	Instrument Flight Rules
ILS	Instrument Landing System
INM	Integrated Noise Model

ISA	Standard Atmosphere
KSDF	Louisville International Airport
LAMAX	maximum A-weighted sound level
LNAV	Lateral Navigation
MIT	Miles-in-Trail
MTDDA	Modified Three Degree Decelerating Approach
NASA	National Aeronautics and Space Administration
NED	North-East-Down frame
NOAA	National Oceanic and Atmospheric Administration
pdf	probability density functions
PIP	Product Improvement Package
PNL	perceived noise level
RAA	Regional Airport Authority
RNAV	Area Navigation
RNP	Required Navigation Performance
SAE	Society of Automotive Engineers
SPL	sound pressure level
TAS	True Airspeed
TASAT	Tool for Analysis of Separation And Throughput
T/D	Top of Descent
TDDA	Three Degree Decelerating Approach
TRACON	Terminal Radar Approach Control
VNAV	Vertical Navigation
WGS 84	World Geodetic System 1984
WHO	World Health Organization

CHAPTER 1

INTRODUCTION

Noise abatement approach and arrival procedures have been shown by previous studies to be a cost effective means of achieving near-and medium-term reductions in noise from arrival aircraft. In addition, noise abatement approach and arrival procedures can be employed to save fuel, reduce emissions, and save flight time. However, because of aircraft trajectory variations due to operational uncertainties, it is difficult for air traffic controllers to predict and maintain separation and adequate spacing between aircraft performing these procedures. Arbitrarily large separation buffers would be used resulting in negative impact on airport throughput. The implementation of noise abatement approach procedures thus has been limited to very few airports under light traffic conditions.

A design and operational framework for implementing noise abatement arrival procedures, and the development of a unique Monte Carlo based aircraft trajectory simulation tool and a new separation analysis methodology for predicting and managing saparation between aircraft performing noise abatement approach and arrival procedures are presented in this thesis. As demonstrated in this thesis, with the developed tool, noise abatement approach and arrival procedures can be implemented to achieve noise reductions and other economic and environmental benefits while maintaining a relatively high level of traffic throughput.

The rest of this chapter is organized as follows. The aircraft community noise issue and existing industry efforts in resolving this issue are discussed first. The historical background of noise abatement approach procedure development and the difficulties associated with the implementation of these procedures are discussed in Section 1.2. Based on the discussions, the problem of modeling and managing separations is formally introduced in Section 1.3. The thesis structure is described in the last section.

1.1 THE AIRCRAFT COMMUNITY NOISE ISSUE

1.1.1 The Effects of Aircraft Noise

In the vicinity of airports, aircraft engine exhaust emissions and aircraft noise are the two most pervasive pollutants resulting from aircraft operations. Anyone who resides or works near an airport knows what a nuisance aircraft noise is, and how it reduces quality-of-life. Beyond this, noise is also a real and present danger to health. According to the World Health Organization's (WHO) Guidelines for Community Noise[1], adverse effects of noise include hearing loss; sleep disturbances; increased risk of ischemic heart disease; as well as anxiety and emotional stress. As a result, work performance and vigilance against error can be impaired.

Aircraft community noise presents a unique type of noise source. For residents living in the vicinity of airports, there are rarely immediate clinical outcomes as a result of a single aircraft noise event because of

the range of sound levels as perceived on ground. Damages to health, however, are developed gradually due to chronic exposure of aircraft noise, and thus represent a more hidden danger. In a recent study, the Road Traffic and Aircraft Noise Exposure and Children's Cognition and Health (RANCH) study[2], researchers from UK examined almost 3,000 children living in the UK, Spain and the Netherlands, the largest ever study on the effect of noise on children's health. Long-term aircraft noise exposure was found related to impaired performance in reading comprehension and recognition memory. The reading age in children exposed to high levels of aircraft noise was delayed by up to two months in the UK for a 5 dB change in noise exposure.

Aircraft noise typically affects areas at considerable distance from the airport. For example, the WHO nighttime limit of 60 dB A-weighted maximum sound level (LAMAX, the unit of LAMAX is also abbreviated as dBA) is frequently exceeded by aircraft noise many miles from an airport, by train noise about 1000 ft or more from the tracks, and by road traffic noise about only 500 to 1000 ft from a highway[3]. Unlike ground noise sources that are more easily shaded by trees and building structures between the noise source and the residents, aircraft noise is emitted from the sky, so the effective noise exposure is greater than from road or rail traffic. The sporadic time pattern of aircraft noise also differs from the relatively steady noise of surface traffic[4]. Aircraft noise is intermittent and depends on the runways in use so it can seem unpredictable from one day to the next. The frequency or the tune of aircraft noise is some times more irritating. For these reasons, aircraft noise seems more annoying than road traffic noise for the same day-night average sound level (DNL) as recognized by many researchers and international organizations[3,5,6,7].

Unlike highway noise and noise from industrial activities, aircraft noise frequently affects communities in rural areas and suburban areas tens of miles away from airports that are otherwise sitting in a peaceful and quiet environment. The recent airline industry trend of shifting more flights to secondary airports[8] that is at some distance from metropolitan areas are making the situation even worse.

The negative impact of aircraft noise to living environment is reflected in the value of residential property located around airports. According to a Federal Aviation Administration (FAA) report published in 1985[4], an increase of 1 dB in DNL usually results in a 0.6 to 2.3% decrease in real estate values.

While the growth of air traffic is driven by, as well as beneficial to, the national and regional economy, it is the local communities near airports that pay the direct environmental price. Although aircraft source noise has been significantly reduced in the past few decades, the number of aircraft movements has increased remarkably during the same period. In fact, since the introduction of jet transport aircraft in the late 1950s and early 1960s, the lateral aircraft noise levels (see definition in the next subsection) have been reduced by approximately 20 dB in effective perceived noise level (EPNL)[9]. On the other hand, according to Air Transport Association (ATA), aircraft departures of US scheduled airlines increased from 3.85 million to 11.18 million during the period from 1960 to 2004[10,11]. Given the public expectation for a lower community noise and improved quality of life, aircraft noise continues to be a limiting factor for the growth of aircraft operations and airport expansion. According to a United States General Accounting Office (GAO) report[12], US airports reported noise concerns as their most serious environmental challenge.

Indeed, airport expansion has seen strong oppositions from communities around airports because of environmental concerns, mainly aircraft noise concerns. For example, Boston Logan Airport started the planning process for a new runway in 1969[13]. The original construction work for the new runway commenced in May 1974 but it was stalled on the very first day by community opponents. A Suffolk Superior Court injunction barring new runways at Logan airport was put in place in 1976. After almost three decades of legal debate, discussions, and thorough environmental assessment, the court did rule that a new unidirectional runway could be built in the same general location. However, when it is completed

in later 2006, the new runway can only be used to reduce delays rather than to increase capacity of the airport. The court ruling stated, the new runway can only be used by private planes and commuter jets when northwest winds exceed 10 knots, and at least three of the existing five runways have to be shut down for weather reasons. The construction work finally started in April 2005.

Existing operations are also subject to restrictions to protect communities around airports from aircraft noise. According to the FAA, as of 2003, noise concerns have resulted in over 600 operational constraints and curfews at US airports.[14] One measure commonly used throughout the US to mitigate aircraft noise impact is soundproofing local residential homes and schools significantly affected by aircraft noise. For example, as of 2004, Chicago O'Hare Airport had spent approximately $212 million to sound insulate 86 schools and the spending is still growing.

1.1.2 Existing Efforts in Relieving the Aircraft Noise Problem

Since its inception, the continuing growth in civil aviation has lead to major economic, social, and cultural benefits to the nation and the world. Civil aviation is strategically important to the economic prosperity. Both FAA[15] and International Civil Aviation Organization (ICAO)[16] have recognized the need to balance air transportation system needs with environmental concerns, and have adopted the concept of "Balanced Approach" to aircraft noise management.

In response to the aircraft noise pollution, major federal legislations have been developed in the US (a historical account of US legislation of aircraft noise pollution can be found in ref. 17, part III) since the late 1960s. In 1968, Congress amended the Federal Aviation Act, authorizing the FAA to include noise considerations in aircraft and engine certification process. The FAA then embarked upon a long-term program of controlling aircraft noise at its source (a brief history of US aircraft noise regulations can be found in ref. 18). In 1969, the FAA issued the first aircraft noise regulations in Title 14, Code of Federal Regulations, part 36 (14 CFR part 36), "Noise Standards: Aircraft Type Certification." The new part 36 became effective on December 1, 1969, and set a limit on noise of large aircraft of new design. In response to the Noise Control Act of 1972, FAA amended 14 CFR part 36 in 1973 to give a stage designation to all newly produced aircraft. The 1969 noise standards became known as the Stage 2 certification standards. Aircraft that have not been shown to comply with the Stage 2 standards are defined as Stage 1 aircraft. Stage 1 aircraft included the first generation commercial jets powered by turbojet engines and very low bypass ratio turbofan engines[19]. Stage 2 aircraft are characterized by low bypass ratio engines with reduced jet exhaust noise and internal noise control features. Under amended aircraft operating rules (in 1976 and 1980) of 14 CFR part 91, Stage 1 aircraft were phased out by January 1, 1985 (extended to not after January 1, 1986 for two-engine aircraft that were to be replaced with Stages 2 or 3 compliant aircraft under an FAA approved replacement plan).

In 1977, the stricter Stage 3 standards became effective. Large aircraft of new design for which new type certificates are applied on or after November 5, 1975 must comply with these standards. Stage 3 aircraft features high bypass ratio turbofan engines. Recognizing the need to balance the air transportation growth with the relief from aircraft noise pollution, Congress passed the Airport Noise and Capacity Act of 1990 (ANCA) on November 5, 1990. Implementing ANCA for controlling aircraft noise at its source resulted in the gradual phasing out of Stage 2 aircraft in contiguous US by December 31, 1999.

The FAA aircraft noise standards are defined by noise level limits at three reference measurement points: lateral (previously sideline), flyover (previously takeoff), and approach. The lateral point is a point 1,476 ft (0.35 nm for aircraft with more than three jet engines when showing compliance with Stage 1 and Stage 2 noise limits) from extended centerline of the runway where the noise level after liftoff is

greatest. The flyover point is a point on the extended centerline of the runway that is 21,325 ft from the start of takeoff roll. The approach point is a point on the extended centerline of the runway that is 6,562 ft from the runway threshold. Aircraft noise level limits are defined in EPNL; and the unit is EPNdB. ICAO adopted similar aircraft noise standards. These standards are prescribed in Chapter 2 (corresponding to Stage 2) and Chapter 3 (corresponding to Stage 3) of the ICAO Annex 16, Environmental Protection, Volume I, Aircraft Noise[20].

The new quieter Stage 4 noise standards became effective on August 4, 2005. The Stage 4 noise standards are the same as the new ICAO Chapter 4 noise standards[20] that specifies a 10 EPNdB cumulative noise reduction (the sum of the reductions in three measurements at the flyover, lateral, and approach points) from Chapter 3 noise levels. The Chapter 4 standards were developed through the Committee on Aviation Environmental Protection (CAEP), which was established by the ICAO in 1983. On and after January 1, 2006, any person filing an application for a new FAA airplane type design must comply with the Stage 4 noise standards[21]. In fact, some later models of aircraft certificated before January 1, 2006 already meet the Stage 4 standards. However, the FAA has no plan to either phase out the production of Stage 3 aircraft, or to impose operational restrictions on Stage 3 aircraft. The timelines of aircraft noise standards and operational restrictions are shown in Fig. 1-1. In Fig. 1-1, the vertical axis represents cumulative noise level – the sum of the three noise level limits at the three measurement points. Because noise level limits are given as functions of the certified aircraft takeoff weight, thus, the vertical axis is not labeled; but the interval between ticks represent a 10 EPNdB difference. The horizontal axis represents calendar year.

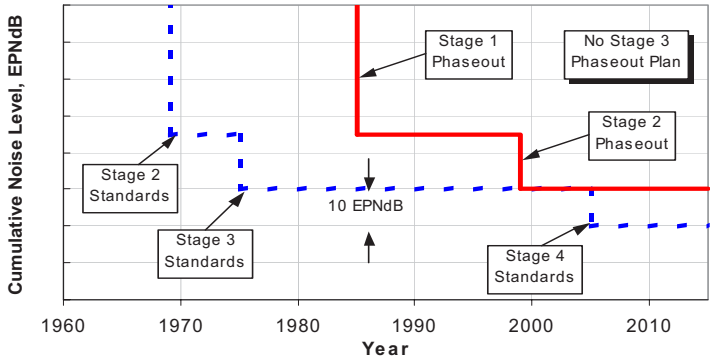

Figure 1-1 Timelines of aircraft noise standards and operational restrictions.

The noise levels of Stage 1 aircraft were dominated by jet exhaust noise because of the very high jet exhaust speed of turbojet engines and early very low bypass ratio turbofan engines[9]. The noise level reductions of Stage 2 aircraft were achieved through slightly increased bypass ratios with decreased jet exhaust velocity and internal noise control features[19]. The noise levels of Stage 3 aircraft, featuring high bypass ratio turbofan engines with significantly reduced jet exhaust velocity, are dominated by fan noise. This is especially true at reduced power and landing approach conditions[9]. To save the cost of replacing older noisier aircraft, hush kit retrofit programs and re-engine programs have been employed by operators to bring those older aircraft up to the then current standard. The engines has been the major source of aircraft noise. However, on modern commercial aircraft, the noise from the airframe moving through the air becomes more and more important. As illustrated by a recent study[22], given constant fan speed at idle thrust, the lateral noise level of the A340 aircraft could be increased by almost 10 dBA if the flaps/slats are extended and the landing gear is down. The noise level reductions since the introduction of high

bypass ratio turbofan engines have been achieved through gradual improvements in engine component design, engine nacelle acoustic performance, and aircraft low-speed aerodynamics.

It is seen that controlling aircraft noise at its source is a long process[21]. For example, Stage 4 noise standards just adopted by the FAA waited 30 years after the Stage 3 noise standards were established in 1975. From the time the Stage 3 noise standard was established in 1975 until the contiguous United States had an all Stage 3 operational fleet at the end of 1999, approximately 25 years had elapsed. Since the introduction of high bypass ratio turbofan engines, it has been very difficult to make additional substantial source noise reductions[9,19]. Nevertheless, technology is not the only factor in this process. Aircraft are very expensive long-term investments. Existing fleet and aircraft that are still in production cannot be easily disposed of within the financial constraint facing the air transportation industry.

For complicated problems like aircraft noise, there is no single solution. Compatible land use in areas adjacent to airports and noise abatement operational procedures are the other two types of important measures[23]. Compatible land use falls under the category of policy and management measures. It involves land use planning and development, zoning, and housing regulation that will limit the uses of land near airports to purposes compatible with airport operations. Financial assistance may be provided to residents to encourage relocation to quieter areas from areas exposed to serious levels of aircraft noise. Land acquisition may also be employed by airports to enclose severe noise exposure within the boundaries of the airport. Before getting into the discussion of noise abatement operational procedures, it is necessary to review some of the background information about flight operations in the terminal area.

From the point of view of aircraft safety, approach and landing phase is the most critical phase of flight. Strict approach and landing procedures must be followed. Most of the time, especially under low visibility conditions, the Instrument Landing System (ILS) is used. The ILS emits glide slope and localizer beams to guide the aircraft vertically to the minimum decision height, and laterally to the approach end of the runway threshold. The glide slope is normally adjusted to 3 deg above horizontal. Because of ground reflections of the glide slope radio wave, false glide slopes may exist above the true ILS glide slope – the first of which is at about 9 deg. Hence, aircraft normally fly a level segment and intercept the ILS glide slope from below in order to avoid capturing the false glide slopes that could lead to inappropriately steep approach angles. Typically, the interception is made about 5 nm to 10 nm from the runway threshold, at a height of approximately 1,500 ft to 3,200 ft above runway elevation.

In current practices, to manage separation between aircraft and to maintain runway throughput, controllers normally direct (vector) aircraft laterally to fly an extended flight path at low altitude, and then turn them onto the final approach course where they intercept the ILS localizer and then capture the glide slope. The level flight segments at low altitude are typically flown at relatively low speeds (say 160-200 kt) with flaps/slats partly extended, requiring relatively high engine power settings (a more detailed analysis is given in Chapter 2). This extends the noise to large residential areas under the flight path, and inevitably increases fuel burn and emissions.

During the takeoff phase, controllers normally adjust spacing by holding the trailing aircraft on the ground for a short period of time. Once aircraft are airborne, normally there is no need to hold them at low altitude. The high thrust to weight ratio of modern turbofan aircraft permits climb angles much higher (5-18 deg) than the ILS glide slope angles. Though thrust is high during the takeoff and climb phase, the aircraft rapidly gain altitude. Because of these differences, the noise footprint could be smaller and is closer to the airport during the takeoff phase than the approach phase.

This is clearly shown in Fig. 1-2 by the approach and takeoff vertical profiles and their corresponding noise contours. The vertical profiles shown in Fig 1-2 are typical of existing operations. They are based on Flight Data Recorder (FDR) data extracted from UPS B767-300 (a Stage 3 aircraft) aircraft performing revenue flights. During the approach, the aircraft flew a step-down vertical profile with level segments at

low altitudes, while during the takeoff the aircraft had very steep Flight Path Angles (FPAs). The total areas of the LAMAX 55 dBA noise contours seemed similar for both takeoff and approach profiles. However, the LAMAX 55 dBA noise contour extended much farther from the runway threshold for the approach profile than that for the takeoff profile (50 nm vs. 31 nm), affecting communities much farther away from the airport. The LAMAX 60 dBA noise contour for the approach profile not only extended much farther away from the runway than that for the takeoff profile (32 nm vs. 13 nm), but also had a larger total area than the noise contour for the takeoff profile. The noise from approach aircraft becomes an increasingly greater problem. Notice that, within 10 nm from the runway threshold, the takeoff noise contours are indeed wider than the approach contours due to the higher thrust during takeoff.

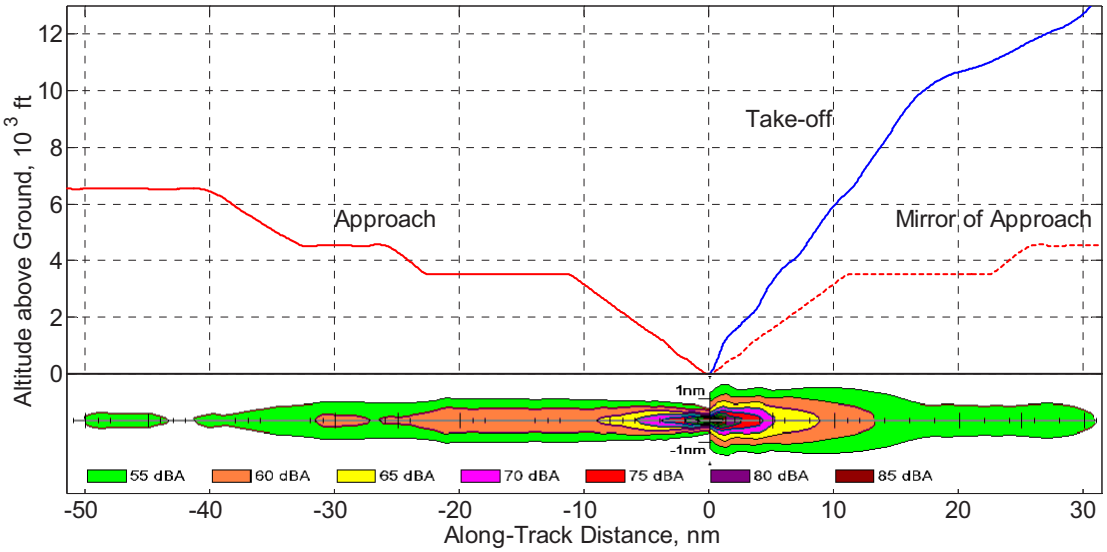

Figure 1-2 Example UPS B767-300 arrival departure profiles and noise contours.

Noise abatement operational procedures seek to reduce the aircraft noise impact on communities by improving the way aircraft are currently operated in the terminal area. Procedure changes have the advantage that noise reductions can be achieved as soon as the procedures are implemented, whereas design improvements that reduce aircraft noise at its source can take many years. New aircraft designs must go through a lengthy development and certification process. Any new noise reduction technologies developed today will not actually start to benefit communities until new aircraft first enter into service several years later, and it will take many years after that until the older, noisier aircraft in the existing fleet are retired. Commercial aircraft normally have an operational life of 20 to 30 years. Noise abatement operational procedures thus could be applied to existing aircraft to reduce noise in the near term at comparatively low cost. Of course, these procedures can also be applied to newly developed aircraft to achieve additional noise reductions.

There are several methods for improving aircraft operations in the terminal area, including preferential runways and routes, as well as noise abatement procedures for takeoff and approach. The purpose of preferential runways and routes is to divert aircraft to avoid densely populated areas around airports. Depending on the physical layout of the airport and its surroundings, aircraft may be directed to follow rivers, highways, or to fly over other non-noise-sensitive areas. The use of preferential runways and routes are widely adopted by airports around the world. Some of these procedures are used throughout the day, and others are used for nighttime operations only for avoiding sleep disturbance.

Noise abatement procedures for takeoff and approach can be combined with preferential runways and routes to minimize noise impact. The most commonly used noise abatement takeoff procedures are thrust cutbacks that can be executed when aircraft are at least 800 ft above runway elevation after takeoff. Two thrust cutback procedures have been recommended by the FAA[24] (in 1993) and the ICAO[25] (in 2001). The first procedure is identified by the FAA as the "close-in" noise abatement departure profile that aims to provide noise reductions to areas close to (within couple miles) the departure end of the runway. The second procedure is identified by the FAA as the "distant" noise abatement departure profile that aims to provide noise reductions to all other areas. The difference between the two procedures is that in the close-in procedure, the thrust cutback is initiated prior to the initiation of flap/slat retraction; while in the distant procedure, the thrust cutback is initiated after the initiation of flap/slat retraction. In both procedures, the reduced thrust level is maintained until the aircraft reaches 3,000 ft above runway elevation, where transition to normal en route climb procedure is initiated. The thrust cutback is limited to the minimum level that is necessary to maintain proper speed and engine inoperative minimum climb gradient (1.2, 1.5 or 1.7 percent for 2, 3 or 4 engine aircraft) for the flap/slat configuration without increasing the thrust of operative engines, in the event of an engine failure. Takeoff thrust cutback procedures are adopted by a number of airports around the world.

Compared with takeoff, noise abatement approach and arrival procedures may achieve additional benefits such as fuel savings and emission reductions. However, as it will be seen, noise abatement approach procedures introduce difficult technical and Air Traffic Control (ATC) challenges because of variations in aircraft trajectories. The research to be presented in this thesis has been established to overcome these challenges. In the next section, the concept and the historical development of noise abatement approach procedures are described to provide a background for further discussions.

1.2 NOISE ABATEMENT APPROACH AND ARRIVAL PROCEDURES

The concept of solving the noise abatement problem through procedural measures emerged in the early 1950's when commercial air transportation boomed after the World War II. In a paper[26] published at the Symposium on Aircraft Noise hosted by the Society of Automotive Engineers (SAE) in 1954, Rosendahl argued that with the fast growing of residential communities near airports and increased volume of airport operations, local communities traditionally seeking for airports shifted their attitude to fighting against having airports located contiguous to their residential and business districts. The paper reviewed actions taken in the areas contiguous to the New York-New Jersey metropolitan airports to solve the aircraft noise problem. The two general strategies used were: 1) reduce the intensity at the noise source, and/or 2) increase the distance between the source and the receiver. These two basic strategies essentially remain unchanged for developing noise abatement operational procedures.

The first operational practice described in the Rosendahl paper was to make maximum possible use of "preferential runways" which would divert numerous operations away from residential areas surrounding airports by routing them over water, open areas, or least congested areas. The novelty of the preferential runway concept was that it permitted a considerable number of landings and takeoffs in certain crosswind situations in which another runway would normally be used. The second operational practice, specific to approach and landing, was to maintain altitudes of at least 1,200 ft above ground level (although still very low compared to today's practice of above 2,000 ft above ground level, as recommended in a 2004 FAA Advisory Circular[27]) as long prior to landings as the characteristics of aircraft permit. Previously, long, low, "drag-in" approaches were performed causing complaints as far as 10 to 15 miles away from the airport. Rosendahl claimed that, those complaints from points at substantial distances from airports had been virtually eliminated with the new higher approaches. These higher approaches with less power also

benefited persons living closer to the airport. Since early 50's, many efforts have been made world wide to develop different noise abatement approach procedures as technology advances.

One way to reduce noise on approach is to keep the aircraft higher through using a steeper descent path. In the later 60's and the early 70's, the National Aeronautics and Space Administration (NASA) examined instrumented two-segment approaches through a series of simulation and flight test programs[28,29]. In this technique, the aircraft initiated the approach at 3,000-4,000 ft above the runway elevation, flew at a steeper descent path (4-7 deg) first and then made a transition to the conventional 3 deg glide slope at 400-1,000 ft to stabilize for landing. Because of the steeper FPA during the upper segment, little power would be required. With the lower power and higher altitude, community noise below the flight path could be reduced between 2-7 nm from the runway. Vertical guidance was provided by an experimental 3D Area Navigation (RNAV) system during the upper segment and by ILS glide slope during the lower segment. Lateral guidance was provided by the ILS localizer during the entire approach. To prevent the aircraft capturing false ILS glide slopes, the ILS glide slope was not armed until the aircraft reached 1,000 ft radio altitude. Although effective at reducing noise, this procedure was not implemented due to safety concerns in the event the transition from the upper steeper segment to ILS glide slop were not properly accomplished.

The early 70's also saw extensive noise abatement approach procedure research and operational trials in Europe[30]. Lufthansa developed a "low-drag, low power" procedure.[31] Lufthansa B727s routinely flew this procedure into Frankfurt and Heathrow under visual conditions, providing simultaneous reductions in both noise footprints and fuel burn. In this procedure, descent to 3,000 ft above the runway elevation was in "clean" configuration, using idle power and optimum speed for the aircraft type. Below 3,000 ft, speed was reduced to 160-170 kt, with flaps in the go around takeoff setting, and engine power engaged to maintain speed. Descent was continued at this speed, and ILS glide slope was captured. Landing gear was extended not until the aircraft reached the height of approximately 500 ft above the normal height for crossing the outer marker. Flaps were also further extended at this point and power increased so that the aircraft can be stabilized in the landing configuration when passing the outer marker. Following this profile, flap/slat and landing gear extensions were significantly delayed as compared with conventional approaches at that time. Considerable noise alleviation was gained up to the outer marker, but beyond this point, no reduction could be achieved. To be fully effective, close co-operation with ATC was necessary. The application of this procedure was limited because of the inability of some other aircraft types to properly follow the profile.

In 1974, Dibley of British Airways proposed a procedure that can be used to reduce noise, and save significant amount of fuel at the same time[32]. In this procedure, ATC gave expected distance measuring equipment (DME) distances and flight levels for bottom of descent points, so that pilots could plan idle thrust descents from the cruise altitude efficiently to bottom of descent points, given suitable forms of guidance. From that point on, aircraft speed is expected to be at least 200 kt Indicated Airspeed (IAS) to enable aircraft to stay in the clean configuration for as long as possible. Ideally, the track miles from the bottom of descent point should allow a 3 deg FPA to smoothly intercept the ILS glide slope with minimum thrust and any need for thrust changes. The height for ILS glide slope interception was increased to 3,000 ft, preferably higher. Landing gear extension was delayed until about 1,500 ft above the runway elevation. Dibley designed a circular slide rule called the Dibley Descent Computer to compute the accurate location of the top of descent for the idle descent path and to provide continuous altitude and distance checks – similar to the Vertical Navigation (VNAV) functionality in modern flight management system (FMS). Wind was accounted for by using ground speed in the calculation. Although a remarkable design, the procedure was not implemented due to the anticipated adverse effects it might have upon the expeditious flow of traffic.

Based on these early studies, the now widely known Continuous Descent Approach (CDA) was developed in UK the later 1970s[33]. The CDA has been pragmatically defined as a descent from 6,000 ft to the interception of the glide slope that contains no or at most one level segment not longer than 2 nm[34]. Noise abatement approach procedures with improvements over the original CDA have also been proposed and studied, but they all achieve community noise reduction through the same two basic techniques used since 1950s: by reducing the overall thrust required during the descent; and by keeping the aircraft higher for longer.

The development of modern Global Positioning System (GPS) based RNAV and FMS technology has enabled new classes of noise abatement procedures with complex 3D descent trajectories starting farther from the runway. For Required Navigation Performance (RNP) procedures[35], more complex 3D approach flight path can be defined and be followed by RNP capable aircraft with very high accuracy. RNP improves airspace use and enables noise abatement approach procedures in complex airspace environment. The acronym CDA is thus also used to refer to the recently developed Continuous Descent Arrival procedures – noise abatement RNAV or RNP procedures that combine the arrival phase (often initiated from cruise altitude) and the approach phase (within the terminal area). In the rest of this thesis, the actual meaning of CDA in the context will be explained as appropriate. The phase "approach procedure" is thus used to refer to procedures confined within the terminal area. The phrase "arrival procedure" is used to refer to procedures that combine both the arrival and the approach phases. Through simulations, flight tests, and few limited implementations modern advanced noise abatement approach and arrival procedures have been shown to be able to achieve near-and medium-term noise reductions, and fuel burn and emissions reductions as well[30,36,37,38,39], to a degree that surpasses their predecessors. However, routine application of these procedures is yet to happen.

The major reason is that the techniques utilize idle or near idle descents, and there are differences and variations in aircraft idle descent trajectories because of aircraft performance differences and operational uncertainties. Because aircraft are continuously descending, variations in aircraft trajectories make it difficult for air traffic controllers to predict future spacing between aircraft[40] and manage the arrival flow. Without proper technology, controllers need to add arbitrarily large buffers, resulted in negative impact on airport capacity. As reported by a widely publicized study of noise abatement approach procedures conducted at Amsterdam Schiphol Airport[41,42,43,44,45], to assure separation during the execution of a Continuous Descent Approach procedure, landing interval was increased from 1.8 to 4 minutes. This represents more than 50% reduction in landing capacity at the airport.

1.3 PROBLEM STATEMENT

As shown in Fig. 1-3, advanced noise abatement approach and arrival procedures allow aircraft to continuously descend from high altitude directly into the ILS glide slope, or GPS based glide slope (illustrated by the solid flight path) without any level flight segment at low altitudes. As mentioned earlier, the higher flight path combined with lower engine thrust significantly reduces noise impact to the community.

Trajectory variations exist in both conventional (or standard) arrival and approach operations and noise abatement arrival and approach procedures. With conventional approaches, controllers frequently vector aircraft to maintain separation until aircraft are established on final approach. However, in order to assure noise reduction benefits, it is preferred that controllers do not intervene with a noise abatement approach by vectoring aircraft, because of doing so would usually require the engine thrust to increase and flight path to be extended. The requirement for air traffic controllers to predict future spacing is thus

higher for noise abatement approaches, and the ability for controllers to adjust spacing is restricted. This explains the anticipated negative impact on airport capacity for noise abatement arrival and approach procedures.

The benefits of noise abatement approach and arrival procedures, on one hand, and the difficulties related their implementation, on the other, form a dilemma. Understanding the uncertainties in aircraft trajectory variations and the interaction between consecutive aircraft is important to resolving the dilemma. Methods must be developed to address the challenges of predicting and mitigating these variations so that separations between aircraft performing these procedures can be managed efficiently by controllers in current and future ATC environments. Only then, noise abatement approach and arrival procedures can be implemented widely to benefit the communities and operators as well as to ease the constraint on traffic growth.

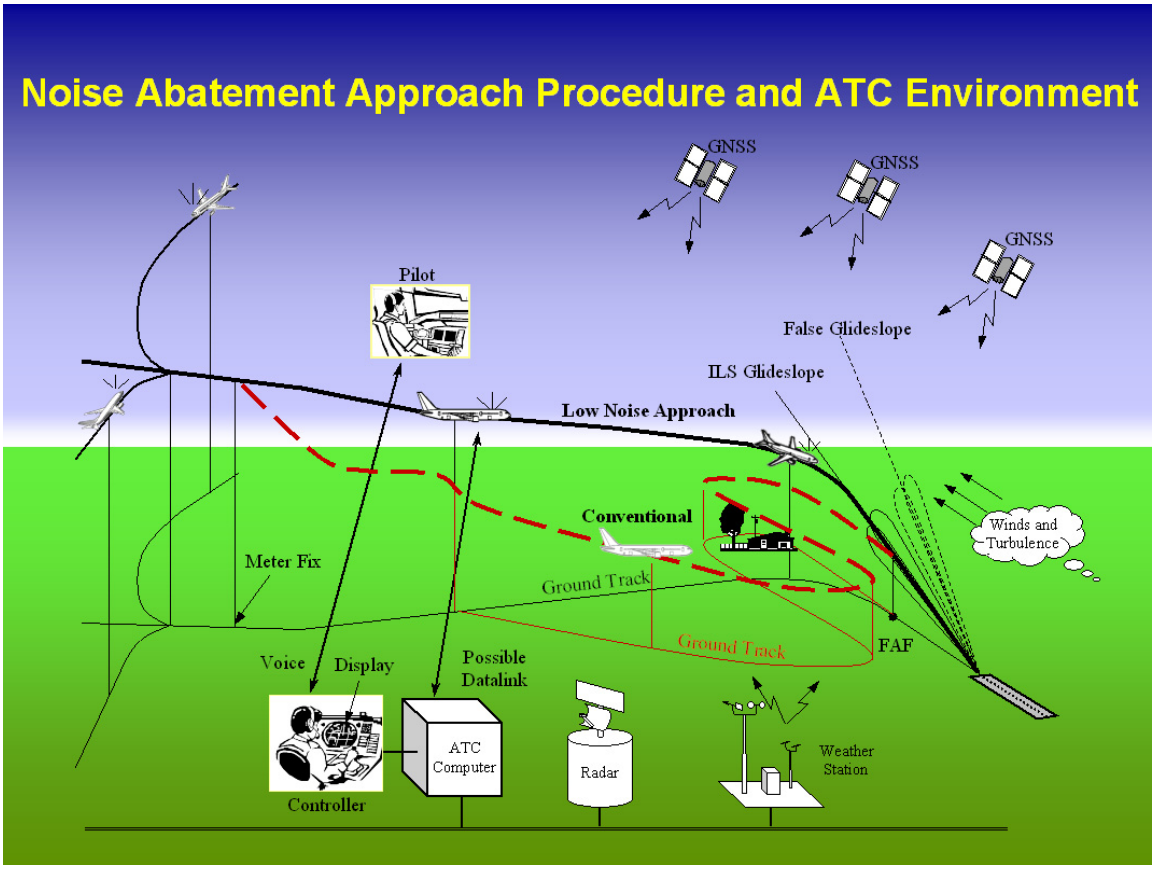

Figure 1-3 Noise abatement approach procedure and ATC environment.

In a recent study, the problem of mitigating aircraft trajectory variations was addressed by developing, first, a methodology to determine the optimum design parameters for a continuous descent approach, and, second, a new pilot cueing system to allow for consistent speed profiles[46]. In another study, a Three Degree Decelerating Approach[36] (TDDA) was modified (i.e. the MTDDA) to mitigate the effects of flight operation uncertainties on aircraft trajectory[47]. This was achieved by holding the initial speed for a certain time after the start of the three-degree descent to runway and then reducing the thrust to idle at a lower altitude to allow for consistent deceleration. The airborne spacing technologies, such as the tool developed by NASA, provide another means to overcome the trajectory variation challenges. However, those technologies probably will not be available in the cockpit any time soon. The work to be presented in this thesis primarily addresses the problem of predicting aircraft trajectory variations and the problem

of efficiently managing separations between aircraft performing noise abatement approach and arrival procedures. Specifically, the objectives of this thesis research were established as follows:

- Identify and model factors contributing aircraft trajectory variations during the execution of noise abatement approach and arrival procedures;
- Develop a tool to simulate aircraft trajectory variations;
- Develop a separation analysis methodology based on trajectory variation analysis to support the procedure design and the control of separation between aircraft;
- Integrate the separation analysis methodology into a proposed procedure design and operational framework and develop a guideline for managing separation between consecutive aircraft performing noise abatement and arrival procedures so that these procedures can be implemented in daily operations under a much wider range of external conditions.

One fundamental philosophy guiding this research is that through using a procedure that is slightly sub-optimal in a noise reduction or separation maintenance sense, the robustness and applicability of the procedure may be significantly improved without sacrificing much of the noise abatement benefits. This may in fact be the best solution overall, because higher traffic throughput can be maintained while achieving noise reductions. In other words, this research sought to develop tools and methodologies that assure separation during the execution of noise abatement approach and arrival procedures with a reasonable – though not absolute – level of confidence without further controller intervention. By accepting some uncertainties in spacing, smaller landing intervals (smaller separation buffers) can be used and traffic throughput can be maintained at a relatively high level. The robustness of the operational concept is achieved by employing alternative plans to cover separation exceptions. Although noise abatement benefits, i.e. community noise, fuel burn, and emissions reductions, may be sacrificed for an individual flight when an exception is handled, the total number of uninterrupted noise abatement operations can be greatly increased, and the procedure can be applied under a wide range of traffic conditions.

1.4 OVERVIEW OF THE THESIS

An introduction to the aircraft community noise issue and the historical development of noise abatement approach procedures has been provided in this Chapter. The need for, and the objectives of the research presented in this thesis have also been introduced by analyzing implementation issues and airport capacity concerns about these procedures. Analyses of aircraft noise impact and aircraft performance during the approach phase of flight, as well as existing ATC terminal area practices are presented in Chapter 2. Based on these analyses, a design and operational framework for noise abatement approach and arrival procedures is proposed. A Monte Carlo based aircraft trajectory simulation tool specifically developed for trajectory variation analysis, and the techniques used in modeling various factors contributing to aircraft trajectory variations are described in Chapter 3. The modeling of wind variation between flights is described separately in Chapter 4, however, due to the complexity of the topic. The theoretical derivation of the separation analysis methodology is given in Chapter 5. An analysis of the trade-off between traffic throughput and level of confidence is also presented. An integration of the separation analysis methodology with procedure implementation is presented in Chapter 6. The application of the framework and the separation analysis methodology is demonstrated through a simulation study. Data collected from flight test are compared with simulation results to show the

effectiveness of the separation analysis methodology. Key contributions, conclusions and implications of the research, as well as a discussion of potential future research directions are provided in Chapter 7. A detailed description of the fast-time aircraft simulator, which is the core of the Monte Carlo simulation tool, is provided in Appendix A. Where applicable, items such as the nomenclature and the reference list are provided for each individual chapter for easy cross-reference.

REFERENCES

[1] "Guidelines for Community Noise," edited, Berglund, B., Lindvall, T., and Schwela, D. H., World Health Organization, Geneva, 2000.

[2] Stansfeld, S., Berglund, B., Clark, C., Lopez-Barrio, I., Fischer, P., Öhrström, E., Haines, M., Head, J., Hygge, S., van Kamp, I., and Berry, B., "Aircraft and Road Traffic Noise and Children's Cognition and Health: A Cross-National Study," *The Lancet*, Vol. 365, No. 9475, 4 Jun. 2005, pp. 1942-1949.

[3] Schomer, P., "A White Paper: Assessment of Noise Annoyance," Schomer and Associates, Inc., Champaign, IL, 22 Apr. 2001.

[4] Newman, J. S., and Beattie, K. R., "Aviation Noise Effects," FAA-EE-85-2, FAA, Office of Environment and Energy, Washington, DC, Mar. 1985.

[5] "WHO Technical Meeting on Aircraft Noise and Health," meeting report, World Health Organization Regional Office for Europe, European Centre for Environment and Health Bonn Office, Bonn, Germany, 29-30 Oct. 2001.

[6] "Public Health Impact of Large Airports," Health Council of the Netherlands: Committee on the Health Impact of Large Airports, 1999/14E, Hague, Netherlands, 1999.

[7] Porter, N. D., Lershaw, A. D., and Ollerhead, J. B., "Adverse Effects of Night-Time Aircraft Noise," NATS R&D Report 9964, Department of Operational Research and Analysis, National Air Traffic Services Ltd., London, UK, Mar. 2000.

[8] Bonnefoy, P. A., "Emergence of Secondary Airports and Dynamics of Regional Airport Systems in the United States," S.M. Thesis, Department of Aeronautics and Astronautics, Massachusetts Institute of Technology, Cambridge, MA, 2005.

[9] International Coordinating Council of Aerospace Industries Associations, "Technology Continues to Play Important Role in Reducing Noise around Airports," *ICAO Journal*, Vol. 59, No. 2, Mar./Apr. 2004, pp 4-7, 27.

[10] "Air Transport 1971 – The Annual Report of the U.S. Scheduled Airline Industry," The Air Transport Association of America, Inc., Washington, DC, 1971.

[11] "Air Transport Association 2005 Economic Report," The Air Transport Association of America, Inc., Washington, DC, 2005.

[12] "Aviation and the Environment – Airport Operations and Future Growth Present Environmental Challenges," GAO/RCED-00-153, Report to the Ranking Democratic Member, Committee on Transportation and Infrastructure, House of Representatives, General Accounting Office, Washington, DC, Aug. 2000.

[13] "Aviation Infrastructure – Challenges Related to Building Runways and Actions to Address Them," GAO-03-164, Report to the Subcommittee on Aviation, House Committee on Transportation and Infrastructure, General Accounting Office, Washington, DC, Jan. 2003.

[14] Wlezien, R. and Maurice , L., "NASA/FAA Environment R&D Activities," Presented to FAA's Research, Engineering and Development Advisory Committee (REDAC)/NASA's Revolutionize Aviation Subcommittee (RAS) Joint Meeting, Alexandria, VA, 17 Sep. 2003.

[15] "Next Generation Air Transportation System – Integrated Plan," Next Generation Air Transportation System Joint Planning & Development Office, Washington, DC, 12 Dec. 2004.

[16] "Consolidated Statement of Continuing ICAO Policies and Practices Related to Environmental Protection," ICAO Assembly Resolution A33-7, Montreal, Canada, Oct. 2001.

[17] Falzone, K. L., "Airport Noise Pollution: Is There a Solution in Sight?" *Boston College Environmental Affairs Law Review*, Vol. 26:769, 1999, pp. 769-807.

[18] "14 CFR Parts 36 and 91 Stage 4 Aircraft Noise Standards," FAA – Notice of Proposed Rulemaking, *Federal Register*, Vol. 68, No. 230, 1 Dec. 2003, pp. 67330-67336.

[19] Smith, M. J. T., "Evolving Noise Issue Could Persist into the Next Century," *ICAO Journal*, Vol. 47, No. 8, Aug. 1992.

[20] ''Environmental Protection, Annex 16 to the Convention on International Civil Aviation, Volume I, Aircraft Noise'', 3rd Ed, ICAO, Jul. 1993, Amendment 7, effective 21 Mar. 2002.

[21] "14 CFR Parts 36 and 91 Stage 4 Aircraft Noise Standards," FAA – Final rule, *Federal Register*, Vol. 68, No. 230, 1 Dec. 2003, pp. 67330-67336.

[22] van Boven, M., "Development of Noise Abatement Approach Procedures," AIAA 2004-2810, *10th AIAA/CEAS Aeroacoustics Conference,* Manchester, UK, 12-14 May 2004.

[23] "Federal Aviation Administration Aviation Noise Abatement Policy Aviation Noise Abatement Policy," FAA, Washington, DC, 18 Nov. 1976.

[24] "Noise Abatement Departure Profiles," AC 91-53A, FAA, Washington, DC, 22 Jul. 1993.

[25] "Procedures for Air Navigation Services – Aircraft Operations, Volume I – Flight Procedures, Part V, Noise Abatement Procedures, Chapter 3, Aeroplane Operating Procedures," ICAO PANS-OPS, Doc 8168, Amendment 11, effective 1 Nov. 2001.

[26] Rosendahl, C. E., "The Aircraft Noise Problem in Airport Vicinities – A Review of the Program and Activities of the National Air Transport Coordinating Committee for the Major Civil Airports in the New York-New Jersey Metropolitan Area," *Symposium on Aircraft Noise*, SAE National Aeronautic Meeting, New York, NY, 12-15 Apr. 1954.

[27] "Visual Flight Rules (VFR) Flight near Noise-Sensitive Areas," AC 91-36D, FAA, Washington, DC, 17 Sep. 2004.

[28] Denery, D. G., Bourquin, K. C., White, K. C., and Drinkwater III, F. J., "Flight Evaluation of Three-Dimensional Area Navigation for Jet Transport Noise Abatement," *Journal of Aircraft*, Vol. 10, No. 4, 1973, pp. 226-231.

[29] Denery, D. G., White, K. C., and Drinkwater III, F. J., "Status and Benefits of Instrumented Two-Segment Approaches; August, 1974," *Journal of Aircraft*, Vol. 12, No. 10, 1975, pp. 791-796.

[30] Reynolds, T. G., Ren, L., Clarke, J.-P. B., Burke, A. S., and Green, M., "History, Development and Analysis of Noise Abatement Arrival Procedures for UK Airports," AIAA 2005-7395, *AIAA 5th Aviation Technology, Integration and Operations Forum*, Arlington, VA, 26-28 Sep. 2005.

[31] "Low Drag, Low Noise," *Flight International*, 25 Sep. 1975.

[32] Dibley, H., "How to Reduce Noise and Save Fuel – Now," *Journal of Guild of Air Pilots & Air Navigators*, Mar. 1974.

[33] "The Noise Benefits Associated with Use of Continuous Descent Approach and Low Power/Low Drag Approach Procedures at Heathrow Airport," CAA Paper 78006, London, UK, Apr. 1978.

[34] "Noise from Arriving Aircraft – Summary," Final Report of the ANMAC Technical Working Group on Noise from Arriving Aircraft, London, UK, 13 Mar. 2000.

[35] "United States Standard for Required Navigation Performance (RNP) Approach Procedures with Special Aircraft and Aircrew Authorization Required (SAAAR)," FAA Order 8260.52, Washington DC, 3 Jun. 2005.

[36] Clarke, J.-P. B., "A System Analysis Methodology for Developing Single Events Noise Abatement Procedures," Sc.D. Thesis, Department of Aeronautics and Astronautics, Massachusetts Institute of Technology, Cambridge, MA, 1997.

[37] "Study of Key Elements Acting on Noise Impact of Aircraft in Operation," SOURDINE/ASP-DOC-D2-001, The European Commission, The Transport RTD Programme, Paris, France, 6 Jul. 1999.

[38] "Noise from Arriving Aircraft – An Industry Code of Practice," Civil Aviation Authority, London, US, Sep. 2001,

[39] Clarke, J.-P. B., Ho, N. T., Ren, L., Brown, J. A., Elmer, K. R., Tong, K.-O., and Wat, J. K., "Continuous Descent Approach: Design and Flight Test for Louisville International Airport," *Journal of Aircraft*, Vol. 41, No. 5, 2004, pp. 1054-1066.

[40] Ho, N. T. and Clarke, J.-P. B., "Mitigating Operational Aircraft Noise Impact by Leveraging on Automation Capability," AIAA 2001-5239, *1st AIAA Aircraft Technology, Implementation, and Operations Forum*, Los Angeles, CA, 2001.

[41] Erkelens, L. J. J., "Research on Noise Abatement Procedures," *Aviation-2000 Prospects Symposium*, Zhukovsky, Russia, 19-24 August 1997; also NLR-TP-98066, Amsterdam, Netherlands, 1998.

[42] Erkelens, L. J. J., "Development of Noise Abatement Procedures in the Netherlands," *New Aviation Technologies International Symposium*, Zhukovsky, Russia, 17-22 Aug. 1999; also NLR-TP-99386, Amsterdam, Netherlands, 1999.

[43] Wubben, F. J. M., and Busink, J.J., "Environmental Benefits of Continuous Descent Approaches at Schiphol Airport Compared with Conventional Approach Procedures," *Internoise Conference*, Nice, France, 27-30 Aug. 2000; also NLR-TP-2000-275, Amsterdam, Netherlands, 2000.

[44] Erkelens, L. J. J., "Research Into New Noise Abatement Procedures for the 21st Century," AIAA-2000-4474, *AlAA Guidance, Navigation and Control Conference and Exhibit*, Denver, CO, 14-17 Aug. 2000.

[45] Erkelens, L. J. J., "Advanced Noise Abatement Procedures for Approach and Departure," AIAA-2002-4858, *AIAA Guidance, Navigation, and Control Conference and Exhibit*, Monterey, CA, 5-8 Aug. 2002.

[46] Ho, N. T., "Design of Aircraft Noise Abatement Approach Procedures for Near-Term Implementation," Ph.D. Thesis, Department of Mechanical Engineering, Massachusetts Institute of Technology, Cambridge, MA, 2005.

[47] Ren, L., Clarke, J.-P. B., and Ho, N. T., "Achieving Low Approach Noise without Sacrificing Capacity," *Proceedings: the 22nd Digital Avionics Systems Conference (22nd DASC)*, Indianapolis, Indiana, 12-16 Oct. 2003, pp. 1.E.3-1.1-9 vol.1.

[48] Weitz, L. A., Hurtado. J. E., Bussink, F. J. L., "Increasing Runway Capacity for Continuous Descent Approaches through Airborne Precision Spacing," AIAA 2005-6142, *AIAA Guidance, Navigation, and Control Conference and Exhibit*, San Francisco, CA, 15-18 Aug. 2005.

CHAPTER 2

NOISE ABATEMENT APPROACH AND ARRIVAL PROCEDURE DESIGN AND OPERATIONAL FRAMEWORK

NOMENCLATURE

C_d	=	drag coefficient
C_l	=	lift coefficient
D	=	aircraft drag
g	=	the acceleration due to gravity
L	=	aircraft lift
L/D	=	aircraft lift to drag ratio
L_{SP}	=	sound pressure level in dB
m	=	aircraft mass
p	=	root-mean-squared sound pressure
p_0	=	standard reference sound pressure, 0.02 mPa
p_i	=	root-mean-squared sound pressure measurement i
S	=	aircraft wing reference area
T_r	=	thrust required
T_i	=	idle thrust
V	=	true speed
V_r	=	true airspeed
ΔL_{SP}	=	difference in sound pressure level in decibel
γ	=	flight path angle
ρ	=	ambient air density

2.1 INTRODUCTION

In a conventional approach, air traffic controllers manage the movement of aircraft and achieve the desired sequencing and spacing on the final approach through vectoring – the process of giving pilots ad hoc altitude, speed and heading commands. The primary benefit of vectoring is that it gives the controller the flexibility that has, to date, been required to achieve a tightly spaced approach queue, thereby maximizing runway throughput when there is high traffic demand. However, vectoring is most frequently conducted at low altitude with extended lateral flight path resulting in flight time, noise, emissions, and fuel burn that are significantly higher than their respective minimum possible levels. Sample ground

tracks of UPS arrivals to Louisville International Airport (KSDF) from the west are shown in Fig. 2-1. These data were extracted from the UPS ground management system. The blue (solid) tracks represent B757-200 (B757) and B767-300 (B767) flights, and the red (dashed) tracks represent flights of other aircraft types. The reason to differentiate B757 and B767 from other aircraft is that these two aircraft types were used in a flight test, which will be described later. As seen in Fig. 2-1, aircraft were directed to perform a variety of heading changes, resulting in substantial increases and variations in flight distance and the extent to which flight tracks span the area around the airport. If these increases and variations could be reduced, the size of noise contours could be significantly reduced, as could the amount of emissions and fuel burn. In addition to the extended lateral path, vectoring also resulted in level flight segments at low altitude that requires high engine thrust. Vertical profiles of the same groups of arrival flights are plotted in Fig. 2-2 as altitude vs. along-track distance. The latter is defined as the distance along each flight's own ground track, thus it reflects the actual distance flown by each aircraft. As seen in Fig. 2-2, vectored flights followed step down vertical profiles and aircraft could fly level flight segments at low altitude that extended to tens of nautical miles. If the level flight segments at low altitude could be reduced or eliminated, the noise level on the ground could be significantly reduced, as would be additional reductions in emissions and fuel burn.

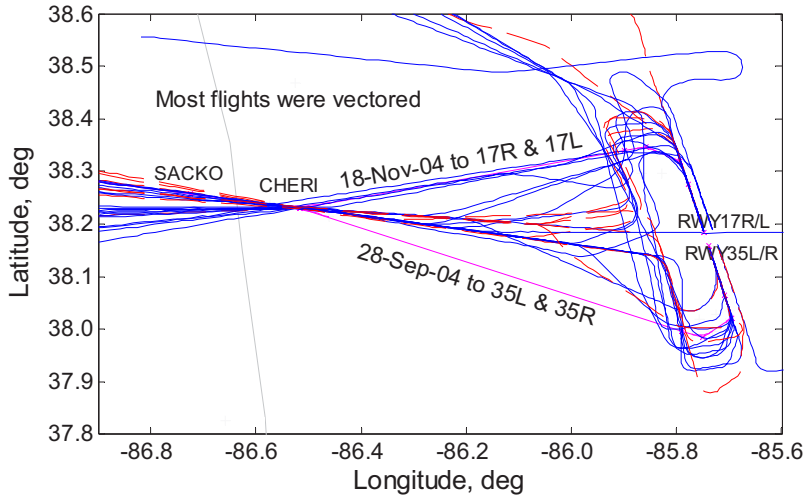

Figure 2-1 Ground tracks of vectored arrival flights.

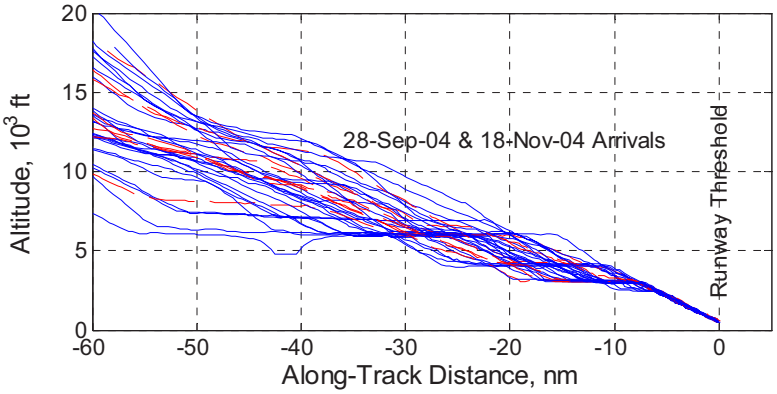

Figure 2-2 Vertical profiles of vectored arrival flights.

The first step in developing noise abatement approach and arrival procedures is to examine how operational parameters such as altitude, speed, and Flight Path Angle (FPA) affect the noise impact from approaching aircraft. Note that the nominal aircraft flap setting is determined by the aircraft weight and the airspeed. Given aircraft flap configuration, altitude, speed, and FPA, the thrust required to maintain the given speed can be obtained from the force equations. Thus the two important noise contribution factors, engine thrust and the nominal aircraft flap configuration, would become known once the afore mentioned operation parameters and aircraft weight are given. Fuel burn, directly contributing to emissions and operating cost, should be examined at the same time. Based on these analyses and the availability of navigation and guidance technologies, a set of high-level noise abatement approach and arrival procedure design guidelines could be derived.

The two fundamental elements in aircraft noise abatement are: 1) reducing noise at its source – lower engine power setting and clean configuration, and 2) moving the noise source farther away – flying at higher altitudes and over less noise sensitive areas. However, for a balanced and feasible procedure design, the operating cost and existing airspace restrictions must also be taken into account. The final noise abatement approach and arrival procedure design should have a shortest lateral path and a continuously descending vertical profile chosen such that airspace restrictions and regulatory operational limits are satisfied at the same time. Naturally, vectoring during the execution of such procedures should be eliminated or at least be minimized. To maintain runway arrival throughput and assure proper spacing between aircraft without extensive use of vectoring, a new procedure design and operational framework is needed. This new framework is the major topic of this chapter.

The remainder of this chapter is organized as follows: The analysis of aircraft noise impact, through numeric examples, is provided in the next section. An analysis of aircraft performance pertinent to noise abatement approach and arrival procedure design is presented in Section 2.3. General guidelines for noise abatement approach and arrival procedure design in light of the recent development of Global Positioning System (GPS) based Area Navigation (RNAV) technology, the Required Navigation Performance (RNP) concept, and the Lateral Navigation (LNAV) and Vertical Navigation (VNAV) capabilities already in place on board modern commercial aircraft are discussed in Section 2.4. The proposed new noise abatement arrival procedure design and operational framework is presented in Section 2.5 to provide the basis for the discussions in the chapters that follow. A summary of this chapter is provided in the last section.

2.2 COMMUNITY NOISE IMPACT FROM APPROACH AIRCRAFT

2.2.1 Noise Metrics

The basic noise metric is the dimensionless sound pressure level (SPL) in decibel (dB). SPL L_{SP} is defined as ten times the logarithm (to the base 10) of the ratio of the root-mean-square (RMS) sound pressure p, squared, and the standard reference sound pressure p_0, squared,

$$L_{SP} = 10\log_{10}\left(p^2 / p_0^2\right) = 20\log_{10}\left(p / p_0\right) \tag{2-1}$$

The standard reference sound pressure p_0 is 20 μPa, which is about the limit of the sensitivity of the human ear, in its most sensitive frequency range. For free plane waves, sound pressure squared is proportional to the sound intensity which is defined as the rate of flow of energy through a unit area

normal to the direction of propagation (see p.7 of ref. 1). For two different sound pressure measurements p_1 and p_2, the difference in SPL is,

$$\Delta L_{SP} = 10\log_{10}\left(p_2^2 / p_0^2\right) - 10\log_{10}\left(p_1^2 / p_0^2\right) = 10\log_{10}\left(p_2^2 / p_1^2\right) = 20\log_{10}\left(p_2 / p_1\right) \qquad (2\text{-}2)$$

If the second sound intensity is twice of that of the first measurement, the difference in SPL can be obtained as,

$$\Delta L_{SP} = 10\log_{10}\left(p_2^2 / p_1^2\right) = 10\log_{10} 2 = 3.0103 \text{ (dB)} \qquad (2\text{-}3)$$

Equation (2-3) indicates that doubling the sound intensity gives a 3 dB increase in SPL, or that halving the sound intensity gives a 3 dB decrease in SPL. It is obvious that a ten times increase in sound intensity gives a 10 dB increase in SPL. Human hearing is directly sensitive to sound pressure. One dB is close to the just noticeable difference for SPL. A 3-dB difference in SPL is noticeable, and a 6-dB difference is clearly noticeable to the human ears.

There are three fundamental families of noise metrics used in measuring aircraft noise. These three families are derived from the A-weighted sound level, C-weighted sound level, and the tone-corrected perceived noise level respectively.

The A-weighted sound level[2,3,4,5] is SPL modified to de-emphasize the low (below 1 kHz) and the high (6.3 kHz and above) frequencies, and to emphasize the frequencies between 1 kHz and 6.3 kHz. It is intended to approximate the relative response of the human ear to different frequencies. In the A-weighting, sound at frequencies where the response of the ear is good is weighted more heavily than sound at frequencies where the response of the ear is poor. Thus, this weighting provides a good approximation of the response of human ear, and correlates well with the average person's subjective judgment of the relative loudness of a noise event, regardless of the sound levels. A-weighted sound level is the most commonly used rating for measuring community and transportation noise.

The C-weighted sound level[2,3] is SPL modified to emphasize the low (between 0.1 kHz to 2 kHz) frequency portions of the spectrum while de-emphasizing other frequencies. However, the weighting remains relatively uniform from 0.0315 kHz to 8 kHz. It provides a better approximation of human perception of the loudness than the A weighted sound level for high level sounds above 90 dB. The C-weighting is often used to measure the peak value of a sound in order to assess the risk of hearing impairment. For aircraft noise, the C-weighted noise levels are commonly used for assessing scenarios dominated by low-frequency sound, e.g., sound level at locations behind start-of-takeoff roll.

The third group of metrics is related to the tone-corrected perceived noise level[2,3,4]. The perceived noise level (PNL) is a computed rating that is most accurate in estimating the perceived loudness of broadband sounds, such as that from aircraft, of similar time duration, which do not contain strong discrete frequency components. Tone-corrected perceived noise level is the PNL adjusted to account for added annoyance due to spectrum irregularity or discrete frequency components, such as tones. The noise metric used in aircraft certification, effective perceived noise level (EPNL), is the value of PNL adjusted for both spectral irregularities and the duration of the noise[6]. Its unit is EPNdB.

To examine the community noise impact from approach aircraft for improving approach procedures, the A-weighted sound level is a natural choice. There are several reasons for this. The A-weighted sound level is simple to compute. The sound level on ground will not be very high (>90 dB) during the approach until the aircraft is very close to the runway threshold. Moreover, the focus of noise abatement procedures is to reduce the community noise impact of the same aircraft type through different

operational procedures rather than to compare differences across different aircraft types. Thus, the use of tone corrected PNL is not necessary.

Within the three metric families, there are three types of metrics[2], namely those that represent the maximum sound levels at a location, metrics that represent the total sound exposures over a given time period, and metrics that represent the time (either in absolute values or as a percentage) that the sound exceeds a specified sound-level threshold. For each individual flight, if the maximum sound level could be reduced, the total sound exposure and the time above a specified sound-level threshold would also be reduced. Therefore, in this section, the maximum A-weighted sound level (LAMAX) is used. LAMAX is presented in decibels and the sound level unit is denoted as dBA to identify it from other sound level metrics.

2.2.2 Noise Impact of Constant Speed Level Flight Segments

As mentioned above, one way to improve approach procedures is to eliminate or at least reduce level flight segments at low altitudes. To quantify how much noise reduction can be achieved, it is necessary to numerically evaluate the community noise impact of these level flight segments as compared with idle-descents. Level flight segments are considered in this subsection. Idle descents are considered in the next subsection. Constant speed level flight requires aircraft engines to maintain certain level of thrust, thus it is of special interest in representing the upper bound of noise levels for approach given all other conditions such as aircraft weight, altitude, and speed equal.

The noise levels of modern commercial transport aircraft are dominated by engine noise. The higher the engine thrust, the higher the engine noise. In constant speed level flight, lift L is equal to aircraft weight mg, and the thrust required T_r is equal to drag D. The lift coefficient C_l can thus be determined as,

$$C_l = \frac{2L}{\rho V_r^2 S} = \frac{2mg}{\rho V_r^2 S} \tag{2-4}$$

where ρ is the ambient air density, V_r is the True Airspeed (TAS), and S is the reference wing area.

It is seen that given altitude (which determines ambient air density) and aircraft weight, the lift coefficient is inversely proportional to the square of TAS. The smaller the TAS, the higher the lift coefficient would be needed to maintain constant speed level flight. The aircraft lift to drag ratio L/D is given by,

$$L/D = \frac{C_l}{C_d} \tag{2-5}$$

where C_d is the drag coefficient. The L/D ratio is a function of the lift coefficient and the flap configuration (defined by flap/slat and landing gear positions). The flap configuration determines the drag polar – the relationship between drag coefficient and lift coefficient. A typical drag polar is shown in Fig. 2-3.

For a given configuration, the L/D ratio increases as the lift coefficient increases from zero, until the maximum L/D ratio is reached. From that point on, the L/D ratio decreases as the lift coefficient increases, until the stall occurs. Commercial transport aircraft are optimized for cruise operational conditions. As the aircraft decelerates to lower speeds to prepare for approach, the lift coefficient will eventually increase to values above the point corresponding to the maximum L/D ratio, and the L/D

ratio will start to decrease. In addition, as the aircraft decelerates further, flaps/slats need to be extended to lower positions to provide high lift coefficient needed to maintain level flight. This results in the drag polar shifting to the right hand side, thus yielding an even lower L/D ratio.

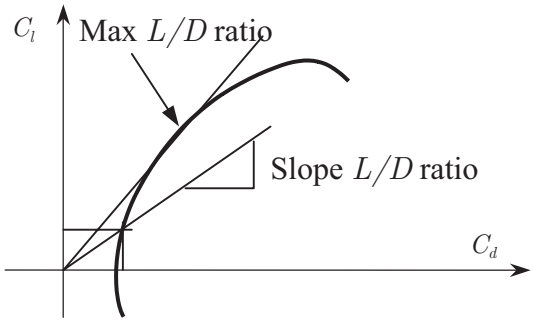

Figure 2-3 Drag polar.

The thrust required for maintain constant speed level flight is given by,

$$T_r = D = \frac{mg}{L/D} \tag{2-6}$$

It is seen that the thrust required is inversely proportional to the L/D ratio. Based on the above discussion, it can be expected that the noise impact from an aircraft performing constant speed level flight would increase with the decrease of the airspeed during approach.

The fast-time aircraft simulator described in Appendix A was used to simulate constant speed level flight segments at altitudes at 500 ft intervals from sea level to 10,000 ft, and over a range of Calibrated Airspeeds (CAS) from 140 kts to 240 kts. The actual altitude simulated for the sea level case was at 50 ft. The altitude range was selected so as to cover the possible range of altitudes at which level flight may be performed during the approach within the terminal area. The speed range was selected to cover the possible speeds during the approach within the terminal area before the aircraft is established on the final approach. Note that Indicated Airspeed (IAS) 250 kt is the regulatory upper speed limit for turbine aircraft operating below 10,000 ft. Most onboard Flight Management Systems (FMSs) use CAS 240 kt as the default speed restriction below 10,000 ft. Modern FMS equipped aircraft have air data computers, and the IAS is corrected to be identical to the CAS. Thus, CAS is used in this analysis.

Two aircraft types were simulated, UPS B757-200 with RB211-535E4 engines and UPS B767-300 with CF6-80C2B6 engines. Aircraft weights for the B757-200 aircraft and the B767-300 aircraft were set to values that are above average UPS package aircraft landing weights but close to average landing weights for passenger aircraft of the same types. They are therefore believed to be representative of the nominal landing weights for the majority of aircraft of these two types. Aircraft flaps/slats were extended at speeds recommended by aircraft operation manuals[7] by the pilot agent built into the fast-time aircraft simulator.

The FAA Integrated Noise Model (INM) Version 6.2[2,8] was used to compute aircraft noise impact. The FAA INM is widely accepted as a standard tool for evaluating community impact of aircraft noise. INM is capable of computing many of the three families of noise metrics, including LAMAX as selected for this analysis. The ground level where noise metric was to be computed was assumed to be at sea level to simplify both the aircraft simulation and noise computation. Because B767-300 with CF6-80C2B6

engines is not available in INM, only the B767-300 with PW4060 engines, the B767-400ER with CF6-80C2F engines was used as a substitute. The principal differences between the -300 and -400ER models are in the shape of the wing tips and the fuselage length. Because community impact of aircraft noise is dominated by noise from the engines, this substitution should be close enough for comparing noise between level flight and idle descent for the same aircraft type.

Outputs from the fast-time aircraft simulator, presented as time history of aircraft state variables, engine thrust and fuel flow in text format, were converted into aircraft profiles in the format required by INM. INM studies[2] were created for the corresponding cases (different altitudes and speeds) simulated using the aircraft simulator. LAMAX at grid points along the simulated straight-line flight path was computed using INM. Results from INM were extracted to form tables of LAMAX at the CAS values and altitude values used in the simulation. The results are presented in Fig. 2-4 and Fig. 2-7 as equal LAMAX contours for B757-200 and B767-300 respectively. Contours were drawn at 5 dBA intervals. A color map was used in these two figures to present gradual changes in LAMAX between contour lines. The dark blue color represents LAMAX of 30 dBA and blow, and the dark brown color represents LAMAX of 110 dBA and above. The gradual color shade change from dark blue to dark brown represents the gradual LAMAX increase from 30 dBA to 110 dBA.

By examining the vertical profiles of vectored arrival flights similar to that shown in Fig. 2-2 and crosschecking with Fig. 2-4 and Fig. 2-7, the noise impact of the constant speed level flight segments in vectored trajectories can also be estimated. For example, due to the level segments at 3,000 ft, it can be estimated that residential communities up to 20 nm (along-track distance) away from the runway could experience noise levels of up to 62 dBA (from B757-200) and 66 dBA (from B767-300). Those communities are mostly in suburban areas where quietness is expected. Note that these INM estimates were based on the assumption that the ground elevation is at mean sea level. If the ground elevation is actually higher, which mostly will be the case, the noise level will be somewhat higher.

It is seen from Fig. 2-4 and Fig. 2-7 that the LAMAX on ground decreases nonlinearly with the increase in altitude. Thus, these results provide information about noise reductions that can be achieved by increasing the altitude of constant level flight segments. At any given speed, the altitude difference between any two adjacent equal LAMAX contours gives the altitude increase that would be needed to reduce noise level by the amount equal to the interval between contour levels (i.e. 5 dBA as in Fig. 2-4 and Fig. 2-7). For the B757-200 aircraft, the altitude of the level segment should be increased from about 1,000 ft to about 1,600 ft (approximately a 600 ft increase) in order to reduce the noise level on ground from 75dBA to 70 dBA. The altitude should be increased from about 1,600 ft to about 2,400 ft (approximately a 800 ft increase) in order to reduce the noise level on ground from 70 dBA to 65 dBA. For the heavier B767-300 aircraft, the altitude should be increased from about 1,400 ft to about 2,200 ft (approximately a 800 ft increase) in order to reduce the noise level on ground from 75dBA to 70 dBA. The altitude should be increased from about 2,200 ft to about 3,200 ft (approximately a 10,00 ft increase) in order to reduce the noise level on ground from 70 dBA to 65 dBA.

Notice that for both aircraft (Fig. 2-4 and Fig. 2-7), the LAMAX on ground increases with the decrease in CAS. This is evidenced by the monotonic increase in altitude for equal LAMAX lines as CAS decreases. The reason for this is that as airspeed decreases, aircraft drag increases and engine thrust must compensate, as explained earlier in this section. This observation suggests that if constant speed level flight segment is not avoidable, they should be conducted at higher speeds.

A third observation is that if the constant speed level flight is conducted above a certain altitude, the noise level on ground could fall below levels that can be viewed as acceptable. For example, if the constant speed level flight were conducted above 5,000 ft, LAMAX would fall below 60 dBA for both B757-200 and B767-300 most of the time. The LAMAX 60-dBA threshold is recommended as a night

time limit by World Health Organization[9] (WHO) to prevent sleep disruption. If the constant speed level flight were conducted above 7,000 ft, LAMAX would fall below 55 dBA for both B757-200 and B767-300 most of the time. Reducing noise level from 60 dBA to 55 dBA would significantly reduce the annoyance because noise levels below 55 dBA are generally tolerable to the human ear. This suggests that vectoring above 7,000 ft may be acceptable from a community noise point of view.

2.2.3 Noise Impact of Constant Speed Idle Descent Segments

Another area of improvement in approach procedures is to allow aircraft engines to operate at lower throttle settings. As emphasized earlier, the way to reduce engine source noise is to use lower throttle settings and fan speeds. The idle throttle represents the lower bound of throttle settings under normal operational conditions, thus idle descents are of special interest in understanding the lower bound of noise levels given other conditions equal.

The fast-time aircraft simulator was used to simulate constant CAS idle descent flight segments. The same two aircraft types, UPS B757-200 and UPS B767-300 were simulated. The aircraft were assumed to perform a straight-in approach. Initial altitude was set to 11,000 ft. The simulations ended when the aircraft reached 50 ft above sea level. Speed was again set at 10 kt intervals from CAS 140 kt to 240 kt. The desired FPA was pre-computed by the FMS module in the aircraft simulator for each selected CAS to allow the aircraft to descend from 11,000 ft to 50 ft at that constant CAS and at the idle throttle setting without using speedbrakes. Because the approach was performed at constant CAS, the flap/slat position was also preset according to the aircraft operation manual[7] before the simulation started. The computation of the FPA for idle constant CAS descent is given in Subsection A.4.3 of Appendix A.

LAMAX noise levels are shown in Fig. 2-5 and Fig. 2-8 for B757-200 and B767-300 respectively. The results are presented in the same manner as for constant CAS level segments, i.e. as equal LAMAX contours. The same color map was used in these two figures to depict gradual changes in LAMAX between contour lines.

It is seen from Fig. 2-5 and Fig. 2-8 that, similar to the results for constant CAS level flight segments, the LAMAX on the ground decreases nonlinearly with the increase in altitude. However, for any given altitude, LAMAX on the ground remained relatively constant for constant CAS idle descent at different CAS values. One reason is that the idle thrust or the idle fan speed remained relatively stable for different CAS values. Another reason could be that the difference in airframe noise due to the difference in CAS and the difference in airframe noise due to the difference in flap configuration offset each other. As shown by a study on airframe noise[10], for the same airspeed, airframe noise increases with the extension of flaps/slats; for the same flap configuration, airframe noise decreases with the decrease in airspeed. In the simulation, at higher speeds, the aircraft was in clean configuration, while at lower speeds, flaps/slats had to be extended. Lastly, the reason could also be that the INM is not accurate enough to capture the small difference in LAMAX due to difference in CAS when the engine throttles was at idle.

By comparing Fig. 2-5 with Fig. 2-4 and Fig. 2-8 with Fig. 2-7, it can be confirmed that, as one might expect, the noise levels for constant CAS idle descent were consistently lower than constant CAS level flight segments for the same altitude and CAS. Each of the equal LAMAX contour lines in Fig. 2-5 (or Fig. 2-8) is lower in altitude than its corresponding equal LAMAX contour line in Fig. 2-4 (or Fig. 2-7). This means that the same LAMAX noise level can be achieved at a lower altitude during the constant CAS idle descent than that during the constant speed level flight. The color shades in Fig. 2-5 and Fig. 2-8 are more toward the blue (lower LAMAX) end of the color map as compared with the color shades in Fig. 2-4 and Fig. 2-7 respectively.

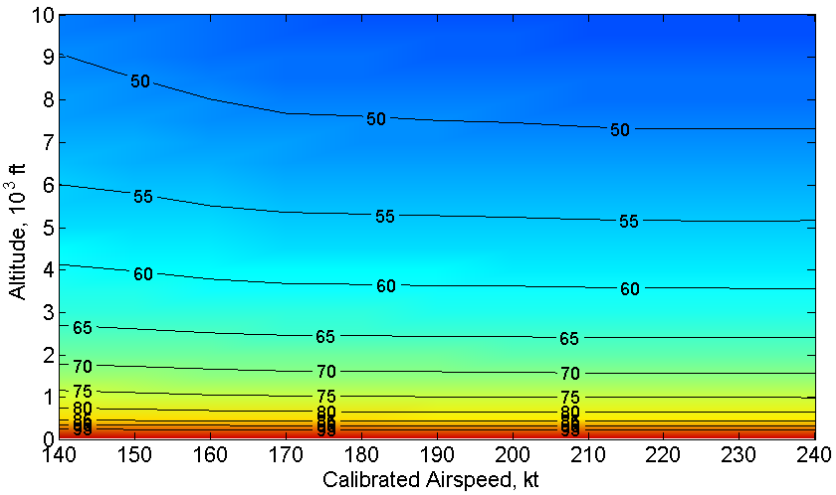

Figure 2-4 B757-200 constant CAS level flight LAMAX, dBA.

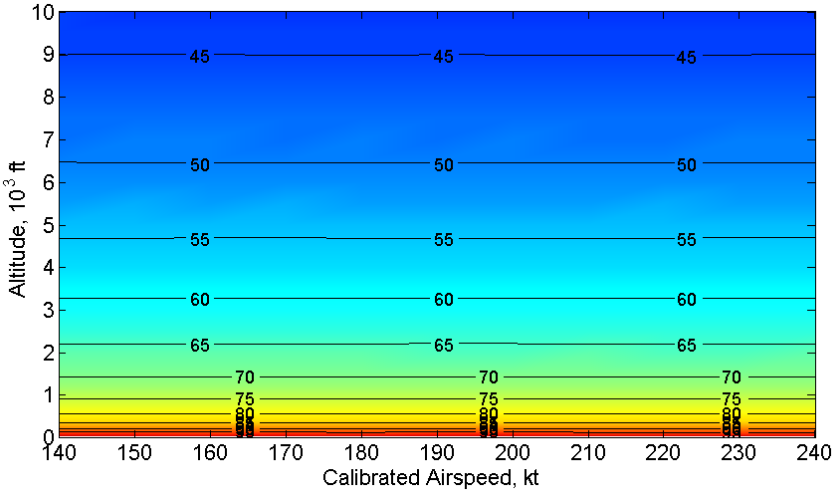

Figure 2-5 B757-200 constant CAS idle descent LAMAX, dBA.

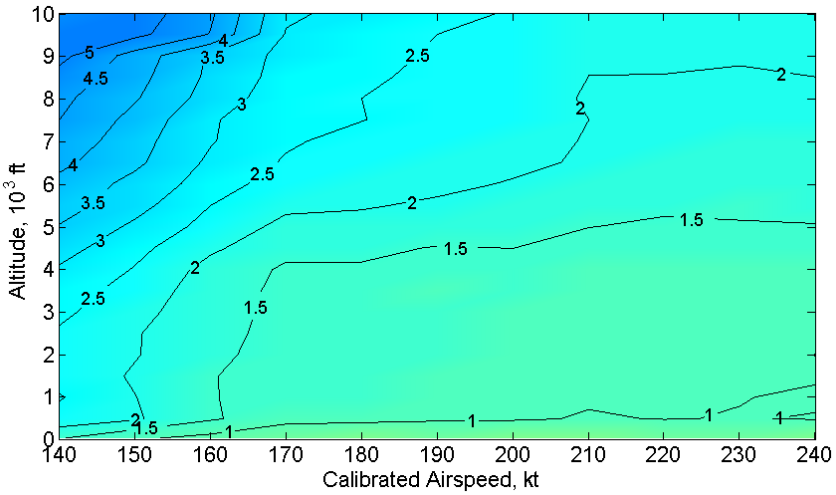

Figure 2-6 B757-200 noise reduction in LAMAX of constant CAS idle descent over level flight, dBA.

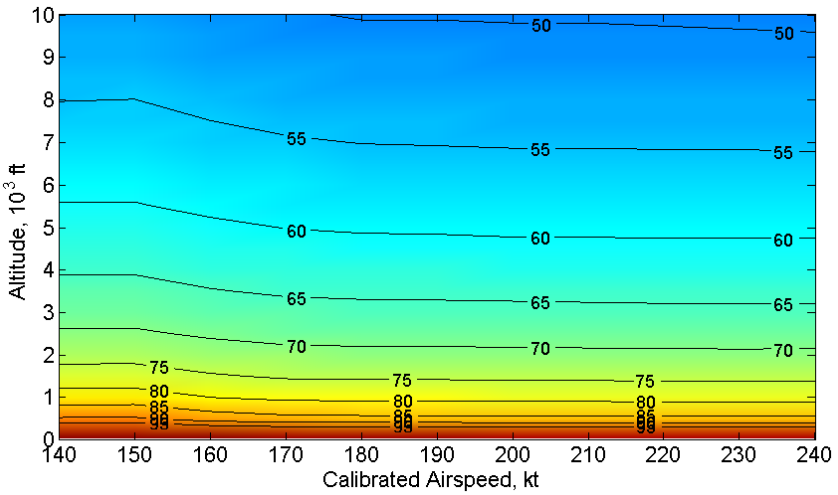

Figure 2-7 B767-300 constant CAS level flight LAMAX, dBA.

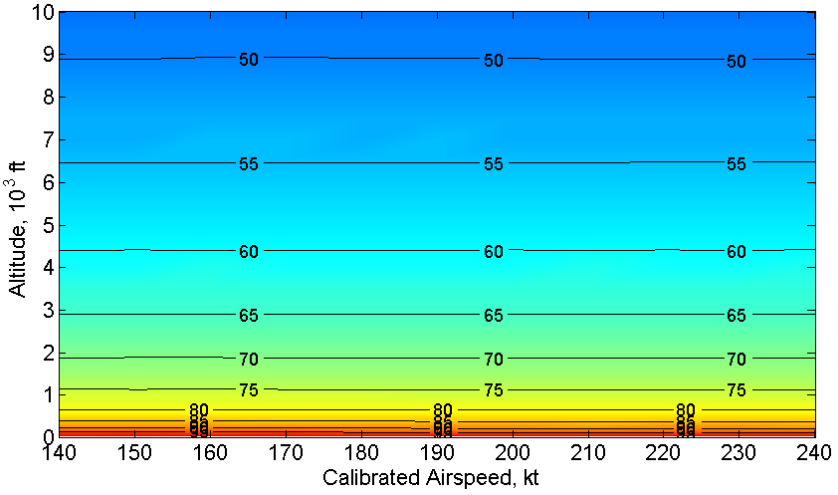

Figure 2-8 B767-300 constant CAS idle descent LAMAX, dBA.

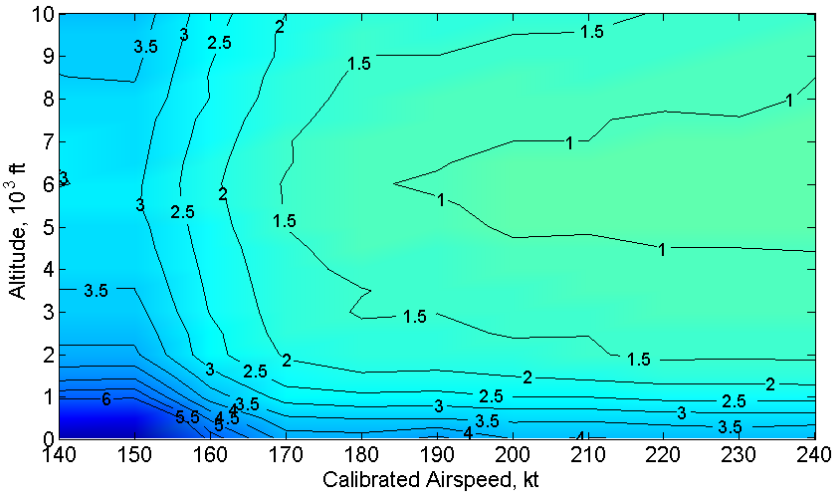

Figure 2-9 B767-300 noise reduction in LAMAX of constant CAS idle descent over level flight, dBA.

To get the magnitude of noise reductions for each aircraft, the LAMAX noise level at each point in the altitude-CAS space for constant CAS level flight was subtracted by the LAMAX noise level for the constant CAS idle descent at the same point. The result is an indicator of the maximum possible noise reductions by setting the throttles to idle with all other parameters such as aircraft weight, altitude, and speed remaining the same. The results are presented as equal LAMAX contours in Fig. 2-6 and Fig. 2-9 for B757-200 and B767-300 respectively. Contours were drawn at 0.5 dBA intervals. A different color map was used in these two figures to present gradual changes in LAMAX reductions between contour lines. A darker blue shade represents a higher magnitude in noise reductions so that the visual impression is consistent with Fig. 2-4, Fig. 2-5, Fig. 2-7 and Fig. 2-8. This is to say that a darker blue shade means a higher noise reduction can be achieved by flying at idle throttle. It is seen from Fig. 2-6 and Fig. 2-9 that, within reasonable altitude and speed ranges, the noise levels on the ground could be reduced by 1 to 3 dBA by using idle throttle. These noise level reductions are noticeable to the human ear. They are equivalent to cutting the noise intensity on the ground by 20% to 50%.

2.2.4 Noise Reductions through Procedure Improvements

Significant noise reduction can be achieved by flying higher vertical profiles and using lower engine throttle settings. Numerical examples are given below to illustrate the possible noise reductions that can be achieved through procedure improvements.

Suppose a vectored approach aircraft descended to 3,000 ft above the ground at a point about 15 to 20 nm (between -20 nm and -15 nm on the horizontal axis in Fig. 2-10) to the runway threshold along the flight track. Further, suppose that from that point on, the aircraft maintained constant speed level flight at CAS 180 kt until the aircraft captured Instrument Landing System (ILS) glide slope at -8 nm. The vertical profile of the vectored aircraft is illustrated by the dashed thick curve in Fig. 2-10. The LAMAX noise levels on the ground below the level flight segment can be obtained from the INM noise computation results presented in Subsection 2.2.2 as 62.5 dBA and 66.1 dBA for B757-200 and B767-300, respectively.

Assume that a hypothetical noise abatement approach procedure were to be designed to reduce community noise impact. Suppose that in this procedure, the aircraft would be 5,000 ft above the ground and descending at CAS 200 kt with engine throttle set to idle when it passed the point at -15 nm. The vertical profile of the hypothetical noise abatement approach procedure is illustrated by the solid thick curve in Fig. 2-10. The LAMAX noise levels on the ground at -15 nm can be obtained from the INM noise computation results presented in Subsection 2.2.3 as 54.0 dBA and 58.4 dBA for B757-200 and B767-300, respectively. Note that these values are below the WHO recommended LAMAX 60-dBA threshold for preventing nighttime sleep disruption. These noise reductions are listed in Table 2-1.

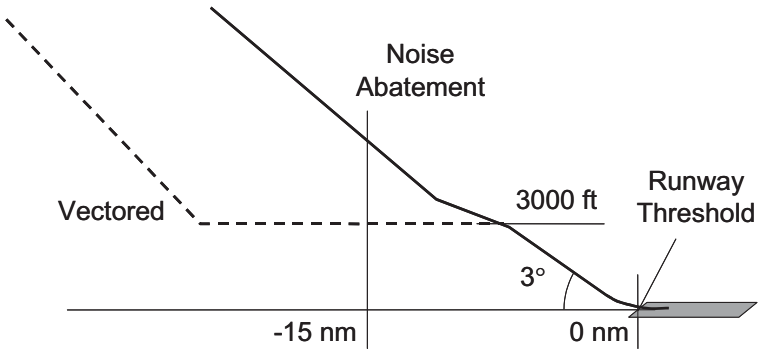

Figure 2-10 Example noise abatement approach procedure.

Table 2-1 Example noise reductions at -15 nm to runway threshold.

Procedure	Vectored	Noise Abatement	Difference
Altitude	3,000 ft	5,000 ft	+2,000 ft
CAS	180 kt	200 kt	+20 kt
Operation mode	Level	Descent	
Throttle	Engaged	Idle	Reduced
LAMAX, B757-200	62.5 dBA	54.0 dBA	6.5 dBA
LAMAX, B767-300	66.1 dBA	58.4 dBA	7.7 dBA

The noise reductions at -15 nm would thus be 6.5dBA and 7.7 dBA for B757-200 and B767-300, respectively. It can also be further deducted from Fig. 2-6 and Fig. 2-9 that the noise reductions at -15 nm simply due to the higher vertical profile and higher speed (without reducing engine thrust from that required for constant speed level flight) were 4.9 dBA and 6.6 dBA for B757-200 and B767-300 respectively. The noise reductions due to reducing engine throttle to idle (at the altitude of 5,000 ft) were 1.6 dBA and 0.9 dBA for B757-200 and B767-300 respectively. In this case, the higher vertical profile contributed more to noise reductions than reducing the engine throttle to idle.

In this example, between -15 nm and -8 nm, noise reductions would gradually decrease when the point moved closer to the runway threshold. Between the start of the level flight segment of the vectored profile and -15 nm, noise reductions would gradually increase as the point moved farther away from the runway threshold.

2.3 AIRCRAFT PERFORMANCE

Aside from community noise impact, aircraft performance is another important aspect that must be considered in noise abatement procedure design. Two performance parameters are of special interest: the total fuel flow rate and the FPA. The total engine fuel flow rate directly contributes to emissions and operating costs, and therefore has become extremely important because of today's high oil prices and environmental concerns. FPA directly determines the aircraft vertical profile and affects required engine thrust; it is also very important in satisfying Air Traffic Control (ATC) restrictions. These two performance parameters are discussed in this section.

2.3.1 Total Fuel Flow Rate

Constant CAS level flight not only defines the upper bound of approach noise levels, but also the upper bound of total fuel flow rate for approach given that all other conditions such as aircraft weight, altitude, and speed are equal. Total fuel flow rate data were extracted from the output files of the constant CAS level flight simulation runs described in Subsection 2.2.2. Results are illustrated in Fig. 2-11 and Fig. 2-12 as approximate equal fuel flow rate contours for the B757-200 and B767-300 respectively. The intervals between consecutive contours are 1,000 lb/h. Again, a color map was used in these two figures to better portray gradual changes in fuel flow between contour lines. The gradual color shade change from blue to brown represents the gradual total fuel flow rate increase.

It is seen from Fig. 2-11 and Fig. 2-12 that total fuel flow rates for constant CAS level flight depend mostly on CAS. They remained roughly the same for the same CAS throughout the altitude range

(10,000 ft and below) shown. As the CAS decreased from 200 kt to 140 kt the total fuel flow rates increased about 50% for both aircraft types. As discussed earlier, this is due to the aircraft drag increase at low speeds. It is thus desired that if level flight segments could not be avoided, they should be conducted at relatively high speed to save fuel.

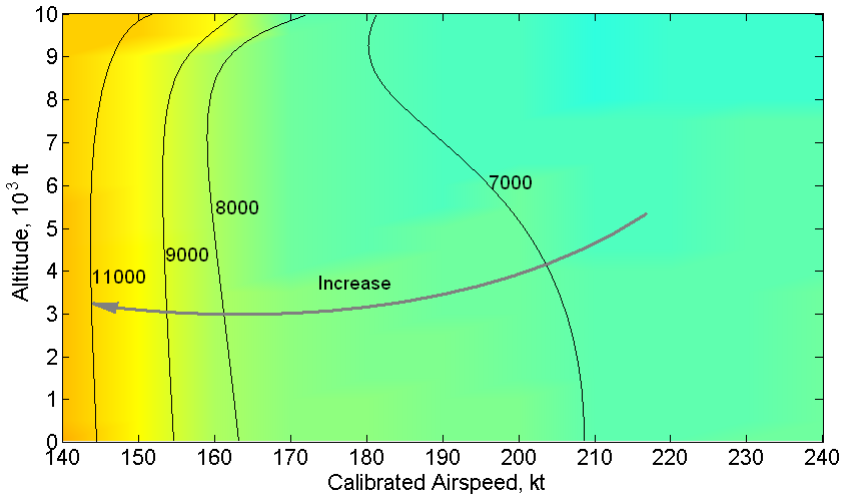

Figure 2-11 B757-200 constant CAS level flight fuel flow rate, lb/hr.

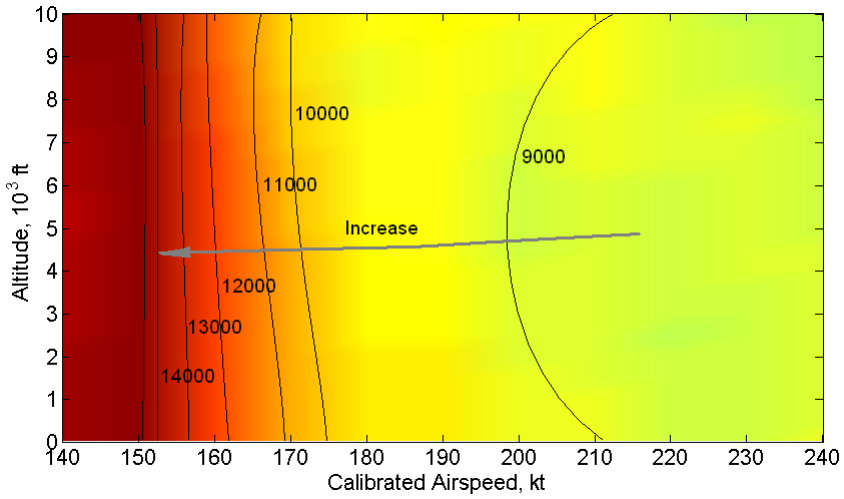

Figure 2-12 B767-300 constant CAS level flight fuel flow rate, lb/hr.

On the other hand, constant CAS idle descents represent the lower bound of total fuel flow rates for approach given that all other conditions such as aircraft weight, altitude, and speed are equal. Total fuel flow rate data were extracted from the output files of constant CAS idle descent simulation runs described in Subsection 2.2.3. Total fuel flow rates for constant CAS idle descents are presented in Fig. 2-13 and Fig. 2-14 as equal percentage contours for B757-200 and B767-300 respectively. The percentages were computed with respect to the corresponding total fuel flow rates for constant CAS level flight. Again, color maps were used to better portray gradual changes in total fuel flow rates between contour lines.

Total fuel flow rates for constant CAS idle descent were significantly lower, approximately 15 to 30% of that for constant CAS level flight for the two aircraft types. Total fuel flow rate for constant CAS idle descent remained relatively constant for different CAS values. The decrease of the percentages at low

CAS values shown in Fig. 2-13 and Fig. 2-14 were due to the significant increase of total fuel flow rates for constant CAS level flight at low CAS values.

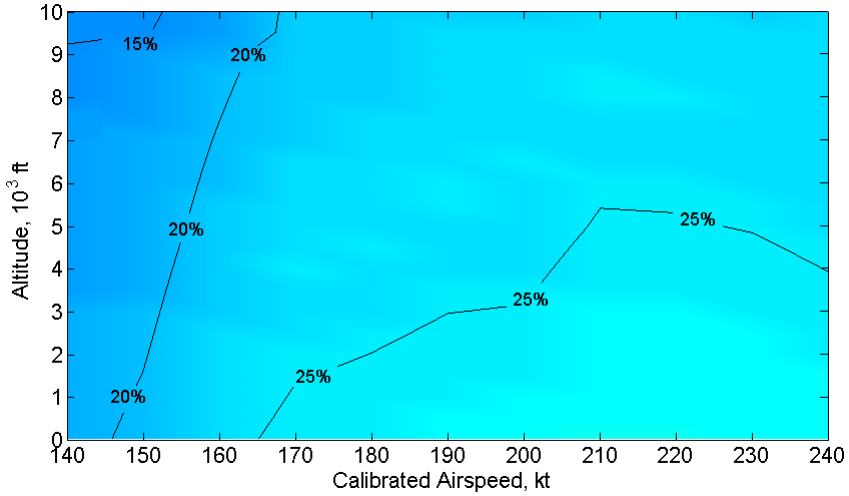

Figure 2-13 B757-200 constant CAS idle descent fuel flow rate, percent of corresponding constant CAS level flight fuel flow rate.

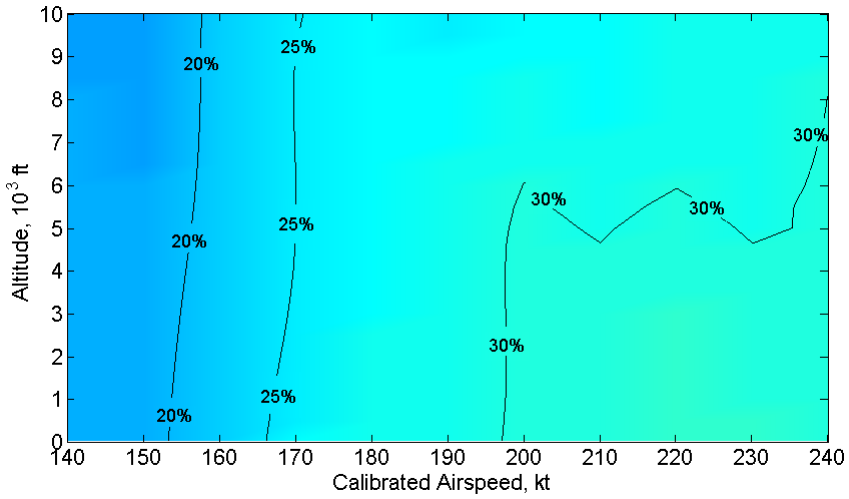

Figure 2-14 B767-300 constant CAS idle descent fuel flow rate, percent of corresponding constant CAS level flight fuel flow rate.

Given today's high oil prices, the fuel savings that can be achieved through improving approach procedures provide great incentives for operators to implement noise abatement approach and arrival procedures and improve the quality of life of residents in communities around airports. Moreover, these reductions in fuel burn also preserve natural resources and improve local air quality without sacrificing the quality of services of air transportation.

2.3.2 The Flight Path Angle

The FPA and the aircraft vertical profile are related to each other. A higher FPA assures a higher vertical profile. If community noise impact were the only concern, high FPAs would naturally be preferred for lower noise on the ground, at least when the aircraft is close to the runway. However, in

noise abatement approach and arrival procedure design, many other factors must also be taken into account.

The FPA is also related to required engine thrust. During constant CAS level flight where FPA equals zero, engine throttle must be fully engaged to overcome drag. As the FPA at which the aircraft is descending becomes steeper, the required engine thrust to maintain a constant speed (such as a given CAS) will decrease. The FPA for constant CAS idle descent represents a critical condition. If the FPA is steeper than the FPA for constant CAS idle descent, speedbrakes must be extended to maintain the given CAS or the CAS will increase during descent. Sustained use of speedbrakes during descents is not desirable because it reduces comfort, increases airframe noise, and wastes the aircraft gravitational potential energy. Thus, constant CAS idle descent represents the upper bound of the magnitude of FPAs from an aircraft performance point of view.

To illustrate the relationship between idle descent FPA and aircraft aerodynamics, consider a simplified case – instantaneous constant true speed descent under zero wind. Because wind is assumed to be zero, the true speed V and true airspeed V_r have the same value. The simplified free body diagram is shown in Fig. 2-15. In the figure, γ denotes FPA, which is negative for descent, and T_i denotes installed idle thrust, which is approximately equal to zero.

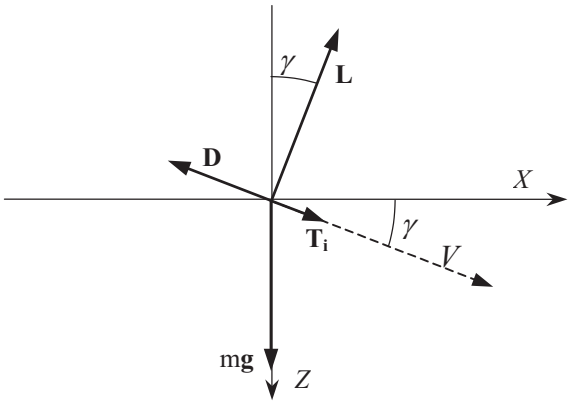

Figure 2-15 Simplified free body diagram for constant true speed idle descent.

For constant true descent, both vertical and horizontal accelerations are zero. The force equations are thus

$$-L\sin\gamma + (T_i - D)\cos\gamma = 0 \tag{2-7}$$

$$L\cos\gamma + (T_i - D)\sin\gamma - mg = 0 \tag{2-8}$$

From Eq. (2-7), the FPA for constant true speed idle descent can be derived as

$$\gamma = \text{atan}\left(\frac{T_i - D}{L}\right) \tag{2-9}$$

Ignoring the installed idle thrust, the FPA for constant true speed idle descent becomes

$$\gamma = -\operatorname{atan}\left(D/L\right) \tag{2-10}$$

It can be seen from Eq. (2-10) that the FPA for constant true speed idle descent is determined by aircraft L/D ratio. The lower the L/D ratio, steeper the FPA will be and vise versa. As mentioned earlier in Subsection 2.2.2, for any given aircraft, the L/D ratio is a function of the lift coefficient and the aircraft configuration (flap/slat and landing gear positions). From Eq. (2-8) and the first half of Eq. (2-4), it can be derived

$$C_l = \frac{2L}{\rho V_r^2 S} = \frac{2[mg - (T_i - D)\sin\gamma]}{\rho V^2 S \cos\gamma} = \frac{2(mg - T_i \sin\gamma)}{\rho V^2 S \cos\gamma} + C_d \tan\gamma \tag{2-11}$$

With the drag polar for a given aircraft configuration known, Eq. (2-10) and Eq. (2-11) can be solved iteratively to obtain the FPA for constant true speed idle descent. Under normal operational conditions, $C_d << C_l$ and the magnitude of FPA γ is small. Eq. (2-11) can be approximated by the lift coefficient for level flight, i.e.

$$C_l \approx \frac{2mg}{\rho V^2 S} \tag{2-12}$$

Based on the discussion in Subsection 2.2.2, the L/D ratio decreases with the decrease in speed. It is thus expected that the magnitude of FPA for constant true speed idle descent will increase as the speed decreases. On the other hand, if the speed is adjusted (by proper trimming) to keep the term mg/V^2 in Eq. (2-12) constant as the aircraft weight varies, the lift coefficient will remain the same; hence, the L/D ratio will remain the same. In other words, the descend speed corresponding to the highest L/D ratio (or the shallowest constant true speed idle descent FPA) varies with the aircraft weight. At heavier weight, the descent speed corresponding to the highest L/D ratio is higher.

Because of the nonlinear relationship between CAS and TAS, and the possible wind changes along altitude, aircraft acceleration is normally not zero during constant CAS descent. The computation of FPA for constant CAS idle descent is thus more complicated. Nonetheless, the analysis of the FPA for constant true speed idle descent does provide insight to the relationship between FPA and aircraft aerodynamic performance, and descent speed. Detailed derivation of the equations used for computing the FPA for idle constant CAS descent is provided in Subsection A.4.3 of Appendix A. They are not iterated here for the sake of clarity.

FPAs for constant CAS idle descent were extracted from the output files of simulation runs described in section 2.2.3. Since FPAs for constant CAS idle descent did not change much for different altitudes with in the range (sea level to 10,000 ft) examined, average values for each CAS value were used to represent the FPA for that speed. The results are presented in Fig. 2-16. The magnitude of FPAs for constant CAS idle descent above CAS 200 kt up to 240 kt (clean configuration) were approximately 3 deg for the given simulation conditions. Below CAS 200 kt, the magnitude of FPAs for the constant CAS idle descent increased rapidly as speed decreased, because flap/slat extensions were initiated at approximately that speed. At 140 kt, the magnitude of FPAs for constant CAS idle descent were about 7 deg – landing gear had been deployed at that speed.

In a practical approach procedure design, the aircraft would normally decelerate as it approaches the runway threshold. Should the aircraft decelerate to about 140 kt, it would normally have been established on the final approach. At that time, the FPA would normally be determined by the ILS glide slope which

is about 3 deg. In other words, as the aircraft decelerates and gets closer to the runway, thrust must be added to maintain stabilized flight because the FPA to remain on glide slope would be far shallower than the FPA required for constant CAS idle descent at low speeds. The requirement to add engine thrust to counter the increased drag – because of the deployment of flaps/slats and landing gear at low speeds and the need to remain on the glide slope – essentially limits the area where noise abatement approach procedures are effective in reducing community noise impact. For this reason, noise abatement approach procedures can not be effective in reducing noise impact once the aircraft is established on the final approach as long as a conventional 3 deg glide slope is used.

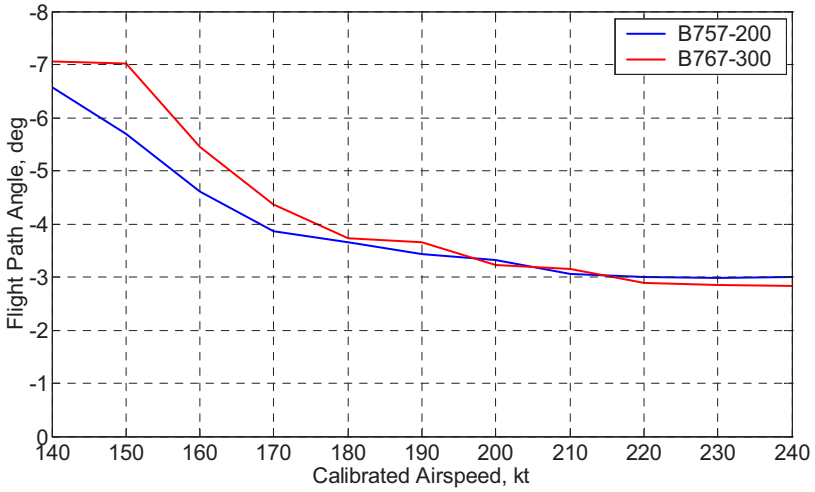

Figure 2-16 Average FPAs for constant CAS idle descent.

A special case is a noise abatement approach procedure that is some times referred to as steeper approach. This procedure resembles a glide-and-dive vertical profile, i.e. an initial approach segment with normal FPA and a final approach segment with steeper FPA (steeper than the normal 3 deg glide slope). If the FPA is steep enough, the final approach could also be performed at or near idle thrust even when the speed is relatively low. However, the majority of commercial jet aircraft are not certified for steeper approaches. The London City Airport is one of the few airports that require the glide-and-dive type steeper approach procedures – only aircraft capable of making an approach at 5.5 deg (-5.5 deg FPA) or steeper are permitted to land at the airport.

The use of different FPAs is also important in satisfying ATC restrictions. For example, if an "at or above" altitude restriction is imposed at a point relatively far from the runway, the FPA between that point and the next lower altitude restriction must be steeper than a certain value. In some cases, the ATC dictated minimum FPA could be slightly higher than the FPA for the constant CAS idle descent corresponding to the assigned CAS for that segment. If this happens, speedbrakes will have to be frequently extended to add drag to keep the aircraft on the vertical path and maintain the assigned speed. This is not desirable because it increases pilot workload. If other conditions permit, the assigned speed for the segment could be lowered so that the FPA for constant CAS idle descent corresponding to the new speed would be higher than the ATC required minimum FPA. With the new speed, an idle descent segment satisfying the altitude restrictions may be built, and be executed without excessive use of speedbrakes[11].

Knowledge of the magnitude of FPA for constant CAS idle descent for various conditions such as aircraft type, weight range, altitude, speed, and wind (which will be discussed in the following chapters) is thus a valuable tool for the design of noise abatement approach and arrival procedures.

2.4 NOISE ABATEMENT APPROACH AND ARRIVAL PROCEDURE DESIGN

The design of noise abatement approach and arrival procedures is determined by overall goal to be achieved through these procedures. The procedures could be designed with the primary objective of reducing aircraft noise impact. Ordinary noise metrics, and residential area and population impacted by aircraft noise at specific levels[5] can be used as objective functions. In this case, the procedures of concern are normally limited within the terminal area. Procedures could also be designed to achieve objectives that are more comprehensive. Aircraft noise impact, engine exhaust emissions, cost of implementation, operating economy, traffic efficiency, and air traffic coordination can all be taken into account to form a balanced approach to procedure development. In this case, the procedures of concern may extend far beyond the boundaries of the terminal area. Procedures that are designed to benefit the most stakeholders will most probably be accepted, implemented, and sustained into the future.

The design of noise abatement approach and arrival procedures also heavily depends on the guidance and navigation technology available for use by the aircraft performing these procedures. Some proposed near term designs, such as the one that relies on a paper based pilot cueing system consisting of gates (i.e., altitude/speed checkpoints) and recommended flap schedule[12], do not require additional automation on board the aircraft. Some other proposed noise abatement procedure designs rely on the availability of new automation such as the Advanced Continuous Descent Approach real-time FMS algorithm[13] and the Low Noise Flight Guidance Concept[14]. Due to the lengthy development and certification process for any airborne system, these approaches to noise abatement procedure design should be considered long-term solutions.

In recent years, as the accuracy and reliability of GPS based RNAV improved and the number of FMS equipped RNAV capable aircraft (either newly built or through retrofit) increased, RNAV terminal area procedures become more and more popular. Aside from the many benefits documented in previous studies[15,16], RNAV terminal area procedures provide an opportunity for implementing noise abatement approach and arrival procedures in the near term. RNP[17,18] is an authoritative statement of aircraft navigation capabilities and performance requirements that are necessary for aircraft to operate in a given airspace or use a given procedure. With the RNP concept, special RNP RNAV noise abatement or arrival approach procedures can be designed for specified aircraft types or specified operators with required capabilities[20], and be approved by aviation authorities for routine use. This regulatory advancement enables maximized use of advanced navigation technology invested by the operators.

RNAV noise abatement arrival procedures, referred to as RNAV Continuous Descent Arrival (CDA) procedures, are RNAV arrival procedures with specially designed vertical and speed profiles that are optimized to reduce aircraft community noise impact. In RNAV CDA, the lateral flight path is defined by a series of waypoints. The lateral path can extend from the final approach fix all the way back to cruise altitude. The vertical and speed profiles are defined by altitude and speed constraints at certain waypoints along the lateral path. The waypoints and the corresponding altitude and speed constraints are preprogrammed in the aircraft FMS navigation database. The FMS LNAV function computes the lateral path from the waypoints and works together with the autopilot to maintain the aircraft on the computed lateral path. The FMS VNAV function computes the vertical and speed profiles that satisfy all constraints and works with the autopilot and autothrottle to control the aircraft to follow the computed vertical and

speed profiles. If no fixed altitude constraint is specified at the higher end of a segment, the VNAV will compute an idle thrust vertical segment consisting of a constant CAS idle descent upper sub segment and an idle deceleration lower sub segment (when deceleration is required). This type of idle thrust vertical segment is referred to as the unrestricted path segment because the flight path angle will be determined by the FMS based on aircraft performance, aircraft weight, and weather conditions (mainly wind). In contrast, geometric segments (with fixed altitude constraints at both ends) with straight-line sub segments may be necessary to accommodate ATC restrictions, or to assure proper transition to final approach. During the execution of RNAV CDA, the pilot monitors the execution of the aircraft, controls the extension of flaps/slats and landing gear at the proper time. The pilot also controls the speedbrakes to add drag when it deems necessary to maintain the desired speed.

The design of the RNAV CDA procedure is thus to: 1) choose a lateral flight path that is most direct to the final approach fix while satisfying lateral ATC restrictions and avoiding noise sensitive residential areas; and, 2) choose altitude and speed constraints that assure a continuously descending vertical profile and a speed profile with delayed deceleration that allows the aircraft to remain in clean configuration as long as possible while satisfying vertical airspace restrictions and regulatory operational limits. The ideal vertical and speed profile design would enable the aircraft engine throttle to remain at idle until the aircraft is established on the final approach. This is essentially a unrestricted path design that will give the highest benefits. Minor adjustment to the unrestricted path design, by employing one or more fine tuned geometric segments, may provide increased predictability or operational flexibility, and accommodate complex ATC restrictions.

For the designed procedure to be approved by aviation authorities for routine application, various regulatory criteria and standard must be satisfied and approval procedure be followed[19]. These include standards for terminal instrument procedures[21,22], standards and guidelines for RNAV or RNP RNAV procedures[20,23,24,25,26,27], procedure operation regulations[28], and procedure approval guidelines[29,30,31].

Once the lateral path and the altitude and speed constraints are determined, fast-time and pilot-in-the-loop simulations are then performed to verify operability and noise impact. Iteration is necessary to search for the best solution until the procedure is ready for flight trials. Depending on the actual situation, negotiation with ATC may be necessary to relax or modify some of the existing ATC restrictions to achieve high noise reduction and other benefits. Well-designed RNAV CDA can significantly reduce community noise, fuel burn, emissions, and flight time while retain benefits of regular RNAV arrival procedures[32,33]. For example, up to 500 lb of fuel were saved by each UPS B767-300 that flew a CDA to KSDF during a flight test conducted in October 2002[32].

The characteristics of the vertical profile of an example RNAV CDA are illustrated in Fig. 2-17. This procedure was designed for a CDA flight test conducted at KSDF in September 2004[33]. The procedure starts at cruise altitude and continues along the FMS computed VNAV descent path until the aircraft is established on the ILS glide slope. The segment above the first vertical constraint is an unrestricted path segment. Ideally, the engine throttle would remain at idle until the aircraft is established on the final approach. Two shallower segments are facilitated by the FMS to allow for proper deceleration. The first of these shallower segments is at 10,000 ft allowing aircraft to decelerate to CAS 240 kt. The second shallower segment is at 3,800, ft allowing aircraft to decelerate to CAS 180 kt, the speed at which the aircraft is configured for the final approach. The segment from the first vertical constraint to the last vertical constraint is a geometric segment that provides a smooth transition to the ILS glide slope interception. The FPA of the geometric segment is slightly shallower than the ILS glide slope to assure proper capture of the ILS glide slope. Comparing with existing standard approaches, aircraft performing CDA will have a higher vertical profile without any level segment, and a lower average throttle setting (mostly idle).

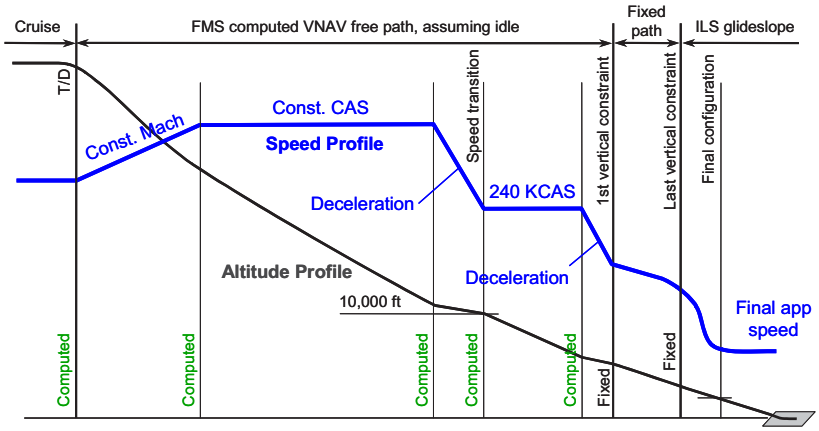

Figure 2-17 Characteristics of the vertical profile of a RNAV CDA designed for KSDF.

The lateral path of the example RNAV CDA is shown in Fig. 2-18. The runway to be used depends on the prevailing winds on a given day. If the wind is from the South, runway 17R is used (the southern flow configuration). If the wind is from North, runway 35L is used (the northern flow configuration). Arrival aircraft from the west follows the path defined by waypoints ZARDA, PENTO, and SACKO, to CHERI. Depending on the runway configuration in use, the aircraft then follows the path defined by waypoints CHERI, TRN17, CHR27, to final approach fix CHRCL, or the path defined by waypoints CHERI, TRN35, CRD27, to final approach fix CARDL. The first vertical constraint is specified at TRN17 and TRN35 for the CDA to runway 17R and runway 35L respectively, and the last vertical constraint is specified at the final approach fix. The RNAV CDA terminates at the final approach fix. By then, the aircraft will have already established on the ILS localizer and the ILS glide slope. This RNAV CDA is used in this thesis as the example procedure for the simulation study.

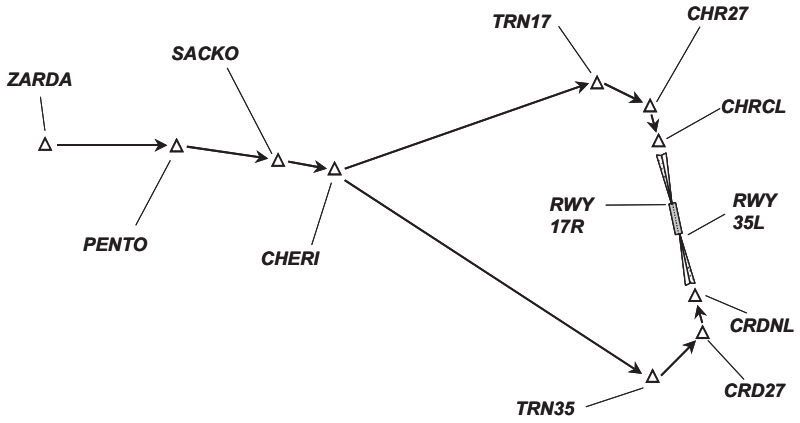

Figure 2-18 The lateral path of a RNAV CDA designed for KSDF.

Specific design parameters of the RNAV CDA designed for the KSDF 2004 flight test will be described later in Chapter 6 when simulation analysis results and flight test results are presented. The

FMS computes the VNAV path through backward integration from the last vertical constraint. Details about how the VNAV path is computed is presented in the next chapter and in Appendix A.

Although the FMS capabilities have been advanced over the years since its inception, the basic FMS VNAV functionalities have been in existence for more than 20 years. In the past, VNAV functionalities have only been used by some aircrews for the descent from cruise to the terminal area boundary. In the vast majority of those cases where VNAV is used, the VNAV is turned off as soon as the aircraft enters the terminal area. There have been two major reasons for this disuse. The first reason is the cognitive related concerns about the use of VNAV in terminal area. Most importantly, the extensive use of vectoring in terminal area for managing separation – as discussed in Subsection 1.1.2 and Section 2.1 – is not consistent with a form of guidance and navigation that requires pre-programmed objectives and planning. In the next section, a proposed procedure design and operational framework is presented. The new framework can be used together with the separation analysis methodology to be presented later in this thesis to maximize the use of VNAV and FMS technology and to achieve environmental and economic benefits.

2.5 PROPOSED PROCEDURE DESIGN AND OPERATIONAL FRAMEWORK

As mentioned earlier in this chapter, in the current ATC practice, the required separation between aircraft is achieved through vectoring. To assure that the noise reduction and other benefits can be achieved as expected, vectoring, especially vectoring at low altitudes, should be avoided. To allow noise abatement approach and arrival procedures to be executed safely and effectively, a new design and operational framework must be put in place. The ultimate goal of the new framework is to allow noise abatement approach and arrival procedures to be implemented at as many sites as possible, and whenever the traffic condition permits to minimize noise impact, fuel burn, emissions, and flight time over time. The philosophy is to develop a methodology to plan a better operation that can be executed without interruption at high level of confidence and to provide alternative plans to cover exceptions, i.e. occasions when separation violations are projected, which occur only with a small probability.

The proposed procedure design and operational framework is shown in Fig. 2-19. In this proposed concept, the role of the air traffic controller during noise abatement approach procedures is divided into four phases: streaming and sequencing; spacing; monitoring, and intervention if separation is projected to be violated; and missed approach. A conceptual intermediate metering point (or simply metering point) separates the descent from cruise and the low noise descent to the runway. The intermediate metering point could be the existing ATC hand off point, a geometric point on the en route control and approach control boundary, or a newly created reference point. A target separation between consecutive aircraft is specified for the intermediate metering point such that separation can be assured – to a desired level of confidence – throughout the low noise descent without further controller intervention. Before the metering point, the controller is free to vector aircraft as necessary for streaming and sequencing, in order to establish the target separation (and altitude and speed, if so desired). With these initial conditions properly set, aircraft can continue the noise abatement approach or arrival procedure without further vectoring. In this phase, the controller monitors the spacing between aircraft, and only intervenes if additional spacing is required to prevent separation violations. The additional spacing can be achieved by adjusting speed; vectoring the aircraft off the procedure lateral path, and returning it to the path when the required separation is reestablished; extending the base leg; or by sidestepping to an alternate runway if it is available. As the aircraft approaches the Final Approach Fix, they will be cleared for final approach in conventional fashion.

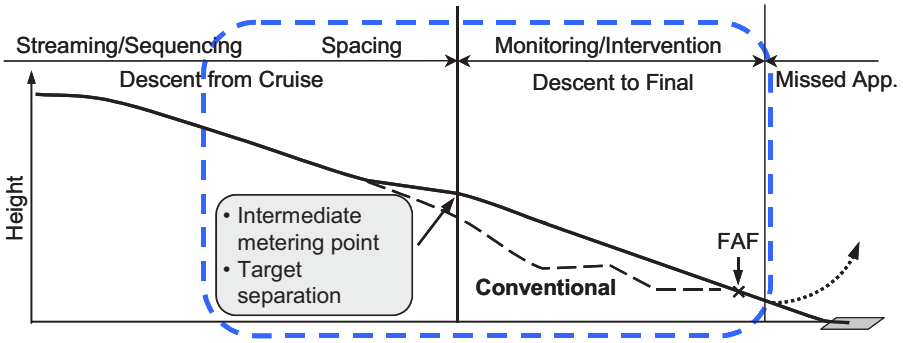

Figure 2-19 Proposed noise abatement approach procedure design and operational framework.

Given this procedure framework, it is apparent that larger trajectory variations during the low noise descent could cause higher variations in the spacing between aircraft, forcing larger target separation to be used, and hence impacting the efficiency of the procedure. All else leaving equal, the longer the low noise descent leg is, the higher the trajectory variations would be. Thus, the location of the intermediate metering point can be tailored to the traffic level. In light traffic situations, it can be moved farther away from the runway to realize more fuel savings and emission reductions in addition to noise reductions. In heavier traffic, it can be moved closer to the runway as long as it is above a certain height (say 7,000 ft) so that noise benefits can be maintained. Alternative metering point locations thus provide operational flexibility for the procedure to be adapted to different traffic levels.

One of the goals of this research, is thus to develop a modeling tool, and a separation analysis methodology to determine the target separation that gives the desired level of confidence at any given intermediate metering point for noise abatement approach and arrival procedures.

2.6 SUMMARY

Typical vectored arrival flight tracks were examined to illustrate areas where arrival procedures can be improved to reduce community noise impact. The definitions of community noise metrics were reviewed, including the rational for choosing the maximum A-weighted sound level (LAMAX) as a figure of merit. Aircraft noise impact of two specific flight modes, constant CAS level flight and constant CAS idle descent were examined through numerical simulation to show the potential of noise reductions that can be achieved through procedure improvements.

By examining the noise impact of constant CAS level flight, three observations were obtained. First, as the altitude of the constant CAS level flight increases, LAMAX on the ground decreases nonlinearly. At low altitudes, the decrease in LAMAX due to the increase of altitude happens faster than that at higher altitudes. This suggests that more noise reduction can be achieved by increasing the altitude of low altitude level flight segments, or eliminating them completely. Second, for the constant CAS level flight, as CAS decreases, LAMAX on the ground increases. The increase in LAMAX due to the decrease in CAS is more obvious when flaps are extended than that when the aircraft is in clean configuration. This suggests that level flight in the terminal area should be conducted at high speeds when the aircraft is in clean configuration, if these level flights cannot be avoided. Third, when the constant speed level flight is conducted above a specific altitude, the noise level on the ground falls below a threshold that can be viewed as acceptable. For example, based on the simulation results, if the constant CAS level flight is

conducted above 5,000 ft, LAMAX will fall below 60 dBA (the WHO recommended nighttime sleep disruption threshold) for both B757-200 and B767-300 most of the time. This suggests that vectoring at high altitudes may be tolerable from a community noise point of view.

By examining the noise impact of constant CAS idle descent, it was observed that although LAMAX on the ground decreased with the altitude in a similar way as for constant CAS level flight, LAMAX on the ground remained relatively constant for different CAS values. For B757-200 and B767-300, LAMAX on the ground is 1 to 3 dBA lower than that for constant CAS level flight, given the same altitude and CAS. These noise level reductions are noticeable by the human ear. They are equivalent to cutting the noise intensity on the ground by 20% to 50%. A hypothetical noise abatement approach procedure using idle descent segment was estimated to reduce LAMAX noise levels at a point 15 nm from runway threshold by 6.5dBA and 7.7 dBA for B757-200 and B767-300 respectively. This reduction is the result of both a higher vertical profile and lower engine thrust as compared with the traditionally vectored flights with level segments at 3,000 ft.

Aircraft total fuel flow rates for constant CAS level flight and constant CAS idle descent were also examined. It was found that by using idle throttle, the total fuel flow rates could be reduced by more than 70% for both B757-200 and B767-300 with respect to the corresponding total fuel flow rates during constant CAS level flight. In light of today's high oil prices, the fuel savings that can be achieved by improving approach and arrival procedures provide great incentives for operators to implement these procedures to improve the quality of life of residents in the communities around airports. Moreover, the reductions in fuel burn also preserve natural resources, and improve local air quality without sacrificing the quality of services of air transportation.

The relationship between FPA, CAS, and engine thrust was also examined through theoretical analysis and simulation for the two aircraft types. At any given altitude and CAS, a zero FPA (level flight) represents the upper bound of required thrust to maintain a constant CAS during approach. The FPA for constant CAS idle descent represents the lower bound of required thrust (idle thrust) to maintain a constant CAS during approach. Anywhere in between, partial thrust will be required unless the aircraft is decelerating. At low speeds, e.g. CAS 140 kt when flaps/slats and landing gear are extended, the magnitude of FPA for constant CAS idle descent could be as high as 7 deg for B757-200 and B767-300. Aircraft normally needs to decelerate to a speed close to its final approach speed once it is established on the final approach. At that time, the FPA would normally be determined by the ILS glide slope, which is about 3 deg. In other words, as the aircraft decelerates and gets closer to the runway, thrust must be added to maintain stabilized flight because the FPA would be far shallower than the FPA desired for constant CAS idle descent. This essentially limits the area where noise abatement approach procedures are effective in reducing community noise impact.

Based on the above observations, general constraints and guidelines for noise abatement approach and arrival procedure design are discussed. As the accuracy and reliability of GPS based RNAV improve and the number of RNAV capable aircraft (either newly built or through retrofit) increases, RNAV Continuous Descent Arrival (CDA) becomes a suitable noise abatement approach procedure for near term implementation. Well-designed RNAV CDA could significantly reduce community noise, fuel burn, emissions, and flight time. Characteristics of RNAV CDA vertical profiles are discussed through a procedure designed for KSDF. This procedure will be used in this research as a numeric example to demonstrate the separation analysis methodology.

The proposed procedure design and operational framework features a conceptual intermediate metering point that separates the descent from cruise and the low noise descent to the runway. The key is to establish a target separation for the intermediate metering point such that separation can be assured – to a desired level of confidence – throughout the rest of the noise abatement procedure without further

controller intervention. On the other hand, the controller is free to vector aircraft before the metering point as necessary for streaming and sequencing, and to establish the target separation. The location of the intermediate metering point can be tailored for the site and the traffic condition to give high operational flexibility and overall efficiency. Contingency plans, such as adjusting speed, vectoring the aircraft off the procedure lateral path and returning later, extending the base leg, or sidestepping to an alternate runway if it is available, can be prepared for the specific site to cover exceptions when separation violation is predicted.

In the following chapters, the development of the modeling tool and the separation analysis methodology for determining the target separation at the intermediate metering point will be presented in detail.

REFERENCES

[1] "Handbook for Industrial Noise Control," NASA SP-5108, prepared by The Bionetics Corporation, NASA, Technology Transfer Division, Washington DC, 1981.

[2] Olmstead, J. R., Fleming, G. G., Gulding, J. M., Roof, C J., Gerbi, P. J., and Rapoza, A. S., "Integrated Noise Model (INM) Version 6.0 Technical Manual," FAA-AEE-02-01, FAA, Office of Environment and Energy, Washington DC, Jan. 2002.

[3] Bennett, R. L., and Pearsons, K. S., "Handbook of Aircraft Noise Metrics," NASA CR-3406, NASA, Scientific and Technical Information Branch, Wahsington DC, 1981.

[4] Newman, J. S., and Beattie, K. R., "Aviation Noise Effects," FAA-EE-85-2, FAA, Office of Environment and Energy, Washington, DC, Mar. 1985.

[5] Clarke, J.-P. B., "A System Analysis Methodology for Developing Single Events Noise Abatement Procedures," Sc.D. Thesis, Department of Aeronautics and Astronautics, Massachusetts Institute of Technology, Cambridge, MA, 1997.

[6] "Tile 14, Code of Federal Regulations, part 36 – Noise Standards: Aircraft Type and Airworthiness Certification," FAA, 1 Jan. 2006.

[7] *UPS B757/767 Aircraft Operating Manual*, Document: UPS33075, UPS Flight Publications, Louisville, Kentucky, 2003.

[8] "INM Version 6.2 Software Update," FAA, Office of Environment and Energy, Washington DC, 19 May 2006.

[9] "Guidelines for Community Noise," edited, Berglund, B., Lindvall, T., and Schwela, D. H., World Health Organization, Geneva, 2000.

[10] van Boven, M., "Development of Noise Abatement Approach Procedures," AIAA 2004-2810, *10th AIAA/CEAS Aeroacoustics Conference,* Manchester, UK, 12-14 May 2004.

[11] Reynolds, T. G., Clarke, J.-P., and Ren, L., "Advanced Continuous Descent Approach Activities at Nottingham East Midlands Airport, UK," Presented at *CDA Workshop No. 3*, Georgia Institute of Technology, Atlanta, GA, 6-7 Sep. 2006.

[12] Ho, N. T., "Design of Aircraft Noise Abatement Approach Procedures for Near-Term Implementation," Ph.D. Thesis, Department of Mechanical Engineering, Massachusetts Institute of Technology, Cambridge, MA, 2005.

[13] Koeslag, M. F. , "Advanced Continuous Descent Approaches, An Algorithm Design for the Flight Management System," Master Thesis, Faculty of Aerospace Engineering, Delft University of Technology, Delft, The Netherlands, Mar. 1999.

[14] Williams, D. H., Oseguera-Lohr, R. M. and Lewis, E. T., "Design and Testing of a Low Noise Flight Guidance Concept," NASA TM-2004-213516, NASA Langley Research Center, Hampton, Virginia, Dec. 2004.

[15] Robinson, S. M., DeArmon, J. S., and Becher, T. A., "Benefits of RNAV Terminal Procedures: Air/Ground Communication Reduction and Airport Capacity Improvements" *Proceedings: the 21st Digital Avionics Systems Conference (21st DASC)*, Vol. 1, Irvine, California, 27-31 Oct. 2002, pp. 2.D.1 - 1-11.

[16] Sprong, K.R., Haltli, B.M., DeArmon, J.S., and Bradley, S., "Improving Flight Efficiency through Terminal Area RNAV," *6th USA/Europe Seminar on Air Traffic Management R & D*, Baltimore, Maryland, 27-30 Jun. 2005.

[17] Meyer, T. and Bradley, J., "The Evolution from Area Navigation (RNAV), Required Navigation Performance (RNP), to RNP RNAV," *ICAO GNSSP IP11 Global Navigation Satellite System Panel Meeting*, Rio de Janeiro, Brazil, 22 Oct.–1 Nov. 2001.

[18] "Roadmap for Performance-Based Navigation – Evolution for Area Navigation (RNAV) and Required Navigation Performance (RNP) Capabilities 2006-2025," Ver. 2.0, FAA, Washington, DC, 5 Jun. 2006.

[19] Tarbert, B., "Area Navigation (RNAV) and Required Navigation Performance (RNP) Program Overview," *The 1st CDA Workshop*, Georgia Institute of Technology, Atlanta, GA, 19 Jan. 2006.

[20] "United States Standard for Required Navigation Performance (RNP) Approach Procedures with Special Aircraft and Aircrew Authorization Required (SAAAR)," FAA Order 8260.52, 1 Jan. 2006.

[21] "United States Standard for Terminal Instrument Procedures (TERPS)," FAA Order 8260.3B CHG 19, 15 May 2002.

[22] "Flight Management System (FMS) Instrument Procedures Development," FAA Order 8260.40B, 31 Dec. 1998.

[23] "Area Navigation (RNAV) Approach Construction Criteria," FAA Order 8260.48, 8 Apr. 1999.

[24] "Civil Utilization of Area Navigation (RNAV) Departure Procedures," FAA Order 8260.44A, 23 Mar. 2000.

[25] "Civil Utilization of Area Navigation (RNAV) Departure Procedures," FAA Order 8260.44A CHG 1, 4 Jun. 2001.

[26] "Special Stand-Alone Area Navigation (RNAV) Transition Procedures," FAA Notice 8000.302, 5 Aug. 2005.

[27] "Special Area Navigation (RNAV) Transition Procedures," FAA Notice 8000.325, 3 Jul. 2006.

[28] "U.S. Terminal and En Route Area Navigation (RNAV) Operations," FAA Advisory Circular 90-100, 7 Jan. 2005.

[29] "Required Navigation Performance (RNP) Airworthiness Approval, Operational Approval, and Design Guidelines for Special Aircraft and Aircrew Authorization Required (SAAAR) Approach Procedures," FAA Notice 8000.300, 5 Jul. 2005.

[30] "Approval Guidance for RNP Procedures with SAAAR," FAA Advisory Circular 90-101, 15 Dec. 2005.

[31] "Approval of U.S. Operators and Aircraft to Operate Under Instrument Flight Rules (IFR) in European Airspace Designated for Basic Area Navigation (B-RNAV) and Precision Area Navigation (P-RNAV)," FAA Advisory Circular 90-96A, 13 Jan. 2005.

[32] Clarke, J.-P. B., Ho, N. T., Ren, L., Brown, J. A., Elmer, K. R., Tong, K.-O., and Wat, J. K., "Continuous Descent Approach: Design and Flight Test for Louisville International Airport," *Journal of Aircraft*, Vol. 41, No. 5, 2004, pp. 1054-1066.

[33] Clarke, J.-P., Bennett, D., Elmer, K., Firth, J., Hilb, R., Ho, N., Johnson, S., Lau, S., Ren, L., Senechal, D., Sizov, N., Slattery, R., Tong, K., Walton, J., Willgruber, A., and Williams, D., "Development, Design, and Flight Test Evaluation of a Continuous Descent Approach Procedure for Nighttime Operation at Louisville International Airport," Report of the PARTNER CDA Development Team, Report No. PARTNER-COE-2006-02, 9 Jan. 2006.

CHAPTER 3

THE MONTE CARLO SIMULATION TOOL

NOMENCLATURE

$\mathrm{B}(\alpha, \beta)$	=	beta function
$\mathrm{E}(\ )$	=	expectation, mean operator
$\hat{\mathrm{E}}(X)$	=	estimation of the mean of random variable X
M	=	random variable of aircraft landing weight
m	=	value of aircraft landing weight
m_{MLW}	=	value of aircraft maximum design landing weight
m_{OEW}	=	value of aircraft spec operating empty weight
$f(x,\alpha,\beta)$	=	probability density function of beta distribution
$\mathrm{STD}(\ )$	=	standard deviation operator
$\hat{\mathrm{STD}}(X)$	=	estimation of the standard deviation of random variable X
$\mathbf{V}$	=	total speed vector
$\mathbf{V}_g$	=	ground speed vector
V_g	=	ground speed
$\mathbf{V}_h$	=	vertical speed vector
V_h	=	vertical speed
$\mathbf{V}_r$	=	true airspeed vector
V_r	=	true airspeed
$\mathbf{W}$	=	horizontal wind vector
W_c	=	the crosswind component
W_h	=	the headwind component
X	=	random variable
x	=	value of random variable X
α	=	the first parameter of beta distribution
$\hat{\alpha}$	=	estimation of the first parameter of beta distribution
β	=	the second parameter of beta distribution
$\hat{\beta}$	=	estimation of the second parameter of beta distribution
γ	=	flight path angle
γ_r	=	flight path angle relative to the air mass
λ_r	=	the angle between the ground speed vector and the wind vector,
μ_r	=	the angle between the projection of true airspeed on the horizontal plane and the ground speed vector

3.1 INTRODUCTION

To study the trajectory variations of aircraft performing noise abatement approach and arrival procedures, and to provide a means to support the application of the procedure design and operational framework introduced in the previous chapter, a fast-time Monte Carlo simulation tool was developed. Because the aircraft system is nonlinear, and because the execution of a procedure is subject to various uncertainties that is varying along altitude, it has been difficult to quantify macro level trajectory variations analytically. This is especially the case for evaluating trajectory variations cumulated through the execution of approach and arrival procedures. Monte Carlo simulation would thus be a proper technique to use. A fast-time aircraft simulator was developed first. External uncertainty factors contributing to trajectory variations could then be fed into the aircraft simulator in a way similar to what would happen to an aircraft in the real world environment. Through a large number of simulation runs – of the procedure under development – with different aircraft types and different operation conditions, a large number of aircraft trajectories could be obtained. With all the elements properly modeled, the simulated aircraft trajectories would reflect variations in trajectories of aircraft performing the same procedure. Simulated aircraft trajectories could then be used in separation analysis to determine the target separation for the selected intermediate metering point.

Depending on the actual procedure design, the propagation of trajectory variation is often a two-stage process. The first stage is the computation of the lateral path and the vertical path of a noise abatement approach or arrival procedure; the second stage is the execution of the procedure. Trajectory variations reflected in the computed vertical flight path could be differences in the computed location of the starting point for each deceleration segment, and differences in the Flight Path Angle (FPA) for each segment. Variations in the computed lateral path would normally be relatively small. Trajectory variations reflected in the execution could be deviations in terms of altitude, speed, and cross track errors, from the flight path computed in the first stage.

Trajectory variations exist between flights in different seasons, flights on different days, or flights during different times of the day. These variations would be reflected by the range of aircraft trajectories spanning the 3D airspace and the range of aircraft states at each point on the flight path, as various external conditions change. Thus, these variations would be very important in analyzing the compatibility of noise abatement approach and arrival procedures with the existing airspace design and other aircraft operations in the same general volume of airspace.

Trajectory variations also exist between consecutive flights on the same procedure. These variations would affect the evolution of the spacing between aircraft. Thus, these variations would be very important in analyzing the separation between aircraft performing noise abatement approach and arrival procedures.

Factors contributing to aircraft trajectory variations were identified as:

- Aircraft type – differences in aircraft dynamics and performance determine; these differences affect both the execution of the procedure and the computation of procedure flight paths if they are performance based,
- Low noise descent path logic – differences in how the descent path is generated for each aircraft due to difference in aircraft equipage; these differences affect the computation of procedure flight paths only, procedure design dependent,
- Pilot technique – differences among pilots and pilot response randomness; these differences affect the execution of the procedure only,

- Aircraft weight – uncertainty due to demand and operational conditions; this uncertainty affects aircraft dynamics and aircraft performance, hence the execution of the procedure, and very likely the computation of procedure flight paths if they are performance based,
- Weather conditions – predominantly winds, both wind variations and forecast uncertainties; these variations and uncertainties affect both the execution of the procedure and the computation of procedure flight paths if they are performance based.

Models of each of the aforementioned factors were developed either as part of the fast-time aircraft simulator, or as individual external modules that will be working with the fast-time aircraft simulator. Elements were carefully integrated together to form a unique Monte Carlo simulation tool.

The remainder of this chapter is organized as follows. A brief introduction to the fast-time aircraft simulator, described in detail in Appendix A, is provided in the next section to lay the groundwork for the discussion that follows. The modeling of pilot response delay, aircraft weight, and winds are described in Section 3.3. Modeling of wind variations, however, is described separately in Chapter 4 because of the complexity of this topic. The process incorporating various components into an integrated Monte Carlo simulation tool is discussed in Section 3.4. A summary of this chapter is given in the last section.

3.2 THE FAST-TIME AIRCRAFT SIMULATOR

The central element of the Monte Carlo simulation tool is the fast-time aircraft simulator. The fast-time aircraft simulator is a batch mode computer program developed based on an early version developed by Ho and Clarke[1] in 2001. It was re-designed for this research as a 4D aircraft trajectory simulator with improved accuracy, expanded functionality, and enhanced capability to simulate different approach and arrival procedures under various conditions[2]. Modeled aircraft types include Airbus A319, Boeing 737-300, 757-200, 767-300, and 747-400. More aircraft types are being added as data become available. A brief description of the aircraft simulator is given in this section to facilitate further discussion. A complete description of this simulator can be found in Appendix A. The block diagram of the aircraft simulator is repeated in Fig. 3-1.

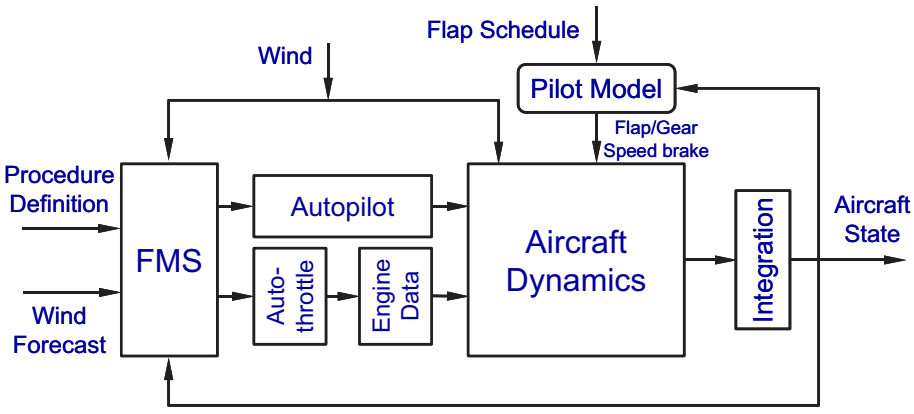

Figure 3-1 Aircraft simulator block diagram.

The aircraft simulator consists of several modular components. The aircraft dynamics module incorporates aerodynamics and kinetics to compute aircraft state derivatives. Attitude control is performed by the autopilot module that is assumed to be able to maintain certain tracking accuracy, thereby eliminating the need for aerodynamic derivatives, rotational moments, and moments of inertial momentum. The engines are controlled by the autothrottle module. Both autopilot and autothrottle were modeled as second order linear controllers. The FMS module builds lateral and vertical flight paths based on entered waypoints and altitude/speed constraints during the preprocessing stage, and provides Lateral Navigation (LNAV) and Vertical Navigation (VNAV) guidance during execution of the procedure. A pilot agent is included to control speedbrakes, flaps/slats and landing gear, and thrust setting and autopilot mode changes when required. The weather module includes the Air Data Computer (ADC) and a user configurable wind and turbulence model. The output of the simulator is a time history of aircraft state variables and system configuration parameters in the format similar to that of the data extracted from a Flight Data Recorder (FDR).

3.2.1 Aircraft Dynamics

The aircraft dynamics module is designed to compute aircraft translational and angular accelerations. By integrating these accelerations, the aircraft state at the next time step can be obtained. The dynamics of the aircraft are determined using a point-mass model based on non-steady-state equations of motion and are thus more accurate in simulating wind effects than a ordinary point-mass model based on steady-state equations of motion, e.g. the early version of the fast-time aircraft simulator.

Lift and drag coefficients were modeled as functions of angle of attack, flap/gear settings, speedbrake position, and Mach number. The instantaneous angle of attack was determined by the aircraft attitude and the wind condition. This gives more accurate results for varying wind conditions, because the contribution of varying wind on angle of attack is directly reflected in lift. A generic side force component (which is normally ignored in steady-state point-mass models) is also included in the aircraft dynamics model to represent the sideslip acceleration behavior of a typical commercial aircraft subject to changing crosswind. Depending on the actual control mode and flight conditions, engine thrust may be at idle, at maximum climb, or somewhere in between as determined by the autothrottle. During the flight, the aircraft weight continuously decreases with time as fuel is consumed. However, because the total fuel flow is relatively small as compared to the total aircraft mass (especially during the descent), at any given time, the aircraft weight is assumed static to simplify computation.

As a simplified model of controls and rotational dynamics, the autopilot module provides aircraft roll rate and pitch rate in the aircraft body frame as outputs. With these two rotational rates, and applying Newton's law for the turning motion, derivatives of the three Euler angles can be obtained.

The low speed drag polars for different flap/gear settings were approximated as parabolic curves for the normal range of lift coefficient. High-speed drag polars for different Mach numbers are given in a look up table. The contribution of speedbrakes was modeled as a drag coefficient increment proportional to the speedbrake position. Installed thrust tables were used to model engine performance. Aircraft performance engineering data provided by aircraft manufacturers were used to build the model of each aircraft.

3.2.2 The Effect of Wind

Wind has a strong impact on aircraft trajectory. It is assumed that the aircraft is flying at True Airspeed (TAS) $\mathbf{V}_r$ and FPA γ, subject to horizontal wind vector $\mathbf{W}$. The angle between the TAS vector and the horizontal plane is γ_r, which represents the flight path angle relative to the air mass. The

geometric relationship between the TAS vector $\mathbf{V}_r$, the vertical speed vector $\mathbf{V}_h$, the ground speed vector $\mathbf{V}_g$, and the total speed vector $\mathbf{V}$, are shown in Fig. 3-2 as collapsed into the vertical plane.

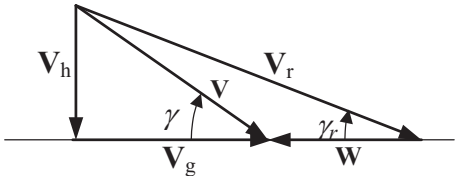

Figure 3-2 Relationship between flight path angle, true airspeed, and ground speed in vertical plane.

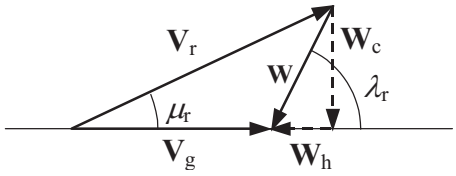

Figure 3-3 Relationship between wind speed, true airspeed and ground speed projected to horizontal plane.

The relationship between speed vectors as projected in the horizontal plane is shown in Fig. 3-3 for the case where λ_r is the angle between the ground speed vector and the wind vector, and μ_r is the angle between the projection of TAS on the horizontal plane and the ground speed vector.

In vector form, the relationship shown in Fig. 3-2 and 3-3 can be expressed as

$$\mathbf{V} = \mathbf{V}_h + \mathbf{V}_g = \mathbf{V}_r + \mathbf{W} \tag{3-1}$$

The value of the ground speed can be obtained as[2]

$$V_g = \sqrt{V_r^2 - V_h^2 - W_c^2} - W_h \tag{3-2}$$

which captures the effect of the headwind component W_h and the crosswind component W_c on ground speed. A positive headwind component causes the ground speed to decrease by the magnitude of the headwind, and a negative headwind component (or tail wind) causes the ground speed to increase by the magnitude of the tail wind. The crosswind component always causes the ground speed to decrease. However, the decrease in ground speed due to the crosswind component is much smaller than that due to the headwind component, if the wind speed is relatively small. As the crosswind component becomes relatively stronger, its relative effect on ground speed also becomes stronger. In the fast-time aircraft simulator, the effects of the headwind and crosswind components were both taken into account.

Because aircraft control and flight procedures are mostly based on Indicated Airspeed (IAS), the effects of wind on aircraft ground speed will result in a change in time-to-fly, e.g. to runway threshold, and a change in the evolution of separation between consecutive aircraft pairs performing the same procedure. Note that Calibrated Airspeed (CAS) is used in this research whenever IAS is required. Uncertainties in wind forecast, and/or change of wind will result in uncertainties in time-to-fly and separation between aircraft.

Wind also affects the FPA. For a flight path segment with a fixed FPA, such as the initial constant CAS segment in a Three Degree Decelerating Approach[3,4] (TDDA) or modified TDDA (MTDDA[5]), the decrease in ground speed due to a headwind or crosswind will result in a shallower flight path angle relative to the air mass. This effect can be seen from Fig. 3-2. This in turn will require higher thrust to maintain the same CAS. The increase in ground speed due to a tailwind will do the reverse, in which case speedbrakes will need to be used. Both thrust change and speedbrake usage have noise implications for the same vertical flight profile. If the engine throttle setting is also fixed, such as in an idle fixed path deceleration segment, a headwind or crosswind will cause the aircraft to decelerate faster, and a tailwind

will cause the aircraft to decelerate slower. This will affect the aircraft's ability to follow a predefined speed profile.

On the other hand, for a flight segment with given flight path angle relative to the air mass, such as a constant CAS idle descent segment, the decrease in ground speed due to a headwind or crosswind will result in a steeper FPA. The increase in ground speed due to a tailwind will result in a shallower FPA. For such a flight segment, the effect of wind is more complicated. Different wind conditions will result in different vertical flight paths. Not only will the altitude profile be different, but for the same CAS profile, the longitudinal acceleration will also be different due to the change in the relationship between TAS and CAS resulting from the change in the vertical profile. A detailed discussion of the effects of wind can be found in Appendix A.

3.2.3 The FMS Model

The FMS module in the aircraft simulator captures the basic RNAV functionalities found onboard modern commercial aircraft. Its function is two-fold. Before the execution of a procedure, the FMS module builds the lateral flight path (LNAV path) based on the location of the given waypoints defining the procedure and the vertical flight path (VNAV path) based on the given altitude/speed constraints at certain waypoints in the similar way an actual FMS does. During the execution of the procedure, the FMS module continuously monitors the states of the aircraft and compares them with the computed LNAV path and VNAV path. It selects the proper modes for, and feeds the altitude, speed, and cross-track error to, the autopilot and autothrottle so that the aircraft can be controlled to follow the computed flight path.

Procedure definition is provided in two separate files. The lateral path definition file contains the list of waypoints defined by their latitude/longitude (or north/east coordinates relative to a reference point) and the lateral tracking modes to be used on each segment. Two lateral modes are modeled: the LNAV Track mode that tracks the cross-track error, and the localizer mode that tracks radial deviation from the extended runway centerline. The lateral turn anticipation is computed from the angle of the turn and projected aircraft speed at the turn.

The vertical path definition file contains the altitude/speed constraints at certain waypoints. Other operational parameters such as the cruise altitude/speed, descent speed, stabilization altitude, and the final approach speed are also contained in the vertical path definition file. The vertical flight path is computed through backward integration of the aircraft dynamics from the lowest altitude/speed constraint to the cruise altitude. The aircraft weight, wind forecast, and flap extension schedule are taken into account in the integration process. The computed VNAV path may include constant Mach idle descent segments, constant CAS idle descent segments, idle deceleration segments, and fixed FPA segments. If proper altitude/speed constraints are given, an idle VNAV path can be built from cruise to final approach fix. However, differences exist in FMS VNAV logic of aircraft from different manufacturers. The final shape of the computed VNAV path is also influenced by aircraft dynamics and performance, FMS descent forecast winds, actual wind at the point where computation is performed (normally at cruise altitude), aircraft weight, temperature, and the nominal flap schedule. A schematic VNAV path and its possible variations are shown in Fig. 3-4.

As shown in the figure, for repeatability and reliability, the constraints at lower altitudes are normally given as "cross at" altitude constraints forcing the FMS to build geometric segments – straight lines in the vertical plane. When there is a difference between the speed constraints at successive waypoints, such as for the segment between the two sets of constraints in the middle, a deceleration is inserted just before the lower waypoint. If the altitude constraint at the higher waypoint of this segment is given as a window

(i.e. at above and/or at below), some FMS may insert a shallow descending deceleration; while yet others may insert a level deceleration. The deceleration point may also be computed differently by different FMS systems. At higher altitudes, to allow for the best performance/economy, altitude constraints are often given as altitude windows (closed or opened). Vertical path, provided it is within the altitude windows, will vary with aircraft types and configurations as shown by the dashed curves in the figure. Some times, due to external conditions, the FMS computed economy path might hit the altitude constraint at the higher end of a segment, resulting in the FMS to re-compute the flight path in a different way. These differences are captured by the FMS module for the aircraft types modeled in the simulator.

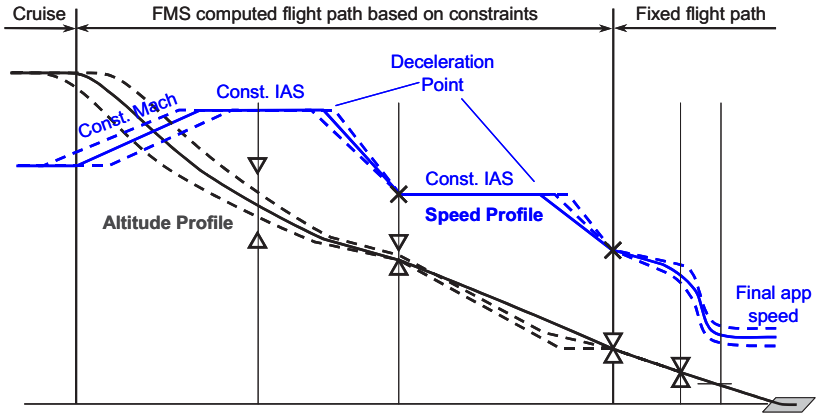

Figure 3-4 FMS VNAV path and its possible variations.

During the execution of the procedure, the FMS compares the aircraft state with the computed flight path, selects proper lateral and vertical modes, and feeds the altitude error, speed error and cross-track error to the autopilot and autothrottle so that they can control the aircraft. All the control modes relevant to performing approach and arrival procedures are modeled. With these modes, the aircraft can be directed to hold a given altitude and speed, to hold a given speed and FPA, or to follow a given vertical flight path defined by altitude, speed, and preferred power setting.

3.2.4 The Pilot Model

Since the fast-time aircraft simulator was designed to run in batch mode, a pilot model (or pilot agent) was also included to perform piloting tasks during the execution of approach and arrival procedures. The pilot model assumes the responsibilities of controlling the extension of flaps/slats, landing gear, and speedbrakes. This is similar to the pilot's responsibility in the real world.

For each procedure to be simulated, a tailored flap schedule is first determined using the information available in aircraft operation manuals[6] that provides speeds at which the flaps/slats and gear should be extended. The speeds are often defined as functions of aircraft weight, and they may be presented as additives to the reference speed. For a specific procedure, the flap/gear schedule may require the extension to a given flap setting be performed at a certain distance (such as at a certain waypoint) from the runway threshold to either assure proper deceleration or to minimize noise. In some procedures, especially when performed by certain aircraft types, flaps/slats or gear be may be required to be extended when the aircraft reaches given altitudes. As such, the flap/gear schedule used by the pilot model could be defined by speeds, distances, or altitudes.

The use of speedbrakes may be necessary when additional drag is needed to keep the aircraft following a given speed profile. This often occurs when the tailwind experienced by the aircraft is

stronger than the wind predicted by the FMS when the VNAV path is computed. Or, it may occur simply because no wind forecast is entered in the descent forecast page, but a tailwind is experienced by the aircraft. The pilot may be required to keep the aircraft within a speed range, such as ±10 kt, from the target speed. This speed range can also be defined in the simulator.

The pilot model performs the controlling task according to the flap/gear schedule and the FMS computed speed profile except that there is a random response delay. Modeling of the pilot response delay is described in the next section.

3.2.5 Simulator Validation

As a tool developed within the time and resource limits of this thesis research, the fast-time aircraft simulator described in this chapter has not yet been validated and certified per industry standards. However, a number of consideration and measures have been taken to make sure the implementation is correct and the simulation is as accurate as possible. These considerations and measures are summarized below:

- The two major assumptions used to simply the design of the fast-time aircraft simulator, the flat earth assumption, and the assumption that the autopilot and autothrottle are able to maintain certain tracking accuracy, were based on careful evaluations. A special coordinate transformation that preserves the distance between consecutive waypoints and the angle of turn at each waypoint was developed to achieve an accurate flat earth approximation. The second assumption is supported by the facts that the autopilot and the autothrottle have been integral parts of advanced commercial jet aircraft, and that advanced navigation technology is available to those aircraft.
- Components of the aircraft simulator were carefully formulated and developed to assure simulation accuracy. These include the use of non-steady state equations of motion, careful formulation of aircraft movement in the wind, and accurate modeling of the FMS logic.
- Aircraft performance engineering data provided by manufactures were used to model each aircraft type.
- The simulator is mainly used to study the macro level relative behavior between simulated trajectories. Should a small bias exist in the simulator, it is not likely to significantly affect the separation analysis results.
- The aircraft simulator has been rigorously tested by simulating different procedure designs at several airports; some of them have complicated airspace restrictions. During this course, various erroneous and unexpected scenarios have been fed to the simulator, intentionally or unintentionally, to verify the simulation design robustness.
- Simulation results have been shown consistent with flight test data and airline pilot training simulation runs. A comparison between flight data and simulated trajectories is given in Subsection A.6.2.

3.3 MODELING EXTERNAL FACTORS CONTRIBUTING TO TRAJECTORY VARIATIONS

Among all the identified factors contributing to aircraft trajectory variations, pilot response delay, aircraft weight, and weather conditions – predominantly wind conditions, are viewed as external to the aircraft model. They are thus modeled as separate elements to the fast-time aircraft simulator.

3.3.1 Pilot Response Delay

Since the pilot assumes the responsibility of controlling the extension of flaps/slats, the landing gear, and speedbrakes, the major contribution of the pilot action to trajectory variation is the deviation from the FMS computed speed profile due to random pilot response. Pilot response delay is the time between a action cue, e.g. a specified speed to extend flaps/slats or the gear being reached, and the time when the flap or gear handle is moved to the next position by the pilot. For each flap setting, there is also a transition time between the time when the flap handle is moved and the time when flaps/slats are extended to the intended position. For a given aircraft type, the flap transition time for each flap setting is a deterministic value, under normal operation conditions. The landing gear has a similar transition time. These transition times were modeled as part of the aircraft dynamics. On the other hand, pilot response delay is a random variable.

The pilot response delay model used in this study was developed by Ho and Clarke through a human-in-the-loop B747-400 cab simulation study[1]. Sixteen active airline pilots were recruited to fly the aircraft simulator in that study. The distribution of the pilot response delay times is reproduced in Fig. 3-5. In the experiment when response times were measured, the flap extension cues were given by the non-flying pilot. The upper chart shows the frequency distribution, and the lower chart shows the cumulative distribution function (cdf). The pilot response time had a mean of 2.8318 seconds, and a standard deviation of 2.2483 seconds. The thick curves in Fig. 3-5 show the fitted normal distribution model of the pilot response time.

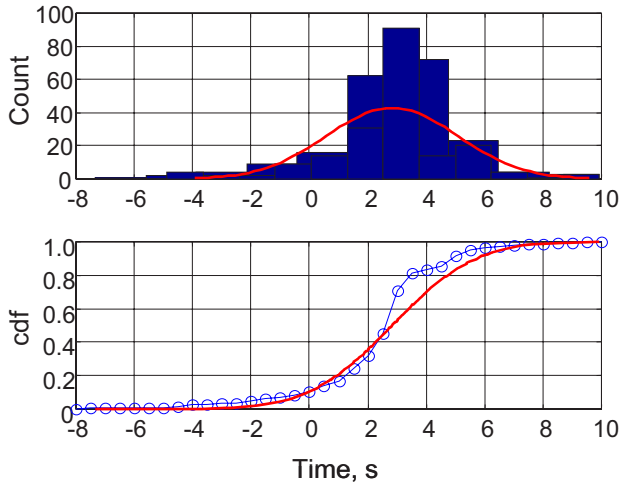

Figure 3-5 Pilot response delay.

Similar to the flap extension under most operational conditions, the extension of speedbrakes is also based on the speed information presented to the pilot. The same pilot response delay model is applied to the control of speedbrakes.

It is seen from Fig. 3-5 that while in most cases pilots started to extend flaps with a positive response delay, some times the pilot extended flaps early. Great flexibility exists in real world operations in terms of flap and gear extension. In current terminal operation environment, because of the uncertainties as to the vectoring, much larger variations exist in pilot response time. However, it is expected that the variation in pilot response time will be reduced and get closer to the aforementioned model as pilots get more and more familiar with noise abatement procedure operations.

3.3.2 Aircraft Weight

The aircraft weight is a very important factor in aircraft performance. Although aircraft weight changes continuously during the flight, because of fuel consumption, the biggest impact of aircraft weight during the arrival and approach phases comes from the large variations in aircraft landing weight from flight to flight within the same aircraft type. Aircraft lift coefficient under any nominal operational condition is directly related to aircraft weight. Thus, variation in aircraft weight will affect the lift/drag ratio under any given nominal operational conditions. In most cases, aircraft flap extension speeds are also determined by the aircraft weight. As a result, the FMS computed VNAV path would be different for different landing weights. The difference would mostly be the in the location of deceleration point, and in the flight path angle of a non-geometric segment. The dynamics of the aircraft will also be different for different weight.

Variations in the landing weight of a given aircraft type are mostly due to uncertainties in local market demand (payload) and operating conditions (fuel consumption). Historical data can be used to model these aircraft weight variations. Table 3-1 shows UPS Boeing 757-200 and Boeing 767-300 package cargo aircraft design weight parameters and statistics of the corresponding aircraft landing weight data collected between April 20 and May 18, 2004 at KSDF. Those statistics were obtained from data of 163 B757-200 and 139 B767-300 arrivals. The probability mass functions based on the aforementioned landing weight data for the two aircraft types are shown as bar charts in Fig. 3-6 and 3-7 respectively.

Table 3-1 Landing weight parameters of UPS cargo aircraft[a], 1000 lb.

	Aircraft Type	
Parameters	B757-200	B767-300
Spec Operating Empty	114.000	188.000
Maximum Design Landing	210.000	326.000
Minimum	146.617	229.271
Maximum	194.534	298.183
Mean	167.539	262.205
Standard Deviation	11.000	18.000

[a] Statistics based on data of 163 B757-200 and 139 B767-300 arrivals to KSDF between 20-Apr-2004 and 18-May-2004.

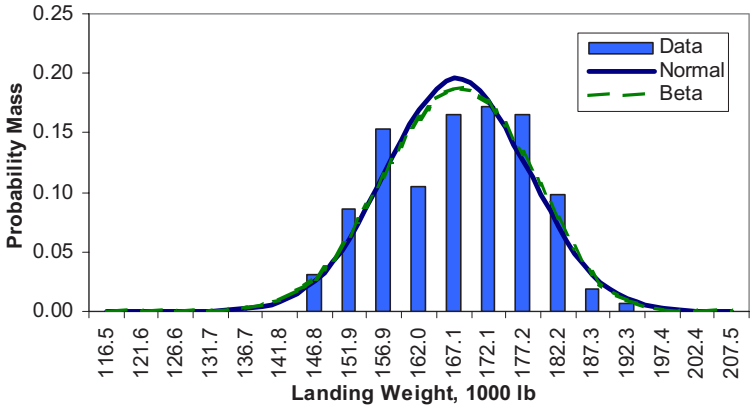

Figure 3-6 UPS B757-200 landing weight distribution.

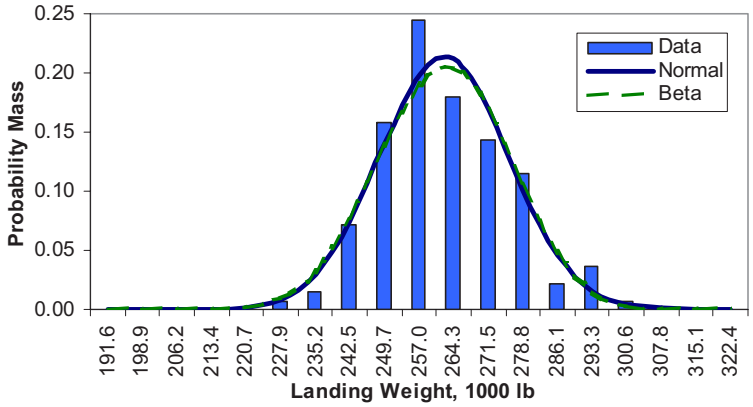

Figure 3-7 UPS B767-300 landing weight distribution.

In each of the figures, the left boundary of the horizontal axis gives the spec operating empty weight of the corresponding aircraft. The right boundary of the horizontal axis gives the maximum design landing weight of the corresponding aircraft. By definition, landing weights are always within the range defined by those two limits for the specific aircraft type. As it can be seen, the landing weights resembled the normal distribution. Thus, a simple model of aircraft landing weight would be a normally distributed random variable for each aircraft type. The random variable should be bounded by the corresponding aircraft's historical minimum landing weight and maximum landing weight to avoid nonrealistic values. Model parameters such as the mean, standard deviation, minimum, and maximum can be estimated using sample statistics. Normal distribution landing weight models based on the sample mean and standard deviation values listed in Table 3-1 are shown in Fig. 3-6 and 3-7 as solid black curves. It is seen that the normal distribution models captured the historical data well. The dashed curves in Fig. 3-6 and 3-7 are beta distribution models, which will be discussed later.

Landing weights of passenger aircraft were also examined. For the purpose of comparison, Delta Air Lines Boeing 757-200 and Boeing 767-300 passenger aircraft landing weights collected between August 1 and August 30, 2005 at Hartsfield-Jackson Atlanta International Airport (KATL) were used. The design weight parameters and statistics of landing weights for these two passenger aircraft are listed in Table 3-2. The corresponding probability mass functions are shown in Fig. 3-8 and 3-9 respectively. Again, in each of the figures, the left boundary of the horizontal axis gives the spec operating empty weight of the corresponding aircraft type. The right boundary of the horizontal axis gives the maximum design landing weight of the corresponding aircraft type.

Table 3-2 Landing weight parameters of Delta passenger aircraft[a], 1000 lb.

	Aircraft Type	
Parameters	B757-200	B767-300
Spec Operating Empty	130.860	186.380
Maximum Design Landing	198.000	300.000
Minimum	140.620	202.500
Maximum	197.872	294.977
Mean	180.258	266.422
Standard Deviation	10.041	16.318

[a] Statistics based on data of 2759 B757-200 and 1184 B767-300 arrivals to KATL between 1-Jul-2005 and 31-Jul-2005.

It is seen that for the same aircraft type, the difference between the spec operating empty weight and the maximum design landing weight is smaller for the passenger version than the cargo version. The historical landing weight data also indicate that the passenger versions had slightly higher mean but lightly lower standard deviation than the cargo versions. However, the most striking difference between the passenger versions and the cargo versions is in the probability mass functions as shown by the figures. The probability mass functions of the passenger aircraft are heavily skewed to the right-hand side. Similar to the treatment of the cargo aircraft, a normal distribution model was built from the sample mean and sample standard deviation for each of the two passenger aircraft types. These normal distribution models are shown as solid black curves in Fig. 3-8 and 3-9. It is seen that the normal distribution models did not capture the data well for the passenger aircraft. To be bounded by the corresponding aircraft's historical minimum landing weight and maximum landing weight to avoid nonrealistic values, a big chuck of the right hand tail of the normal distribution has to be cut off. This will further decrease the modeling accuracy.

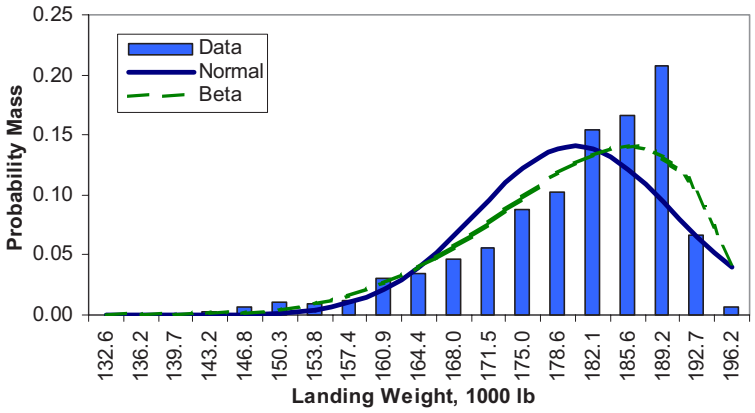

Figure 3-8 Delta B757-200 landing weight distribution.

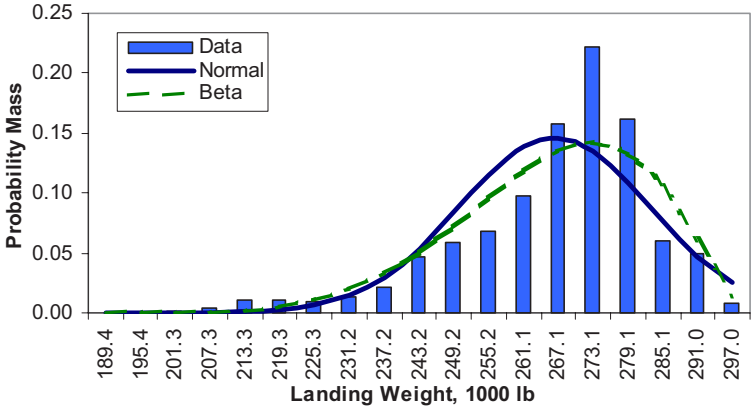

Figure 3-9 Delta B767-300 landing weight distribution.

A commonly used distribution to model variables that are lower and upper bounded is the beta distribution[7]. The probability density function (pdf) of beta distribution is defined on the interval [0, 1]

$$f(x,\alpha,\beta) = \frac{1}{\mathrm{B}(\alpha,\beta)} x^{\alpha-1}(1-x)^{\beta-1} \tag{3-3}$$

where α and β are parameters that must be positive and $\mathrm{B}(\alpha, \beta)$ is the beta function

$$\mathrm{B}(\alpha,\beta) = \int_0^1 u^{\alpha-1}(1-u)^{\beta-1} du \tag{3-4}$$

The mean and standard deviation of the beta random variable X with parameters α and β are

$$\mathrm{E}(X) = \frac{\alpha}{\alpha+\beta} \tag{3-5}$$

$$\mathrm{STD}(X) = \frac{1}{\alpha+\beta}\left(\frac{\alpha\beta}{\alpha+\beta+1}\right)^{1/2} \tag{3-6}$$

If the estimated mean $\hat{\mathrm{E}}(X)$ and the estimated standard deviation $\hat{\mathrm{STD}}(X)$ are known, the two parameters of the beta distribution can be estimated

$$\hat{\alpha} = \hat{\mathrm{E}}(X)\left(\frac{\hat{\mathrm{E}}(X)\left(1-\hat{\mathrm{E}}(X)\right)}{\hat{\mathrm{STD}}^2(X)} - 1\right) \tag{3-7}$$

$$\hat{\beta} = \left(1-\hat{\mathrm{E}}(X)\right)\left(\frac{\hat{\mathrm{E}}(X)\left(1-\hat{\mathrm{E}}(X)\right)}{\hat{\mathrm{STD}}^2(X)} - 1\right) \tag{3-8}$$

For an aircraft with spec operating empty weight m_{OEW} and maximum design landing weight m_{MLW}, the normalized aircraft landing weight x for a given landing weight m can be defined as

$$x = \frac{m - m_{OEW}}{m_{MLW} - m_{OEW}} \tag{3-9}$$

The estimated mean $\hat{\mathrm{E}}(X)$ and the estimated standard deviation $\hat{\mathrm{STD}}(X)$ of the normalized aircraft landing weight can then be computed from the estimated mean $\hat{\mathrm{E}}(M)$ and the estimated standard deviation $\hat{\mathrm{STD}}(M)$ of the aircraft landing weight as

$$\hat{\mathrm{E}}(X) = \frac{\hat{\mathrm{E}}(M) - m_{OEW}}{m_{MLW} - m_{OEW}} \tag{3-10}$$

$$\hat{\mathrm{STD}}(X) = \frac{\hat{\mathrm{STD}}(M)}{m_{MLW} - m_{OEW}} \tag{3-11}$$

With the normalized estimates from Eq. (3-10) and Eq. (3-11), using Eq. (3-7) and Eq. (3-8), estimates of parameters α and β of the beta distribution model can be obtained. The parameters of the beta

distribution models for each of the four aircraft types examined thus far are listed in Table 3-3. The modeled beta distributions are shown as dashed curves in Fig. 3-6, Fig. 3-7, Fig. 3-8, and 3-9 respectively.

Table 3-3 Parameters of beta distribution landing weight models.

Aircraft Type	$\hat{\alpha}$	$\hat{\beta}$
UPS B757-200	11.5102	9.1285
Delta B757-200	5.6602	2.0330
UPS B767-300	13.3679	11.4924
Delta B767-300	6.4060	2.6874

It is seen that the beta distribution models were very close to the normal distribution models for the two UPS cargo aircraft types. The beta distribution models were much better than the normal distributions for the two Delta passenger aircraft types. Moreover, a beta distribution is bounded by the lower and upper boundaries (spec operating empty weight and maximum landing weight in this case) – one does not have to worry about nonrealistic values generated during the simulation. Thus, the beta distribution models are a better choice in modeling aircraft landing weight distributions. However, the simulation of a beta distribution model is more difficult than a normal distribution model. For aircraft landing weight distribution similar to that of the UPS B757-200 and B767-300 aircraft, normal distribution models would be comparably good but very easy to implement in the simulation.

3.3.3 Wind Variations

Wind conditions can be modeled using both long-term statistical expectations (such as mean wind and 2-σ wind) to reflect the magnitude of the wind that an aircraft would expect to experience during its descent to the runway, and short-term variations to reflect wind changes between consecutive flights arriving on the same lateral path. The long-term statistical models represent nominal wind conditions under which the analysis is done. The short-term variations between consecutive flights represent uncertainties in the wind.

Archived Aircraft Communications Addressing and Reporting System (ACARS) automated weather reports from commercial aircraft were used to develop the wind models. A mode decomposition and autoregressive technique was developed to model wind variations between flights. In this technique, wind variations were calculated between consecutive descending ACARS profiles that were separated by less than 15 min upon arrival at the destination airport. Wind variations were modeled using the east wind and north wind components. The two components – east wind and north wind variation components – were viewed as two independent stochastic processes. To cope with the non-stationary behavior of wind variation along altitude, an unique mode decomposition approach was used to separate each of the east and north wind variation components into a zero-mean higher frequency signal, a zero-mean lower frequency signal and a static (DC) signal. Each decomposed signal was then treated as a stationary stochastic process.

For simplicity, and to make maximum use of the large ACARS data set, the wind variation signals were approximated as autoregressive (AR) signals. AR models for the higher frequency components and lower frequency components were obtained from the averages of covariances of the respective decomposed signals. Second order AR models were used in simulating the wind variations. To avoid the high frequency artifacts of the AR model for the lower frequency signals, the outputs of the lower frequency AR models were fed through a low pass filter to obtain smooth simulated signals similar to the

original decomposed lower frequency signals. Outputs from the higher frequency AR models were used directly. The DC signals were simply simulated as random variables. Simulated components were then combined to give simulated wind variations.

The final step was to incorporate simulated wind variations with a nominal wind profile to obtain the actual wind profile for each simulation run. A complete description of the modeling technique for wind variation between flights is given in Chapter 4.

3.3.4 Other Factors Contributing to Aircraft Trajectory Variations

Aside from the factors introduced in the previous subsections, temperature, performance difference between each individual aircraft in the same type fleet, uncertainties in the position of aircraft Center of Gravity (CG), procedure design, the use of FMS descent forecast, and the timing of computing FMS VNAV path also contribute to aircraft trajectory variations.

Temperature significantly affects engine thrust, especially thrust at higher throttle settings. Generally, higher temperature means lower thrust for the same throttle setting. Compared with other weather conditions such as winds, short-term variations in temperature is relatively small. The effects of temperature on aircraft trajectories are more evident when a long time span (such as over a month, a season, or even a year) is considered. For the analysis of separation between consecutive aircraft pairs, temperature is a less important factor. Thus, in this research, the international standard atmosphere is used.

In addition to significant performance differences between different aircraft types (including different engine variants), performance differences exist between individual aircraft in the same type fleet. The differences between individual aircraft in the same type fleet include differences in both aerodynamics and engine performances. These differences are due to differences in wearing, weathering, and adjusting. These performance differences affect the execution of a procedure. Normally, if the FMS computed profile is used, the computed profile will not be affected by these performance variations of each individual aircraft because the FMS uses a pre-loaded aircraft performance model. However, a specific aircraft type may have a production life of two to three decades. Significant improvements may have been made to the aircraft type over the years. Newly manufactured aircraft may have improved engines and improved avionics systems (including FMS). If the differences are large, the older and the newer aircraft of the same type may be modeled as different aircraft types. In the current implementation of the aircraft simulator, average aerodynamic and engine performance data are used for each modeled aircraft type. Performance differences between individual aircraft of the same type fleet may be modeled in the future as an enhancement.

The position of the aircraft CG affects aircraft trimming; hence, it also affects aircraft drag polars. For simplicity, in the current fast time aircraft simulator, only one predetermined fixed CG position is implemented. This is reasonable because during normal operations, aircraft CG are carefully adjusted to be as close to the ideal position as possible through arranging payloads. The aircraft simulator can also be improved through using multiple sets of drag polars to allow variations in aircraft CG position.

Some procedure designs will have larger aircraft trajectory variations than others. For example, procedures allowing optimal vertical profile for each aircraft will minimize noise impact and save more fuel, but they are likely to have larger aircraft trajectory variations than procedures that have fixed altitude and speed constraints all the way down to the final approach. The latter probably will have slightly higher noise impact and save less fuel. Because aircraft trajectories can be simulated for each procedure design separately, the effects of procedure design on trajectory variations are well accommodated by the simulation tool.

As discussed in Subsection 3.2.3, FMS descent forecast winds influence the FMS computed VNAV paths. In addition to this effect, large errors in descent forecast, or not entering any descent forecast results in large discrepancies between the FMS computed VNAV flight path and actual operating conditions. These large discrepancies would increase the flight path tracking error and demand more pilot efforts for managing the speed profile. The results are larger trajectory variations. Thus to reduce trajectory variations, the FMS descent forecast needs to be entered and it should be as accurate as possible. Since FMS descent forecast functionality is implemented in the FMS model, the effect of descent forecast can be simulated.

Similar to the effects of FMS descent forecast winds, the earlier the FMS VNAV path is computed, the larger the discrepancies between the FMS computed VNAV flight path and actual operating conditions would be. Hence, the timing of FMS VNAV path computation will also affect trajectory variations. One way to cope with this is to force the FMS to re-compute the VNAV path right before the intermediate metering point rather than totally rely on the VNAV path computed before top of descent, which is normally more than one hundred nautical miles away from the runway. To force the FMS to re-compute the VNAV path, the pilot can re-enter the altitude/speed constraints at any of the down stream waypoints.

3.4 THE INTEGRATED MONTE CARLO SIMULATION TOOL

The random pilot response model, the random aircraft weight model, and the stochastic wind variation model are incorporated with the fast-time aircraft simulator to form a Monte Carlo simulation tool. Arrival procedures can be executed hundreds of times with different aircraft types and configurations under different wind conditions. Separation and throughput analysis can then be applied on simulated trajectories[8]. The Monte Carlo engine and the separation analysis methodology to be presented are collectively referred to as the Tool for the Analysis of Separation And Throughput (TASAT) as illustrated in Fig. 3-10.

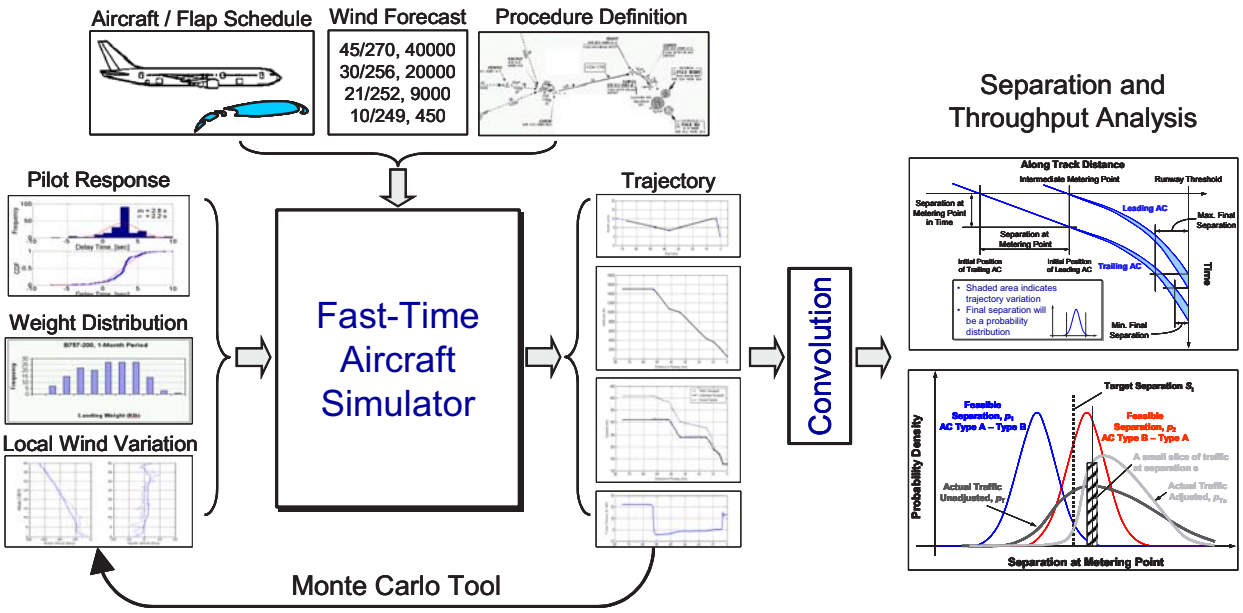

Figure 3-10 Tool for the Analysis of Separation And Throughput (TASAT).

During each simulation run, for a given aircraft type, a unique aircraft landing weight will be generated by the random landing weight model. The wind profile will also be different for each simulation run. Pilot response time will be randomly generated for each control action. Procedure definition, FMS descent forecast winds (zero if not provided), and aircraft flap/gear schedule (as given to the pilots for real world operations) are provided to the simulator as deterministic inputs. It is assumed that there are no direct interactions between consecutive flights performing the same procedure. Thus, when multiple aircraft types are involved in performing a procedure, each aircraft can be simulated separately.

The application of the wind model needs special attention. To make best use of the inter-flight wind variation model, flights are identified as leading flights and trailing flights. For a given nominal wind condition, this can be done as following. For each aircraft type, an ensemble of flights can be simulated with the fixed nominal wind condition while retaining variations in other factors such as the pilot response and the aircraft weight. Another ensemble of flights can be simulated with nominal wind condition plus a stochastic inter-flight wind variation profile in addition to other random factors. A simulated trajectory from the leading ensemble and a simulated trajectory from the trailing ensemble can be selected to form a random flight pair. By enumerating flights from each ensemble, a large number of flight pairs can be constructed. Separation analysis (discussed in a separate chapter later) can then be applied on those flight pairs accordingly.

3.5 SUMMARY

A Monte Carlo simulation tool built around a fast-time aircraft simulator was developed to simulate variations in flight trajectories for noise abatement approach and arrival procedures. The fast-time aircraft simulator was developed with a careful trade-off between simplicity, fast execution, accuracy, and the capability to simulate 3D aircraft trajectories. Focus is given to macro level aircraft trajectories rather than micro dynamic behavior. Because wind is the most important single factor affecting aircraft trajectory variations, non-steady state equations of motion were used in the aircraft dynamics model. This would allow aircraft behavior under various wind conditions to be accurately simulated. Major aircraft navigation and control systems such as the FMS and the autopilot models were included in the simulator. A pilot model was also included in the simulator to control the extension of flaps, landing gear, and speedbrakes during simulation runs. A previously developed probability distribution pilot response delay model, a newly developed probability distribution aircraft landing weight model, and a newly developed stochastic process wind variation model were incorporated with the fast-time aircraft simulator to form the Monte Carlo simulation tool. The tool enables approach and arrival procedures to be simulated hundreds of times for each aircraft type under various external conditions with a short amount of time and at very low cost. The large pool of aircraft trajectories obtained through these simulation runs can then be used to analyze variations in aircraft trajectories for the specific procedure design and operating environment.

Future enhancements of the Monte Carlo simulation tool could include incorporating performance variations due to differences in wearing, weathering, and adjusting between individual aircraft units within the same aircraft type. A probability distribution model of aircraft CG position could also be developed. The model of aircraft drag polars in the fast-time aircraft simulator could be revised to enable the effect of aircraft CG position being accurately simulated. Limitations to these future enhancements mostly rely on data available to support the modeling efforts.

REFERENCES

[1] Ho, N. T. and Clarke, J.-P. B., "Mitigating Operational Aircraft Noise Impact by Leveraging on Automation Capability," AIAA-2001-5239, *1st AIAA Aircraft Technology, Implementation, and Operations Forum*, AIAA, Los Angeles, California, 2001.

[2] Ren, L., Ho, N. T., and Clarke, J.-P. B., "Workstation Based Fast-Time Aircraft Simulator for Noise Abatement Approach Procedure Study," AIAA-2004-6503, *AIAA 4th Aviation Technology, Integration and Operations (ATIO) Forum*, Chicago, Illinois, 20-22 Sep. 2004.

[3] Clarke, J.-P. B., "A System Analysis Methodology for Developing Single Events Noise Abatement Procedures," Sc.D. Thesis, Department of Aeronautics and Astronautics, Massachusetts Institute of Technology, Cambridge, MA, 1997.

[4] Clarke, J.-P. B., "Systems Analysis of Noise Abatement Procedures Enabled by Advanced Flight Guidance Technology," AIAA 97-0490, *Journal of Aircraft*, Vol. 37, No.2, Mar.-Apr. 2000, pp.266-273.

[5] Ren, L., Clarke, J.-P. B., and Ho, N. T., "Achieving Low Approach Noise without Sacrificing Capacity," *Proceedings: the 22nd Digital Avionics Systems Conference (22nd DASC)*, Indianapolis, Indiana, 12-16 Oct. 2003, pp. 1.E.3-1.1-9 vol.1

[6] *UPS B757/767 Aircraft Operating Manual*, Document: UPS33075, UPS Flight Publications, Louisville, Kentucky, 2003.

[7] Evans, M., Hastings, N., and Peacock, B. *Statistical Distributions*, 3rd ed., John Willey & Sons, Inc., New York, 2000, pp. 34-42.

[8] Ren, L., and Clarke, J.-P. B., "Development and Application of Separation Analysis Methodology for Noise Abatement Approach Procedures," *AIAA-2005-7397, AIAA 5th Aviation Technology, Integration and Operations (ATIO) Forum*, Arlington, Virginia, 26-28 Sep. 2005.

CHAPTER 4

MODELING AND SIMULATING WIND VARIATIONS BETWEEN FLIGHTS

NOMENCLATURE

a_i	=	the coefficients of an AR model
$\hat{a}_i$	=	estimated coefficients of an AR model
$\hat{a}_{Ei}$	=	estimated coefficients of the AR model of east wind variation
$\hat{a}^H_{Ei}$	=	estimated coefficients of the AR model of higher frequency signal of east wind variation
$\hat{a}^H_{Ni}$	=	estimated coefficients of the AR model of higher frequency signal of north wind variation
$\hat{a}^L_{Ei}$	=	estimated coefficients of the AR model of lower frequency signal of east wind variation
$\hat{a}^L_{Ni}$	=	estimated coefficients of the AR model of lower frequency signal of north wind variation
$\hat{a}_{Ni}$	=	estimated coefficients of the AR model of north wind variation
b_i	=	the coefficients of an FIR filter
$\mathrm{E}(\ )$	=	expectation, mean operator
$H(z)$	=	filter
h_n	=	ACARS wind profile re-sampling altitude
n	=	discrete sequence index
$\hat{K}(\theta)$	=	estimated power spectra density function
N	=	number of measurements in a finite sequence
m	=	discrete sequence index
p	=	the order of an AR model
q	=	the order of an FIR filter
$w^{DC}_{j,E}$	=	DC signal of east wind variation observed by flight j
$w^{DC}_{j,N}$	=	DC signal of north wind variation observed by flight j
$w^f_{j,E}(h_n)$	=	filtered east wind variation observed by flight j at altitude h_n
$w^f_{j,N}(h_n)$	=	filtered north wind variation observed by flight j at altitude h_n
$w^H_E[n]$	=	simulated higher frequency signal of east wind variation
$w^H_{j,E}(h_n)$	=	higher frequency signal of east wind variation observed by flight j at altitude h_n
$w^H_{j,N}(h_n)$	=	higher frequency signal of north wind variation observed by flight j at altitude h_n
$w^H_N[n]$	=	simulated higher frequency signal of north wind variation
$\mathbf{W}_j(h_n)$	=	re-sampled wind profile from flight j at altitude h_n
$W_{j,D}(h_n)$	=	wind direction of re-sampled wind profile from flight j at altitude h_n
$W_{j,E}(h_n)$	=	east wind component of re-sampled wind profile from flight j at altitude h_n
$W_{j,N}(h_n)$	=	north wind component of re-sampled wind profile from flight j at altitude h_n
$W_{j,V}(h_n)$	=	wind speed of re-sampled wind profile from flight j at altitude h_n

$w_E^L[n]$ = simulated lower frequency signal of east wind variation
$w_{j,E}^L(h_n)$ = lower frequency signal of east wind variation observed by flight j at altitude h_n
$w_{j,N}^L(h_n)$ = lower frequency signal of north wind variation observed by flight j at altitude h_n
$w_N^L[n]$ = simulated lower frequency signal of north wind variation
$x[n]$ = generic sequence
$\Delta W_E[n]$ = simulated east wind variation component
$\Delta W_{j,D}(h_n)$ = wind variation in direction observed by flight j at altitude h_n
$\Delta W_{j,E}(h_n)$ = east wind variation component observed by flight j at altitude h_n
$\Delta W_{j,N}(h_n)$ = north wind variation component observed by flight j at altitude h_n
$\Delta W_{j,V}(h_n)$ = wind variation in speed observed by flight j at altitude h_n
$\Delta W_N[n]$ = simulated north wind variation component
γ_ν = innovation variance
$\hat{\gamma}_\nu$ = estimated innovation variance
$\kappa_x[m]$ = covariance sequence of generic sequence x
$\hat{\kappa}_x[m]$ = covariance sequence of generic sequence x
$\nu[n]$ = white sequence
$\nu_E[n]$ = white noise sequence for simulating the east wind variation
$\nu_E^H[n]$ = white noise sequence for simulating the higher frequency signal of east wind variation
$\nu_N^H[n]$ = white noise sequence for simulating the higher frequency signal of north wind variation
$\nu_E^L[n]$ = white noise sequence for simulating the lower frequency signal of east wind variation
$\nu_N^L[n]$ = white noise sequence for simulating the lower frequency signal of north wind variation
$\nu_N[n]$ = white noise sequence for simulating the north wind variation

4.1 INTRODUCTION

Wind is arguably the most significant single factor that influences aircraft trajectory. Separation analysis requires an accurate model of wind variations in speed and direction between consecutive flights conducting the same approach or arrival procedure. Such a model requires large amount of data. One source of this data is the Aircraft Communications Addressing and Reporting System (ACARS) automated weather reports. ACARS is an air-ground communication system managed by Aeronautical Radio Inc. (ARINC). Airlines use this system to transmit digital messages between the aircraft and ground. Weather reports are automatically transmitted by the aircraft to ground at certain intervals[1]. Using ACARS metrological reports, it is possible to create a large set of inter-flight wind variation profiles from which the model is derived. The wind variation model may then be used in the Monte Carlo simulation tool described in the previous chapter to simulate aircraft trajectory variations with high accuracy.

A modeling approach was developed to model wind variations between consecutive flights. In this modeling approach, wind variation profiles are viewed as stochastic processes along the altitude. Because these processes deems non-stationary, a unique mode decomposition approach is used to separate each wind variation component profile – the east wind or the north wind profile – into a zero mean higher frequency signal, a zero mean lower frequency signal, and a static (DC) signal. Each separated signal is then viewed as a stationary process. The decomposed wind variation signals are then approximated as autoregressive (AR) signals. The final AR model for each decomposed signal is built based on the average of estimated covariances of data samples of the corresponding component signal.

As mentioned in the previous chapter, the winds experienced by a pair of consecutive flights are assumed the sum of a nominal wind profile that is common to both the leading and trailing flights, and a wind variation profile that is only applied to the trailing flight. This is a simplified scenario in that the nominal wind profile and the wind variation profile can be modeled separately. The selection of the nominal wind profile is site dependent. The nominal wind profile could be either selected to signify the most common wind conditions or any wind conditions with a special concern at the airport.

The rest of this chapter is organized as follows. Details of the ACARS wind data, as compared with other data sources available in the US, are explained in Section 4.2. The modeling approach is introduced in the section to lay the ground for more detailed discussions that follow. The process for the mode-decomposition of raw ACARS wind variation profiles, and the process for modeling the decomposed signals as autoregressive signals are discussed in Sections 4.3 and 4.4 respectively. Finally, the process whereby the wind variation model is used in simulating trajectories of aircraft performing noise abatement approach and arrival procedures is explained in Section 4.5. Examples are also presented to demonstrate the accuracy and the effectiveness of the modeling technique. The summary of this chapter is provided in the last section.

4.2 DATA SOURCE AND MODELING APPROACH

Details of the data used in the numerical examples are presented below, along with a discussion of the modeling approach that is used in the context of aircraft trajectory simulation for separation analysis. This is to lay the ground for more detailed discussions of modeling and simulating wind variations in the subsequent sections.

4.2.1 Data Source

In recent years, National Oceanic and Atmospheric Administration's (NOAA's) Global Systems Division (GSD; previously Forecast Systems Laboratory, or FSL) of the Earth System Research Laboratory (ESRL) has made available ACARS metrological reports for research use[2]. These reports include wind data measured by airborne sensors sampled at intervals on the order of tens of seconds to minutes. Wind data are reported in the form of wind speed and direction, along with the time, altitude, and latitude and longitude at which the measurement was observed by the sensors on board the aircraft. A sample ACARS flight track is shown in Fig. 4-1. This aircraft landed at Louisville International Airport (KSDF) at approximately 1:09AM on 25 September 2004. This flight is referred to as the "sample flight" throughout this chapter. Note that the airport elevation at KSDF is 501 ft. The wind data

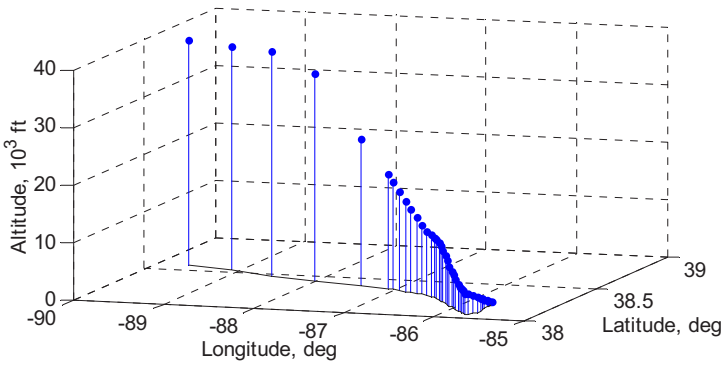

Figure 4-1 ACARS flight track of the sample flight.

from the sample flight, as a function of altitude, are shown in Fig. 4-2. NOAA GSD has made available current near real time ACARS wind data covering the entire US airspace and many other airports around the world. These ACARS data are provided to NOAA GSD by participating airlines including major airlines in the US and some international airlines. Historical data back to 1 July 2001 are also available to the research community. Since the ACARS wind data were measured by airborne sensors, they represent what was experienced by aircraft in the past. Thus, they provide a good basis for modeling winds, at sites where sufficient data are available.

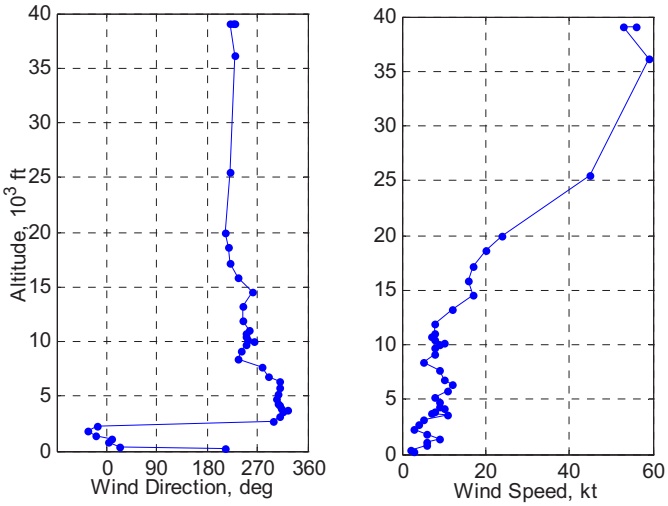

Figure 4-2 ACARS wind profile from the sample flight.

As with any source of meteorological data, these data are not perfect. The resolution of the data points is not very high. As shown in Fig. 4-2, at high altitudes, the vertical interval between data points could be as high as ten thousand feet. There are also sensor noise and measurement errors. Nevertheless, compare with other data sources, such as the Doppler radar (which relies on reflections from particles floating in the air to detect wind speed) and the Wind Profiler[3] (limited availability) etc, ACARS data are still considered to be one of the best data sources. NOAA GSD provides each data point with an error tag and other properties, thus for modeling purpose, erroneous data points identified by GSD can be eliminated from data samples.

ACARS data are provided in Network Common Data Form (netCDF) format, which is a compact binary data format used to present scientific data[4]. Data points are identified by GSD encrypted tail numbers. Thus, data points with the same encrypted tail number could be extracted to form a flight track. A set of software tools has been developed to decode, filter, and extract data from the NOAA ACARS data set. Individual flight tracks can then be used for further processing. Figure 4-1 was generated from such a flight track.

Data filtering criteria can be tailored to serve different applications at different airports. Of course, because airlines participate in the NOAA ACARS data program at voluntary bases, the availability of data varies airport by airport. Especially, international airports have much less coverage due to weaker international participation.

4.2.2 Modeling Approach

For a wind model to be effective in modeling aircraft trajectory uncertainties, two important elements must be modeled. The first element is the nominal wind field; the second element is the variation in the wind field between flights.

A complete model of the wind field could be represented by 3-D grid points spanning the airspace. Aircraft destined to the same airport via the same arrival would normally follow a similar vertical profile. Thus, for aircraft trajectory planning and separation analysis, the 3-D wind field is often simplified as a sequence of points along altitude. This is normally referred to as a wind profile. Traditionally, wind profiles are given in wind direction and wind speed as functions of altitude such as the one shown in Fig. 4-2. Mean wind and 2σ (mean plus two standard deviations) wind have been used to represent wind strength and direction at a given point.

The wind profiles in Fig. 4-3 are based on NOAA ACARS flight tracks from aircraft destined to KSDF from the west. Three wind profiles are shown: mean wind, 2σ wind, and maximum observed wind. To obtain the wind profiles, ACARS wind data from each flight track were interpolated at every thousand feet. Statistics were then obtained at each of the altitudes. Mean wind speed and 2σ wind were calculated directly from wind speed regardless of the wind direction at each data point. Mean wind direction was calculated using the unit vector method where the wind direction at each data point was represented by an unit vector. Mean direction was determined by the direction of the mean unit vector of all data points. Another method to calculate mean wind direction is to use wind direction at each data point weighted by the wind speed at that data point. The later method would have a better representation of the direction at higher winds.

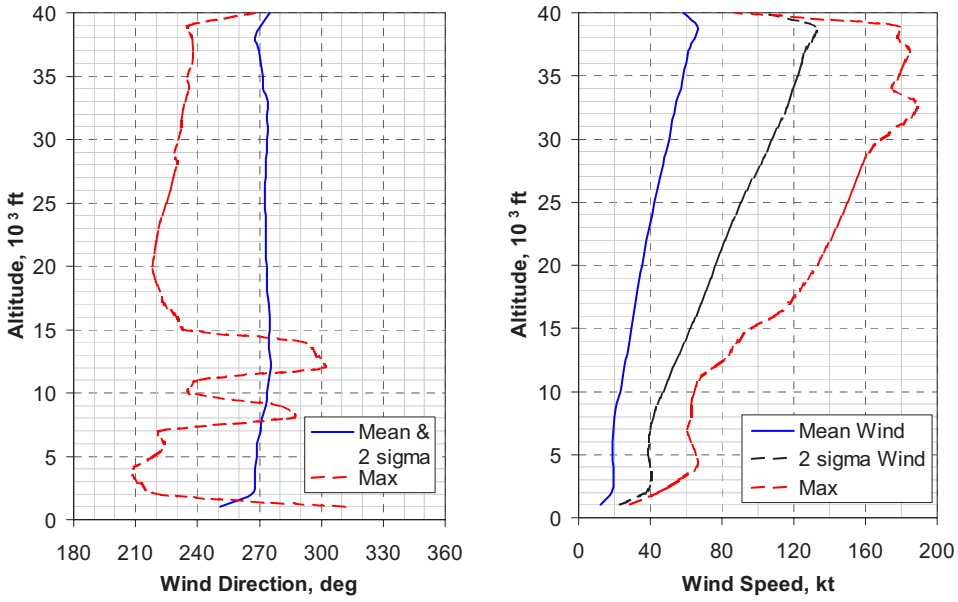

Figure 4-3 KSDF wind profiles based on ACARS flight tracks from the west.

If an airport experiences strong wind from different directions during different periods of the day, or in different seasons of the year, special wind profiles representing these conditions should be obtained in addition to the mean wind and 2σ wind profiles. For example, an airport may frequently experience northwest only winds during the winter, but southeast only winds during the summer. In this case, it makes sense to model the seasonal winds separately.

Wind variations between flights are of great concern because these variations would affect the interactions between trajectories of consecutive flights. In this research, wind variations are defined as changes in wind direction or speed (or east wind and north wind components) at same altitudes during the time between the passages of consecutive flights through the same altitude. As such, the winds experienced by a pair of consecutive flights are assumed to share a common wind profile, and a wind variation profile that is only experienced by the trailing flight. The common (or nominal) wind profile is modeled as one of the wind profiles mentioned in the previous paragraphs. The inter-flight wind variation profile is modeled separately. While the nominal wind profile is deterministic for any given conditions, the wind variation profile would be a stochastic process possessing the same stochastic characteristics as historic data.

A two-step process was employed to model the wind variation. The first step was to decompose each of wind variation profile component into a zero mean higher frequency signal, a zero mean lower frequency signal, and a DC signal. The next step was to model the decomposed wind components as AR signals. The final AR model for each component was built on the average of estimated covariances of data samples of the corresponding component. Details of this modeling approach are described in the next two sections.

Once both the nominal wind profile model and wind variation model are developed, they can be combined to simulate realistic wind fields. To simulate a consecutive pair of aircraft, the wind profile for the leading aircraft can be a pre-selected nominal wind profile; the wind profile for the trailing aircraft can be the nominal wind profile plus simulated wind variation profile.

4.2.3 Data for the Numeric Examples

To use the wind variation model in a Continuous Descent Arrival (CDA) flight test project at KSDF[5], the modeling effort used wind data reported by arrival aircraft flying into KSDF from the west. ACARS reports within a time widow of 5 hours starting 10:00 PM to 3:00 AM local standard time were used. Ideally, as much data as available (at least one year worth) should be used for a reliable wind model. Due to database access issues, only six-month worth of data were used to develop the model. The data covered 10 February 2004 through 12 August 2004. For the selected time window at KSDF, on each weekday, 10 to 17 flight tracks were extracted. Most of them were UPS flights clustered in groups. Data from these flight tracks match the need of the CDA project at KSDF perfectly. These data are used as the numeric examples throughout this chapter.

4.3 MODE DECOMPOSITION OF THE WIND VARIATION SIGNAL

The first step of the mode decomposition and AR approach is presented in this section. The method for extracting the wind variation profiles from ACARS flight tracks is described first. Criteria used to pair flight tracks and select usable data range are discussed. It follows the description of the mode decomposition method that separates wind variation profile components into categorized frequency signals.

4.3.1 Extracting Wind Variation Profiles

As shown in Fig. 4-2, the raw ACARS reports are not evenly distributed along altitude. Altitudes of data points vary from flight to flight. To simplify the processing, wind data from each flight track are re-sampled at 250 ft altitude intervals using linear interpolation. This altitude interval was selected to match

the sampling rate of the most detailed wind profiles from the raw ACARS data. Because the new wind samples have regular intervals along altitude, wind variations can be easily obtained by a direct comparison of data points from consecutive flight pairs at the same altitude. The re-sampled wind profile is denoted as $\mathbf{W}_j(h_n)$, where subscript j identifies each individual flight, and h_n denotes the re-sampling altitudes.

Flights are first sorted by arrival time at the destination airport. Wind variation is then calculated between consecutive flight pairs that are separated by less than 15 minutes. Wind variation, in terms of wind speed and direction, as experienced by each trailing flight j at each altitude could be obtained as:

$$\begin{cases} \Delta W_{j,V}(h_n) = W_{j,V}(h_n) - W_{j-1,V}(h_n) \\ \Delta W_{j,D}(h_n) = W_{j,D}(h_n) - W_{j-1,D}(h_n) \end{cases} \tag{4-1}$$

In Eq. (4-1), subscripts V and D denote wind speed and direction respectively. Subscript *j-1* identifies the leading flight in front of flight *j*. Wind direction change, computed by the second equation, has values within the range of (-180, 180] deg. Wind variation, in terms of east wind and north wind components, could be obtained as

$$\begin{cases} \Delta W_{j,E}(h_n) = W_{j,E}(h_n) - W_{j-1,E}(h_n) \\ \Delta W_{j,N}(h_n) = W_{j,N}(h_n) - W_{j-1,N}(h_n) \end{cases} \tag{4-2}$$

In Eq. (4-2), subscripts E and N denote east and north wind components respectively. The wind variation profile for the sample flight is shown in Fig. 4-4 in terms of wind direction and wind speed in a) on the left, and in east and north wind components in b) on the right.

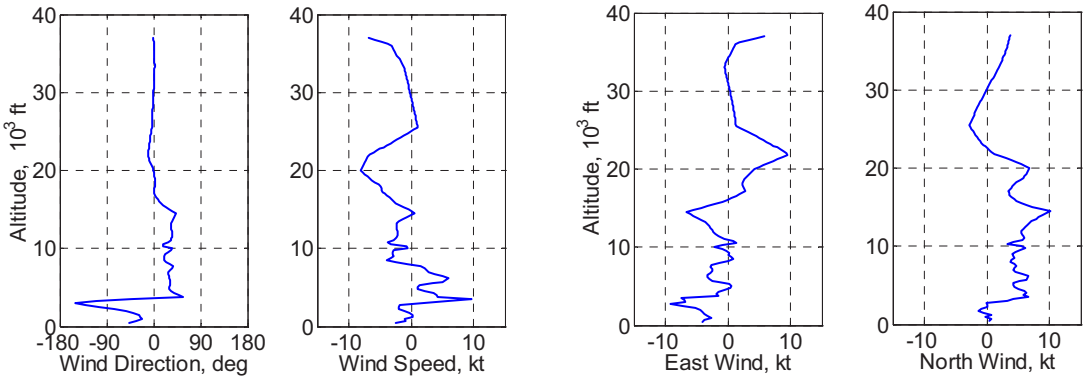

a) Direction and speed b) East and north components

Figure 4-4 Wind variations observed by the sample flight, ACARS data.

A maximum time interval of 15 minutes was used to maximize data usage. This is because within the terminal area, flights that are separated by more than 15 minutes in arrival time would not likely be a factor to each other. To verify the suitability of using 15 minutes as the maximum time interval between consecutive flights, statistics were obtained for east and north components of wind variation at each altitude. The mean and the standard deviation of these components of the wind variation are shown in Fig. 4-5 versus time interval at 11,000 ft. The statistics were based on 1048 consecutive flight pairs that were separated by less than 15 minutes in arrival time. Mean and standard deviation for data point in Fig. 4-5 was computed from wind variations of 10% of all the consecutive flight pairs centered at that point.

Thus, Fig. 4-5 can be viewed as a moving statistics chart. It can be seen that the standard deviation of wind variation components stayed roughly the same as the time interval increases. This observation is consistent through all altitudes.

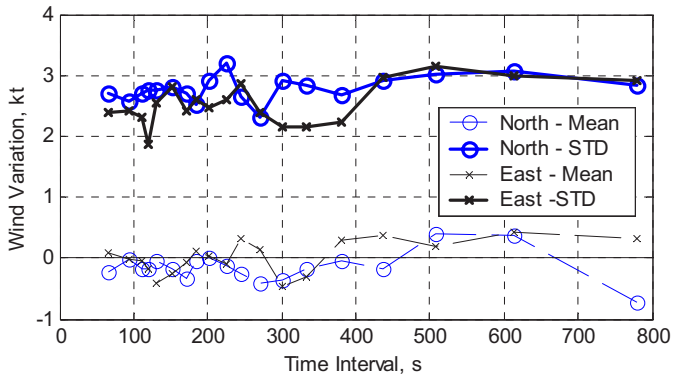

Figure 4-5 Wind variation versus time interval, 11,000 ft.

The mean and the standard deviation of the east and north components of the wind variation are shown in Fig. 4-6 versus wind speed at 11,000 ft. The mean and the standard deviation for each wind speed was computed in the same way as that in Fig. 4-5. The standard deviation of wind variation components stayed roughly the same as wind speed increases; except when wind speed is above 35 kt (roughly above mean wind plus σ), when a slight increasing trend in standard deviation is observed. This tendency is slight more obvious at altitudes below 10,000 ft, and is hardly identifiable above 12,000 ft.

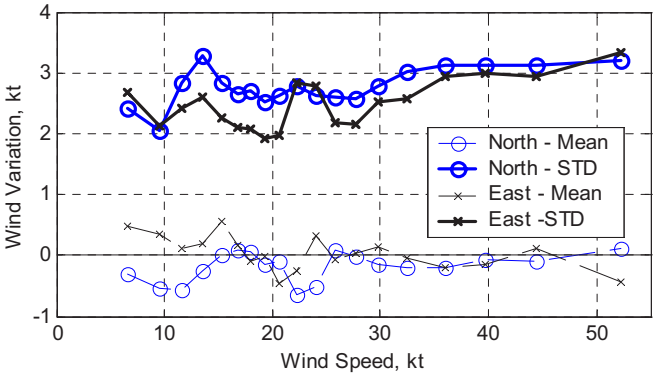

Figure 4-6 Wind variation versus wind speed, 11,000 ft.

Because separation is only a concern for aircraft on the same procedure that are between 1 to 3 minutes apart, wind variation can be modeled as being independent of the time interval between flights. As an approximation, wind variation could also be modeled as being independent of wind speed.

Wind variation could be modeled either by variation in wind direction and speed, or by variation in east and north components. As shown in Fig. 4-4a, there are distinctive differences between the variation in wind direction and the variation in wind speed. Actually, very large wind direction variation often occurs when wind speed is relatively small. On the other hand, east and north wind components could be viewed as two equally positioned contribution factors to the total wind variation.

Sample correlation coefficient between east and north wind components was obtained at each altitude. As shown in Fig. 4-7, the correlation between east and north was very weak. An examination of the actual distribution of the east and north components at each altitude indicated that the east and north

components could be assumed to be two independent processes. Thus, wind variation was modeled in east and north components.

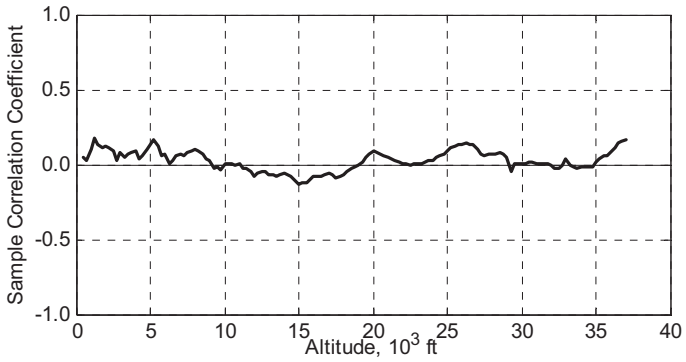

Figure 4-7 Sample crosscorrelation coefficient between east and north wind variations versus altitude.

As shown in Fig. 4-4b that, given altitude as the independent variable, the east and north wind variation components were not stationary, although their variation in magnitude and frequency was much less than that of the wind direction change. This is a natural observation since differences in air movement exist in different atmosphere layers. As mentioned earlier, raw ACARS data have a much lower sampling rate at high altitude. The frequency differences at different altitudes as reflected by ACARS data may well contain artifacts due to the difference in sampling rate. Thus, it is worth a closer look before further analysis. The wind profile extracted from Flight Data Record (FDR) data of the sample flight is shown in Fig. 4-8. By comparing Fig. 4-8 and Fig. 4-2, it is seen that the ACARS data captured the overall wind profile relatively well.

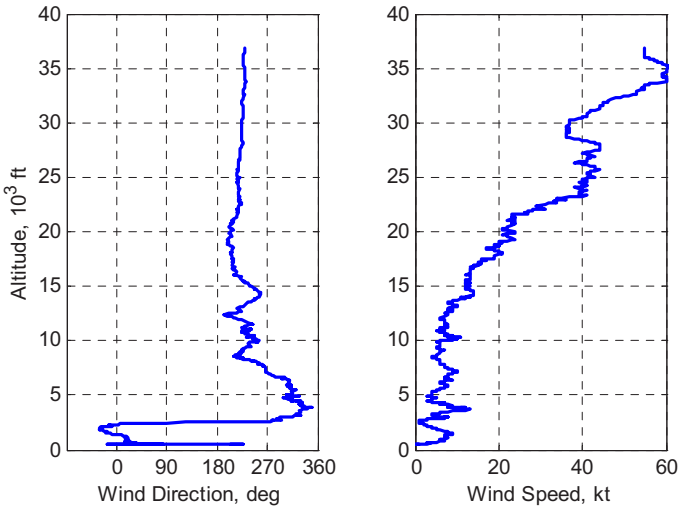

Figure 4-8 FDR wind profile from the sample flight.

Using FDR data from the sample flight and that of the aircraft immediately in front of it, a wind variation profile was derived. The wind variation profile is shown in Fig. 4-9. Comparing Fig. 4-9 with Fig. 4-4b, it is seen that due to the overall lower sampling rate, use of ACARS data resulted in a smoother wind variation profile. Additionally, high frequency contents were cut off in the ACARS data. This should not pose a problem as high frequency contents reflect turbulence and measurement noise. The

turbulence would mostly affect the micro-level aircraft dynamics. With proper guidance and control, the macro-level aircraft trajectory will not likely be significantly affected by those high frequency wind contents. Below 20,000 ft, wind variations reflected by FDR data was also captured by the ACARS data relatively well. Interestingly, at about 3,000 ft, there was a relatively large wind shift in the FDR data; this was also captured by the ACARS data. This relatively large wind shift at lower altitude is a common phenomenon at KSDF, and it is more visible in same data samples than in others. This phenomenon has been identified by both pilots and air traffic controllers in real world operations. However, as expected, due to the very low sampling rate at high altitude, ACARS data did not capture the wind variation well at high altitude. This is especially true above 20,000 ft, at least for the data sample shown in Fig. 4-4b. It is obvious that FDR data would be a good source for modeling the wind and wind variations. However, due to organizational constraints, FDR data could not be easily obtained in large volume and for a great number of days.

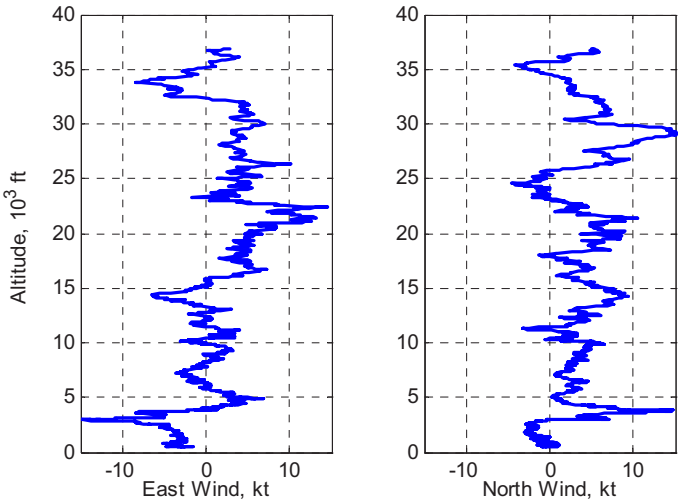

Figure 4-9 Wind variation observed by the sample flight, FDR data.

4.3.2 Mode Decomposition

To model wind variations using ACARS data, two issues must be resolved. As mentioned earlier, wind variations along altitude are non-stationary random processes. The second issue is the low sampling rate at high altitude. Thus, even using nonlinear methods, a very accurate model would not be obtained if the methods were applied to ACARS data directly. One way to cope with these two issues could be to use both FDR data and ACARS data in the modeling effort. Non-stationary analysis method, such as the Hilbert-Huang Transform[6], could be applied to the FDR to obtain the energy-frequency-altitude distribution of wind variations. Classic statistics method could be applied to the large ACARS data set to obtain statistic characteristics of the wind variation along altitude. Analysis results using the FDR data set and the ACARS data set could be combined to build a wind variation model in the form of digital shaping filter, which could then be implemented to simulate wind variation profiles from a white noise sequence. The parameters of the shaping filter could be functions of altitude. One of the problems with this approach is that, although the ACARS data set may be large enough to fully represent the actual wind variations, the FDR data is still limited and it may not be large enough to fully represent the energy-

frequency-altitude distribution of wind variations over a wide variety of wind conditions. On the other hand, the frequency distribution information contained in the large ACARS data set is not utilized.

For simplicity and to make maximum use of the large ACARS data set, the wind variation profile was approximated as AR signals[7]. An AR model has been previously used in the Dryden wind turbulence model[8] in which the longitudinal wind turbulence component was approximated as a first order AR signal. To avoid the problem raised by the low sampling rate of ACARS data at high altitude, only wind data between 3,000 ft and 20,000 ft were used. To cope with the problem of the wind variation being a non-stationary process, a mode decomposition approach was used to separate each of the two components – the east and north wind variation components – of the wind variation profiles into a zero mean higher frequency signal, a zero mean lower frequency signal, and a DC signal. By doing this, each separated signal within the aforementioned altitude range was treated as a stationary process. It is worth to point out that the upper bound of usable data was selected based on ACARS data sampling rate, so it could be viewed as site independent. The lower bound of the usable data however was selected based on observations. It thus should be viewed as site dependent.

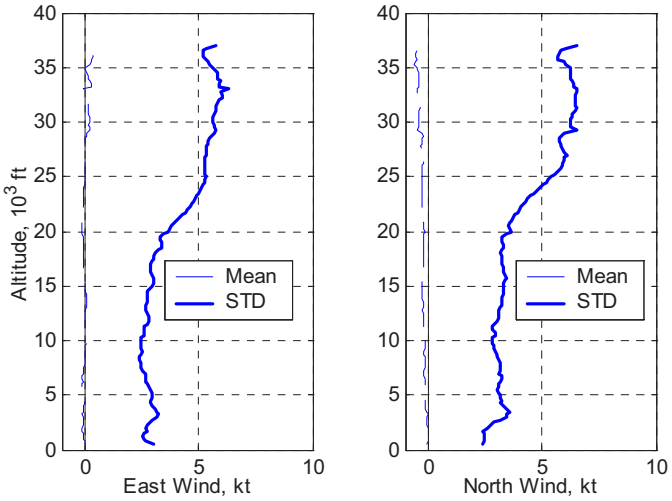

Figure 4-10 Sample mean and standard deviation of wind variations versus altitude.

AR models could be built based on the characteristics of the higher frequency signal and lower frequency signal. Then the AR models could be tuned to fit the wind variation characteristics below 3,000 ft and above 20,000 ft to cover the whole range of altitude if such fidelity is required. The mean and standard deviation of the east and north wind components at each altitude are shown in Fig. 4-10. The corresponding data points were obtained from the entire ensemble of wind variation profiles. The mean values shown in Fig. 4-10 are ensemble means. The standard deviation values are derived using the autocorrelation functions at zero altitude difference. It is seen that the sample ensemble mean values were essentially zero. Within the range of 3,000 ft to 20,000 ft, the standard deviation values remained roughly the same. Above 20,000 ft, the standard deviation values tended to increase with altitude. Assuming the only information lost due to the lower sampling rate at high altitude is frequency information, the tendency of standard deviation to increase with altitude could be viewed as reflecting the true characteristics of wind variation at high altitude. It is also seen that below 3,000 ft, the standard deviation tended to decrease with altitude. Data shown in Fig. 4-10 could be used to tune the wind variation intensity of the AR models.

However, for the purpose of aircraft trajectory simulation within the terminal area, accuracy below 20,000 ft is more important. Based on an inspection of the data set, it was assumed that by simply extending the model below 3,000 ft, the wind variation would be slightly over estimated. Because aircraft would normally be established on the Instrument Landing System (ILS) localizer and the ILS glide slope, it's believed that extending such developed wind variation model down below 3,000 ft without further adjustment would still produce reasonable results.

The mode decomposition was done as following. The east and north components of wind variation profiles were first passed through a Finite Impulse Response (FIR) low pass filter to obtain two corresponding smooth curves. The smooth curves were then subtracted from their corresponding raw wind variation components to obtain the higher frequency signals of the wind variation. The DC signals were simply the mean of the smooth curves given by the FIR filter. The lower frequency signals were obtained by subtracting the DC signals from their corresponding smooth curves. The separated signals of the east and north wind variation components observed by the sample flight are shown in Fig. 4-11. Notice that for demonstration purposes, the mode decomposition shown in Fig. 4-11 was done for the full altitude range. The actual wind variation model was built based on data within the altitude range of 3,000 ft to 20,000 ft. A mathematical description of this process is presented below.

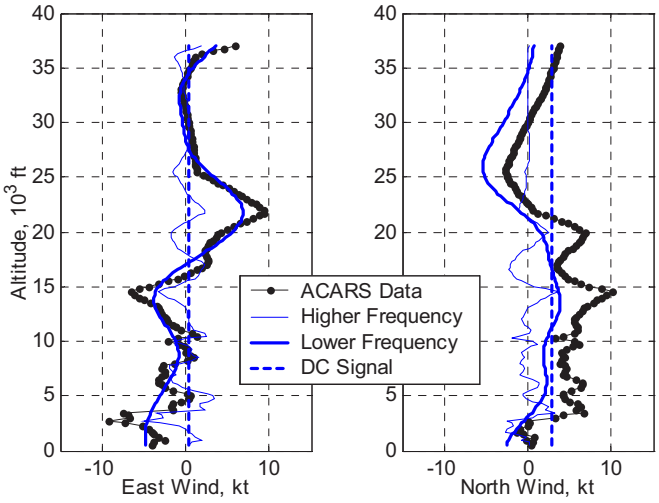

Figure 4-11 Mode decomposition of wind variation observed by the sample flight.

The transfer function of a qth order FIR filter can be expressed as[9]

$$H(z) = b_0 + b_1 z^{-1} + b_2 z^{-2} + \ldots + b_q z^{-q} \tag{4-3}$$

In the numerical example, the FIR filter was designed with an order of 100 and a digital cut off frequency of 0.06 (0.03 times sampling rate). Because data were re-sampled at every 250 ft, the cut off frequency was actually 0.03/250, 1/ft. This is equivalent to 1 cycle for every 8,333 ft. The order and cut off frequency of the FIR filter were manually selected after running a large number of wind variation profiles. It was selected such that the filtered smooth curves would capture the general trend of wind variation along altitude. The N+1 coefficients, $\{b_i$, for $i = 0, 1, \ldots, q\}$, were determined using the window method. Details of the window method are out of the scope of this document. The readers are referred to

Chapter 9 of reference 9. To avoid aliasing toward the start and end altitudes, padding was applied to both ends of the wind variation profiles. Before the start altitude, q points with the corresponding values at the start altitude were added to the east and north wind variation components respectively. After the end altitude, q points with the corresponding values at the end altitude were added to the east and north wind variation components respectively. The padded east and north wind variation components were passed through the FIR filter. The filtered data sequences were then aligned with the east and north wind variation components and truncated to yield the smooth curves $w^f_{j,E}(h_n)$ for the east wind variation component and $w^f_{j,N}(h_n)$ for the north wind component. The higher frequency signals of the wind variation could be obtained as

$$\begin{cases} w^H_{j,E}(h_n) = \Delta W_{j,E}(h_n) - w^f_{j,E}(h_n) \\ w^H_{j,N}(h_n) = \Delta W_{j,N}(h_n) - w^f_{j,N}(h_n) \end{cases} \tag{4-4}$$

The DC signals of the wind variation could be obtained as

$$\begin{cases} w^{DC}_{j,E} = E\left(w^f_{j,E}(h_n)\right) \\ w^{DC}_{j,N} = E\left(w^f_{j,N}(h_n)\right) \end{cases} \tag{4-5}$$

Notice that the mean in Eq. (4-5) should be computed across altitude, thus the re-sampling altitudes were dropped on the left hand side of the two equations. Finally, the lower frequency signals of the wind variation could be obtained as

$$\begin{cases} w^L_{j,E}(h_n) = w^f_{j,E}(h_n) - w^{DC}_{j,E} \\ w^L_{j,N}(h_n) = w^f_{j,N}(h_n) - w^{DC}_{j,N} \end{cases} \tag{4-6}$$

The wind variation component in each direction can be reconstructed by adding the DC signal, the lower frequency signal, and the higher frequency signal together. The decomposed wind variation signals can be interpreted as the wind variations at different geographical scales. The DC signals reflect the overall wind variation between flights, i.e. wind variation spanning the entire arrival phase. The lower frequency signals reflect wind variations at a scale of tens of nautical miles. The higher frequency signals reflect wind variations from 500 ft (corresponding to the Nyquist rate for re-sampling interval of 250 ft) up to about 26 nm (corresponding to the cut off frequency of the FIR filter, estimated based on a flight path angle of -3 deg).

4.4 THE AUTOREGRESSIVE WIND VARIATION MODEL

The second step of the mode decomposition and AR modeling approach is presented in this section. A brief description of the AR model is given first. The estimation of autocovariance sequences of wind variation signals is presented next. The estimated autocovariance sequences are the bases for determining the AR model parameters. Finally, analyses of estimated power spectral density are presented to demonstrate the effectiveness of the mode decomposition method.

4.4.1 Formulation of Autoregressive Model

An AR model has a general form of

$$x[n] = -a_1 x[n-1] - a_2 x[n-2] - \cdots - a_p x[n-p] + \nu[n] \tag{4-7}$$

where $\nu[n]$ is a white sequence that is uncorrelated with past values of $x[n]$, that is,

$$\mathrm{E}\big(\nu[n]x[n-m]\big) = 0, \quad \text{for all } n \text{ and all } m \ > 0. \tag{4-8}$$

and

$$\mathrm{E}\big(\nu[n]x[n]\big) = E\big(\nu[n]^2\big) = \gamma_\nu \tag{4-9}$$

Parameter γ_ν is called the innovation variance. Thus for a pth order AR model, there are p+1 parameters, $\{\gamma_\nu, a_1, \ldots, a_p\}$. These parameters can be obtained from the autocovariance sequence $\kappa_x[m]$ using Yule-Walker equations[9]

$$\begin{bmatrix} \kappa_x[0] & \kappa_x[1] & \cdots & \kappa_x[p-1] \\ \kappa_x[1] & \kappa_x[0] & \cdots & \kappa_x[p-2] \\ \vdots & \vdots & \cdots & \vdots \\ \kappa_x[p-1] & \kappa_x[p-2] & \cdots & \kappa_x[0] \end{bmatrix} \begin{bmatrix} a_1 \\ a_2 \\ \vdots \\ a_p \end{bmatrix} = -\begin{bmatrix} \kappa_x[1] \\ \kappa_x[2] \\ \vdots \\ \kappa_x[p] \end{bmatrix} \tag{4-10}$$

$$\gamma_\nu = \kappa_x[0] + a_1\kappa_x[1] + \cdots + a_p\kappa_x[p] \tag{4-11}$$

Because the autocovariance sequence $\kappa_x[m]$ of the signal to be modeled $x[n]$ is not known, an estimation must be made to obtain the AR model.

4.4.2 The Estimation of Covariance Sequences of Wind Variation Signals

For the set of measurements $\{x[n], 0 \le n \le N\text{-}1\}$ of a zero mean signal, the estimated autocovariance sequence can be computed using the formula[9],

$$\hat{\kappa}_x[m] \equiv \frac{1}{N} \sum_{i=0}^{N-1-m} x[i]x[i+m], \quad 0 \le m \le p \tag{4-12}$$

In the equation above, the hat denotes that the autocovariance sequence was estimated from measurements. The same naming convention will be used for all estimated values. For the numerical example, autocovariance sequences were computed based on data points between 3,000 ft and 20,000 ft. The estimated autocovariance sequences of the raw ACARS east and north wind variation components observed by the sample flight are shown in Fig. 4-12. The estimated autocovariance sequences of the raw wind variation components are noisy, and large differences exist between the autocovariances of the each and north wind variation components.

Figure 4-13 and Fig. 4-14 show estimated autocovariances of the higher and lower frequency signals respectively. By comparison, it is seen that the higher frequency signals reflected the shorter-term autocorrelation, the lower frequency signals reflected the longer-term autocorrelation. It is also seen that

in the decomposed higher frequency and lower frequency signals, the two directional components demonstrated similar behavior. This is not clearly seen in the autocovariances of the raw wind variation components shown in Fig. 4-12.

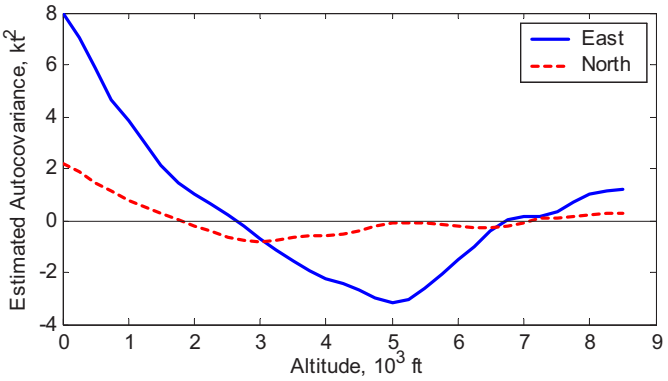

Figure 4-12 Estimated autocovariances of raw wind variation components observed by the sample flight.

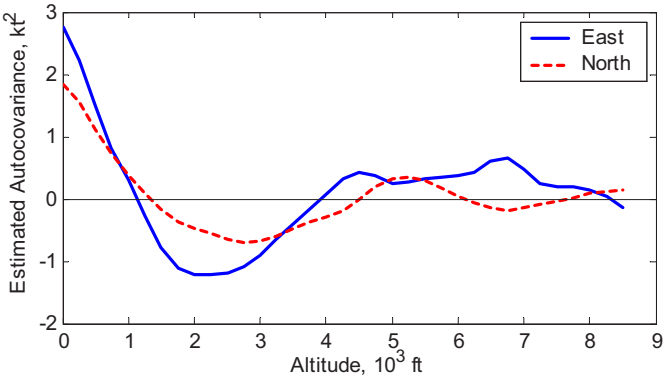

Figure 4-13 Estimated autocovariances of higher frequency signals from wind variations observed by the sample flight.

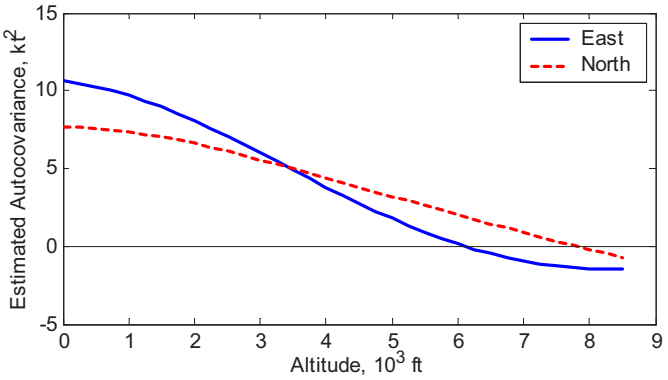

Figure 4-14 Estimated autocovariances of lower frequency signals from wind variations observed by the sample flight.

Estimated autocovariances of the raw wind variation components, the higher frequency signals, and the lower frequency signals, are shown in Fig. 4-15, 4-16, and 4-17 as averages over 1029 flights from the period of ACARS data that were available. The autocovariances were not only much smoother; the east and north autocovariances were closer to each other too.

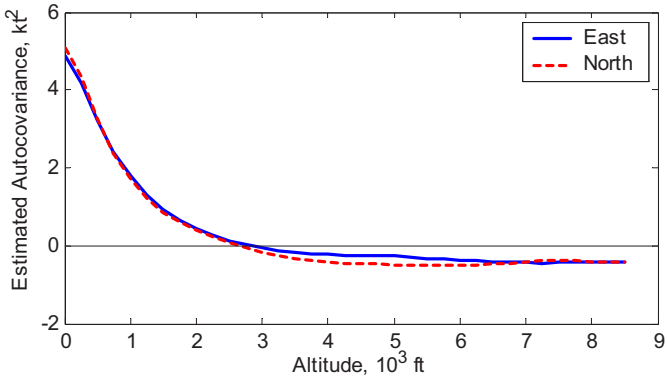

Figure 4-15 Estimated autocovariances of raw wind variation components averaged over 1029 flights.

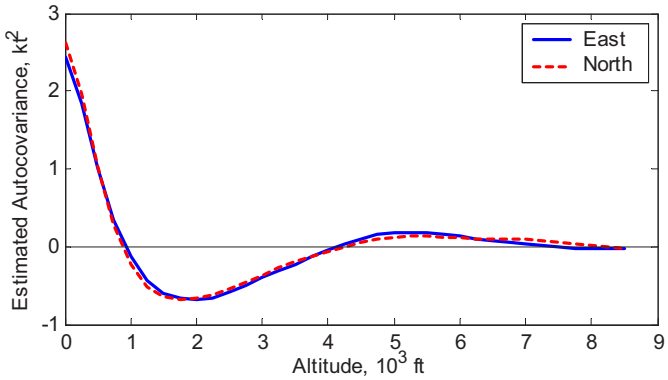

Figure 4-16 Estimated autocovariances of higher frequency signals averaged over 1029 flights.

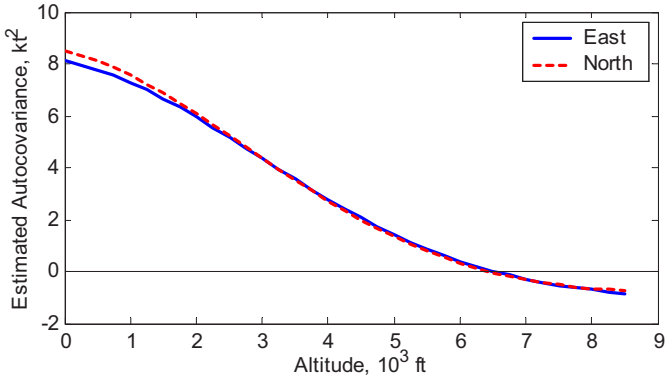

Figure 4-17 Estimated autocovariances of lower frequency signals averaged over 1029 flights.

The effectiveness of mode decomposition is clearly illustrated in Fig. 4-15, 4-16, and 4-17. The raw wind variation components were decomposed into higher frequency signals that have weaker autocorrelation, and lower frequency signals that have stronger autocorrelation. With the autocovariance sequences estimated, the AR model parameters can be solved.

4.4.3 Solving Autoregressive Model Parameters

AR models could be developed using either averaged autocovariance sequences of the raw wind variation components, or that of the higher frequency signals and lower frequency signals. Referring to Eq. (4-7), the pth order AR models of the raw east and north wind variation components ΔW_E and ΔW_N can be written as,

$$\begin{cases} \Delta W_E[n] = -\hat{a}_{E1}\Delta W_E[n-1] - \hat{a}_{E2}\Delta W_E[n-2] - \cdots - \hat{a}_{Ep}\Delta W_E[n-p] + \nu_E[n] \\ \Delta W_N[n] = -\hat{a}_{N1}\Delta W_N[n-1] - \hat{a}_{N2}\Delta W_N[n-2] - \cdots - \hat{a}_{Np}\Delta W_N[n-p] + \nu_N[n] \end{cases} \tag{4-13}$$

In Eq. (4-13), subscription j is no longer used, indicating that the wind variation components are simulated values. Sequence index n denotes simulated values at altitude h_n, n-1 denotes simulated values at altitude h_{n-1} and so on. Note that the two white noise sequences ν_E and ν_N are independent of each other. Coefficients $\hat{a}_{Ei}$ and $\hat{a}_{Ni}$ are the solutions of the corresponding Yule-Walker equations for east and north wind variation components. Similarly, the pth order AR models of the higher frequency signals and the lower frequency signals can be written as,

$$\begin{cases} w_E^H[n] = -\hat{a}_{E1}^H w_E^H[n-1] - \hat{a}_{E2}^H w_E^H[n-2] - \cdots - \hat{a}_{Ep}^H w_E^H[n-p] + \nu_N^H[n] \\ w_N^H[n] = -\hat{a}_{N1}^H w_N^H[n-1] - \hat{a}_{N2}^H w_N^H[n-2] - \cdots - \hat{a}_{Np}^H w_N^H[n-p] + \nu_N^H[n] \end{cases} \tag{4-14}$$

$$\begin{cases} w_E^L[n] = -\hat{a}_{E1}^L w_E^L[n-1] - \hat{a}_{E2}^L w_E^L[n-2] - \cdots - \hat{a}_{Ep}^L w_E^L[n-p] + \nu_N^L[n] \\ w_N^L[n] = -\hat{a}_{N1}^L w_N^L[n-1] - \hat{a}_{N2}^L w_N^L[n-2] - \cdots - \hat{a}_{Np}^L w_N^L[n-p] + \nu_N^L[n] \end{cases} \tag{4-15}$$

The Levinson-Durbin algorithm[9] could be used to solve the Yule-Walker equations with orders from 1 up to p for each signal through one execution. This allows comparison of different orders of the AR models so that the most suitable ones could be selected. The Levinson-Durbin algorithm is a computationally efficient algorithm, especially when all orders of the Yule-Walker equations up to pth order are solved at the same time. Specifically, in this algorithm, the solution (AR model parameters) to lower order equations is updated using the next element of the autocovariance sequence to obtain the solution to the next higher order equations.

Table 4-1 Numerical example of 2nd order AR model parameters.

Parameters		$\hat{a}_1$	$\hat{a}_2$	$\hat{\gamma}_\nu$
Raw	East	-1.0852	0.2655	1.1994
Wind Variation	North	-1.1077	0.2969	1.2494
Higher	East	-1.0139	0.3449	0.9282
Frequency Signal	North	-1.0307	0.3748	0.9829
Lower	East	-1.1205	0.1417	0.2932
Frequency Signal	North	-1.1120	0.1352	0.3366

From the estimated autocovariances presented earlier, AR models with orders from 1 up to 32 were obtained. For example, parameters of the 2nd order AR models are listed in Table 4-1. For the sake of simplicity, other superscriptions and subscriptions of the model parameters were dropped in the table since the model type and wind components are clearly annotated. With all parameters available, power spectral density analysis could be performed to compare different orders of AR models. This analysis is presented in the next subsection.

4.4.4 Power Spectral Density Analysis

The AR model parameters can also be used to estimate the power spectral density (PSD) function,

$$\hat{K}_x(\theta) = \hat{\gamma}_v \left| \frac{1}{1 + a_1 e^{-j\theta} + a_2 e^{-j2\theta} + \cdots + a_p e^{-jp\theta}} \right|^2 \tag{4-16}$$

The estimated PSDs from the 2nd order AR models of the raw wind variation components are shown in Fig. 4-18. It is seen that the 2nd order PSDs were very smooth, thus they were probably relative crude depictions of the true PSDs.

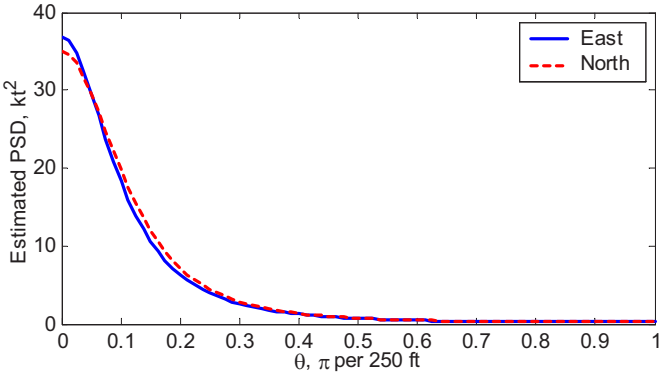

Figure 4-18 Estimated power spectral density from 2nd order AR models of raw wind variation components.

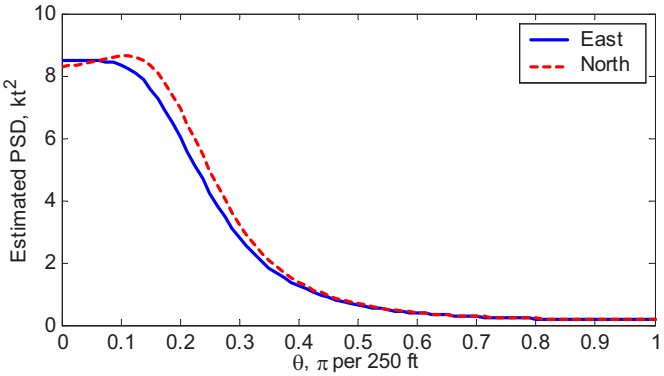

Figure 4-19 Estimated power spectral density from 2nd order AR models of the higher frequency signals.

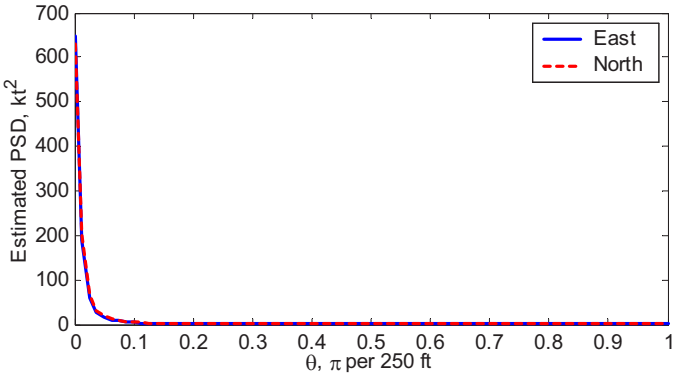

Figure 4-20 Estimated power spectral density from 2nd order AR models of the lower frequency signals.

The estimated PSDs from the corresponding 2nd order AR models of the higher frequency signals and the lower frequency signals are shown in Fig. 4-19 and 4-20 respectively. These estimates are very smooth and lack subtle details too. The estimated PSDs of the higher frequency signals have band-limited frequency contents, indicating band-limited white noise like behavior. The estimated PSDs of the lower frequency signals had a very narrow spike at the lower end of the frequency spectrum, indicating that the general trend of the simulated wind variation would be dominated by the lower frequency component.

The estimated PSDs from the 32nd order AR models of the raw wind variation components are shown in Fig. 4-21. They have details not seen in the estimated PSDs from the 2nd order AR models. It is also noticeable that the peak frequencies were different. The estimated PSDs from the 32nd order AR models had slightly higher peak frequency, and there was a small hump around digital frequency of 0.085π.

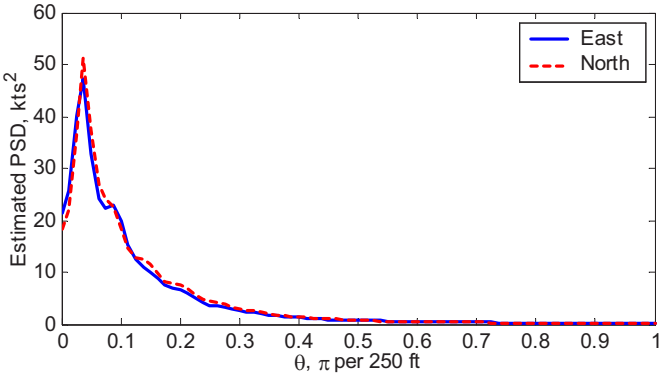

Figure 4-21 Estimated power spectral density from 32nd order AR models of raw wind variation components.

The estimated PSDs from the 32nd order AR models of the higher frequency signals and the lower frequency signals are shown in Fig. 4-22 and 4-23 respectively. Again, the estimated PSDs from 32nd order AR models have features not seen in the estimates from the 2nd order AR models. The peak frequencies in these two figures are now standing out by themselves; and the peak frequencies of the higher frequency signals and the lower frequency signals are distinct from each other.

Comparing Fig. 4-22 and 4-23 with Fig. 4-21, the power of the mode decomposition approach in identifying different frequency contents is clearly seen. The frequency separation is barely seen in Fig. 4-

21 as a small hump at round digital frequency of 0.07π. Without using mode decomposition, even with high degree AR models such as that shown in Fig. 4-21 the characteristics of the original signals may not always be fully captured. This will be further demonstrated in the next section.

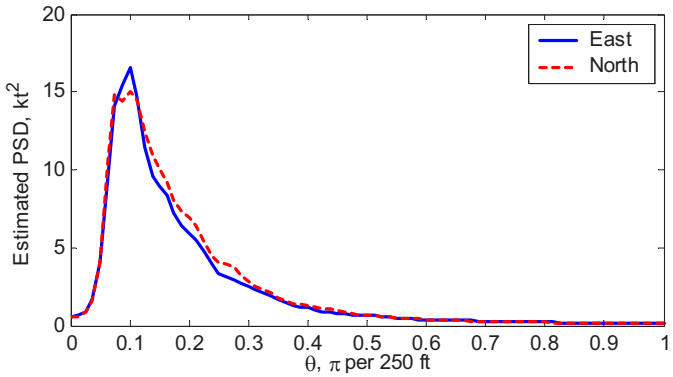

Figure 4-22 Estimated power spectral density from 32nd order AR models of the higher frequency signals.

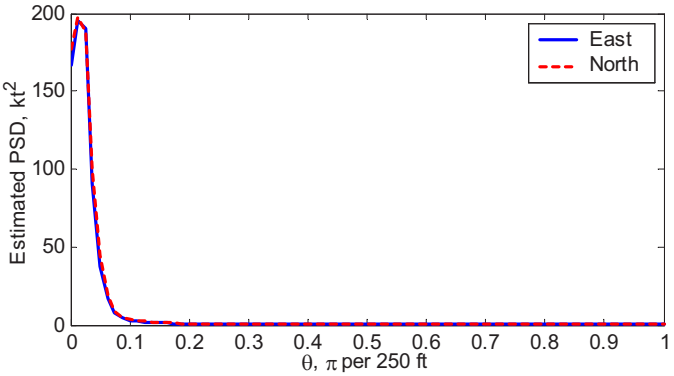

Figure 4-23 Estimated power spectral density from 32nd order AR models of the lower frequency signals.

For higher accuracy, high order AR models would definitely be better choice. However, for a specific application such as the modeling of wind variations between flights for aircraft trajectory simulation, lower order AR models may serve the same purpose well. In the next section, the selection of the order of the AR models through comparing simulation results of the KSDF numerical examples is discussed.

4.5 SIMULATION WITH AUTOREGRESSIVE WIND VARIATION MODELS

The AR models that have been developed can be used to simulate wind variations between flights. For the purpose of comparison, the AR models based on the raw wind variation components are examined first. The AR models based on mode decomposition are examined next. The latter will be used in aircraft trajectory simulations. Finally, the application of the wind variation model is briefly discussed.

4.5.1 Simulation Using AR Models Based on Raw Wind Variation Components

With the AR model parameters known, wind variations can be simulated using Eq. (4-13). To start up the simulation process of a pth order AR model, sequence index n is initially set to zero and all elements of the output sequence with negative indices are treated as if they are zero. The first simulated p elements starting from $n = 0$ are then dropped from the output sequence to allow for the simulation to stabilize. Thus, the pth element of the simulated output sequence are considered to be the first usable element. This process was used for all simulations discussed in this section.

Examples of simulated results using the 2nd order AR models are shown in Fig. 4-24. Examples of simulated results using the 32nd order AR models are shown in Fig. 4-25. Interestingly, the differences between 2nd order AR models and 32nd order AR models are not obvious from the simulated wind variation components. This suggests that higher order model might not be necessary to achieve higher fidelity. Recall that, in the Dryden wind turbulence model, the longitudinal turbulence component was modeled as a first order AR signal. To the scale of aircraft trajectory simulation, especially when the focus is on how the distance traveled evolves over time, higher order AR models probably will not yield significantly more accurate results.

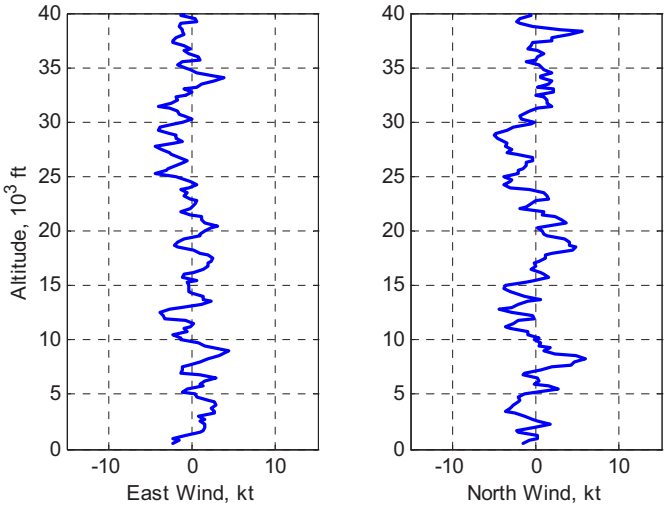

Figure 4-24 Simulation results of 2nd order AR models based on raw wind variation components.

One might notice that the simulated wind variation components have a lower magnitude compared with the raw wind variation shown in changes in Fig. 4-4b. This could be explained partially by the fact that the raw wind variation components observed by the sample flight were from a large pool of data reported by many flights, and that the simulated results were from a large pool of all possible simulation results. The magnitude thus may not necessarily be the same for the two specific individual samples. Another reason is that the wind variation components shown in Fig. 4-4b did not necessarily have zero mean. However, in the AR modeling approach, wind variation components are treated as having zero mean.

Another observation from Fig. 4-24 and 4-25 is that the simulated wind variation components lack the non-stationary characteristics demonstrated by the raw wind variation components. However, those non-stationary characteristics may very well contribute to the aircraft trajectory variations. Thus, the AR models directly based on the raw wind variation components are deemed unacceptable.

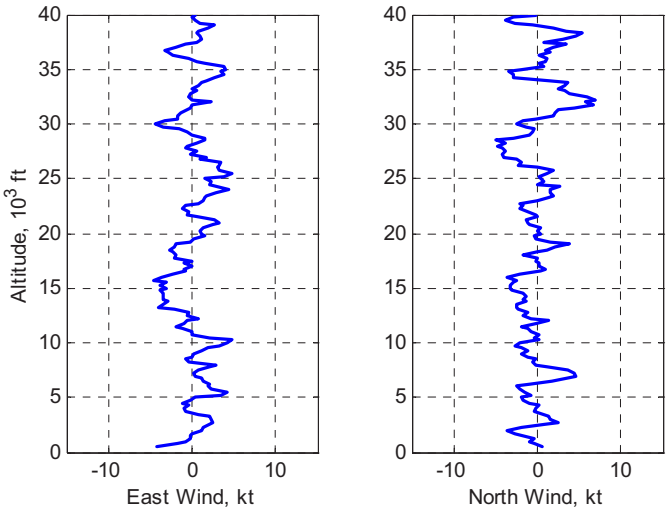

Figure 4-25 Simulation results of 32nd order AR models based on raw wind variation components.

4.5.2 Simulation Using AR Models Based on Mode Decomposition

With the AR models based on mode decomposition, each of the final simulated east and north wind variation components are the summation of three signals: a higher frequency signal, a lower frequency signal, and a random DC signal.

The higher frequency signals were the direct outputs of the corresponding AR models. Examples of simulated higher frequency signals from the 2nd order AR models are shown in Fig. 4-26. The random DC signals were simply normally distributed random numbers bounded by the corresponding maximum and minimum values of source data. If any of such obtained DC signals exceeded the range of the corresponding source data, that value was regenerated again until a new value within the range was obtained.

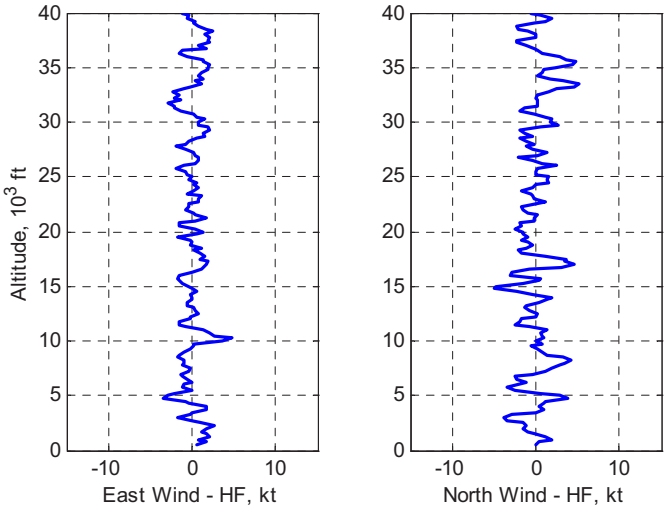

Figure 4-26 Simulation results of 2nd order AR models based on higher frequency signals.

Special attention is needed to simulate the lower frequency signals. To avoid high frequency artifacts of the AR models, the outputs of the lower frequency AR models were filtered using the same FIR filter that were used in the mode decomposition. High frequency artifacts of the AR models exist because the filtered lower frequency signals from the wind variation profiles were not exactly AR signals. If those high frequency artifacts are not properly removed, they will couple with the higher frequency signals that are simulated separately, yielding inaccurate results. Examples of simulated lower frequency signals from the 2nd order AR models are shown in Fig. 4-27. It is obvious that within the altitude range, the simulated lower frequency signals demonstrated non-stationary characteristics, although the AR models were developed as stationary models. If the altitude range were large enough, the simulated lower frequency signals would look more like stationary processes. The low cutoff frequency assures that for the practical range of altitudes, the simulated lower frequency processes do depict the non-stationary characteristics of the data. This again shows the effectiveness of the mode decomposition approach in modeling non-stationary signals.

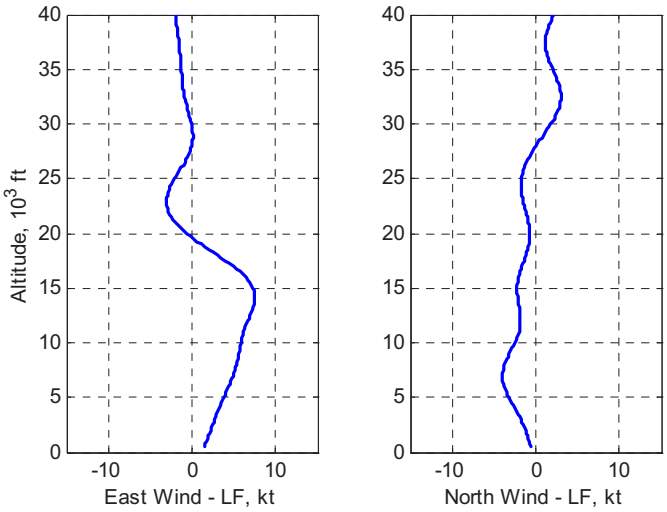

Figure 4-27 Simulation results of 2nd order AR models based on lower frequency signals.

The simulated higher frequency signals, low frequency signals, and the random DC signals are then added together to give simulated wind variation components. Wind variation components obtained from adding the separately simulated signals discussed above are shown in Fig. 4-28. In addition to the non-stationary characteristics, simulated wind variation components normally do not have zero mean. The magnitudes are also higher, at least as seen in the example results. Comparing Fig. 4-28 with Fig. 4-24 and 4-25, the simulated wind variation based on mode decomposition were much more closer to the wind variation reflected in the data.

Examples of simulated wind variation components from the 32nd order AR models are shown in Fig. 4-29. It is again seen that the simulated results from the 2nd order models and the high order models were very similar. Thus for aircraft trajectory simulation, the 2nd order models are good choice. If computational time is not a concern, high order models could definitely be used.

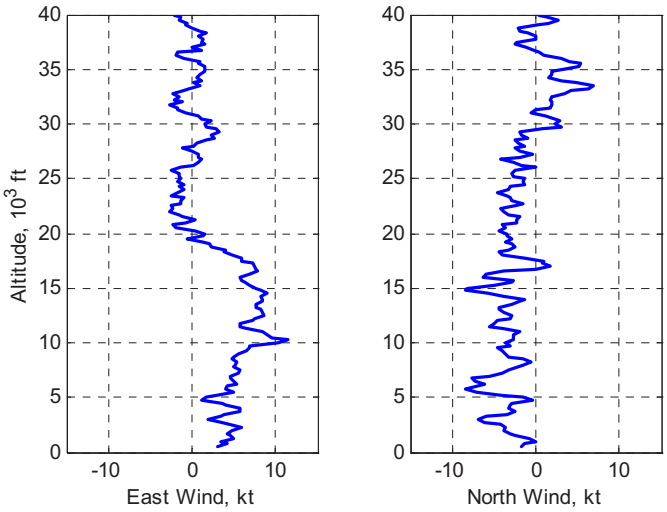

Figure 4-28 Simulated wind changes of 2nd order AR models based on mode decomposition.

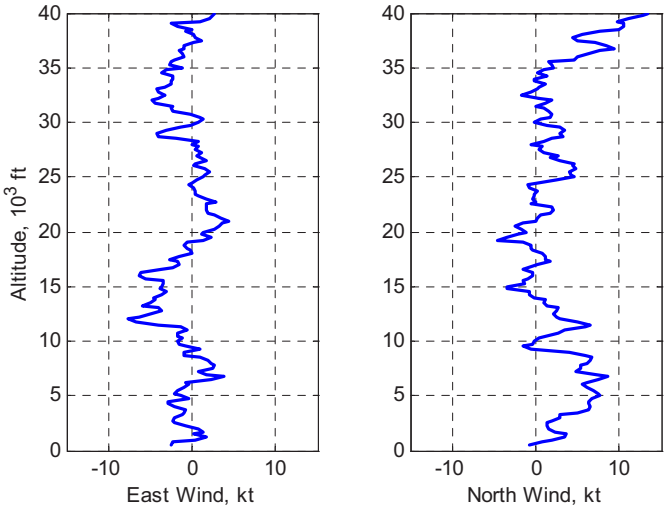

Figure 4-29 Simulated wind changes of 32nd order AR models based on mode decomposition.

4.5.3 Application of the Wind Variation Model

The final step is to incorporate simulated wind variation components with the nominal wind profile to obtain actual wind profile for use in aircraft trajectory simulation. For analyzing separation between flight pairs, the nominal wind profile is used as the wind profile for the leading flight; and the nominal wind profile plus a simulated wind variation profile is used as the wind profile for the trailing flight. If the mean wind is used as the nominal wind profile, then the wind profile for the trailing flight will be the mean wind profile plus a simulated wind variation profile, as the example shown in Fig. 4-30. The solid curves are the east and north wind components of the mean wind profile. The dotted curves are the east

and north wind components of the mean wind profile plus a simulated wind variation profile. The dotted wind profile was obtained by adding the mean wind profile shown in Fig. 4-3 and the wind variation components shown in Fig. 4-28.

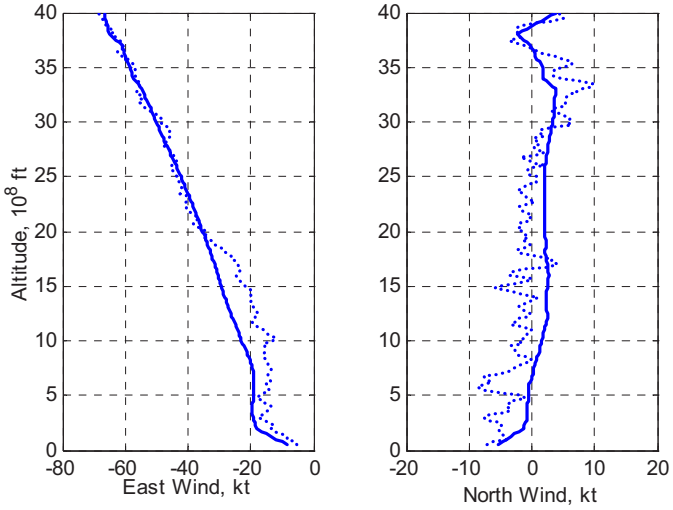

Figure 4-30 Simulated wind variation supper imposed on mean wind profile.

For simulating large numbers of aircraft trajectories, each of the leading flight can be simulated with the fixed nominal wind profile but with all other uncertainty factors taking into account. The pool of simulated leading trajectories will reflect trajectory variations without wind variations. Each of the trailing flight can be simulated with all other uncertainty factors taking into account, plus a wind variation profile freshly generated for each flight that is supper imposed on the fixed nominal wind profile. Thus, the pool of simulated trailing trajectories will reflect trajectory variations with wind variations. Flight pairs can then be formed by randomly picking a trajectory from the leading pool and randomly picking a trajectory from the trailing pool. Separation analysis can then be performed upon the large pool of random flight pairs.

As an improvement of the wind variation model, the simulated wind variation (east and north) components can be tuned to fit additional magnitude variations along altitude. This could be done as follows. Statistics similar to that shown in Fig. 4-10 could be normalized such that, the values of the curves within the altitude range of 3,000 ft to 20,000 ft is equal to 1. The values of the curves above 20,000 ft would be higher than 1 and the values of the curves below would be lower than 1. The simulated wind variation components could then be multiplied by the corresponding curves for magnitude adjustment.

4.6 SUMMARY

To tackle the problem of simulating wind variation between consecutive flights, a unique mode decomposition approach was developed to decompose the wind variation components into categorized frequency content signals. These frequency content signals include zero mean higher frequency signals, zero mean lower frequency signals, and random DC signals. The higher frequency signals and lower frequency signals are modeled as AR signals. Through numerical examples, the effectiveness of the

mode decomposition modeling approach was demonstrated. To overcome the shortcomings of AR method in modeling the lower frequency signals, FIR filtering is employed to obtain satisfactory results. This process provides an integrated wind variation modeling approach that is an essential part of the tool for analyzing trajectory variations of aircraft performing approach and arrival procedures.

The numerical examples of wind variation modeling were based on ACARS wind data reported within the altitude range of 3,000 ft to 20,000 ft by aircraft landing to KSDF from the west. Model improvements were suggested to adapt to the characteristics of actual wind field above 20,000 ft and below 3,000 ft. A simple way to do this would be to only adjust the magnitude of the simulated wind variation components, and leave the frequency spectrum as unchanged. Another possible way would be to adapt both frequency spectrum and variance at the same time. Using the latter approach, the final model parameters would become functions of altitude themselves. In digital simulation, varying model parameters along altitude would not impose any problem. The biggest challenge would be collecting enough data to support this effort. The lower sampling rate of ACARS data at high altitude would not be sufficient.

Although the numeric examples given in this chapter were based on ACARS data, these data are not available at all sites. In this case, data from other sources could also be used to model wind variation using the same modeling approach. One example of such data sources is the Mesosphere-Stratosphere-Troposphere (MST) Radar at Aberystwyth in UK. MST is unique in being able to provide continuous measurements of the three-dimensional wind vector over the altitude range of 2-20 km at high resolution (typically 300 m in altitude and a few minutes in time)[10]. It could therefore be used to model wind variation in that area when the amount of ACARS data is not sufficient.

REFERENCES

[1] Moninger, W. R., Mamrosh, R. D., and Pauley, P. M., "Automated Meteorological Reports from Commercial Aircraft," *Bulletin of the American Meteorological Society*, Vol. 84, Jan. 2003, pp. 203-216.

[2] "NOAA/ESRL/GSD Aircraft Data Web," [online database] URL: http://acweb.fsl.noaa.gov/ [cited 10 Jun. 2006].

[3] Benjamin, S. G., Schwartz, B. E., Szoke, E. J., and Koch, S. E., "The Value Of Wind Profiler Data in U.S. Weather Forecasting," *Bulletin of the American Meteorological Society*, Vol. 85, Dec. 2004, pp. 1871-1886.

[4] Russ Rew, Glenn Davis, Steve Emmerson, and Harvey Davies, *The NetCDF Users' Guide - Data Model, Programming Interfaces, and Format for Self-Describing, Portable Data*, NetCDF Version 3.6.1, Unidata Program Center, University Corporation for Atmospheric Research, Boulder, CO, May 2005.

[5] Clarke, J.-P., Bennett, D., Elmer, K., Firth, J., Hilb, R., Ho, N., Johnson, S., Lau, S., Ren, L., Senechal, D., Sizov, N., Slattery, R., Tong, K., Walton, J., Willgruber, A., and Williams, D., "Development, Design, and Flight Test Evaluation of a Continuous Descent Approach Procedure for Nighttime Operation at Louisville International Airport," Report of the PARTNER CDA Development Team, Report No. PARTNER-COE-2006-02, 9 Jan. 2006.

[6] Norden E. Huang, Zheng Shen, Steven R. Long, Manli C. Wu, Hsing H. Shih, Quanan Zheng, Nai-Chyuan Yen, Chi Chao Tung and Henry H. Liu, "The Empirical Mode Decomposition and The Hilbert Spectrum for Nonlinear and Non-Stationary Time Series Analysis," *Proc. R. Soc. Lond. A 454*, London, 1998.

[7] Brown, R. G. and Hwang, P. Y. C., *Introduction to Random Signals and Applied Kalman Filtering – with MATLAB Exercises and Solutions*, John Wiley & Sons Inc., New York, 1997.

[8] MIL-HDBK-1797, *Flying Qualities of Piloted Aircraft*. Department of Defense Handbook, 19 Dec. 1997.

[9] Boaz Porat, *A Course in Digital Signal Processing*, John Willey & Sons, Inc. New York, 1997.

[10] "Services & Facilities Annual Report – FY April 2004 to March 2005," The NERC MST Radar Facility at Aberystwyth, UK, 2005.

CHAPTER 5

SEPARATION ANALYSIS METHODOLOGY

NOMENCLATURE

C	=	traffic throughput in aircraft per hour
C_i	=	traffic throughput for aircraft sequence i
D	=	along track distance
D_0	=	along track distance at the intermediate metering point
$dP_{T,i,s}$	=	infinitesimal total probability for aircraft sequence i at separation s, unadjusted traffic
$dP_{Ta,i,s}$	=	infinitesimal total probability for aircraft sequence i at separation s, adjusted traffic under sequence-specific target separation
$E(\ )$	=	expectation, mean, average operator
$f(\ )$	=	aircraft trajectory function
$f_l(\ )$	=	aircraft trajectory function, leading aircraft
$f_t(\ )$	=	aircraft trajectory function, trailing aircraft
$f^{-1}(\ )$	=	inverse aircraft trajectory function
$f_l^{-1}(\ )$	=	inverse aircraft trajectory function, leading aircraft
$f_t^{-1}(\ )$	=	inverse aircraft trajectory function, trailing aircraft
i	=	index of aircraft sequence in arrival traffic
P_i	=	probability of aircraft sequence i in arrival traffic
p_i	=	probability density of feasible separations at metering point for aircraft sequence i
P_{Ri}	=	conditional level of confidence for aircraft sequence i
P_T	=	total level of confidence
p_T	=	probability density of spacing in arrival traffic
P_{Ta}	=	total level of confidence under adjusted arrival traffic
p_{Ta}	=	probability density of spacing in adjusted arrival traffic
P_{Tai}	=	total probability for aircraft sequence i, adjusted traffic under sequence-specific target separation
$P_{Ta,i}$	=	total probability for aircraft sequence i, adjusted traffic under sequence-independent target separation
p_{Tai}	=	probability density of spacing in adjusted arrival traffic under sequence-specific target separation for aircraft sequence i
$P_{T,i}$	=	total probability for aircraft sequence i, unadjusted traffic
s	=	spacing
S	=	target separation for unadjusted traffic
s_f	=	spacing at runway threshold
S_f	=	separation minimum at runway threshold

S_I = target separation
S_{Ii} = sequence-specific target separation for aircraft sequence i
s_T = spacing in unadjusted arrival traffic
s_{Ta} = spacing in adjusted arrival traffic
T = inter-arrival time at intermediate metering point
t = normalized time
$t_{l,f}$ = leading aircraft normalized time when leading aircraft is at runway threshold
$t_{t,f}$ = trailing aircraft normalized time when leading aircraft is at runway threshold
x = generic variable
β_f = final separation buffer

5.1 INTRODUCTION

A separation analysis methodology was developed to analyze the evolution of spacing between consecutive aircraft pairs conducting the same noise abatement approach and arrival procedure, and to determine the target separation at the intermediate metering point. This methodology can also be used to evaluate under what traffic condition the proposed operational framework may be applied. This methodology is based on the availability of a large number of aircraft trajectories such as that from the Monte Carlo simulation tool, or from radar tracking data. This methodology also assumes a set of predefined separation minima that must be obeyed. Existing separation minima are described in the following paragraphs.

Under Instrument Flight Rules (IFR), for aircraft at the same altitude, the FAA radar separation minima are 3 nm between aircraft operating within 40 nm (60 nm for single sensor ASR-9 radar with Mode S) of the radar antenna site, and 5 nm between aircraft operating beyond 40 nm (or 60 nm) from the antenna site (FAA Order 7110.65 5-5-4.a[1], AIM 4-4-10[2]). These minima may be increased or decreased in certain specific situations.

Wake turbulence procedures specify increased separation minima required for certain classes of aircraft because of the possible effects of wake turbulence (FAA Order 7110.65 5-5-4.e,f,g[1] and AIM 7-3-9[2]). For the purposes of defining wake turbulence separation minima, aircraft are classified according to maximum certificated takeoff weight as Heavy (more than 255,000 lb), Large (more than 41,000 lb, up to 255,000 lb), and Small (41,000 lb or less). Note that B757 is a Large aircraft but is treated specially when it is in a leading position. Wake turbulence separation minima between arrival aircraft are summarized in Table 5-1. These minima apply when the trailing aircraft is operating directly behind, or directly behind and less than 1,000 feet below, or following an aircraft conducting an instrument approach except otherwise noted in the table.

Besides the separation minima, letters of agreement between adjacent facilities may define some higher miles-in-trail (MIT) restrictions (such as 10 nm or higher) limited to specified routes and/or sectors/positions during certain periods of the day.

The remainder of this Chapter is organized as follows. The relationship between trajectory variation and the variability in spacing during noise abatement approach and arrival procedures is analyzed in the next section. The basic concept of determining the target separation from the probability distribution of final spacing at the runway threshold for given spacing at the metering point is presented. This is followed by a discussion in Section 5.3 about the solution to the inverse separation analysis problem – obtaining the probability distribution of "feasible separations" at the metering point for given final separations – which is more efficient. The conditional probability separation analysis method that is

Table 5-1 IFR wake turbulence separation minima matrix, nm

	Trailing Aircraft		
Leading Aircraft	Heavy	Large	Small
Heavy	4	5	5/6[a]
B757	4	4	5
rge	2.5[b]	2.5[b]	4[a]
Small	2.5[b]	2.5[b]	2.5[b]

[a] When leading aircraft is over the runway landing threshold.

[b] When aircraft established on the final approach course within 10 nm of the landing runway, radar operating in single sensor slant range mode, and average runway occupancy time of 50 seconds or less.

directly based on the distribution of feasible separations is presented in Section 5.4. The total probability separation analysis method is presented in Section 5.5. In this method, the aircraft mix and the actual spacing in the arrival stream are taken into account to determine the target separation. Thus, the total probability method is more realistic in reflecting the confidence levels. A theoretical analysis of the tradeoff between target separations and traffic throughputs is presented in Section 5.6. The summary of this chapter is provided in the last section.

5.2 TRAJECTORY VARIATION AND SEPARATION

Distance versus time (as depicted in Fig. 5-1) is the most important relationship when analyzing the separation between consecutive aircraft flying along the same path. In the figure, the horizontal axis represents the along track distance, and the vertical axis represents time. The shaded areas represent the region of uncertainty in the distance-time space where the aircraft could be in the future. Note that in reality, the segment on the trailing aircraft trajectory prior to the intermediate metering point would also be a shaded area. This segment is presented in Fig. 5-1 as a straight line for the sake of simplicity. It represents the case where every aircraft is flying at the same ground speed prior to the intermediate metering point. For a given spacing at the metering point (measured when the leading aircraft is at the metering point), the final spacing (measured when the leading aircraft is at runway threshold) would have

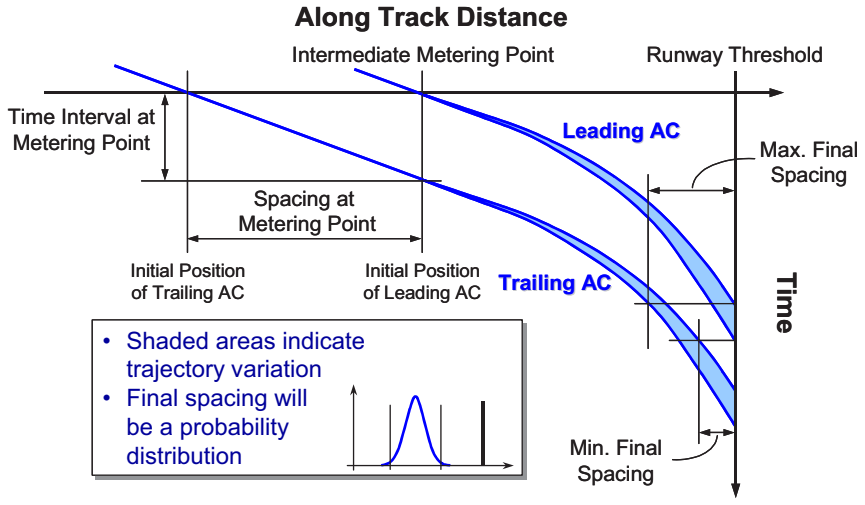

Figure 5-1 Trajectory variations and separation.

a probability density function (pdf) similar to that shown in the panel in the figure. The minimum value of the final spacing would be given by the slowest leading trajectory and the fastest trailing trajectory, and the maximum value would be given by the fastest leading trajectory and slowest trailing trajectory.

As indicated in a previous simulation study[3], the minimum spacing between any pair of consecutive aircraft will most probably occur when the leading aircraft is at the runway threshold because of the separation compression due to deceleration, and the variations in their trajectories. Thus, although different separation minima are in effect at different stages of the arrival, the separation minima in effect at the runway threshold are the binding constraints. The target separation for a given pair of aircraft may therefore be determined by the spacing at the metering point that gives a minimum value of the final spacing that is equal to the separation minimum for that pair. However, the target separation determined in this way is conservative in terms of throughput because one would be protecting against a rare worst-case scenario. Furthermore, the tail of the spacing distribution might never be known through practical means.

On the other hand, the pdf of the final spacing for a given spacing at the metering point may be estimated through analysis of large numbers of aircraft trajectory pairs. Therefore, the target separation can be determined by adjusting the spacing at the metering point and the resulting estimated distribution of the final spacing until there is sufficient confidence (i.e., probability) that the final spacing will be greater than or equal to the separation minimum. This process is illustrated in Fig. 5-2. The level of confidence is the integral of the pdf from the separation minimum to infinity.

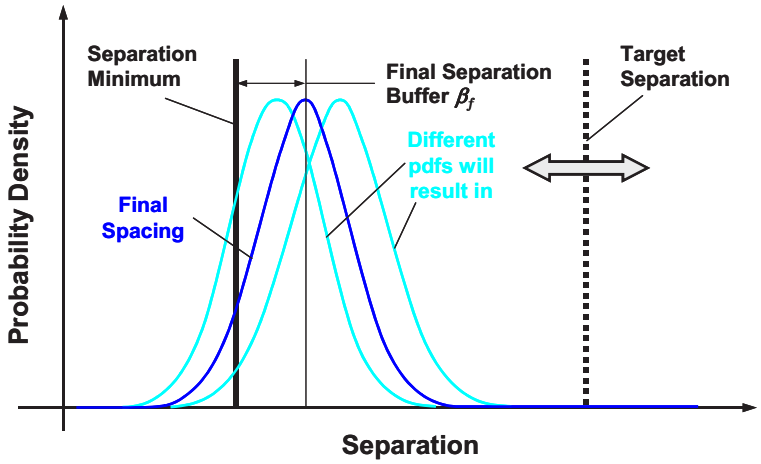

Figure 5-2 Adjusting spacing at metering point for final separation.

The final separation buffer β_f, is a measure of how much the final spacing will be above the separation minimum, and it is computed by taking the difference between the mean of the final spacing s_f and the separation minimum. This measure can be used as an indicator of efficiency for the given target separation or level of confidence. Another parameter to measure the efficiency is the average traffic throughput C computed at the metering point in terms of aircraft per hour (1/h) and given by

$$C = 3600 / E(T) \tag{5-1}$$

where $E(T)$ is the mean of inter-arrival time T in seconds measured at the intermediate metering point.

It is worth to mention that, because of the non-linearity in the distance-time relationship, a different pdf will be resulted in each time the spacing at the metering point is adjusted. That is to say, not only will

the pdf of the final spacing shift left or right (see Fig. 5-2), its standard deviation will also change. Thus, it is not computationally efficient to determine the target separation by adjusting the spacing at the metering point and then examining the final spacing. It is also difficult to visualize the relationship between the target separation and the level of confidence using this method. In the next subsection, a method is introduced for determining the pdf of the "feasible separations" at the metering point that ensures separation minima. Using the new pdf of feasible separations, the above-mentioned shortcomings are overcome.

5.3 THE INVERSE SEPARATION ANALYSIS PROBLEM

Consider a large pool of paired aircraft trajectories. For a specific pair of trajectories, the shaded areas in Fig. 5-1 would reduce to two curved lines, as shown in Fig. 5-3. Assume that the leading trajectory and the trailing trajectory in the pair are independent of each other. As a simplified case, the feasible separation – the spacing at the metering point that ensures the separation minima for the specific trajectory pair – can be determined by moving the trailing trajectory in the direction parallel to the time axis until the final spacing is equal to the separation minimum in effect at the runway threshold. For a separation minimum at the runway threshold, feasible separations (measured when the leading aircraft is at the metering point) would have a pdf similar to that shown in the panel in the figure. In reality, different separation minima would be in effect at different stages of the arrival phase, and that the trailing aircraft could be faster than the leading at some points on the flight path. Thus, to determine the feasible separation for a trajectory pair, separation minima throughout the arrival flight, not just the final separation minimum, should be protected (see the red dashed curve in Fig. 5-3).

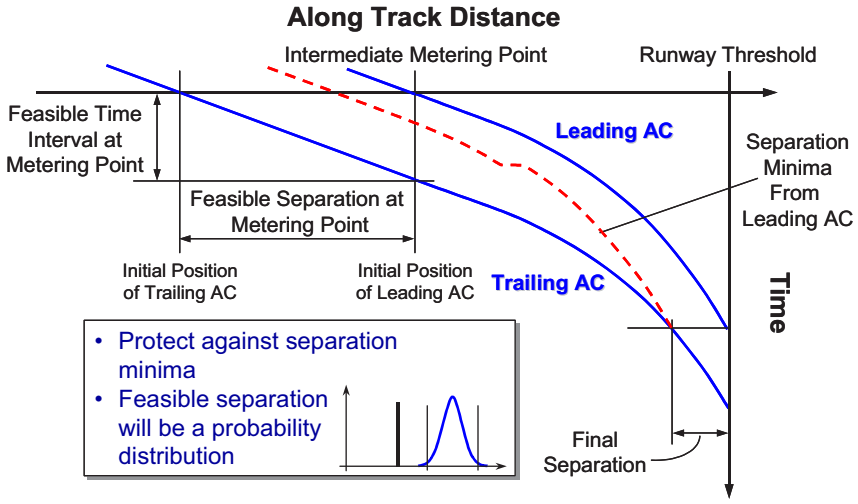

Figure 5-3 The inverse separation analysis problem.

The feasible separation for a specific trajectory pair can be derived mathematically as follows. Assume that aircraft trajectories are expressed in the form of along track distance as a function of normalized time

$$D = f(t) \tag{5-2}$$

Along track distance has a positive sense along the direction of flight and it is defined as equal to zero at the runway threshold. Normalized time is defined as at zero when the aircraft is at the metering point. By definition, the location of the metering point is

$$D_0 = f(0) \tag{5-3}$$

The inverse function of the Eq. (5-2) gives normalized time as a function of along track distance

$$t = f^{-1}(D) \tag{5-4}$$

If spacing between the two aircraft exactly equals the separation minimum S_f when the leading aircraft is at the runway threshold, the normalized times for the leading and trailing trajectories at that moment would be

$$\begin{cases} t_{l,f} = f_l^{-1}(0) \\ t_{t,f} = f_t^{-1}(-S_f) \end{cases} \tag{5-5}$$

where subscripts l and t denote leading and trailing respectively. Note that the two normalized times in Eq. (5-5) are actually the same moment to an external observer. Referring to Fig. 5-1, the feasible separation can be obtained as

$$s = f_l(0) - f_t(t_{t,f} - t_{l,f}) = D_0 - f_t(t_{t,f} - t_{l,f}) \tag{5-6}$$

The separation minima at other points along the flight path and the case when the trailing aircraft is significantly slower than the leading aircraft on the final approach should also be protected. To do this, the feasible separation could be determined such that the spacing at any point on the approach flight path between the metering point and the runway threshold is equal to or greater than the separation minimum in effect at that point. A simplified method to achieve this is to apply the process defined by Eq. (5-5) and (5-6) to the final approach fix in addition to the runway threshold. The larger of the two spacing values determined is then the feasible separation for the trajectory pair. Because of the natural separation compression, it might not be always necessary to apply this process at higher altitudes though.

It can be seen from the above derivation and Fig. 5-1 and 5-3 that the feasible separation depends on the separation minimum, the location of the metering point, and the characteristics of both the leading and the trailing trajectories. If the leading aircraft is slow and the trailing aircraft is fast, a relatively large feasible separation would be expected and vice-versa.

Applying this process to all possible trajectory pairs, a large number of feasible separation values could be obtained. By definition, the frequency density distribution of these values normalized by the total number of values would, as the number of values gets very large, become the pdf of feasible separations that result in the required final separation. The relationship between the target separation, and the level of confidence derived using the resulting pdf of feasible separations (by integrating the pdf from zero to the target separation), would be equivalent to that obtained using the pdf of possible final spacing for the given target separation (by integrating the pdf from the separation minimum to infinity), but without the need to regenerate the pdf of possible final spacing for each target separation.

The integral of the pdf of feasible separations from zero to the target separation, i.e. the cumulative probability, is the probability that the feasible separation is less than the given target separation. In other

words, this cumulative probability indicates the likelihood that no separation violations will occur during the execution of the procedure, should the aircraft pair arrive at the metering point with the given target separation. The cumulative probability is thus a conditional probability, and the corresponding level of confidence is therefore also conditional. With the pdf of feasible separations known, a chosen target separation immediately gives the conditional level of confidence of uninterrupted operation.

5.4 CONDITIONAL PROBABILITY SEPARATION ANALYSIS METHOD

The sequence of aircraft in a consecutive pair is important for determining the target separation, as aircraft trajectories are functions of the dynamics of the specific aircraft involved, and the separation minima depend on aircraft weight classes. This is illustrated in Fig. 5-4 by the pdfs of feasible separations for complementary sequences: the first for aircraft type A leading type B; the second for aircraft type B leading type A. One reason for the difference between the pdfs would be the difference in the weight classes of the aircraft. For example, when a Heavy aircraft is leading a Large aircraft, the separation minimum is greater than in the complementary case. Thus, the feasible separations would probably be larger. Another reason would be the difference in the performance characteristics of the aircraft. For example, if one aircraft descends at a steeper angle than the other does, the steeper aircraft will have a higher ground speed for longer even if the two aircraft descend at the same Calibrated Airspeed (CAS). Notice that the sequences with aircraft of the same type—aircraft type A leading type A and type B leading type B—are not shown in Fig. 5-4 for the sake of simplicity.

5.4.1 Sequence-Independent Target Separation

Given the probability density p_i of feasible separations for aircraft sequence i, and a target separation S_I, the conditional level of confidence P_{Ri} is

$$P_{Ri} = \int_0^{S_I} p_i ds \tag{5-7}$$

The conditional level of confidence is the probability that there will be no separation violations in an

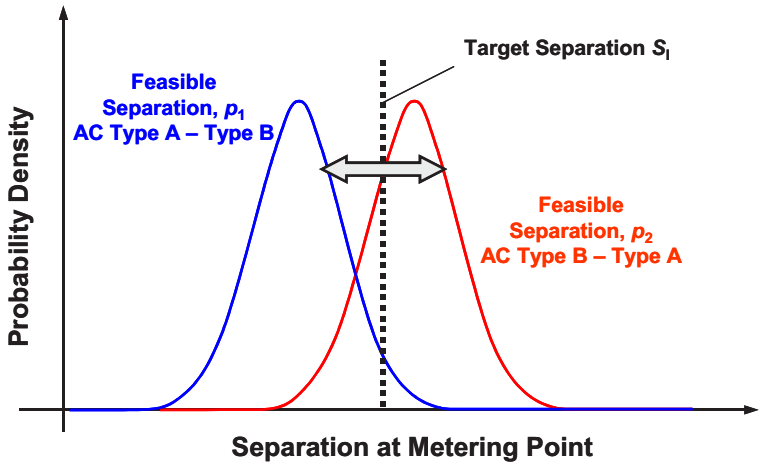

Figure 5-4 Sequence-independent conditional probability method.

uninterrupted noise abatement approach or arrival if (on the condition that) the spacing at the metering point is exactly equal to the selected target separation.

If different aircraft sequences have different pdfs of feasible separations, as shown in Fig. 5-4, different aircraft sequences will have different conditional levels of confidence for the same target separation. Thus, if a single target separation is desired, to be consistent with the current practice of using a single MIT restriction for the entire traffic stream at the hand-off or metering point, it could be determined by finding the minimum S_I such that every single P_{Ri}, or the average of P_{Ri} is greater than or equal to the desired value.

5.4.2 Sequence-Specific Target Separation

To have the same conditional level of confidence for all sequences, each aircraft sequence must have a different target separation. While such a scheme is more complex, there is a strong motivation for it. If a single target separation is used, it will be too conservative for some aircraft sequences. By using sequence-specific target separations, throughput may be increased.

The conditional probability separation analysis method using sequence-specific target separations is illustrated in Fig. 5-5. The light gray dotted vertical line in the middle denotes the sequence-independent target separation for both aircraft sequences. This target separation would give a certain average conditional level of confidence. However, for each of the aircraft sequences, the sequence-independent target separation would give a different conditional level of confidence. The dotted vertical line on the left corresponds to the target separation for aircraft type A leading type B with a conditional confidence level that is equal to the average level given by the sequence-independent target separation. The dotted vertical line on the right is the corresponding target separation for aircraft type B leading type A.

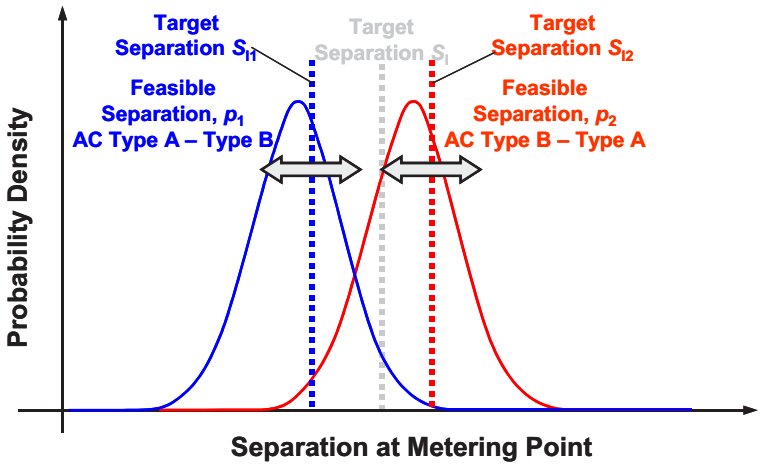

Figure 5-5 Sequence-specific conditional probability method.

For relatively high confidence levels, the use of sequence-specific target separations would give a lower average target separation. This is further illustrated in Fig. 5-6. In this figure, cumulative probabilities for the two aircraft sequences are shown as individual functions and as an average. If sequence-specific target separations with the same confidence level are used, as indicated in the figure, a smaller target separation would be needed when aircraft type A is leading type B, and a larger target separation would be needed when aircraft type B is leading type A. For the confidence level shown, the

decrease in the target separation for aircraft type A leading type B is greater than the increase for aircraft type B leading type A.

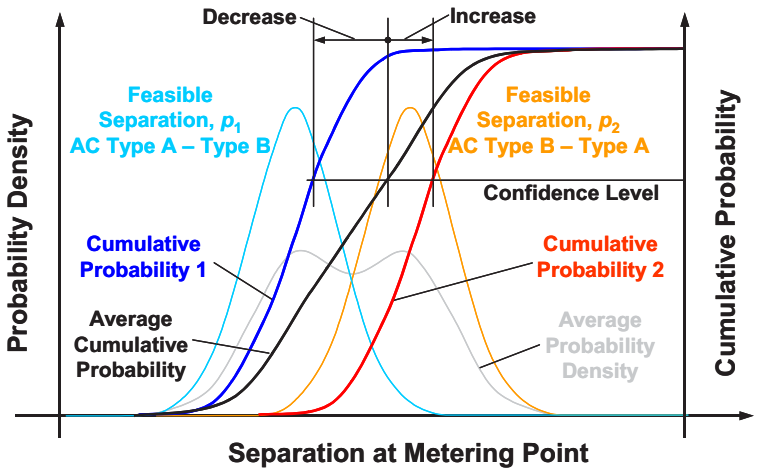

Figure 5-6 Sequence-specific separation capacity savings.

As the confidence level increases, the difference would be even greater, giving an even smaller average target separation thus greater throughput. In other words, this would result in a smaller final separation buffer. Given the target separation S_{Ii} for aircraft sequence i, Eq. (5-7) now becomes

$$P_{Ri} = \int_0^{S_{Ii}} p_i ds \tag{5-8}$$

5.5 TOTAL PROBABILITY SEPARATION ANALYSIS METHOD

A key assumption in the conditional probability separation analysis method is that the spacing at the metering point is exactly equal to the target separation. The reality is that neither controllers nor automation are this precise, nor does the traffic level guarantee the target separation can be exactly met. Thus, there will always be some variability in the spacing at the metering point, and this variability must be accounted for if the total probability of no separation violations is to be determined.

5.5.1 The Characteristics of Spacing in Arrival Stream

To this end, it is necessary to characterize the actual spacing in the arrival stream at the metering point. A hypothetical pdf of the spacing at the metering point for under an existing MIT restriction at that metering point is illustrated by the solid black curve in Fig. 5-7. The traffic stream under the existing MIT restriction is referred to as the unadjusted traffic.

Should a higher target separation be used, as a result of controllers' effort to achieve that target, the pdf of the spacing at the metering point will be shifted towards higher values, i.e. rightwards. This is illustrated by the gray curve in Fig. 5-7. The traffic stream with the increased target separation is referred to as the adjusted traffic. The shapes of the pdfs are not symmetrical because controllers normally only need to adjust the spacing that could fall below the target separation. Notice that in the figure the tails of the pdfs extend to the left of target separations. This is to illustrate that, on rare occasions, the spacing

may actually be less than the target separations. However, this is typically not an issue as the target separations are often much higher than the separation minima in effect at the metering point.

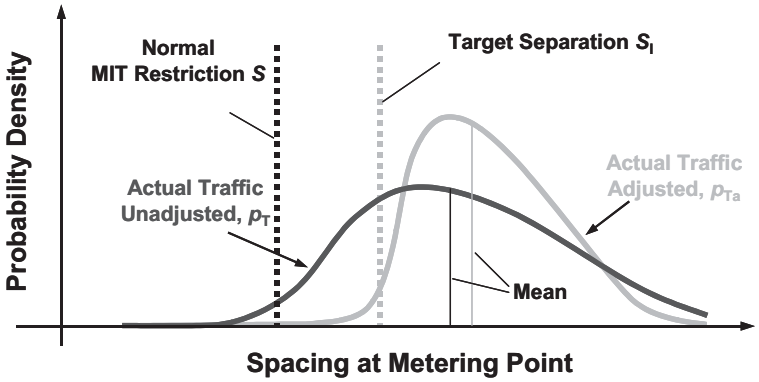

Figure 5-7 Spacing distribution in arrival traffic stream.

The mean spacing at the metering point in the unadjusted traffic stream, an indicator of arrival traffic volume, is given by

$$E(s_T) = \int_0^\infty p_T s ds \tag{5-9}$$

The mean spacing for the adjusted traffic stream is simply

$$E(s_{Ta}) = \int_0^\infty p_{Ta} s ds \tag{5-10}$$

In practice, the lower integration limit in Eq. (5-9) and (5-10) would be the separation minimum in effect at the metering point because the integral from zero to the separation minimum should be zero. However, zero is used as the lower integration limit for the sake of simplicity.

When the arrival rate is below the runway acceptance rate, the mean of spacing in the unadjusted traffic will be much higher than the separation minimum that is in effect at the metering point. As the arrival rate increases, the pdf of the spacing at the metering point will become narrower, and the mean of spacing in the unadjusted traffic will be closer to the separation minimum.

A natural metering point at which the requisite data can be collected is the boundary between the Air Route Traffic Control Center (Center) and the Terminal Radar Approach Control (TRACON), as this is the point where the hand-off of aircraft occurs. The distribution of the spacing in the unadjusted traffic can be obtained from radar tracking data, as can the distribution of the spacing in the adjusted traffic. The distribution of the spacing can also be obtained through controller-in-the-loop simulations.

5.5.2 Total Probability for Unadjusted Traffic

Once the pdf of the spacing in the unadjusted traffic, such as that shown in Fig. 5-7 is known, a total probability can be computed. For the pdf p_T of the spacing in the unadjusted traffic, the probability (referring to Fig. 5-8 and based on Eq. (5-7)) that aircraft sequence i contained in the small slice of traffic at spacing s, and could execute the procedure without any separation violations is

$$dP_{T,i,s} = p_T ds \int_0^s p_i dx \tag{5-11}$$

On the left hand side of Eq. (5-11), subscript T denotes that the probability is from the pdf of unadjusted traffic spacing. The integral on the right hand side of Eq. (5-11) is actually the cumulative probability of feasible separations. The total probability that no separation violation will occur for aircraft sequence i under the given traffic condition, i.e. the total level of confidence P_{Ti} for aircraft sequence i can be obtained as

$$P_{T,i} = \int_0^\infty \left(\int_0^s p_i dx \right) p_T ds \tag{5-12}$$

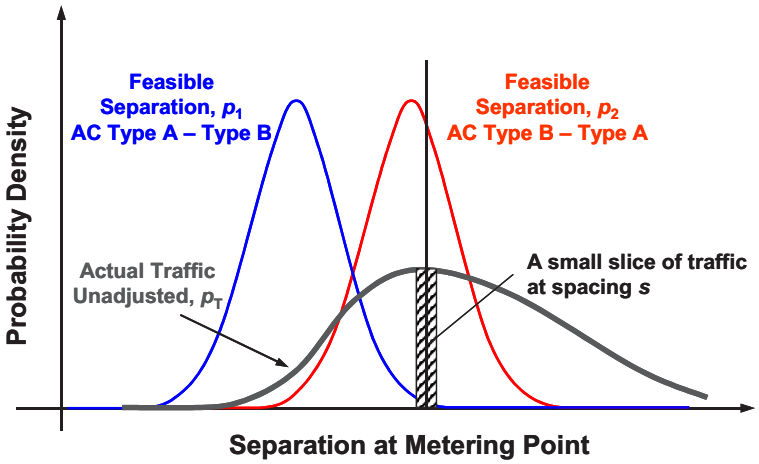

Figure 5-8 Probability under normal traffic flow.

For the probability P_i that aircraft sequence i is in the arrival traffic stream, the overall total probability P_T that no separation violation will occur under the given traffic condition is a weighted average of total probabilities for all aircraft sequences, that is

$$P_T = \sum_i P_i P_{T,i} = \sum_i P_i \int_0^\infty \left(\int_0^s p_i dx \right) p_T ds \tag{5-13}$$

The probability given by Eq. (5-13) now depends on the actual traffic condition, i.e. traffic mix and the distribution of the spacing in the unadjusted traffic. For example, if there is only a small percentage of a sequence where a heavy is leading a small – a sequence with large feasible separations, and a pdf farther to the right than other sequences – that sequence will not contribute much to the overall total probability. Note that once the pdf of the spacing in the unadjusted traffic and ground speed are known, the average arrival rate can be estimated. However, the pdf of the spacing in the unadjusted traffic is not unique for a given average arrival rate even if ground speed is fixed. Equations (5-12) and (5-13) not only account for the arrival rate, it also accounts for the randomness in the arrival stream. For the same average arrival rate, higher randomness will give a flatter P_T, yielding lower total probability.

The overall total probability gives an estimated percentage of flights in the arrival stream that could execute the procedure without any separation violations. This total probability is an indicator of how well the procedure fits into the actual traffic flow, i.e. without the need to impose a higher target separation at the intermediate metering point. Under lighter traffic conditions, the pdf p_T will shift to the right, yielding higher values of P_T. This means the procedure could be executed with higher levels of confidence. Under heavier traffic conditions, the pdf p_T will shift to the left, yielding lower values of P_T. This means the procedure would be executed with lower levels of confidence.

5.5.3 Sequence-Independent Target Separation

When a higher target separation is used, the pdf of the observed spacing would be similar to the thick gray curve in Fig. 5-9. Following the same derivation described in the previous subsection, the total level of confidence for aircraft sequence i under the adjusted traffic P_{Ta} is given by

$$P_{Ta,i} = \int_0^\infty \left(\int_0^s p_i dx \right) p_{Ta} ds \tag{5-14}$$

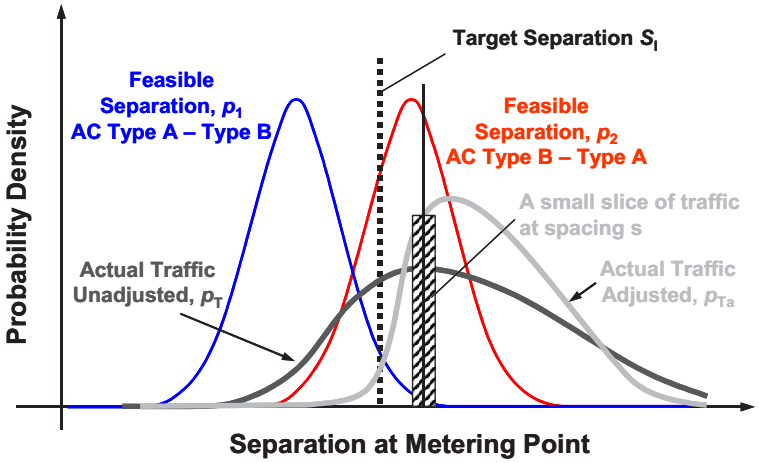

Figure 5-9 Probability under adjusted traffic flow.

The overall total probability P_{Ta} that no separation violation will occur under the adjusted traffic is

$$P_{Ta} = \sum_i P_i \int_0^\infty \left(\int_0^s p_i dx \right) p_{Ta} ds \tag{5-15}$$

As shown in Fig. 5-9, the pdf of the spacing in the adjusted traffic is to the right of the pdf for the unadjusted traffic, resulting in a higher total level of confidence. Thus, the goal of the total probability method is to find a minimum target separation S_I such that the resulting probability density p_{Ta} would assure an overall total probability P_{Ta} that is greater than or equal to the desired value.

When traffic is not heavy, the mean of observed spacing would increase at a much slower rate than the increase in the target separation. In other words, the arrival rate would decrease at a much slower rate than the rate at which the target separation is increased. This is because, when traffic is not heavy, the use of an increased target separation would mostly reduce spacing randomness in the arrival stream rather than increase the mean of observed spacing. However, when traffic is heavy, the increase in the target separation would cause at some point the arrival rate to decrease. In this case, a tradeoff must be made between noise abatement approach and arrival procedure benefits and throughput. This will be discussed in more detail later.

5.5.4 Sequence-Specific Target Separation

The total probability separation analysis method using sequence-specific target separations is illustrated in Fig. 5-10. By using sequence-specific target separations, the spacing at the metering point for each aircraft sequence will be adjusted by the controller based on the target separation for that specific

aircraft sequence, as shown by the pdfs (thick gray curves) for adjusted traffic spacing in Fig. 5-10. Notice that both the means and shapes of the pdfs of the spacing in the adjusted traffic would be different for different target separations. However, these pdfs will likely only depend on the pdfs of the spacing in the unadjusted traffic and the target separations used, but not the aircraft sequence, because controllers probably would not treat each aircraft differently. Based on this assumption, a generic model of pdfs of the spacing in the adjusted traffic may be developed that would be applicable to different aircraft types.

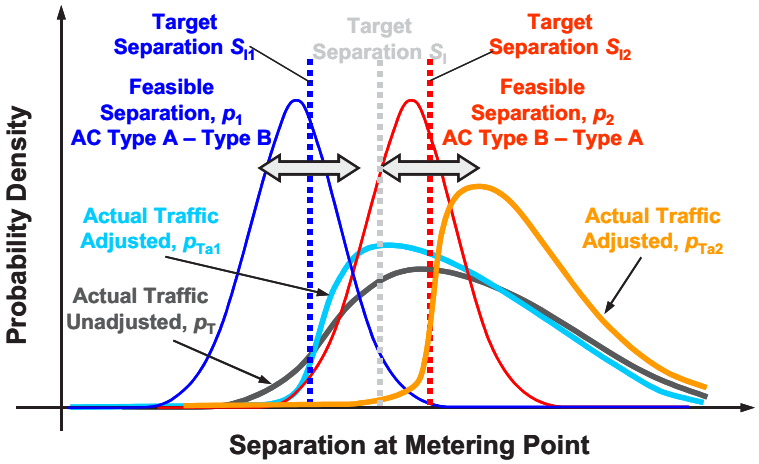

Figure 5-10 Sequence-specific total probability method.

Now the pdf of the spacing in the adjusted traffic stream for aircraft sequence i becomes p_{Tai}. Referring to Fig. 5-8 and 5-9, the probability that aircraft sequence i contained in the small slice of traffic at spacing s could execute the procedure without any separation violations is

$$dP_{Tai,s} = p_{Tai} ds \int_0^s p_i dx \tag{5-16}$$

In Eq. (5-16), subscripts Tai denote that the probability is from the pdf of the spacing in the adjusted traffic under the target separation for aircraft sequence i. Similarly, the total probability that all aircraft pairs of sequence i in the traffic stream could execute the procedure without any separation violations is

$$P_{Tai} = \int dP_{Tai,s} = \int_0^\infty \left(\int_0^s p_i dx \right) p_{Tai} ds \tag{5-17}$$

The overall total level of confidence for all aircraft sequences then becomes

$$P_{Ta} = \sum_i P_i P_{Tai} = \sum_i P_i \int_0^\infty \left(\int_0^s p_i dx \right) p_{Tai} ds \tag{5-18}$$

Note that the sum of probability P_i for all aircraft sequences in the arrival traffic stream is equal to one. Thus, by selecting S_{Ii} such that P_{Tai} is equal to the desired confidence level, the resulting overall total level of confidence would also be equal to the same desired confidence level. This observation offers a simple way to determine sequence-specific target separations using the total probability method, i.e. by determining each target separation independently.

5.6 TRADEOFF ANALYSIS

In both the conditional probability and the total probability separation analysis methods, the individual sequence-specific target separations for each of the aircraft sequences can be determined independently with the same level of confidence. Target separations determined this way treat each of the aircraft sequences equally even though their contribution to throughput or overall level of confidence may very well be different. Under some situations, it may be better to assign different levels of confidence for different aircraft sequences.

For instance, if a specific aircraft sequence requires larger feasible separations than other sequences, and the sequence is rare in the arrival stream, it might not be prudent to simply use a large target separation for this aircraft sequence. Rather, a moderate target separation could be used for this specific aircraft sequence if there is some tolerance for aircraft in this sequence being vectored during the descent when deemed necessary. On the other hand, target separations slightly higher than what are specified by the average confidence level could be used for aircraft sequences that require smaller feasible separations to allow more aircraft of these sequences to perform noise abatement approach and arrival procedures without interruptions. The benefits of this strategy are two folds. First, by using sequence-specific target separations that are determined with different levels of confidence, the throughput may be increased even for the same overall level of confidence, or higher overall level of confidence may be achieved for the same throughput. Second, by eliminating the use of very large target separations that might be nominally required by some rare aircraft sequences, excessive delay to other aircraft behind those aircraft sequences may be avoided.

5.6.1 Trade-off Analysis through Solving Optimization Problems

Two optimization problems can be formulated for sequence-specific target separations using the total probability method. In the first optimization problem, traffic delay is minimized for given overall total level of confidence (the minimum delay problem). Mean adjusted traffic spacing at the metering point is used as the indicator of traffic delay caused by spacing adjustment. A more direct indicator of traffic delay would be the average inter-arrival time. The connection between the two is ground speed. The mean adjusted traffic spacing subject to a single target separation is given in Eq. (5-10). The objective in this problem is to choose sequence-specific target separations S_{Ii} to minimize the mean adjusted traffic spacing

$$E(s_{Ts}) = \sum_i P_i \int_0^\infty p_{Tai} s ds \tag{5-19}$$

subject to the constraint

$$P_{Ta} = \sum_i P_i \int_0^\infty \left(\int_0^s p_i dx \right) p_{Tai} ds \geq P_{Ta}\Big|_{given} \tag{5-20}$$

In the second optimization problem, the objective is to choose S_{Ii} to maximize the overall total level of confidence (the maximum level of confidence problem) as given in Eq. (5-18), for given traffic conditions, i.e. the mean adjusted traffic spacing shall not exceed the mean unadjusted traffic spacing

$$E(s_{Ta}) \leq E(s_T) \tag{5-21}$$

In other words, no additional delay shall be introduced. The mean unadjusted traffic spacing is given in Eq. (5-9). For the sake of clarity, the second problem is rewritten as choosing S_{Ii} to maximize

$$P_{Ta} = \sum_i P_i \int_0^\infty \left(\int_0^s p_i dx \right) p_{Tai} ds \tag{5-22}$$

subject to the constraint

$$\sum_i P_i \int_0^\infty p_{Tai} s ds \le \int_0^\infty p_T s ds \tag{5-23}$$

In the first optimization problem (the minimum delay problem), defined by Eq. (5-19) and (5-20), additional delay may have to be introduced as the given level of confidence increases. In the second optimization problem (maximum level of confidence problem), defined by Eq. (5-22) and (5-23), the level of confidence may be limited to a certain level when the traffic is heavy. The solution from maximum level of confidence problem gives the highest overall level of confidence that could be achieved without introducing additional delay. The solution from the minimum delay problem, on the other hand, gives the maximum throughput (connected to minimum spacing via ground speeds) that could be achieved for the given desired overall total level of confidence.

Although detailed analyses of noise abatement approach and arrival procedure benefits and delay penalties are out of the scope of this thesis, the formulation of the two optimization problems provides bases for more rigorous tradeoff analysis in the future. This tradeoff may be illustrated as follows. To maintain throughput, the average spacing at the metering point needs to be kept as low as possible so that additional delay is not imposed to upper stream traffic. This suggests the selection of a target separation that is as close as possible to the separation minima or MIT restrictions currently being used, or the use of a relatively low level of confidence. However, the benefits of noise abatement approach and arrival procedures are best achieved when there are no interruptions to the low noise descent leg. This suggests the selection of larger target separations, or a relatively high level of confidence. The optimum solution is a tradeoff between the solutions of the two problems. It is important to note that this tradeoff is only possible because of the controller's ability to predict separation violations and intervene when necessary. Additionally, the location of the intermediate metering point may be moved towards or away from the runway to search for a better design if the optimal solution at the current metering point is not satisfactory.

5.6.2 Simplified Optimization Problems

Since knowledge of pdf p_{Iai} of adjusted traffic for any arbitrary target separation is not readily available, the above two optimization problems could not be easily solved. However, they can be reduced to a simplified form. Assuming only the aircraft mix is known, the minimum delay problem becomes to choose sequence-specific target separation S_{Ii} to minimize the weighed average target separation

$$E(S_{Ii}) = \sum_i P_i S_{Ii} \tag{5-24}$$

subject to the constraint that the weighed average of conditional levels of confidence is greater than or equal to the given value, i.e.

$$E(P_{Ri}) = \sum_i P_i \int_0^{S_{Ii}} p_i dx \geq P_R\Big|_{given} \tag{5-25}$$

The maximum level of confidence problem becomes to choose squence-specific target separation S_{Ii} to maximize the weighed average of conditional levels of confidence

$$E(P_{Ri}) = \sum_i P_i \int_0^{S_{Ii}} p_i dx \tag{5-26}$$

subject to the constraint that the weighed average target separation is less than or equal to the given value, i.e.

$$E(S_{Ii}) = \sum_i P_i S_{Ii} \leq S_I\Big|_{given} \tag{5-27}$$

The same tradeoff principle can now be applied to the solutions of the two simplified optimization problems to obtain sequence-specific target separations.

5.6.3 On the Use of Sequence-Specific Target Separations

In current practice, MIT restrictions at the metering point or hand-off point are given as a single number for the entire traffic stream at any given time. Using sequence-specific target separations will increase the number of variables for the controller to work with. For example, with two aircraft types A and B, four aircraft sequences exist, i.e. type A leading type A, type A leading type B, type B leading type A, and type B leading type B. As the number of aircraft types increases, the number of aircraft sequences increases geometrically. To be practical, the number of sequence-specific target separations must be limited to a manageable level.

More over, MIT restrictions are discretized[4], often in increments of 5 nm. However, the optimal target separations are continuous variables and thus may fall between the discrete MIT restriction values currently in use. These target separations must also be discretized to some degree for easy handling. As an option, aircraft sequences with similar feasible separation distributions could be consolidated to simplify the scenario. The optimization method could then be modified to accommodate the discretization requirement. In any case, for optimal performance, the discretization step size will have to be reduced from the commonly used 5 nm.

5.7 SUMMARY

A methodology for analyzing separation between consecutive aircraft performing the same noise abatement approach or arrival procedure was presented. This methodology provides means to determine target separations at the intermediate metering point to allow for uninterrupted operation of noise abatement approach or arrival procedures with certain levels of confidence. The methodology also provides means to evaluate the suitability of the procedure operation concept under given traffic conditions. The methodology could be applied using aircraft trajectories obtained from radar tracks or simulation.

The conditional probability method directly connects target separations at the intermediate metering point with conditional levels of confidence. The total probability method, utilizing probability

distribution of the spacing in the arrival traffic, gives more realistic estimation of levels of confidence for given target separations in real world environment. The sequence-independent target separation is easy to use, but sequence-specific target separations may provide additional throughput benefits. The selection of which method to use should be based on data availability, traffic conditions, and existing controller practices at the site. Further discussion on this can be found in the next chapter.

The formulation of the minimum delay optimization problem and the maximum levels of confidence problem provides bases for rigorous tradeoff analysis. Solving these two problems and detailed analyses of noise abatement benefits and delay penalties provide research opportunities for the future.

Although the methodology was specifically developed for solving the separation analysis problems for noise abatement approach and arrival procedures, it may also be used more generally for any approach or arrival procedure, such as the Area Navigation (RNAV) arrival procedures[5], that have a predefined lateral flight path.

REFERENCES

[1] "Air Traffic Control," FAA Order 7110.65R, February 16, 2006

[2] "Aeronautical Information Manual – Official Guide to Basic Flight Information and ATC Procedures," FAA, February 16, 2006.

[3] Ren, L., Clarke, J.-P. B., and Ho, N. T., "Achieving Low Approach Noise without Sacrificing Capacity," *Proceedings: the 22nd Digital Avionics Systems Conference (22nd DASC)*, Vol. 1, Indianapolis, Indiana, Oct. 12-16, 2003, pp. 1.E.3 - 1-9.

[4] Kopardekar, P., Green, S., Roherty T., and Aston, J., "Miles-In-Trail Operations: A Perspective," AIAA-2003-6700, *AIAA's 3rd Annual Aviation Technology, Integration and Operations (ATIO) Forum*, Denver, Colorado, Nov. 17-19, 2003.

[5] Ren, L. and Clarke, J.-P., "A Separation Analysis Methodology for the Design of RNAV Arrival Procedures," Under review, submitted to *Journal of Guidance, Control, and Dynamics*.

CHAPTER 6

THE UTILITY AND APPLICATION OF THE DESIGN FRAMEWORK, METHODOLOGY, AND TOOLS

NOMENCLATURE

C	=	traffic throughput in aircraft per hr
C_i	=	traffic throughput for aircraft sequence i
$E(\ )$	=	expectation, mean, average operator
$\hat{E}(\ )$	=	sample mean
i	=	index of aircraft sequence in arrival traffic
k	=	order of Erlang probability density function
$\hat{k}$	=	estimated order of Erlang probability density function
P_{Ri}	=	conditional level of confidence for aircraft sequence i
P_T	=	total level of confidence
P_{Ta}	=	total level of confidence under adjusted arrival traffic
s	=	spacing
s_i	=	spacing for aircraft sequence i
S_I	=	target separation
S_{Ii}	=	sequence-specific target separation for aircraft sequence i
β_f	=	final separation buffer
β_{fi}	=	final separation buffer for aircraft sequence i
λ	=	parameter of Erlang probability density function
$\hat{\lambda}$	=	estimated parameter of Erlang probability density function
σ	=	standard deviation
σ_s	=	standard deviation of spacing in arrival stream
$\hat{\sigma}_s$	=	sample standard deviation of spacing in arrival stream

6.1 INTRODUCTION

The procedure design and operational framework, the Monte Carlo based aircraft trajectory simulation tool, and the separation analysis methodology form a Tool for Analysis of Separation And Throughput (TASAT). As a vital part of this research, the application of TASAT has been demonstrated through a simulation study and a flight test. As stated earlier in this thesis, the goal of this research is to efficiently manage separation between aircraft performing noise abatement approach and arrival procedures so that these procedures can be implemented widely to benefit the communities and operators, as well as to ease

the constraint on traffic growth. Pertinent to this goal, analyses have also been done to determine the impact of operational conditions and procedure design parameters on traffic throughput.

The TASAT is currently being applied to approach and arrival procedure development projects at a number of airports in the US and Europe. These airports include Nottingham East Midlands Airport[1] and London Gatwick Airport[2] in UK, Los Angeles International Airport[3] and Hartsfield-Jackson Atlanta International Airport[4] in the US, and several other airports. The Continuous Descent Arrival (CDA) flight test conducted in September 2004 at Louisville International Airport (KSDF) was the first project in which the separation analysis methodology was successfully applied. The CDA procedure developed for the KSDF 2004 flight test was used as the numeric example in the simulation study to be presented. The analyses of data collected during the KSDF 2004 CDA flight test are also to be presented in this chapter to demonstrate the effectiveness of the tool developed. It is thus necessary to provide some background information about the flight test project and to provide details of the procedure design before proceeding to further discussions.

KSDF is the major hub for UPS overnight package delivery operations. Due to the nature of its business, most UPS flight operations at KSDF occur during the night. Each weekday, about 100 jet transport aircraft (mostly UPS package freighters) land at KSDF in a four-hour period between 10:00 PM and 03:00 AM. This is the period when residents are most sensitive to noise disturbance. Thus, KSDF becomes a perfect candidate site for conducting noise abatement arrival procedure studies. KSDF has three runways: runway 17R/35L, its parallel runway 17L/35R, and runway 11/29. Because of the ramp configuration of the UPS sorting facility at the airport, runway 17R/35L is the preferred runway for the majority of UPS night arrivals.

In an effort to advance the development of noise abatement approach procedures, a research team consisting of members from Massachusetts Institute of Technology, Boeing, Federal Aviation Administration (FAA), Louisville Regional Airport Authority (RAA), National Aeronautics and Space Administration (NASA), and UPS designed a continuous descent approach procedure for runway 17R at KSDF. The research team conducted a flight demonstration test at KSDF in 2002 using UPS B767-300 revenue flights to evaluate the operational characteristics and to demonstrate the noise-reducing potential of this advanced noise abatement procedure. This procedure was shown to reduce the maximum A-weighted sound level (LAMAX) noise at seven locations along the flight path by 3.9 to 6.5 dBA and reduce the fuel burn during approach by 400 to 500 lb[5].

In 2004, to further the development and the implementation of CDA procedures, the research team undertook the development of a CDA procedure that could be used regularly during nighttime by UPS aircraft destined to runways 17R or 35L at KSDF from origins in the Western United States. A flight test involving 12 to 14 UPS B757-200 and B767-300 revenue flights each night was conducted to demonstrate the consistency of the procedure and the effectiveness of the separation analysis methodology; to measure the reductions in noise, emissions, fuel burn and time; and to obtain the data necessary for approval to use the procedure on a regular basis. In the KSDF 2002 study, managing separation between consecutive flights was purposely omitted to expedite the research project in that only one flight performed a continuous descent approach each night. However, managing separation effectively is essential for the implementation of CDA procedures in a real world environment; as such, it became an integrated part of the 2004 research effort.

The arrival chart used in the KSDF 2004 CDA flight test is shown in Fig. 6-1. As mentioned earlier in this thesis, this is an Area Navigation (RNAV) based CDA. The lateral flight path would be managed by the Flight Management System (FMS) Lateral Navigation (LNAV) function. The nominal lateral flight path was a routing via waypoints CENTRALIA, ZARDA, PENTO, SACKO, to CHERI and then to either runway 17R or 35L. The runway to be used depends on the prevailing winds on a given day. If the wind

were from the south, the CDA to runway 17R would be in effect (southern flow). If the wind were from north, the CDA to runway 35L would be in effect (northern flow). The vertical profile would be a continuous descent starting at cruise altitude and follow the FMS computed Vertical Navigation (VNAV) defined by altitude and speed constraints given at waypoints TRN17, CHR27, and CHRCL for the CDA to runway 17R, or waypoints TRN35, CRD27, and CRDNL for the CDA to runway 35L. The characteristics of the vertical profile are shown in Fig. 2-16. Ideally, the engine throttle would remain at idle until the aircraft is established on the final approach. Two shallower segments are facilitated by the FMS to allow proper deceleration. The first of these shallower segments is at 10,000 ft allowing aircraft to decelerate to a Calibrated Airspeed (CAS) of 240 kt. For turbojet aircraft operating below 10,000 ft, Air Traffic Control (ATC) requires that the speed shall not exceed an Indicated Airspeed (IAS) of 250 kt. CAS 240 kt is used by many FMS as the default value to leave a 10 kt speed buffer. Note that for aircraft with FMS, the airspeed displayed to the pilot is the same as CAS. The second shallower segment is at 3,800 ft allowing aircraft to decelerate to CAS 180 kt; the speed at which the aircraft is configured for the final approach. During the flight test, the waypoint SACKO was used as the intermediate metering point.

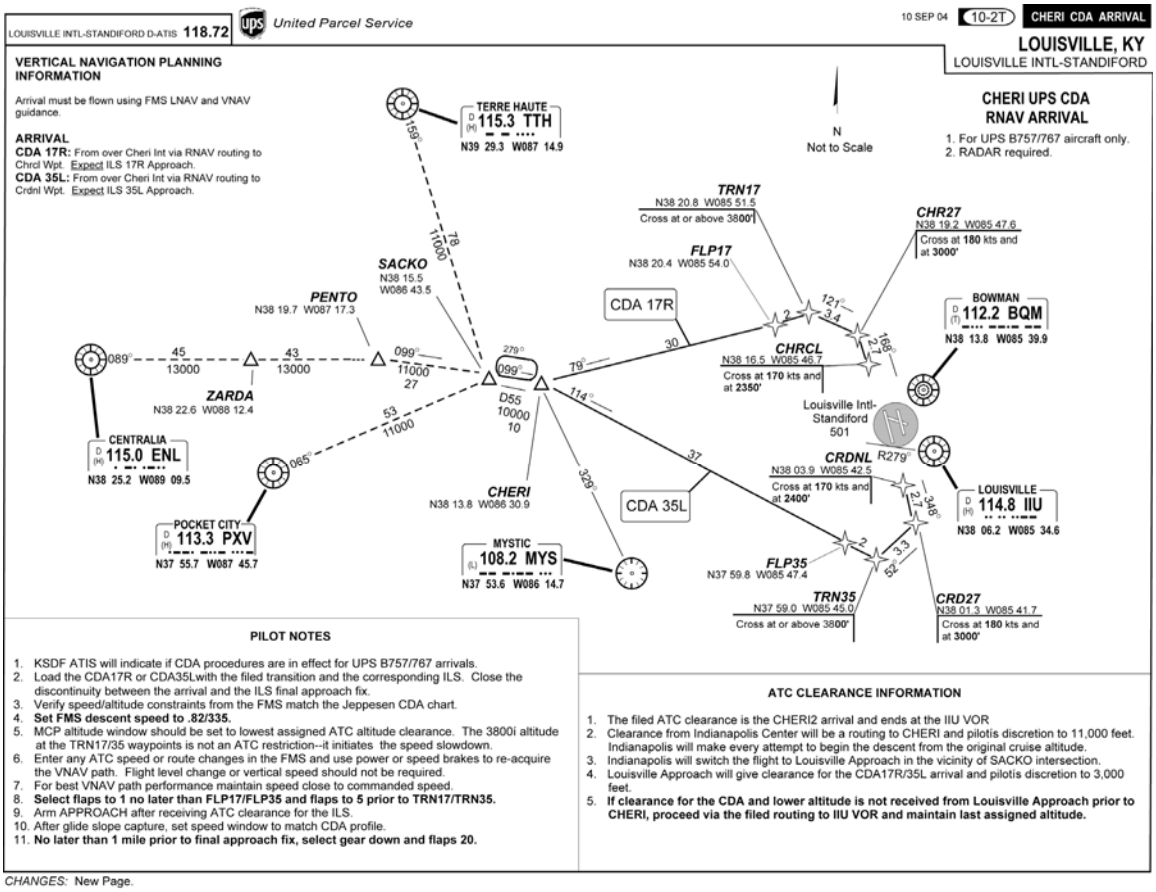

Figure 6-1 Chart used in the KSDF 2004 RNAV CDA flight test.

The remainder of this chapter is organized as follows: The results of the simulation studies are presented in the next section. The application of the separation analysis methodology is demonstrated through applying the conditional probability separation analysis method and the total probability separation analysis method on simulated aircraft trajectories. The contributions of winds and the effect of the location of the intermediate metering point are also presented. The analyses of data collected during the KSDF 2004 CDA flight test are presented in Section 6.3. Spacing in the arrival stream at the

intermediate metering point and observations on separation management during the flight test are described in detail. It follows a separation analysis based on aircraft trajectories extracted from radar tracks. Flight test results are compared with simulation results to show the effectiveness of the Monte Carlo simulation tool and the separation analysis methodology. The summary of this chapter is provided in the last section.

6.2 THE SIMULATION STUDY

A simulation study was conducted to both illustrate how the separation analysis methodology and the Monte Carlo simulation tool are applied, and to determine the impact of winds and the location of the intermediate metering point on traffic throughput. The results of this study are presented in this section.

6.2.1 Simulation Setup

The noise abatement arrival procedure used in the simulation study to be presented was based on the RNAV CDA developed for the KSDF 2004 flight test. To be concise, only the results for the CDA to runway 35L are presented in detail. This runway configuration was selected because it was the most commonly used configuration due to the local wind conditions. The altitude and speed constraints that define the vertical profile of the simulation procedure are listed in Table 6-1. Notice that the altitude constraint at waypoint TRN35 for the simulation procedure is 200 ft higher than the flight test procedure. The reason is that the altitude constraint at TRN35 was reduced from 4,000 ft to 38,000 ft for the flight test procedure to assure proper capturing of Instrument Landing System (ILS) glide slope from below. However, the separation analysis results to be presented should be valid for both procedures. The descent speed was CAS 335 kt from cruise to 10,000 ft, and CAS 240 kt (the FMS default value) from 10,000 ft to the point where the aircraft began decelerating to satisfy the first speed constraint.

Table 6-1 Vertical constraints for CDA to runway 35L.

Waypoint	Distance, nm	Altitude, ft	CAS, kt
TRN35	-11.45	Above 4000	/
CRD27	-8.14	3000	180
CRDNL	-5.79	2400	170
Runway	0	/	/

Two aircraft types, B757-200 (B757) and B767-300 (B767), were simulated with random landing weights as defined in Table 6-2. The random pilot response model described in Subsection 3.3.1 was used. Nominal wind profiles and inter-flight wind variation were modeled using ACARS data reported between 10:00 PM–3:00 AM local standard time each day during a period of 6 months from February 10 to August 12, 2004. Three nominal wind profiles were used in the simulation: the mean wind profile, the zero wind profile, and a hypothetical head wind profile. The mean wind profile for KSDF (shown in Fig. 4-30 as the solid curves) would be a tail wind condition during most part of the arrival, and a crosswind

Table 6-2 Landing weight parameters, lb.

	B757-200	B767-300
Mean	167,539	262,205
Standard Deviation	11,000	18,000
Minimum	146,617	229,271
Maximum	194,534	298,183

condition during the final approach. The hypothetical head wind profile had the same wind speed profile but with the wind directions flipped about the line of longitude at the airport so that it would be experienced as a head wind condition during most of the arrival and as a crosswind condition during the final approach. For a given scenario, each aircraft type was simulated 200 times in the leading position and 200 times in the trailing position. For the two aircraft types, a total of 800 trajectories were simulated in each scenario.

6.2.2 Feasible Separations, the Target Separation and the Application of Conditional Probability Method

In this scenario, the KSDF mean wind profile was used as the nominal wind profile. The probability density functions (pdfs) of the feasible separations at SACKO, which is a waypoint at along track distance of -60.46 nm or about 10 nm west of the Terminal Radar Approach Control (TRACON) boundary, were obtained from simulated trajectories. Note that the along track distance is defined as the distance along the nominal flight path in the direction of flight, with zero at the runway threshold. The results are shown in Fig. 6-2. Among the four possible aircraft sequences, the sequence of B767 leading B757 had the largest values of feasible separations. This was partially because this sequence has the largest final separation minimum among the four – 5 nm while the other three sequences require 4 nm. Another factor was that the B757 aircraft, which was in the trailing position, had larger trajectory variations. This latter factor can also be seen by comparing the sequence of B757 leading B757 with the sequence of B767 leading B767.

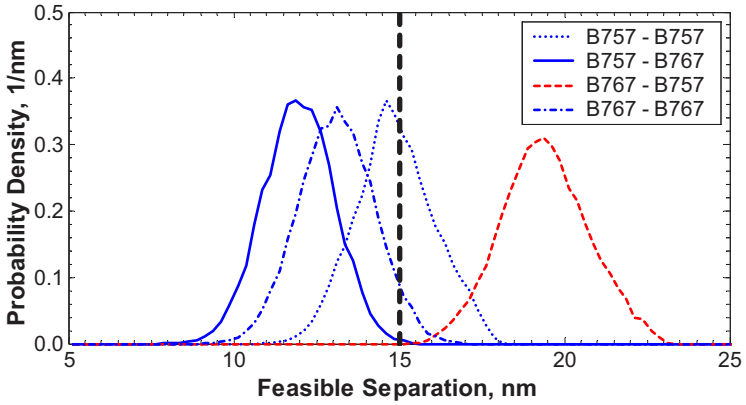

Figure 6-2 Feasible separations at SACKO.

The pdfs of the final spacing are shown in Fig. 6-3 for a hypothetical target separation of 15 nm at SACKO. The two vertical lines indicate the separation minima at the runway threshold. The vertical line on the right is for the sequence of B767 leading B757, the vertical line on the left is for the other three aircraft sequences.

The traffic throughput of an ideal case was examined first. The ideal case implies that trajectory variations were predicted precisely as they would happen and that the spacing at the metering fix for each consecutive aircraft pair was set exactly to the corresponding feasible separation for that aircraft pair. This means there would be no capacity loss in accommodating uninterrupted noise abatement arrival procedure execution, and that the final separation buffer would be nearly zero. Thus, throughputs for the ideal case indicate system capacity for the given aircraft mix and wind condition. For the ideal case, the traffic throughput C and the mean $E(s)$ of spacing at the intermediate metering point for each aircraft sequence i for the ideal case are listed in Table 6-3 as the group on the left. The average throughput

values in the table are not averages of the individual aircraft sequences. They were directly computed from the mean of time intervals at SACKO. The average throughput was 31.40 aircraft per hr for the ideal case.

Table 6-3 Conditional levels of confidence and traffic throughputs.

Aircraft Type/Sequence	Ideal Case C_i 1/hr	Ideal Case $E(s_i)$ nm	S_I = 15 nm P_{Ri}	S_I = 15 nm C_i 1/hr	S_I = 15 nm β_{fi} nm
B757 – B757	32.04	14.88	55.5%	31.78	0.05
B757 – B767	37.42	11.96	99.9%	30.08	1.01
B767 – B757	24.84	19.41	0.0%	31.78	-1.30
B767 – B767	34.24	13.11	95.2%	30.08	0.62
Average	31.40	14.84	62.7%	30.91	0.09

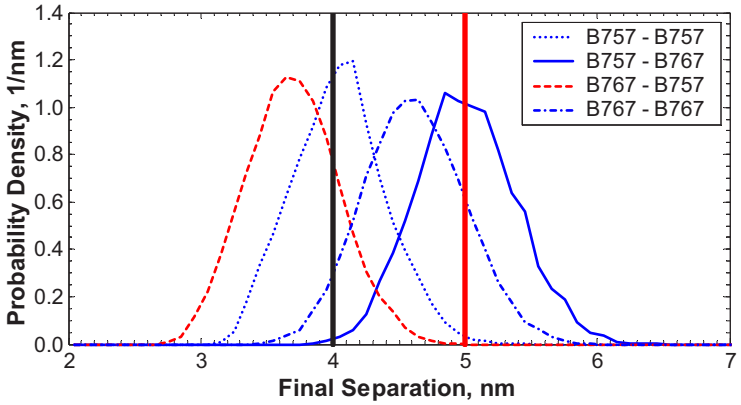

Figure 6-3 Final spacing given 15 nm at SACKO.

For a sequence-independent target separation of 15 nm (the target separation used in the flight test), conditional levels of confidence for the four aircraft sequences can be computed using either the pdfs of the feasible separations shown in Fig. 6-2, or the pdfs of the final spacing shown in Fig. 6-3. The results are listed in Table 6-3 as the group on the right. Again, it is important to note that for a different target separation, the pdfs need to be regenerated for the final spacing while the pdfs for the feasible separations can be reused for any target separation values. The 15 nm target separation yielded an average conditional level of confidence P_R of 62.7% and an average final separation buffer β of 0.09 nm. However, the conditional level of confidence and final separation buffer vary drastically from aircraft sequence to aircraft sequence. The average throughput for a 15 nm target separation was 30.91 aircraft per hr, very close to the average throughput for the ideal case. Note that the averages in Table 6-3 were not weighted. Thus, they are only applicable to scenarios where there is 50% of each aircraft type. For the CDA to runway 17R, the average conditional level of confidence was 68.2%, and the average throughput was 29.62 aircraft per hr.

To illustrate the effect of sequence-specific target separations on traffic throughput, a conditional level of confidence of 75% was chosen. The corresponding sequence-independent target separation was determined to give an average conditional level of confidence of 75%. The corresponding sequence-specific target separations were determined to give the conditional confidence level of 75% for each aircraft sequence. The target separations, traffic throughputs, and final separation buffers are listed in

Table 6-4 for both cases. The sequence-independent target separation determined was 17.07 nm. The average of the sequence-specific target separations was 15.63 nm, or 1.44 nm lower than the sequence-independent target separation. This 1.44 nm reduction in average target separations was the benefit of using sequence-specific target separations for the conditional level of confidence of 75%. It is seen from Table 6-4 that for the same average conditional level of confidence, by using sequence-specific target separations, the final separation buffer was reduced and more evenly shared by all aircraft sequences. The average traffic throughput was increased from 27.31 to 29.85, by more than 2 aircraft per hr. Based on queueing theory, as the system is operating at near capacity, even a small improvement in traffic throughput would significantly reduce system delay[6].

The traffic throughput values listed in Tables 6-3 and 6-4 only have theoretical meaning because in real world situations, the actual spacing at the intermediate metering point would not be exactly equal to the target separations.

Table 6-4 Sequence-independent vs. sequence-specific target separations.

	S_I = 17.07 nm			P_{Ri} = 75.0 %		
Aircraft Type/Sequence	P_{Ri}	C_i 1/hr	β_{fi} nm	S_{Ii} nm	C_i 1/hr	β_{fi} nm
B757 – B757	96.3%	28.08	0.67	15.67	30.47	0.25
B757 – B767	100.0%	26.59	1.73	12.69	35.34	0.24
B767 – B757	3.7%	28.08	-0.71	20.29	23.80	0.30
B767 – B767	100.0%	26.59	1.31	13.89	32.39	0.25
Average	75.0%	27.31	0.75	15.63	29.85	0.26

To further illustrate the relationship between the sequence-independent target separation and the corresponding sequence-specific target separations, a series of conditional levels of confidence were examined. For each of the conditional levels of confidence, sequence-independent target separation and sequence-specific target separations were determined in the same way as the values in Table 6-4 were determined. The sequence-independent target separations and the averages of sequence-specific target separations are plotted in Fig. 6-4 versus conditional levels of confidence. It is seen that, at lower levels of confidence, i.e. below 65% in the simulated case, sequence-specific target separations would actually reduce efficiency. As the level of confidence became greater than 65%, sequence-specific target separations began to improve efficiency; the higher the levels of confidence, the higher the benefits sequence-specific target separations would provide relative to a sequence-independent target separation. The reason behind this is graphically illustrated in Fig. 5-5, and explained earlier in Chapter 5.

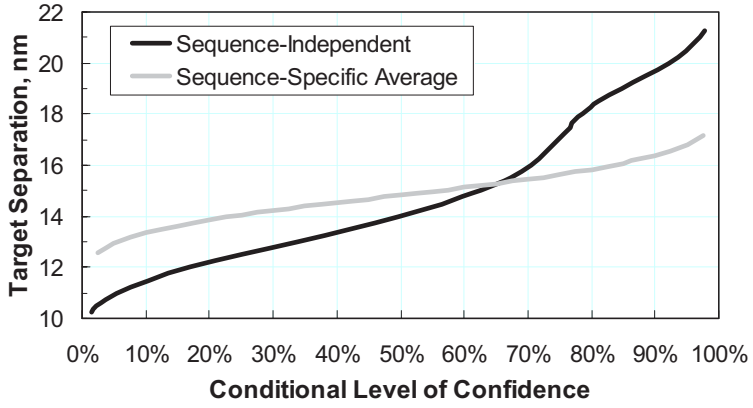

Figure 6-4 Target separation vs. level of confidence.

6.2.3 The Application of the Total Probability Method

As discussed before, the total probability method can be used to examine how well the procedure fits into a given unadjusted traffic flow. To demonstrate the application of the total probability separation analysis method, the spacing in the arrival stream at SACKO was extracted from Automated Radar Terminal System (ARTS) data via the UPS ground management system. Details of the ARTS data used in this analysis are explained in Subsection 6.3.1 of this chapter. Flights arrived between 22:00 PM and 3:00 AM local standard time on 28 days between September 14 and December 1, 2004 were examined. On 18 of these 28 days, the normal 10 nm Miles-in-Trail (MIT) restriction was in effect. On the remaining 10 days, i.e. during the CDA flight test period from September 14 to September 25, a 15 nm target separation was in effect. In total, 131 flight pairs were selected from the arrival stream under the 10 nm MIT, and 69 flight pairs were selected from the arrival stream under the 15 nm target separation. The criteria for selecting these flight pairs were: a) the spacing at SACKO between a flight pair was less than or equal to 30 nm – larger spacing are considered as gaps in the arrival flow; b) no flights from other entry points had landed on the same runway between the flight pair – sepaaration values become meaningless between the pair of aircraft.

The estimated pdfs of the spacing in the arrival stream are shown as bar charts in Fig. 6-5. Traffic under the 10 nm MIT and the 15 nm target separation are denoted as the unadjusted traffic and the adjusted traffic respectively. It is normal that at times, the MIT restrictions might not be satisfied, as shown by the bars on the left of vertical lines at 10 nm and 15 nm for the unadjusted traffic and the adjusted traffic respectively. However, there were no observations of spacing below the separation minimum of 5 nm in effect at SACKO. Estimated parameters of the spacing in the arrival stream such as mean $E(s)$ and standard deviation σ_s are listed in Table 6-5. It is seen that although the average traffic spacing was increased by using a larger target separation (or a larger MIT restriction), the standard deviation was decreased – indicating a reduction in randomness. It is also seen that as the target separation increases, the average traffic spacing increases by a smaller amount than the corresponding increase in the target separation.

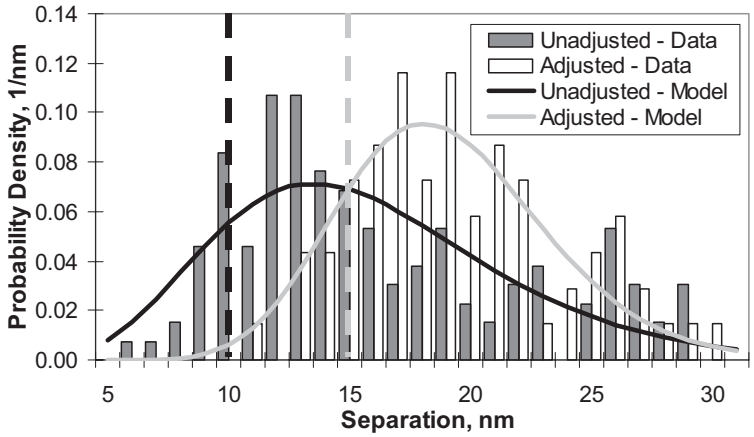

Figure 6-5 Traffic spacing at SACKO.

An Erlang probability density function[6] was fit to model the spacing data. The Erlang distribution is bounded to positive values, and it has a smaller standard deviation (randomness) than the exponential distribution that is commonly used to model inter-arrival times. Because spacing in an arrival stream are adjusted by the controller to meet the separation minima or MIT restrictions, Erlang pdf could be a proper one to use. The Erlang pdf is given by

$$p(s) = \begin{cases} \dfrac{\lambda^k s^{k-1} e^{-\lambda s}}{(k-1)!} & k = 1, 2, \ldots; s \geq 0 \\ 0 & \text{otherwise} \end{cases} \tag{6-1}$$

where s is the spacing in the arrival stream; and k is referred to as the order of the Erlang pdf. For any set of given parameters, the mean and variance of the Erlang distribution are

$$\begin{cases} E(s) = k / \lambda \\ \sigma_s^2 = k / \lambda^2 \end{cases} \tag{6-2}$$

Given estimated mean and variance (denoted by hat), from Eq. (6-2), parameters of the Erlang model can be estimated as

$$\begin{cases} \hat{k} = \text{round}(\hat{E}^2(s) / \hat{\sigma}_s^2) \\ \hat{\lambda} = \hat{k} / \hat{E}(s) \end{cases} \tag{6-3}$$

The Erlang approximations to the pdfs of traffic spacing are shown as the solid black curve and the light gray curve in Fig. 6-5 for the 10 nm MIT and 15 target separation respectively. The estimated model parameters are listed in Table 6-5. It is seen from Fig. 6-5 that the models fit the data well. With sufficient radar data or simulation data, a generic model for a specific metering point may be developed as a function of the mean of spacing in the unadjusted traffic, the standard deviation of the unadjusted traffic spacing, and the target separations. This provides another opportunity for future research.

Table 6-5 Spacing parameters in arrival traffic.

Traffic Condition	Traffic Data		Model	
	$E(s)$ nm	σ_s nm	$\hat{k}$	$\hat{\lambda}$, 1/nm
Unadjusted	15.79	5.88	7	1.050
Adjusted	19.05	4.28	20	0.443

With the distributions of the spacing in the arrival stream known, the total levels of confidence for the unadjusted traffic and the adjusted traffic can be computed using Eq. (5-13) and Eq. (5-15) respectively. The results listed in Table 6-6 are for a 50-50 traffic mix of B757 and B767 that is randomly sequenced such that there is 25% of each of the four aircraft sequences. The computation was based on the pdfs of the feasible separations shown in Fig. 6-2 and the models of the spacing in arrival traffic shown in Fig. 6-5.

Table 6-6 Total levels of confidence assuming 50-50 traffic mix of B757 and B767.

Sequence	P_T (S_I = 10 nm)	P_{Ta} (S_I = 15 nm)
B757–B757	52.0%	83.6%
B757–B767	72.1%	96.4%
B767–B757	25.5%	45.4%
B767–B767	64.3%	92.8%
Overall	53.5%	79.6%

Comparing Table 6-6 with Table 6-3 and Fig. 6-4, it is seen that the total levels of confidence are higher than the conditional levels of confidence for the same target separation. For a target separation of 10 nm, the average (as if weighted by 50-50 traffic mix) of the conditional levels of confidence was less than 10%, while the total level of confidence was 53.5%. For a target separation of 15 nm, the average of the conditional levels of confidence was 62.7%, while the total level of confidence was 79.6%. While the conditional level of confidence of 62.7% seems not to be very high, it worked well during the flight test, because the actual probability seen by the controllers was the total level of confidence – an estimated value of 79.6% which is higher. The total levels of confidence for the CDA to runway 17R were 58.7% and 85.0% for the unadjusted and the adjusted traffic respectively. The total confidence levels were higher for the CDA to runway 17R because the flight path was about 7 nm shorter than the CDA to runway 35L.

As these results illustrate, the total probability method provides a more complete view of the relationship between the target separations and the levels of confidence in a real world environment. However, extra effort is needed to obtain the distribution of the spacing in the traffic stream. Often, data are not readily available for adjusted traffic with different target separations. Nevertheless, it is very important to at least check traffic conditions such as traffic mix and arrival rate even if the total probability method were not to be applied due to cost and time constraints. It is also important to note that, should the same level of confidence be desired, the total probability method would yield a smaller target separation.

Given the minimum acceptable total level of confidence, the traffic condition allowing CDA to be performed can be determined. More data collected from the field will be needed to determine what would be the acceptable level of confidence, and what are the factors affecting the acceptable level of confidence. This would be an opportunity for future research. In current applications[3,4], 70% is often used as a starting point[*].

6.2.4 The Contributions of Winds

The effects of inter-flight wind variations were examined first. In this analysis, the mean wind profile was used as the nominal wind profile, and the pdfs of feasible separations were obtained from trajectories simulated without inter-flight wind variations. The results are shown in Fig. 6-6. A comparison with Fig. 6-2 will reveal that without inter-flight wind variations, the distribution of the feasible separation became narrower. This is further illustrated by a comparison of means and standard deviations in Table 6-7. Although there is no big difference between the means of the feasible separations, the standard deviations were reduced significantly when there were no wind variations. This means that larger wind variations would normally reduce conditional levels of confidence for a given target separation. The effect would be most significant when sequence-specific target separations were to be used. These results suggest that it is important to model wind variation accurately.

The effects of the magnitude of the nominal wind profile were also examined. Simulations were conducted with different nominal wind profiles: the mean wind profile, the zero wind profile, and a

[*] In response to a question about if a level of confidence of 70% is acceptable during the third CDA workshop hosted at Georgia Institute of Technology September 6-7, 2006, Walter White of Southern California TRACON stated that 70% is a balance between workload and efficiency. It is a starting point to be evaluated. In many cases today, the operational level of confidence can be as low as 10%, meaning that up to 90% of the approach flights require controller intervention in the form of either a speed assignment or vector to maintain separation or to keep proper spacing.

Table 6-7 The effect of inter-flight wind variations.

	With wind variations		Without Wind Variations	
Sequence	$E(s_i)$ nm	σ nm	$E(s_i)$ nm	σ nm
B757–B757	14.88	1.18	14.84	0.597
B757–B767	11.96	1.06	12.00	0.451
B767–B757	19.41	1.31	19.37	0.724
B767–B767	13.11	1.13	13.15	0.578
Average	14.84		14.84	

hypothetical head wind profile. The mean wind profile for KSDF would be experienced as a tail wind during most part of the arrival, and as a crosswind during the final approach. It is therefore referred to as tail wind profile in the following discussions. The hypothetical head wind profile had the same wind speed profile but with the wind directions mirrored about the line of longitude at the airport so that it would be experienced as a head wind during most part of the arrival and as a crosswind during the final approach. Distributions of the feasible separations were obtained for each wind profile. The means and standard deviations are shown in Fig. 6-7. The standard deviations are presented as error bars on top of the mean values. The means and standard deviations of feasible separations for the tail wind, zero wind, and head wind profiles are listed in Table 6-8.

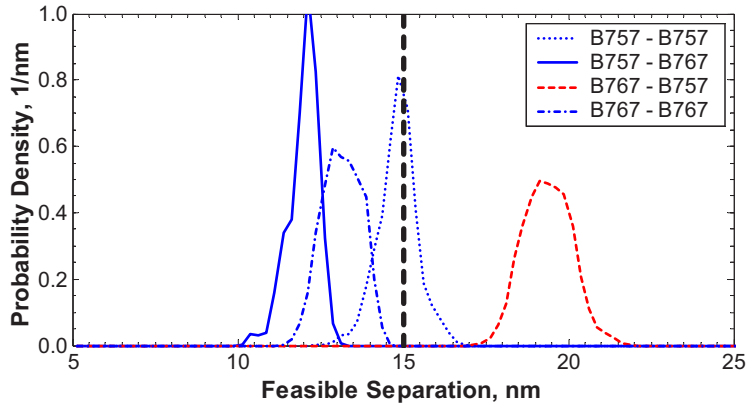

Figure 6-6 Feasible separations at SACKO, without inter-flight wind variations.

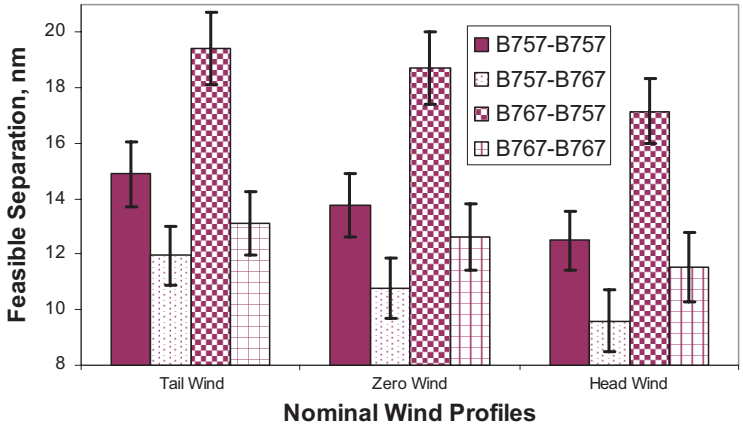

Figure 6-7 The effect of nominal wind profiles.

Table 6-8 The tail wind, zero wind and head wind results, nm.

	Tail Wind		Zero Wind		Head Wind	
Sequence	$E(s_i)$	σ	$E(s_i)$	σ	$E(s_i)$	σ
B757–B757	14.88	1.18	13.78	1.13	12.49	1.04
B757–B767	11.96	1.06	10.78	1.09	9.60	1.11
B767–B757	19.41	1.31	18.70	1.30	17.16	1.17
B767–B767	13.11	1.13	12.60	1.20	11.52	1.26
Average	14.84		13.97		12.69	

From Fig. 6-7 and Table 6-8, it is seen that the means of the feasible separations were higher under the tail wind and lower under the head wind relative to the zero wind. The sequence-independent target separations at SACKO for an average conditional level of confidence of 62.7% were 15 nm, 14.12 nm, and 12.94 nm for the tail wind, the zero wind, and the head wind respectively. These results suggest that different target separations could be used for different wind conditions, especially when the differences in wind speeds are large.

6.2.5 The Effect of the Location of the Intermediate Metering Point

The effect of the location of the intermediate metering point on target separations was also studied. To this end, the distributions of the feasible separations were determined at three additional waypoints: CHERI (the current ATC handoff point, at along track distance -50.38 nm), a point at -35 nm, and a point at -25 nm. The distances between points are 10 to 15 nm. At -25 nm on the flight path, the altitude of a noise abatement approach procedure could still be around 7,000 ft. Noise reduction benefits can still be preserved. The mean wind profile was used as the nominal wind profile. The means and standard deviations of feasible separations for each of the metering points are shown in Fig. 6-8. It is seen that as the metering point moved closer to the runway, both the means and the standard deviations became smaller. The averages of the means and standard deviations were 14.84/1.17, 13.95/1.07, 10.56/0.75, 9.18/0.51 nm at SACKO, CHERI, -35 nm, and -25 nm respectively.

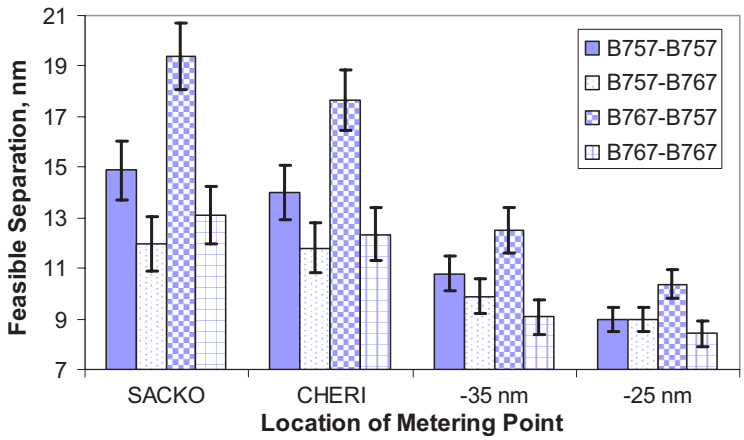

Figure 6-8 The effect of the locations of metering point.

To determine the impact of metering point location on throughput, a sequence-independent target separation was obtained for the conditional level of confidence of 75% at each of the four points. The

resulting final separation buffer and throughput for each target separation are listed in Table 6-9. As seen from the table, the sequence-independent target separation to achieve the same average conditional level of confidence became smaller as the metering point moved closer to the runway threshold. The sequence-independent target separation was reduced from 17.07 nm at SACKO to 9.64 nm at 25 nm from runway threshold. At the same time, the throughput increased as the metering point moved closer to the runway threshold; from 27.31 at SACKO to 29.98 at 25 nm from the runway threshold.

Table 6-9 Final separation buffer and throughput for average conditional level of confidence of 75%.

Metering Point		SACKO	CHERI	-35 nm	-25 nm
S_I [a]		17.07	15.76	11.62	9.64
B757–B757	β_f[a]	0.67	0.58	0.32	0.34
	C	28.08	28.44	29.98	29.92
B757–B767	β_f	1.73	1.40	0.73	0.34
	C	26.59	27.14	27.75	30.03
B767–B757	β_f	-0.71	-0.61	-0.33	-0.38
	C	28.08	28.44	29.98	29.92
B767–B767	β_f	1.31	1.20	1.10	0.63
	C	26.59	27.14	27.75	30.03
Average	β_f	0.75	0.65	0.46	0.23
	C	27.31	27.78	28.82	29.98

[a] Target separations and final separation buffer are in nm.

Aside from reducing the target separation and increasing the theoretical throughput, an intermediate metering point closer to the runway threshold would give controllers more time and airspace to adjust the spacing between aircraft. Thus, it is reasonable to expect that spacing in the adjusted traffic stream (similar to that shown in Fig. 6-5) would have a narrower distribution and higher percentage satisfying the target separation at a metering point that is closer to the runway. This in turn would give an even higher total level of confidence for the same average conditional levels of confidence.

This analysis suggests that, for a given procedure, target separations could be provided at alternative metering points along the noise abatement arrival procedure flight path to allow for operational flexibility in accommodating different traffic loads. At lower traffic densities, intermediate metering points farther away from the airport could be used to allow more fuel and time savings per flight. By using an intermediate points farther away from the airport, especially when the metering points are at or beyond the Air Route Traffic Control Center (Center)/TRACON boundary, more responsibility would be given to the Center controller. However, because this would occur during low traffic period, it should not be a big concern, but the operators would benefit from more fuel savings and the public would benefit from reduced environmental impact. At higher traffic densities, intermediate metering points closer to the runway threshold could be used to allow more flights to perform noise abatement approach procedures albeit starting at a lower altitude. Moreover, traffic throughput can be maintained. At very high traffic densities such as those exceeds the system capacity, the system would have to be reverted to the conventional mode – all aircraft would have to be vectored. This is an extreme case in that the "intermediate metering point" would have to be moved to the final approach fix.

6.3 FLIGHT TEST RESULTS

The analyses of the data collected during the KSDF 2004 CDA flight test are presented in this section to further demonstrate the application, and to show the effectiveness of the Monte Carlo simulation tool and the separation analysis methodology. The flight test and the data collected during the flight test are described first. Observed spacing in the arrival stream at the intermediate metering point and observations on separation management during the flight test are presented in Subsection 6.3.2. A separation analysis using aircraft trajectories extracted from radar tracks is provided in the last subsection.

6.3.1 The Flight Test

The design of the flight test CDA procedure is described in section 6.1. Prior to the flight test, the research team selected SACKO as the intermediate metering point. As mentioned earlier, this is a waypoint 10 nm to the west of the TRACON boundary. It was selected for two reasons: 1) to allow aircraft hand off to occur before the speed transition from the descent speed of CAS 335 kt to CAS 240 kt occurring at 10,000 ft; 2) to save more fuel.

The existing MIT restriction at the boundary between Indianapolis Center (the Center that covers Louisville TRACON) and TRACON boundary is 10 nm. To determine a target separation for the CDA flight test, simulation using the Monte Carlo simulation tool was performed with B757 and B767 aircraft both flying the CDA to runway 35L and the CDA to runway 17R under various conditions. These conditions included different combinations of nominal wind conditions such as zero wind, mean wind, and 2σ wind; with and without variations in pilot response delay; and random, minimum, mean, and maximum landing weight. The conditions were selected to cover a broad range, from normal operation conditions to cases that required high target separation, e.g., the 2σ wind, which is a strong tail wind condition at KSDF.

Separation analysis was done for both runways, and all the simulated conditions. Target separations that would guarantee separation (at 100% level of confidence based on simulated trajectories) ranged from 11.58 nm to 22.64 nm depending on the aircraft sequence, wind condition, and the range of aircraft weight used in the simulation. Results were presented to the research team. To adapt to the current practice of giving MIT restrictions in 5 nm increments, the research team determined that a target separation of 15 nm at SACKO would give an acceptable level of confidence.

During the flight test, Indianapolis Center was asked to make every effort to begin the descent from the original cruise altitude, and to maintain 15 nm separations between aircraft. Aircraft were handed off to Louisville TRACON at SACKO. The clearance from Indianapolis Center would be a routing to CHERI and pilots discretion of 11,000 ft. Louisville TRACON would clear aircraft to proceed with CDA to runway 35L (or 17R) and maintain 3,000 ft. Prior to the waypoint FLP35 (or FLP17, refer to Fig. 6-1), Louisville TRACON would issue another clearance to maintain 3,000 ft until establish on the Instrument Landing System (ILS) localizer. This clearance served as a reminder to the pilot to prepare for the deceleration to 180 kt. The aircraft would then be handed off to Louisville Tower Control.

Pilots were required to select the CDA35L (or the CDA17R) procedure and the appropriate ILS procedure prior to the Top of Descent (T/D). During the descent, pilots were asked to keep the aircraft in FMS LNAV/VNAV path mode to best enable compliance of the altitude and speed constraints and the intended CDA profile. Minimum thrust or drag could be added as necessary to maintain the speed as close as possible to the VNAV target speed. Pilots were also required to select flaps 1 no later than FLP35 (or FLP17), and to select flaps 5 no later than TRN35 (or TRN17). These flap extension requirements were necessary to enable proper deceleration before capturing the ILS localizer.

Should the spacing at cruise altitude be sufficient and the descent profile be properly managed, no vectoring would be necessary by either Center or TRACON controllers during the descent. In this case, the engine throttle would likely remain at idle from T/D until aircraft is established on the final approach. Should the spacing at SACKO be projected as less than the 15 nm target separation, the Center controller would use speed adjustment, lateral vectoring, or both to maintain a 15 nm separation. If the 15 nm target separation at SACKO were met, in most cases no vectoring by the TRACON controller would be needed. In any case, should the TRACON controller project that a separation violation were likely to occur, the aircraft would be vectored, or sent to the parallel runway.

The KSDF CDA flight test began on Tuesday, September 14 and ended on Saturday, September 25, 2004. The flights involved in the test were all scheduled to arrive within the one hour period between UTC 5:30 (1:30 AM local day light savings time) and UTC 6:30 (2:30 AM local day light savings time) each morning.

The initial plan called for 12 CDA flights on Tuesdays through Fridays, and 14 CDA flights on Saturdays. However, due to changes in aircraft assignments (where B757 or B767 replaced A300, or vice versa) and the request to participate by the crew of one flight that was not planned to fly CDA, a total of 126 flights were finally cleared to proceed with CDA. Among those 126 flights, 125 aircraft performed the CDA and 1 aircraft was later cleared for visual approach upon request from the crew because of a navigation database issue.

All the flights on September 16 and 24 and 1 flight on September 23 flew the CDA to runway 17R; the remainder of the flights flew the CDA to runway 35L. The numbers of CDA flown by each aircraft type to each runway are summarized in Table 6-10. Some of the flights that flew the CDA to runway 35L actually landed on runway 35R following instructions from controllers to ensure separation. The need for these landings on runway 35R will be explained later.

Table 6-10 Number of CDA flights.

		September										
Date		14	15	16	17	18	21	22	23	24	25	Total
35L	B757	6	7		5	8	6	7	7		8	54
	B767	6	5		6	6	6	6	5		6	46
17R	B757			6						6		12
	B767			6					1	6		13
Total		12	12	12	11	14	12	13	13	12	14	125

ARTS data for the two-week CDA flight test period were retrieved from the UPS surface management system. These data provide flight identification, aircraft position, altitude, and ground speed at a rate of once every 4 to 10 seconds. On each day, the data covered a time span of about 3 hours around the scheduled CDA arrival time except on September 25 when only 2 hours worth of data were available. The data covered a spatial area of 55 nm radial from the airport. All UPS flights arrived during the 3 hour period were included. Although there were occasional flights from other operators during this time of the day, their numbers were small; and only a few of them came from the west where the CDA flights arrived. The ARTS data provided a good basis for separation analysis in the terminal area. In the data retrieved from the UPS surface management system, aircraft position was represented as latitude and longitude. It appeared that the magnetic variation was not corrected by the system while converting ARTS X-Y coordinates into latitude and longitude. This was corrected by converting the latitude and longitude into bearing and range relative to the reference point at the airport, rotating the bearing

counterclockwise by 3 deg (the magnetic variation at KSDF), then converting bearing and range back to latitude and longitude. The corrected ground tracks closely matched the waypoints on CDA arrivals.

Data for 8 CDA flights on September 25 were missing or incomplete due to the data availability issue mentioned before. Data for 1 flight on September 23 was also missing because it was delayed by more than an hour thus arrived after the 3-hour period. Flight Data Recorder (FDR) data of 6 of those 9 flights were available and thus were used in place of ARTS data. Non-CDA flights that arrived from the west along CDA flights were also included in the analysis to provide a complete view of the scenario. During the flight test period, voice communications between the aircraft and the TRACON controller were also recorded using a commercial radio scanner and equipment hosted by the Noise Office of Louisville RAA. The recorded voice communications provide additional information for interpreting the ARTS data. Enhanced Traffic Management System (ETMS) data were also used to help identify non-UPS flights and the vectoring outside the ARTS data coverage area.

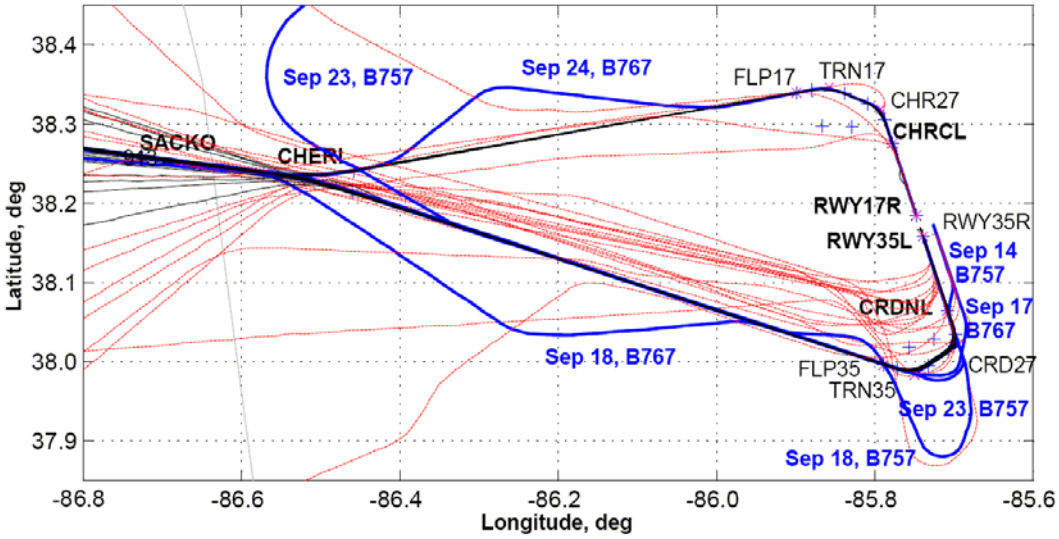

Figure 6-9 KSDF CDA flight test ground tracks.

Figure 6-9 shows the ARTS ground tracks of all CDA flights and some non-CDA flights from the west that arrived while the CDA flight test was active. The solid thin tracks (black, followed all waypoints) were normal CDA flights. The thick tracks (blue, annotated with date and aircraft type) were CDA flights vectored for separation during the flight test. The dotted thin tracks (red) were non-CDA flights from the west that had similar ground tracks as CDA flights. It is seen from the figure that the ground tracks of the normal CDA flights were extremely consistent. The thick blue B757 track on September 23 that joined the CDA lateral path after waypoint CHERI was the flight not originally planned to fly CDA. Except for that B757 flight, a total number of 6 CDA flights were laterally vectored for separation during the flight test. Details of these vectored CDA flights are explained in the next subsection.

During the flight test, the TRACON controller purposely vectored a number of non-CDA flights to follow the CDA lateral path to see how well non-CDA flights can be blended into the CDA arrival stream. It is seen from Fig. 6-9 that the amount of lateral vectoring was reduced for those non-CDA flights that followed the CDA lateral path. The contrast can be easily seen by referring to vectored ground tracks during regular operations shown in Fig. 2-1. This suggests that some of the vectoring

techniques that were developed to handle heavy traffic might have been used by controllers constantly even when the traffic is not heavy. Thus, the number of heading commands maybe reduced by some degree during non-busy periods through modifying vectoring strategies.

During the flight test, pilots reported that missing, incorrect, or out-of-place information was observed in the latitude, longitude, and altitude/speed constraints when the procedure was loaded into the FMS. In most of these cases, the pilot manually entered the missing altitude/speed constraints, or manually corrected the incorrect data. There were still occasions in which the FMS VNAV path was not computed as desired. It was discovered after a discussion with the FMS manufacturer that the database issues can be resolved through revising pilot procedures and FMS database management procedures.

Analysis revealed that, on average, approximately 2 minutes flight time was saved by flying CDA. An average of 118 lb of fuel was saved by each B757-200 CDA flight, and an average of 364 lb of fuel was saved by each B767-300 CDA flight, as compared with flights of same aircraft types performed conventional approach procedures. Up to 6 dBA peak level noise reduction, up to 30% noise contour area reduction[7], and up to 34% local emissions reduction (below 3,000 ft) were achieved by flying the CDA. Other aspects of the flight test can be found in the report by the KSDF 2004 CDA flight test research team[8].

6.3.2 Observed Spacing and Spacing Adjustment during the Flight Test

The actual spacing in the CDA arrival stream at SACKO (measured when the leading aircraft was at SACKO) during the flight test were extracted from the ARTS data. Spacing for 69 flight pairs were selected for analysis. Other flight pairs were removed either because the spacing between a flight pair was larger than 30 nm (considered as a gap in the arrival stream), or because another flight had landed between the pair of flights (spacing for the flight pair becomes meaningless). Among the 69 selected flight pairs, 9 were non-CDA pairs. The remainder 60 flight pairs involved at least one CDA flight.

The frequency distribution of spacing in the 69 selected flight pairs is shown in Fig. 6-10. The spacing shown in the figure included 56 flight pairs to runway 35L and 13 flight pairs to runway 17R. Because SACKO was selected as the common intermediate metering point for both runways, and the same target separation of 15 nm was used, flights to the two runways should have been treated in the same way by Center controllers. The frequency distribution shown in Fig. 6-10 were the bases of the probability densities and Erlang models shown in Fig. 6-5 for spacing in the adjusted traffic.

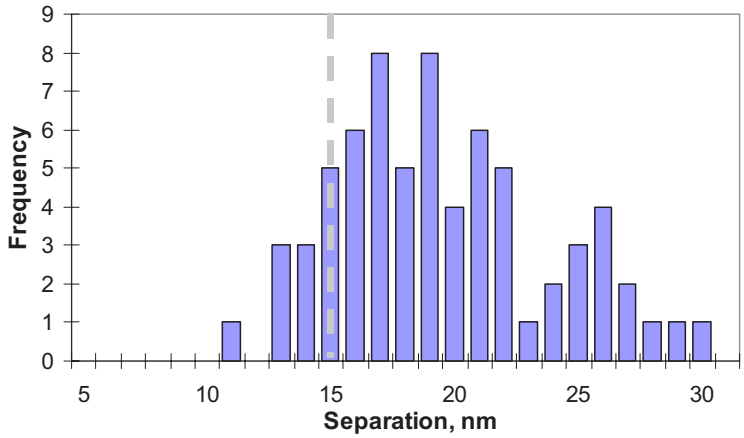

Figure 6-10 Frequency distribution of spacing at SACKO in the CDA arrival stream.

It is seen from Fig. 6-10 that among the 69 selected flight pairs, 12 flight pairs (all involved at least 1 CDA flight) indicated a spacing less than the recommended target separation of 15 nm at waypoint SCAKO. This illustrates that in real world environment, the recommended target separation might not be satisfied under some situations. The 12 flight pairs that had spacing less than 15 nm at SACKO are summarized in Table 6-11 and are examined in the following paragraphs. Among them, the trailing aircraft in 4 of the flight pairs were laterally vectored for separation after the aircraft were handed off to the TRACON controller and cleared to proceed with CDA.

Table 6-11 Flight pairs with spacing less than 15 nm at SACKO.

Date	Aircraft Leading-Trailing	Spacing, nm SACKO/Final (Minimum)[a]	Laterally Vectored	Comments[c]
14-Sep	B767-B757	10.9/3.7[b] (5)	Yes	Crew accepted to maintain visual separation. Later vectored to side step to parallel runway 35R.
15-Sep	B767-B757	13.8/9.4 (5)	No	No controller intervention observed.
16-Sep	A300-B767	13.1/5.1 (4)	No	The leading aircraft (a non-CDA) was kept above 10,000 ft and at faster speed for longer than normal.
16-Sep	B767-B767	13.8/7.2 (4)	No	Center directed aircraft to descend at lower speed (first IAS 290 kt, then IAS 270 kt) before 10,000 ft.
17-Sep	B757-B767	13.9/3.0[b] (4)	Yes	Vectored to extended base, and then side step to parallel runway 35R.
17-Sep	B767-B767	14.9/4.8 (4)	No	Crew accepted to maintain visual separation, deceleration before the turn started early.
18-Sep	B757-B767	14.3/5.4 (4)	Yes	Vectored off the CDA path then directed to return the CDA path before turning to final.
21-Sep	B767-B767	14.6/10.0 (4)	No	Center directed aircraft to descend at lower speed (IAS 270 kt) before 10,000 ft.
22-Sep	B757-B767	14.9/7.7 (4)	No	No controller intervention observed.
24-Sep	B767-B767	12.3/3.9 (4)	Yes	Vectored off the CDA path then directed to return the CDA path before turning to final.
24-Sep	B757-B767	12.5/2.5 (4)	No	Crew accepted to maintain visual separation, no controller intervention observed.
25-Sep	B767-B757	14.2/3.2 (5)	No	Crew accepted to maintain visual separation, no controller intervention observed.

[a] Numbers in parenthesis are separation minima in effect at runway threshold.

[b] Projected as if no action were taken, actual value unknown as aircraft were on different runway.

[c] About trailing aircraft except indicated otherwise.

On September 14, runway 35L was in use. This is the first day of the CDA flight test. For the vectored B757 (see the first flight pair in Table 6-11), the spacing at SACKO was 10.9 nm. The TRACON controller decided not to vector the aircraft immediately. Rather, the aircraft was let to continue on CDA without interruption so that the controller could gain first hand experience on how the spacing would evolve as the CDA proceeded. The crew accepted instructions from the controller to maintain visual separation from the leading aircraft which was a CDA flight as well. When visual

separation is used upon instructions from the controller, the pilot provides his or her own separation by maneuvering the aircraft as necessary. Visual separation requires less spacing between aircraft than radar separation, thus the interruptions to CDA execution can be reduced. For the flight pair, the spacing decreased to 5 nm at TRN35. Because spacing would continue to decrease as the aircraft turned to the final approach course, the aircraft was directed to side step to the parallel runway 35R. Close examination of the aircraft trajectory revealed that, should this aircraft stay on the final approach to runway 35L, the final spacing could have dropped below 3.7 nm. Spacing at SACKO for all the other flights on the same day were greater than 15 nm, and proper final separation were ensured without controller intervention. After the first day of flight test, the research team gained great confidence in the operational concept and the selected target separation.

In the following paragraphs, flight pairs with spacing less than 15 nm at the intermediate metering point SACKO are examined. Vectored flights are examined first. These flight pairs can be divided into 2 categories.

1. **Aircraft vectored to extend base or to side step to the parallel runway**
   The vectoring of the B757 on September 14mentioned above represents the first category of vectoring used during the flight test. Initially, the crew accepted instructions from the controller to maintain visual separation. As the procedure progressed, the separation compressed due to deceleration. Given the spacing at the time and the projected further separation compression, before the aircraft turned to final approach course, the controller gave clearance for the aircraft to side step to the alternative runway. Another case of this type of vectoring was the vectored B767 on September 17 (see the 5th flight pair in Table 6-11, runway 35L was in use that day). The spacing was 13.9 nm at SACKO, and the spacing decreased to 6.1 nm at TRN35. The aircraft was cleared to extend the base leg (the segment prior to final approach segment) and to side step to runway 35R. Should the controller not intervene, the final spacing would have dropped to approximately 3.0 nm.
2. **Aircraft vectored as soon as they entered TRACON boundary**
   In the second category, the controller vectored the aircraft not long after the aircraft was handed off when spacing at the metering point was below the recommended target separation. Should the vectoring be effective, the aircraft could later return to the CDA and land on the originally assigned runway. This included the cases of the vectored B767 on September 18 (see the 7th fight pair in Table 6-11, runway 35L was in use on that day) and the vectored B767 on September 24 (see the 10th flight pair in Table 6-11, runway 17R was in use on that day). The vectoring was a moderate heading change (turn 30 deg off the CDA lateral path), and flying the new heading for a certain distance and then returning to re-join CDA. As seen from Table 6-11, in both cases, the Instrument Flight Rules (IFR) separation minima were assured. Examining the FDR data of the B767 on September 24 revealed that while the aircraft was vectored off the CDA lateral path, the aircraft remained on the VNAV path, and the engine throttle remained at idle. This is an encouraging finding. It suggests that similar vectoring techniques may be used to adjust spacing during CDA without losing much noise abatement and fuel saving benefits.

No lateral vectoring was observed for the other 8 flight pairs that had spacing less than 15 nm at SACKO. These cases can be divided into four categories.

1. **No additional air/ground communications were observed**
   In the first category, no additional air/ground communications were observed except the basic clearances for a CDA flight. This included a flight pair with a trailing B757 on September 15 (see the 2nd fight pair in Table 6-11) and a flight pair with a trailing B767 on September 22 (see the 9th fight pair in Table 6-11). For the case on September 15 with a trailing B757, the spacing

was 13.8 nm at SACKO and was 11.1 nm at TRN35. For the case on September 22 with a trailing B767, the spacing was 14.9 nm at SACKO and was 10.8 nm at TRN35. It appeared that no separation violations for the two flight pairs were predicted by the controller as the CDA proceeded, thus no intervention was needed.

2. **Crew accepted instructions from the controller to maintain visual separation**

   In the second category of flight pairs, the crew of the trailing aircraft accepted instructions from the controller to maintain visual separation. This included three flight pairs: In the flight pair with a trailing B767 on September 17 (see the 6th fight pair in Table 6-11), the deceleration before the turn to the final approach course started early for the trailing B767. Thus, the final spacing was 4.8 nm – greater than the IFR wake turbulence separation minimum of 4 nm. In the other two flight pairs, the one on September 24 with a trailing B767 (see the 11th fight pair in Table 6-11) and the one on September 25 with a trailing B757 (see the 12th fight pair in Table 6-11), no special actions were observed. For the first pair, the spacing was 12.5 nm at SACKO and the final spacing was 2.5 nm. For the second pair, the spacing was 14.2 nm at SACKO and the final spacing was 3.2 nm. The final spacing was less than the IFR wake turbulence separation minima of 4nm and 5 nm respectively.

3. **Trailing aircraft descent speed was lower than specified in the procedure**

   In the third category of flight pairs, the descent speed of the trailing aircraft prior to the deceleration at 10,000 ft was lower than the descent speed of CAS 335 kt specified for CDA flights. This included a flight pair on September 16 with a trailing B767 (see the 4th fight pair in Table 6-11) and a flight pair on September 21 with a trailing B767 (see the 8th fight pair in Table 6-11). For the first pair, the trailing B767 was directed by Indianapolis Center to descend at CAS 290 kt and later to descend at CAS 270 kt before hand off. For the second pair, the trailing B767 was directed to descend at CAS 270 kt before hand off. The spacing at SACKO was 13.8 nm for the first pair, and 14.6 nm for the second pair. The speed reductions appeared to be the Center controller's efforts to establish the 15 nm target separation at SACKO. The aircraft continued at the reduced descent speeds until the deceleration at 10,000 ft. After the deceleration at 10,000 ft, the aircraft resumed the normal CDA speed profile, i.e., descending at CAS 240 kt until the deceleration before turning on to the final approach course. The deceleration at 10,000 ft automatically isolated the speed adjustment initiated by the Center controller from the normal CDA speed profile below 10,000 ft. Because the deceleration at 10,000 ft was much closer to the runway than the metering point at waypoint SACKO, the speed reduction initiated by the Center controller also contributed to adjusting the spacing after the aircraft were handed off. The final spacing was 7.2 nm for the first pair, and 10.0 nm for the second pair.

4. **Leading non-CDA was vectored**

   In the last category of the four, the leading aircraft, which was a non-CDA, was vectored. For a flight pair on September 16 involving a trailing B767 (see the 3rd fight pair in Table 6-11), the leading aircraft was an Airbus 300 (A300) not flying CDA. The spacing was 13.1 nm at SACKO. The non-CDA aircraft was vectored by the controller to follow the CDA lateral path, and at the same time, it was directed to maintain 10,000 ft (without reducing speed) for slightly longer. Normally the clearance for a non-CDA flight at the same stage would be to descend and maintain at a lower altitude such as 7,000 ft. At altitude above 10,000 ft, speed higher than CAS 250 kt can be used. For the same CAS, the ground speed would also be higher at higher altitudes. With the vectoring of the leading A300, wake turbulence separation minima was assured. On the other hand, the separation between the A300 and the flight in front of it (another B757 doing CDA) were maintained – the final spacing was 4.3 nm as compared with the wake turbulence separation

of 4 nm. This is a perfect example of how non-CDA flights can be blended into CDA arrival stream.

Table 6-12 Flight pairs with proper spacing at SACKO but small spacing at threshold.

Date	Aircraft Leading-Trailing	Spacing, nm SACKO/Final (Minimum)[a]	Laterally Vectored	Comments[b]
22-Sep	B757-B767	25.4/2.6 (4)	No	Crew accepted to maintain visual separation, leading aircraft too slow. No intervention observed.
25-Sep	B767-B757	16.3/4.0 (5)	No	Crew accepted to maintain visual separation, no controller invention observed.

[a] Numbers in parenthesis indicate separation minima at runway threshold.

[b] About trailing aircraft except indicated otherwise.

Among the 69 selected flight pairs, 2 flight pairs that had spacing greater than 15 nm at SACKO ended up with final spacing less than the corresponding IFR wake turbulence separation minima. These 2 were CDA flight pairs. They are summarized in Table 6-12.

1. **Leading aircraft too slow**
   In the first flight pair, the leading B757 had a much shallower vertical profile than all other CDA flights on the same day, thus it was much slower. The crew of the trailing B767 accepted instructions from the controller to maintain visual separation. The spacing at SACKO was 25.4 nm, a relatively large value. The final spacing was 2.6 nm, less than the IFR wake turbulence separation minimum of 4 nm. Apparently, the CDA VNAV path was not properly computed for the leading B757. Because of lack of data, it was not clear why this occurred. The altitude and speed constraints probably were not properly loaded into the FMS.
2. **Normal case of feasible separation greater than 15 nm**
   In the second flight pair of this type, both the leading and trailing aircraft had proper CDA VNAV path. The crew of the trailing B767 accepted instructions from the controller to maintain visual separation. The spacing at SACKO was 16.3 nm. The final spacing was 4.0 nm, less than the IFR wake turbulence separation minimum of 5 nm. This flight pair represents a normal case in that spacing greater than 15 nm at SACKO would be needed to assure the IFR wake turbulence separation minima throughout the procedure.

Table 6-13 Other vectored flights not included in the selected 69 flight pairs.

Date	Aircraft Leading-Trailing	Spacing, nm SACKO/Final (Minimum)[a]	Laterally Vectored	Comments[b]
18-Sep	DC8-B757	33.7/4.5 (5)	Yes	Vectored to extend base because the non-CDA in front was vectored, thus disrupted separation.
23-Sep	B757-B757	/ (4)	Yes	Vectored to extend base. The aircraft in front (a non-planned CDA) had difficulty to manage speed.

[a] Data in parenthesis indicate separation minima at runway threshold.

[b] About trailing aircraft except indicated otherwise.

The other 2 flight pairs involving laterally vectored trailing aircraft were not included in the 69 selected flights based on the criteria described earlier in this subsection. These 2 flight pairs are

summarized in Table 6-13. In these 2 pairs, the trailing aircraft were vectored due to unexpected situations.

1. **Leading aircraft was vectored to avoid traffic from a different direction**
   In the flight pair on September 18 (the first flight pair in Table 6-13), the spacing at SACKO was 33.7 nm. The leading aircraft (a DC8) in this flight pair was a non-CDA flight that was vectored to avoid traffic from a different direction, thus forced the trailing B767 to be vectored as well. Close examination of the FDR data revealed that the lateral flight path of the trailing B767 was extended by about 13 nm. The flight path of the leading aircraft was extended about the same amount. The amount of overall flight path extension could have been reduced if better traffic coordination tools and mechanisms were in place.
2. **Leading aircraft was a unplanned CDA that had difficulties to manage speed**
   In the flight pair on September 23, the spacing at SACKO was not computed because the two aircraft were on different lateral flight path at the time. The leading B757 was the unplanned CDA that joined CDA upon request from the flight crew. Because the leading B757 joined CDA late, it had difficulties to manage the speed. This resulted in a very slow speed profile. Thus, the trailing B757, an originally planned CDA, was vectored to extend base. The vectoring of the trailing B757 should thus be viewed as an exception event.

In summary, among the 125 flights that performed CDA, 6 flights, or 4.8% of them was laterally vectored for separations. Four of the flights were vectored due to insufficient spacing (less than 15 nm) at the intermediate metering point SACKO. Two of the flights were vectored due to unexpected events. A total number of 69 consecutive flight pairs that had spacing less than or equal to 30 nm at SACKO and had no other aircraft landed between the pair were selected for further examination. In 60 of the selected 69 flight pairs, at least 1 CDA flight was involved.

Among the 69 flight pairs, 12 pairs (all involved at least 1 CDA flights), or 17.4% had spacing less than 15 nm at SACKO. The 4 flights vectored for separation were all included in the 12 flight pairs that had spacing less than 15 nm at SACKO. These 4 vectored flights involved 5.8% of the 69 selected flight pairs (or 6.7% of the 60 CDA flight pairs) and 33.3% of the 12 flight that had spacing less than 15 nm at SACKO. The other 8 flight pairs that had spacing less than 15 nm at SACKO were handled as follows. Speed reductions prior to 10,000 ft were applied to the trailing aircraft in 2 of the flight pairs. The speed of the leading aircraft (a non-CDA) was adjustment in 1 of the flight pairs. The crew of the trailing aircraft accepted instructions from the controller to maintain visual separation in 2 of the flight pairs; and the final spacing were less than the IFR wake turbulence separation minima. The crew of the trailing aircraft accepted instructions from the controller to maintain visual separation in another flight pair, and the final spacing was above the IFR wake turbulence separation minimum. Spacing adjustment was not need in the other 2 of the 12 flight pairs. This means in 9, or 75% of the 12 flight pairs that had spacing less than 15 nm at SACKO, were vectored one way or another, or were cleared to maintain visual separation. The controller projected that separation violation would occur in these 9 cases if non actions were to be taken. In 2 of the flight pairs that had spacing greater than or equal 15 nm at SACKO, the crew accepted instructions from the controller to maintain visual separation; and the final spacing were less than the IFR wake turbulence separation minima.

In short, the final spacing in 11 flight pairs, or 15.9% of the 69 flight pairs would be less than the IFR wake turbulence separation minima if the controller had not intervened. This is equivalent to a total level of confidence of 84.1%. Based on the 60 CDA flight pairs, the total level of confidence would be 81.7%. This is in between the simulated total levels of confidence of 79.6% and 85.0% for the CDA to runway 35L and 17R respectively, as presented in subsection 6.2.3.

As described above, after gaining experience managing the CDA flights, TRACON controllers were able to develop techniques for predicting future separations between aircraft performing CDA. The 15 nm target separation at SACKO was mainly recommended for Center controllers to establish separation between consecutive flights in a way similar to what the existing MIT restrictions are used. The target separation was also used by TRACON controllers as a reference aid for predicting future separations between aircraft on the CDA. When the spacing between a consecutive aircraft pair was greater than the 15 nm target separation, the controller would not be too concerned about future separations between pair of aircraft during the monitoring phase, because separation violations would be less likely to occur. When the spacing between an aircraft pair was less than the 15 nm target separation, the controller would pay much closer attention to the separation between the pair of aircraft, as evidenced by increased voice communications to negotiate with the crew and to provide crew with information about the relative speed and spacing with respect to the aircraft in front. In this case, the crew was normally instructed to maintain visual separation from the aircraft in front, visibility permitting. Because the lateral flight path was managed by the onboard FMS during the execution of CDA, the speed and the altitude became the only variables determining the aircraft state in the airspace. An interview with controllers revealed that, after observing a number of uninterrupted CDA operations, controllers were able to establish mental models of the probable CDA speed profiles. Air/ground communications indicated that controllers frequently referenced to the relative speed of the trailing aircraft with respect to the leading aircraft in predicting the future separation between aircraft. Controllers acknowledged that differences in predicting accuracy existed, indicating that the predicting accuracy could be improved should they gain more experience.

6.3.3 Separation Analysis Using Radar Tracks

In the previous subsection, the observed spacing between successive flight pairs were described. In this subsection, separation analysis using ARTS radar tracks is presented. The question of great interest is, given the CDA trajectories known, what would be feasible separations at the intermediate metering point, namely SACKO, in order to assure separation minima throughout the execution of CDA. Trajectories of flights that performed the CDA as desired were selected for this purpose. Note that the criteria used in selecting the CDA flights in this subsection differ from that used in the previous subsection. The criteria used in selecting flight pairs to obtain the spacing distribution in the CDA arrival stream were based on the spacing at waypoint SACKO, regardless of how well the procedure was performed by each aircraft involved. The criteria used in this subsection are based on how well the procedure was performed by each CDA flight, regardless of the actual spacing between consecutive flights. Some CDA flights were removed either because they were vectored (the trajectory would not reflect uninterrupted CDA execution), or because their VNAV paths were not properly computed due to FMS database issues (these issues would have been corrected should the procedure be formally implemented). From the selected flight trajectories, CDA flight pairs were formed. These CDA flight pairs were not necessarily the consecutive flight pairs during the flight test. In rare occasions, a third flight might have landed between the pair of flights. For CDA to runway 35L, 73 flight pairs were formed. For CDA to runway 17R, 18 flight pairs were formed. The numbers of CDA flight pairs for different aircraft sequences are listed in Table 6-14.

Trajectories of the selected CDA flights on September 14 are shown in Fig. 6-11. Trajectories on other days were in similar pattern. In the figure, the horizontal axis represents along track distance. The vertical axis represents time since the aircraft passed SACKO, pointing downwards. All trajectories were aligned at SACKO to show the variation between flights. At any given point on the horizontal axis, the variation represents differences between flight times from SACKO to that point. At any given time on the

vertical axis, the variation represents differences between the aircraft locations. To ensure safe execution of uninterrupted CDA, proper spacing (the feasible separations) must be given at SACKO to accommodate trajectory uncertainties. The larger the variations between flight trajectories were, the larger the feasible separations would be.

Table 6-14 Selected CDA flight pairs for applying separation analysis methodology.

	Aircraft	September										Sub
	Sequence	14	15	16	17	18	21	22	23	24	25	Total
35L	B757-B757	2	4		1	3	4	2	2		2	20
	B757-B767	2	2		3	3	2	2	2		3	19
	B767-B757	1	1		2	2	1	2	1		3	13
	B767-B767	3	3		2	2	3	4	3		1	21
17R	B757-B757			4						3		7
	B757-B767			2						3		5
	B767-B757			1						2		3
	B767-B767			2						1		3

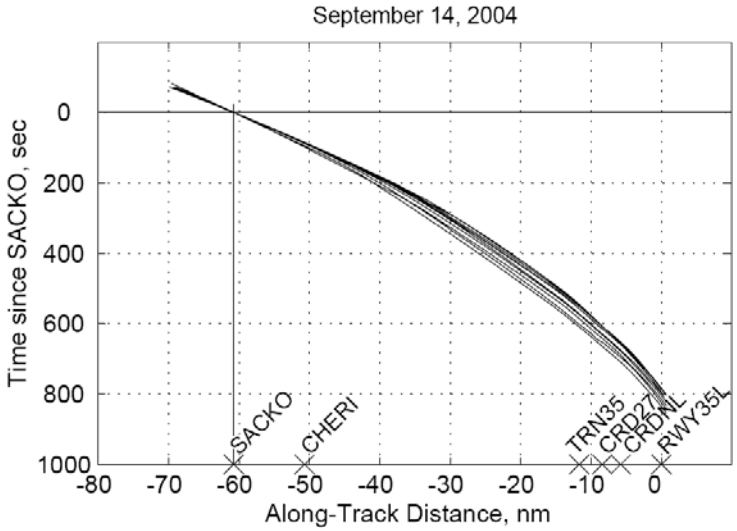

Figure 6-11 Sample CDA trajectories from ARTS data.

To obtain feasible separations from flight trajectories extracted from the ARTS data, it is assumed that the trajectories would remain the same when the spacing at the metering point between consecutive flights are slightly adjusted. This is not exactly true in the real world. However, it can be assumed that the effects of the adjustment would be canceled out if the analysis is applied to a very large pool of flight pairs. The process described in Chapter 5 was applied to the consecutive flight trajectory pairs to obtain feasible separations at SACKO. The distribution of estimated feasible separations at SACKO for the CDA to runway 35L is shown in Fig. 6-12. The distribution of estimated feasible separations at SACKO for the CDA to runway 17R is shown in Fig. 6-13. The distributions of estimated feasible separations were based on all flight pairs listed in Table 6-14. Because the small sample size, different aircraft sequences are not identified in these two figures. The distributions in Fig. 6-12 and Fig. 6-13 thus indicate weighted average based on the traffic mix listed in Table 6-14.

The minimum and maximum values of the estimated feasible separations for the CDA to runway 35L were 5 nm and 20.5 nm respectively. The minimum and maximum values of the estimated feasible separations for the CDA to runway 17R were 6.4 nm and 22.5 nm respectively. As seen from Fig. 6-12, in 69.9% of the cases the feasible separations were less than or equal to 15 nm for the CDA to runway 35L. This number could be viewed as an estimate of the weighted average (by the actual traffic mix shown in Table 6-14) of conditional levels of confidence for the CDA to runway 35L given a 15 nm sequence-independent target separation at SACKO. As seen from Fig. 6-13, in 72.2% of the cases the feasible separations were less than or equal to 15 nm for the CDA to runway 17R. This number could be viewed as an estimate of the weighted average of conditional level of confidence for the CDA to runway 17R given a 15 nm sequence-independent target separation at SACKO.

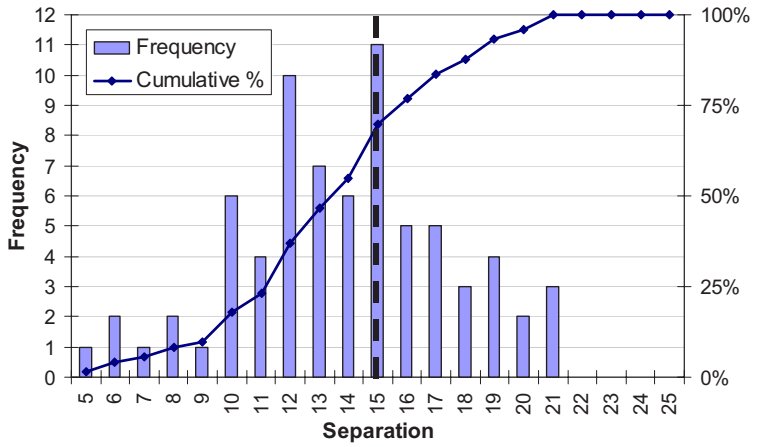

Figure 6-12 Sample frequency distribution of feasible separations for CDA to runway 35L.

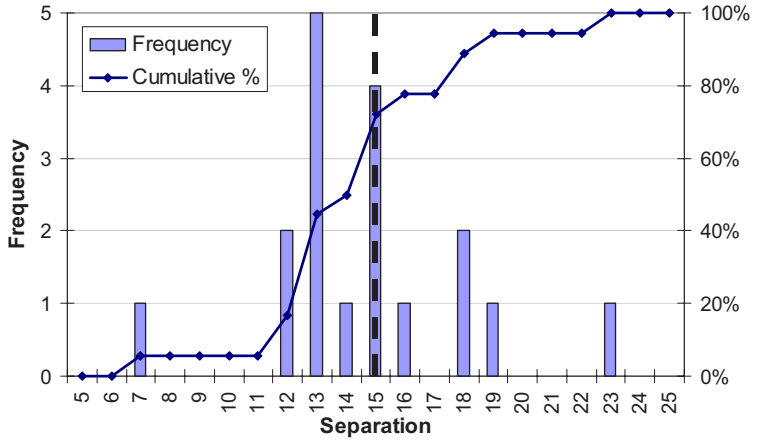

Figure 6-13 Sample frequency distribution of feasible separations for CDA to runway 17R.

The estimates of conditional levels of confidence for a 15 nm sequence-independent target separation are listed in Table 6-15, along with the simulation results that have been presented in subsection 6.2.2. In

Table 6-15, the average values from the simulation were arithmetic average, and the weighted average values were weighted by the traffic mix data shown in Table 6-14. It is seen that the weighted average values are very close to the flight test results.

Table 6-15 Comparison of conditional levels of confidence given 15 nm sequence-independent target separation.

	Simulation Results		
	Average	Weighted Average	Flight Test Results
CDA to 35L	62.7%	68.6%	69.9%
CDA to 17R	68.2%	72.5%	72.2%

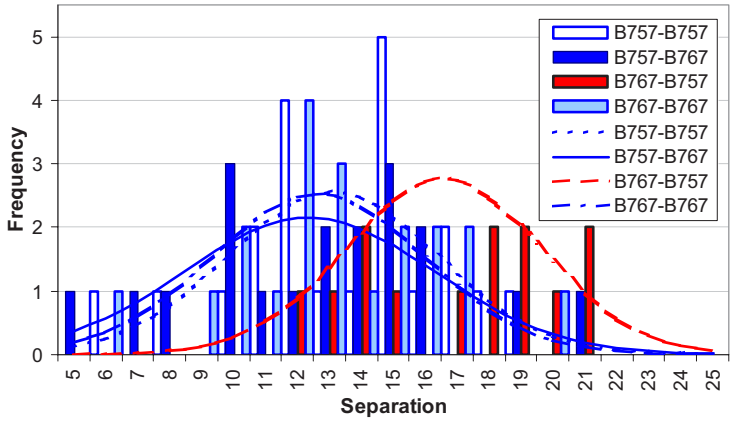

Figure 6-14 Sample frequency distributions of feasible separations for different aircraft sequences, CDA to runway 35L.

Frequency distributions of estimated feasible separations for the four different aircraft sequences were also obtained for the CDA flights to runway 35L. The results are shown in Fig. 6-14. Because the sample sizes become even smaller after the flight pairs are divided into the four sequences, the data become even more scattered. To illustrate the trend in the data, normal distributions were fit to the data. These normal distributions are shown as curves in Fig. 6-14. By comparing Fig. 6-14 with Fig. 6-2, it is seen that the central tendencies in the flight test results are similar to the simulation results. The spread in the flight test data, however, seems larger than the simulation data. There could be several possible reasons for this. Due to schedule and operational issues, it was not possible to conduct extensive crew training on CDA operations before the flight test – the flight test was a learning process itself. It was observed from FDR data that some flights used different descent speeds (for the descent from cruise to 10,000 ft) from that specified in the procedure chart. The use of FMS wind forecast was not consistent across flights. Larger variations in flap and speedbrake usage, mainly due to existing inconsistent practices under vectored environment, were also observed. Although operational consistency improved greatly in the second week of the flight test, it was still some distance away from stabilized operations. The effects of these elements were reflected in the flight test data. There is also the nuisance of very small sample sizes. Thus, it is believed as the flight crews become more familiar with the procedure, and

the operational consistency improves, the spread of feasible separations will be reduced. On the other hand, more data collected from the field will also provide an opportunity to improve the model accuracy.

6.4 SUMMARY

A simulation study and analyses of data collected from a CDA flight test at KSDF with B757-200 and B767-300 aircraft were presented. For the CDA to runway 35L, the simulation results indicated that a 15 nm sequence-independent target separation at the selected intermediate metering point SACKO would give an average conditional level of confidence of 62.7% for a 50-50 traffic mix of B757-200 and B767-300 aircraft. This gives a theoretical average traffic throughput of 30.91 aircraft per hr. The ideal case, in which trajectory variations are exactly predicted and thus no capacity loss would occur, gives an average traffic throughput of 31.40 aircraft per hr. The throughput for the ideal case represents system capacity.

For a given conditional level of confidence of 75%, the sequence-independent target separation would give an average theoretical throughput of 27.31 aircraft per hr, while sequence-specific target separations would give an average theoretical throughput of 29.85 aircraft per hr. The traffic throughput increase from 27.31 aircraft per hr to 29.85 aircraft per hr is significant improvement. This is because system delay would be significantly reduced by a small throughput increase as the system is operating at near capacity. Simulation indicated that for relatively high conditional levels of confidence (>65% for the simulated CDA to runway 35L), using sequence-specific target separations would always improve traffic throughput. The higher the conditional level of confidence, the more benefits can be gained by using sequence specific target separations.

In a real world operating environment, spacing at the metering point will not be exactly as specified by target separations or MIT restrictions. The analysis of the ARTS data collected at KSDF for night arrival traffic from the west revealed that, when a 10 nm MIT was in effect, the average traffic spacing was 15.79 nm with a standard deviation of 5.88 nm. When a 15 nm target separation was requested, the average traffic spacing became 19.05 nm with a standard deviation of 4.28 nm. This represents an increase of the average spacing of 3.26 nm (vs. 5 nm increase in the MIT restriction) and a decrease of the standard deviation of 1.60 nm. This observation leads to the conclusion that as the target separation increases, the average traffic spacing increases by a smaller amount than the corresponding increase in the target separation. Using a larger target separation will not just simply increase the traffic spacing, it also decrease the randomness in arrival traffic.

An Erlang distribution model for the distribution of the spacing in the unadjusted traffic and adjusted arrival traffic was developed based on ARTS data collected at KSDF. The total probability method was applied to the simulation results to obtain total levels of confidence. For the CDA to runway 35L, the total level of confidence for a sequence-independent target separation of 15 nm was 79.6% while the average of conditional levels of confidence for the same target separation was 62.7%. The total probability method provides a more complete view of the relationship between the target separations and the levels of confidence in a real world environment.

Simulation results revealed that winds have a strong impact on the feasible separations. A head wind condition would yield lower feasible separations, and a tail wind would yield higher feasible separations. If efficiency is a big concern, such as in relatively busy terminal areas or during relatively busy time of the day, different sets of target separations should be developed for different wind conditions. In this case, a strong tail wind condition would need larger target separations, and a strong head wind condition would need smaller target separations.

Simulation results also revealed that, for the same conditional level of confidence, traffic throughput will be significantly improved as the intermediate metering point is moved closer to the runway threshold. For the CDA to runway 35L, sequence-independent target separations for a given conditional level of confidence of 75% were obtained for four different intermediate metering point locations: SACKO, CHERI, a point at -35 nm, and a point at -25 nm. The target separations were 17.07, 15.76, 11.62, and 9.64 nm for the four metering points respectively. The corresponding average theoretical traffic throughput were 27.31, 27.78, 28.82, and 29.98 aircraft per hr respectively. Thus, for a given procedure, target separations could be provided at alternative metering points along the noise abatement approach or arrival procedure flight path to allow for operational flexibility in accommodating different traffic loads.

The effectiveness and the accuracy of the Monte Carlo simulation tool and the separation analysis methodology (collectively referred to as TASAT) were successfully demonstrated during the KSDF 2004 CDA flight test. Examining the ARTS data revealed that for a 15 nm target separation, a total confidence level of 81.7% was observed. This is close to the predicted total level of confidence of 79.6% (CDA to runway 35L) and 85.0% (CDA to runway 17R) by the simulation study.

Separation analysis was also done using aircraft trajectories extracted from the ARTS data. The analysis revealed that for a sequence-independent target separation of 15 nm, the estimated conditional level of confidence for the CDA to runway 35L was 69.9%, which is also very close to the value of 68.6% predicted by the simulation study. Because of the very small sample size, frequency distributions of feasible separations were hardly visually discernible. However, the central tendencies reflected by the feasible separations from the ARTS data and from simulated aircraft trajectories were very similar.

Feasible separations from ARTS data do reflect slightly larger spread (or standard deviations) than simulated aircraft trajectories. Possible reasons include: unplanned use of different descent speed from cruise altitude, inconsistent use of FMS wind forecast, and larger variations in flap and speedbrake extension actions. On one hand, these variations are expected to decrease in formal implementations of CDA procedures as pilots gain more experience with these procedures through training and daily operations. On the other hand, these variations reflected by flight test data provide an opportunity to further improve the model accuracy.

After gaining experience on managing CDA flights, controllers were able to develop techniques for predicting future separations between aircraft on the same procedure. Because the lateral flight path was fixed, controllers relied on their mental models of the probable CDA speed profile and the relative speed of the trailing aircraft with respect to the leading aircraft to predict if spacing would be less than separation minima in the future.

Two strategies were used by controllers to adjust the spacing between aircraft during the execution of CDA. The first strategy was to vector the aircraft early when the spacing at the metering point was less than the given target separation. The second strategy was to vector when the aircraft was close to turning on to the final approach course and when the controller was certain that a separation violation would occur if no action were taken. If the first strategy is used, some of the aircraft might have been vectored when in fact the separation could eventually be ensured without intervention. As demonstrated in the flight test, a moderate heading change command could still be performed at idle thrust if managed early. If the second strategy is used, the number of aircraft to be vectored could be reduced. However, as actions are taken later during the procedure, the aircraft would probably have to be vectored to substantially extend the base leg and fly level segments at relatively low altitudes if an alternative parallel runway is not available for use.

Controllers were also able to handle the arrival traffic flow with mixed aircraft types when the CDA flight test was active. A number of non-CDA flights were fed into the gaps between CDA flights and

were vectored to follow the CDA lateral flight path. In several cases, speed commands were assigned to non-CDA flights to maintain separation – allowing CDA flights to continue without interruption.

REFERENCES

[1] Reynolds, T. G., Clarke, J.-P. B., and Ren, L., "Advanced Continuous Descent Approach Activities at Nottingham East Midlands Airport, UK," Presented at *CDA Workshop No. 3*, Georgia Institute of Technology, Atlanta, Georgia, 6-7 Sep. 2006.

[2] Reynolds, T. G., Ren, L., Clarke, J.-P. B., Burke, A. S., and Green, M., "History, Development and Analysis of Noise Abatement Arrival Procedures for UK Airports," AIAA 2005-7395, *AIAA 5th Aviation Technology, Integration and Operations Forum*, Arlington, Virginia, 26-28 September 2005.

[3] White, W. and Clarke, J.-P. B., "Details and status of CDA procedures at Los Angeles International Airport (LAX)," Presented at *CDA Workshop No. 3*, Georgia Institute of Technology, Atlanta, Georgia, 6-7 Sep. 2006.

[4]Staigle, T. and Nagle, G., "Details and status of CDA procedures for early morning arrivals at Hartsfield-Jackson Atlanta International Airport (ATL)," Presented at *CDA Workshop No. 3*, Georgia Institute of Technology, Atlanta, Georgia, 6-7 Sep. 2006.

[5] Clarke, J.-P. B., Ho, N. T., Ren, L., Brown, J. A., Elmer, K. R., Tong, K.-O., and Wat, J. K., "Continuous Descent Approach: Design and Flight Test for Louisville International Airport," *Journal of Aircraft*, Vol. 41, No. 5, 2004, pp. 1054-1066.

[6] Larson R.C. and Odoni, A.R., Urban Operations Research, Prentice-Hall, Englewood Cliffs, New Jersey, 1981.

[7] Sizov, N. V., Clarke, , J.-P. B., Ren, L., Elmer, K. R., and Shivashankara, B. N., "Noise Impact Study of A New 2004 Noise Abatement Procedure at Louisville Airport," *The Institute of Noise Control Engineering's Annual Conference - NOISE-CON 2005*, Minneapolis, Minnesota, 17-19 Oct. 2005.

[8] Clarke, J.-P. B., Bennett, D., Elmer, K., Firth, J., Hilb, R., Ho, N., Johnson, S., Lau, S., Ren, L., Senechal, D., Sizov, N., Slattery, R., Tong, K., Walton, J., Willgruber, A., and Williams, D., "Development, Design, and Flight Test Evaluation of a Continuous Descent Approach Procedure for Nighttime Operation at Louisville International Airport," Report of the PARTNER CDA Development Team, Report No. PARTNER-COE-2006-02, 9 Jan. 2006.

CHAPTER 7

CONTRIBUTIONS, CONCLUSIONS, AND FUTURE RESEARCH DIRECTIONS

A practical and theoretically rigorous approach for supporting air traffic controllers managing separation between aircraft performing noise abatement approach and arrival procedures under normal traffic conditions has been presented in this thesis. The contributions of the research presented are summarized in Section 7.1. Major findings and observations, and implications of this research are summarized in Section 7.2. Possible future research directions are discussed in 7.3.

7.1 CONTRIBUTIONS

Major challenges exist for routing implementation of noise abatement approach and arrival procedures under normal or high traffic conditions. These challenges are: 1) variations in aircraft trajectories due to differences between aircraft types and uncertainty factors, and 2) difficulties for controllers to predict and control separation between aircraft. One way to overcome these challenges is to reduce aircraft trajectory variations by improving aircraft guidance and control systems. Another way is to develop tools and strategies for controllers to efficiently manage the separation between aircraft given that the variations do exist. The research presented in this thesis has been focused on the latter. Specifically this research has contributed:

- **Developed a procedure design and operational framework for implementing noise abatement arrival procedures that can be adapted to different traffic flow levels**
  The philosophy guiding the operational framework is to plan a better operation that can be executed with a reasonably high level of confidence, and to prepare alternative plans to cover exceptions so that traffic throughput can be maintained. The operational framework features an intermediate metering point that separates the descent from high altitude and the low noise descent to the runway. The key is to give a target separation for the intermediate metering point such that separation can be ensured – to a desired level of confidence – during the low noise descent to the runway without further controller intervention so that noise can be minimized. The location of the intermediate metering point can be tailored to the specifics of the site and the traffic conditions thereby giving high operational flexibility and overall efficiency. Contingency plans, i.e. occasional vectoring during the low nose descent, are prepared to cover exceptions when separation violation is predicted by the controller. Procedure robustness is thus significantly improved. With this operational framework, noise abatement approach and arrival procedures can be implemented at as many sites as possible, and whenever the traffic condition permits to minimize noise impact, fuel burn, emissions, and flight time over time.

- **Identified and modeled the key factors contributing to aircraft trajectory variations**
  Aircraft type, low noise descent path logic, pilot response delay, aircraft weight, and winds were identified as major sources of trajectory uncertainties. Models of aircraft type and low noise descent path logic were developed as part of the fast-time aircraft simulator. A previously developed pilot response delay model was used. The aircraft weights were modeled from data collected from airline operations as either normal distributions or beta distributions. Aircraft Communications Addressing and Reporting System (ACARS) meteorological reports from commercial aircraft were used to build wind models. The winds were modeled as long-term statistical expectations (such as mean wind and two-sigma wind) to reflect the magnitude of the wind that an aircraft would expect to experience during its descent to the runway, and short-term variations to reflect wind changes between consecutive flights.
- **Developed a mode-decomposition and autoregressive approach for the modeling of wind variations between consecutive flights**
  For separation analysis, wind variations between consecutive flights on the same approach and arrival procedure are extremely important. A unique mode decomposition approach employing a Finite Impulse Response (FIR) low pass filter was developed to decompose the wind variation components into categorized frequency content signals. These included zero mean higher frequency signals, zero mean lower frequency signals, and Direct Current (DC) signals. The higher frequency signals and lower frequency signals were modeled as autoregressive (AR) signals, and the DC signals were modeled as random variables. To overcome the shortcomings of AR method in modeling the lower frequency signals, FIR filtering was applied to the output of AR models to obtain satisfactory results. Simulated components were then assembled to form a unique inter-flight wind variation sample for each individual simulation run.
- **Developed an unique fast-time Monte Carlo simulation tool for simulating aircraft trajectory variations**
  A fast-time aircraft simulator was developed with careful trade-offs between simplicity, fast execution, accuracy, and the capability of simulating 4D aircraft flight trajectories. Focus was given to macro level aircraft trajectories. Non-steady state equations of motion were used to allow aircraft behavior under various wind conditions to be accurately simulated. Major aircraft navigation and control systems such as the Flight Management System (FMS) and autopilot model were included in the simulator. A pilot agent was also included in the simulator to control the extension of flaps/slats, landing gear, and speedbrakes during simulation runs. The aircraft simulator and models of factors contributing to aircraft trajectory variations were combined to form a unique fast-time Monte Carlo simulation tool. The tool enables arrival procedures being simulated hundreds of times for each aircraft type under various external conditions within a short amount of time and at very low cost. The large pool of simulated aircraft trajectories can then be used to analyze variations in aircraft trajectories for the specific procedure design and operating environment.
- **Developed a new separation analysis methodology**
  A methodology for analyzing the separation between consecutive aircraft performing the same noise abatement approach and arrival was developed. The methodology provides the means to determine the target separations at the intermediate metering point. The concept of feasible separation was conceived, that is the minimum spacing at the intermediate metering point that ensures that the required separation minima is not violated throughout the remainder of the procedure. The method for obtaining probability density functions (pdfs) of feasible separations from radar tracks or simulated aircraft trajectories was developed. The conditional probability

method directly connects target separations at the intermediate metering point with conditional levels of confidence. The total probability method gives a more realistic estimate of levels of confidence for given target separations in real world environment. The sequence-independent target separation is easy to use, but sequence-specific target separations could provide additional throughput benefits. In order to rigorous analyzing trade-off between level of confidence and traffic throughput, a theoretical framework for was also formulated that consists the minimum delay optimization problem and the maximum levels of confidence problem.

- **Demonstrated the applicability and utility of the Monte Carlo simulation tool and the separation analysis methodology**
  The applicability and the effectiveness of the Monte Carlo simulation tool and the separation analysis methodology were demonstrated through a simulation study and a flight test project. The simulation study demonstrated that with aircraft trajectories generated from the Monte Carlo simulation tool, the application of the conditional probability method is straightforward. The value of the total probability method and the benefits of using sequence-dependent target separations over a sequence-independent target separation were also demonstrated through simulation analysis. Analysis of target separations and traffic throughput for different wind conditions and different locations of the intermediate metering point proved the flexibility of the operational framework. The Monte Carlo simulation tool and the separation analysis methodology were successfully applied in the Continuous Descent Arrival (CDA) flight test conducted in September 2004 at Louisville International Airport (KSDF). The flight test demonstrated that the separation analysis methodology is very effective in providing a target separation for the controller to manage the CDA traffic flow. Analysis of flight test data revealed that both conditional probability and total probability from the simulation results closely matched what occurred during the flight test.
- **Developed a model of spacing in arrival traffic stream from flight test data**
  Data collected during the KSDF 2004 CDA flight test, including Automated Radar Terminal System (ARTS) data, Flight Data Recorder (FDR) data were carefully examined and rigorously analyzed. Based on these analyses, an Erlang distribution model of the spacing in unadjusted and adjusted traffic streams was developed. The modeling approach and resulting models developed provide bases for developing more generic models that can be used in the application of the total probability method at other sites in the future.
- **Identified controller techniques for predicting and adjusting spacing**
  Data collected during the KSDF 2004 CDA flight test, including ARTS data, FDR data, and air/ground voice communications, were carefully examined to identify controller techniques used in predicting and adjusting spacing between aircraft during the flight test were identified. This effort is important for expanding the implementation of noise abatement arrival procedures at other sites in the future.

The design framework, the Monte Carlo simulation tool, and the separation analysis methodology form a Tool for Analysis of Separation And Throughput (TASAT). In addition to the KSDF 2004 CDA flight test project, the procedure design and operational framework and the tool has been and are currently being applied in approach and arrival procedure development projects at a number of airports in the US and Europe. These airports include Nottingham East Midlands Airport and London Gatwick Airport in UK, Los Angeles International Airport, Hartsfield-Jackson Atlanta International Airport, and several other airports

Although the methodology was specifically developed for solving the separation analysis problems for noise abatement approach and arrival procedures, it may also be used more generally for any approach or

arrival procedures that have a predefined lateral flight path, such as the Area Navigation (RNAV) arrival procedures or Required Navigation Performance (RNP) approach and arrival procedures.

7.2 CONCLUSIONS AND IMPLICATIONS

The research work presented in this thesis covered several aspects of the design and implementation of noise abatement approach and arrival procedures. The conclusions are divided into three specific areas: procedure design, separation analysis methodology, and observations from the KSDF 2004 CDA flight test. These conclusions are summarized in the following three subsections respectively. The implications of this research are discussed in the last subsection.

7.2.1 On Noise Abatement Arrival Procedure Design

Flight tracks of existing vectored arrival flights were examined to illustrate areas that can be improved to reduce community noise impact. Aircraft noise impact and fuel flow of two special flight modes, constant Calibrated Airspeed (CAS) level flight and constant CAS idle descent, were examined through simulation to determine the potential noise reductions and fuel savings that can be achieved through procedure improvements. It has been concluded that:

- As the altitude of the constant CAS level flight increases, the maximum A-weighted sound level (LAMAX) on ground decreases nonlinearly – the rate of decrease is higher at low altitudes than that at higher altitudes. More noise reduction can be achieved by increasing the altitude of level flight segments that are currently observed at low altitudes, or by eliminating them at all.
- As the CAS of the constant CAS level flight decreases, the LAMAX on ground increases. The increase in LAMAX due to the decrease in CAS is more obvious when flaps are extended than that when the aircraft is in clean configuration. Level flight in the terminal area should be conducted at high speeds when the aircraft is in clean configuration, if these level segments cannot be completely avoided.
- When the constant CAS level flight is conducted above a certain altitude, the noise level on ground will fall below a certain threshold that can be viewed as acceptable. This suggests that vectoring at high altitudes may be tolerable from a community noise point of view.
- LAMAX on ground can be reduced by reducing the engine thrust from that required for constant CAS level flight to idle. However, this noise reduction can be easily surpassed by the noise reduction by increasing the altitude. It is more important to maintain a higher vertical profile in some cases, especially during the lower part of the noise abatement arrival procedures.
- The aircraft engine fuel flow can be significantly reduced by maintaining engine power at idle. Compared with this, the effects of other procedure parameters, such as speed and altitude, on engine fuel flow become secondary. It is very important to maintain the engine power at idle as long as possible to save fuel.
- At any given altitude and speed, the level flight represents the upper bound of required thrust to maintain a given constant CAS during the arrival and approach phase of flight. The Flight Path Angle (FPA) for constant CAS idle descent represents the lower bound of required thrust (idle thrust) to maintain the same constant CAS. At any FPA in between, either the thrust will need to be added to maintain a given CAS, or the aircraft will decelerate. As the aircraft decelerates and gets closer to the runway, thrust must be added to maintain stabilized flight because the FPA would be constrained by the Instrument Landing System (ILS) glide slope. This essentially limits

the area where noise abatement approach and arrival procedures are effective in reducing community noise impact.

- The operational framework presented in this thesis features an intermediate metering point that separates the descent from cruise and the low noise descent to the runway. By giving proper target separations for the intermediate metering point such that separation can be ensured – to a desired level of confidence – throughout the low noise descent to the runway, the operational framework is able to accommodate noise abatement arrival and approach procedures and give controller the flexibility to manage traffic flow.

7.2.2 On The Separation Analysis Methodology

The separation analysis methodology presented in this thesis may be used to determine the target separation at a selected intermediate metering point that will allow aircraft to perform noise abatement approach and arrival procedures to a desired level of confidence without interruption. The methodology utilizes aircraft trajectories from radar tracks or computer simulation. In the accompanying Monte Carlo based aircraft trajectory simulation tool that has been developed to support the application of this methodology, various uncertainty factors such as pilot actions, aircraft landing weight, and winds are modeled to provide accurate and reliable estimates of aircraft trajectory variations. Based on the theoretical analysis and the results of the numeric simulation, the following conclusions can be drawn:

- The conditional probability method is a useful way to determine target separations because it directly connects target separations at the intermediate metering point to conditional levels of confidence. The relationship is shown by the pdfs of feasible separations and the application of the method is straightforward.
- The total probability method gives more realistic estimates of the levels of confidence for the given target separations. Additionally, it can be used to evaluate the feasibility of a noise abatement approach and arrival procedure under given traffic conditions, and to determine target separations that best fit the given traffic conditions. However, it takes additional effort to obtain the data required to generate the pdfs of the actual traffic spacing.
- There are significant benefits in using sequence-specific target separations relative to current practice of using a single Miles-in-Trail (MIT) restriction or target separation. However, the use of multiple target separations increases the number of variables that controllers must use as the number of aircraft sequences is proportional to the square of the number of aircraft types in the arrival stream. Sequence-specific target separations will need to be consolidated to keep the number of variables within a manageable level.
- The current practice of giving MIT restrictions in increments of 5 nm is not efficient, as the computed target separations are not integer multiples of 5 nm. Thus, it is necessary to reduce the discretization increment step from 5 nm to a smaller number.
- Winds have a strong impact on the feasible separations. If efficiency is a big concern, such as in relatively busy terminal areas or during relatively busy times of the day, different sets of target separations should be determined for different nominal wind conditions. In this case, a strong tail wind condition would need larger target separations, and a strong head wind condition would need smaller target separations.
- For the same conditional level of confidence, traffic throughput will be significantly improved as the intermediate metering point is moved closer to the runway threshold. Thus, for a given procedure, target separations could be provided at optional metering points along the noise

abatement arrival procedure flight path to allow for operational flexibility in accommodating different traffic loads.

7.2.3 Observations from the Flight Test

The separation analysis methodology presented in this thesis was applied in the KSDF 2004 CDA flight test involving UPS B757-200 and B767-300 revenue flights. Based on simulation and analysis results, a 15 nm target separation was recommended for the selected intermediate metering point SACKO. Based on the analysis of radar tracking data and air/ground voice communications, it is observed that:

- The recommended 15 nm target separation was used by both Air Route Traffic Control Center (Center) controllers and the Terminal Radar Approach Control (TRACON) controllers, but in different ways. The target separation was used by Center controllers as a MIT restriction to deliver traffic to TRACON controllers. On the other hand, the target separation was used by TRACON controllers as a reference aid for predicting future separations between aircraft on the CDA.
- The use of larger target separation reduces randomness in the arrival flow. Although the average spacing in the arrival stream was increased by using a larger target separation (or a larger MIT restriction), the standard deviation was decreased. As the target separation increased, the average traffic spacing increased by a amount smaller than the corresponding increase in the target separation.
- The spacing in the arrival stream under MIT restrictions followed Erlang distributions. The left side tail of the distribution extended to the spacing values less than the target separations. This indicates that at times the MIT restrictions might not be satisfied. However, there were no observations of spacing below the separation minimum of 5 nm.
- After gaining experience managing the CDA flights, controllers were able to develop techniques for predicting future separations between aircraft on the same procedure. Since the lateral flight path was fixed, controllers used their mental models of the probable CDA speed profiles and relied on the relative speed of the trailing aircraft with respect to the speed of the leading aircraft to predict if spacing would be less than separation minima in the future.
- The techniques used by controllers to adjust spacing maintained noise abatement benefits in most cases. These techniques included directing the aircraft to side step to the parallel runway, vectoring the aircraft 30 deg off CDA path and return later, and adjust descent speed prior to the deceleration at 10,000 ft.
- In some cases, when the weather condition permitted, visual separation was used when controllers predicted that the Instrument Flight Rules (IFR) separation minima could be violated. When using visual separation, a pilot sees the aircraft in front, and provides his own separation from the aircraft in front. Because visual separation requires less spacing between aircraft than radar separation, interruption to the execution of CDA was reduced.
- Two strategies were used by controllers to adjust the spacing between aircraft during the execution of CDA. The first strategy was to vector the aircraft early when the spacing at the metering point was less than the given target separation. The second strategy was to vector the aircraft when aircraft was close to turning on to the final approach course and that the controller was certain that a separation violation would occur if no action were to be taken. If the first strategy is used, some of the aircraft may have been vectored when in fact the separation could eventually be ensured without intervention. If the second strategy is used, the number of aircraft to be vectored could be reduced. However, as the actions are to be taken later in the procedure,

the aircraft would probably have to vectored substantially to extend the base leg and fly level segments at relatively low altitudes if an alternative parallel runway is not available for use.

- Controllers were also able to handle the arrival traffic flow with mixed aircraft types when the CDA flight test was active. A number of non-CDA flights were fed into the gaps between CDA flights and were vectored to follow the CDA lateral flight path. In several cases, speed commands were assigned to non-CDA flights to maintain proper spacing – allowing CDA flights to continue without interruption.

7.2.4 Implications of This Research

Aircraft noise is a significant concern to communities near airports, and therefore a constraint to the growth of aviation. Advanced noise abatement approach and arrival procedures are a cost effective means of achieving near- and medium-term noise reductions. Additionally, these procedures can be employed to reduce fuel burn, emissions, and flight time. However, because of the aircraft trajectory variations due to operational uncertainties, and because the aircraft is continuously descending during noise abatement approach and arrival procedures, it is difficult for air traffic controllers to predict and maintain separation. Without proper decision support tools, negative impact on airport capacity is anticipated for implementing noise abatement approach and arrival procedures. The benefits of noise abatement approach and arrival procedures on one hand and the anticipated negative impact on capacity from their implementation on the other form a dilemma. This is essentially one of the major reasons why noise abatement approach and arrival procedures have not been routinely implemented in the past.

The research presented in this thesis demonstrated through the KSDF 2004 CDA flight test that with the developed framework and tools, noise abatement arrival procedures can be implemented in near-term to achieve noise reductions and other economic and environmental benefits while maintaining a certain level of traffic throughput. Although the flight test was conducted during the middle of the night, because of the nature of UPS's over-night package delivery operations, the traffic level could be at times relatively high. Additionally, while the CDA flight test was active, UPS B757-200 and B767-300 were not the only aircraft types in the arrival flow. There were other UPS aircraft types, and occasional aircraft from other carriers in the arrival flow. Those aircraft were not expected to fly CDA. However, controllers were able to manage the arrival traffic with mixed types, CDA, and non-CDA. Similar traffic conditions exist at many airports. For example, early morning arrivals from the west coast, at major east coast airports could be very good candidates to fly CDA. Nighttime cargo operations at other airports can also fly CDA. Similar traffic conditions could exist during daytime at certain airports, especially for traffic from certain entry points. These are also windows of opportunity for implementing CDA. Under this implementation scheme, although only a fraction of flights fly CDA, the benefits add up quickly giving today's large number of aircraft operations – over 10 million departures per year. If 10% of the flights can perform CDA, that would be 1 million CDA per year. In fact, in several current projects, noise abatement arrival procedures are already being developed for implementation under this scheme.

The research presented in this thesis also demonstrated through simulation analysis that with the developed framework and tools, noise abatement approach and arrival procedures can be implemented in the near-term under relatively high traffic conditions. This can be achieved by using an intermediate metering point closer to the runway threshold, and using sequence-specific target separations. It is also important to allow the use of target separations presented in discretization step sizes smaller than the 5 nm discretization step size currently used for MIT restrictions. With CDA implemented under higher traffic, an even larger number of flights can perform CDA.

Under queueing theory, system delay comes from uncertainties, or randomness in arrival traffic and the services handling the traffic. The procedure design and operational framework implies increased level of coordination between Center and TRACON as demonstrated by the KSDF CDA flight test. The target separations are determined based on the analysis of trajectory variations. The use of such determined target separations can be viewed as applying traffic regulators that reduce randomness in the traffic flow. Thus, the procedure design framework, the supporting Monte Carlo simulation tool and the separation analysis methodology provides a means to reduce system delay. The application of the tools are thus not limited to noise abatement approach or arrival procedures. They can be applied to generic RNAV and RNP arrivals as well. With some changes, the tools can even be applied to the conventional approach to determine the optimal MIT restrictions, thus improving system efficiency. In contrast, in the current operational environment, MIT restrictions are purely determined based on experience.

The framework and the tools presented in this thesis were developed with the open-loop control assumption, i.e. pilots flying aircraft to track pre-computed profiles without interacting with other traffic. Controller intervention is needed when adjustment to spacing is necessary. This does not imply that when new technology – such as airborne spacing – is available in the cockpit, the framework, and the separation analysis methodology would become obsolete. On the contrary, the framework and the tools would still be a valuable means for strategic planning tasks so that the high gain control actions by each individual aircraft can be minimized to maintain procedure benefits to the highest level. On the other hand, should airborne spacing technology or the required time of arrival technology be used, the traffic throughput for noise abatement approach and arrival procedures could be maintained at an even higher level. This is because additional leverage would be available for adjusting spacing. The airborne spacing would enable the use of lower levels of confidence that is defined based on open-loop aircraft trajectory control.

The procedure design and operational framework also presents a methodology to manage uncertainties in a more generic sense. Instead of employing ad hoc actions to respond to operational uncertainties, a nominal plan can be developed with a reasonable – though not absolute – level of confidence without the need for ad hoc response actions. By accepting some uncertainties, near-optimal plan can be used to achieve operational goals. Alternative measures or contingency plans can be developed to cover exceptions.

7.3 FUTURE RESEARCH WORK

The simulation tool and the analysis methodology have been improved over the course of growing applications in different projects in both US and Europe. Future efforts to expand the research presented in this thesis include:

- **Modeling more aircraft types**
  One of the continuing efforts is to add new aircraft types to the fast-time aircraft simulator. Specifically, more commercial transport aircraft types from Airbus and regional jets could be added to expand the capability of the simulator so that it can be used for future projects with more diverse fleet mix.
- **Enhancing the aircraft performance model**
  Future enhancements of the Monte Carlo simulation tool could include incorporating performance variations within each aircraft type due to differences in wearing, weathering, and adjustment. Probability distribution model of aircraft CG positions could also be developed. These future enhancements mostly rely on the data available to support the modeling efforts.

- **Expanding the wind model**
  Special wind profiles can be developed to study the procedure flyability and separation requirement under different wind conditions. These may include seasonal wind profiles and wind profiles for certain runway configurations. The wind variation model may be expanded to use other available data sources at sites where no sufficient ACARS are available.
- **Improving the pilot response delay model**
  A previously developed pilot response model was used in the current Monte Carlo simulation tool. Larger variations in flap and speedbrake usage were observed during the KSDF 2004 CDA flight test. It is believed that training would improve operational consistency, but the larger variations observed could also be partially due to difference between pilot response in line operations and pilot response in a tightly controlled experiment with a specially designed procedure. Data collected from the field or further experimental studies could thus be used to calibrate the pilot response delay model.
- **Developing a generic model of spacing in the arrival traffic stream under different MIT restrictions**
  Probability distributions of spacing in the arrival stream under different MIT restrictions are very important for evaluating the suitability of noise abatement approach and arrival procedures (and RNAV arrival procedures) under real world traffic conditions and determining optimal target separations. Radar data tracking under different MIT restrictions are often not readily available. Controller-in-the-loop simulation studies could be used to collect these data. With sufficient data, a generic model for the spacing in arrival stream may be developed as a function of the mean of unadjusted traffic spacing, the standard deviation of unadjusted traffic spacing, and the target separations.
- **Tradeoff analysis through solving the separation optimization problems**
  The formulations of the minimum delay optimization problem and the maximum levels of confidence problem provide bases for rigorous tradeoff analysis. With the generic model of spacing in the arrival traffic stream developed, the tradeoff optimization problems can be solved to determine different sets of target separations for combined scenarios with different wind conditions, traffic mix, and traffic load. This would allow for as many aircraft as possible to perform uninterrupted noise abatement approach and arrival procedures (and RNAV procedures) within a manageable limit even during relatively busy periods. Detailed analyses of noise abatement benefits and delay penalties to upstream traffic under MIT restrictions provide another research opportunity for the future.
- **Solving the traffic coordination problem for merging arrival routes**
  The research presented in this thesis has been focused on the case of a single file of arrival aircraft performing the same noise abatement approach or arrival procedure. The separation analysis methodology can also be extended to merging traffic on different arrival procedures from different entry points leading to the same runway. In the case of merging traffic, the target separation problem becomes a traffic coordination problem. Two new elements associated with winds come into play. The first is the nominal wind profile. Given the same nominal wind profile, the headwind and crosswind components will be different for different arrivals due to differences between their lateral paths. The other is the wind variation between flights on different arrival paths. Aside from the influence of winds, aircraft trajectories in terms of distance versus time will have systematic differences on different arrival procedures, mainly due to differences in procedure parameters. Aircraft pairs will have to be treated as sequence/procedure combinations rather than sequences only. However, the fundamental

principle of the separation analysis presented in this thesis is still applicable. Instead of spacing at the metering point between a pair of consecutive aircraft on the same procedure, distances of the "trailing" aircraft to its own metering point – measured at the time when the "leading" aircraft on the other procedure is at own its metering point – can be used for the analysis. The analysis could even be more straightforward if it were based on time of arrival to each procedure's respective metering point. The solution to the traffic coordination problem would be an essential step to more broad application of noise abatement approach and arrival procedures and RNAV/RNP arrival procedures alike.

- **Applying the methodology to departure and en route operations**
  The procedure design and operational framework and the separation analysis methodology can also be extended in include departure and en route operations. The goal is to streamline the merging of departure flights into en route traffic flow, and to minimize vectoring of en route flights when they are handed off from one sector to another.

APPENDIX A

THE FAST-TIME AIRCRAFT SIMULATOR

NOMENCLATURE

$\mathbf{A}$	=	transformation matrix, from NED to Body frame
a_c	=	centrifugal acceleration
C_d	=	drag coefficient
$C_{dSBfull}$	=	drag coefficient increment of fully extended speedbrake
C_l	=	lift coefficient
C_l^α	=	lift curve slope
C_{l0}	=	lift coefficient at zero angle of attack
C_y	=	side force coefficient
D	=	drag
F_c	=	centrifugal force
f_f	=	total fuel flow
F_y	=	side force
F_n	=	engine net thrust
F_n/δ	=	corrected engine net thrust
g	=	gravitational acceleration
h	=	aircraft altitude above mean sea level
k_i	=	drag polar parameters, $i = 0, 1, 3$
L	=	lift
m	=	aircraft mass
n	=	number of engines of an aircraft
p	=	X component of aircraft angular velocity in Body frame
p_{SB}	=	speedbrake usage in %
q	=	Y component of aircraft angular velocity in Body frame
R	=	radius of turn
r	=	Z component of aircraft angular velocity in Body frame
S	=	aircraft wing reference area
T	=	total net thrust
u	=	X component of aircraft velocity in Body frame
u_r	=	X component of true airspeed in Body frame
$\mathbf{V}$	=	aircraft speed vector
v	=	Y component of aircraft velocity in Body frame
V_c	=	calibrated airspeed
V_g	=	ground speed

V_h = vertical speed
V_r = true airspeed
v_r = Y component of true airspeed in Body frame
$\mathbf{W}$ = wind vector
w = Z component of aircraft velocity in Body frame
W_c = crosswind component
$\mathbf{W}_F$ = wind forecast vector
W_{Fc} = crosswind component of wind forecast
W_{Fh} = headwind component wind forecast vector
W_h = headwind component
W_E = East wind component
W_N = North wind component
w_r = Z component of true airspeed in Body frame
W_u = X component of wind in Body frame
W_v = Y component of wind in Body frame
W_w = Z component of wind in Body frame
X_{NED} = North coordinate in NED frame
xte = cross track error
Y_{NED} = East coordinate in NED frame
Z_{NED} = Down coordinate in NED frame
α = aircraft angle of attack
β = sideslip angle
δ = ambient pressure ratio, p/p_0
ϕ = roll angle
γ = flight path angle
γ_r = the angle between true airspeed vector and the horizontal plane
λ = track angle
λ_r = incidental angle between wind vector and ground speed in horizontal plane
μ_r = angle between true airspeed and ground speed in horizontal plane
θ = pitch angle
ρ = ambient air density
ψ = yaw angle

A.1 INTRODUCTION

Flight test is the ultimate means of studying aircraft trajectory characteristics and researching flight operation procedures. However, it is also a costly and time-consuming process. Simulations have thus been extensively used in flight operation procedure design and flight test planning. Full fidelity dedicated simulators such as the National Aeronautics and Space Administration (NASA) Ames B747-400 full motion flight simulator[1] have all the major flight crew interfaces and are very accurate in representing real aircraft dynamics. Experiments with these simulators usually involve qualified airline pilots. Due to the relatively high cost of operating such simulators, and the difficulties in scheduling and recruiting pilot subjects, the number of simulation runs on a full fidelity dedicated simulator in an experiment is limited. A workstation based aircraft simulator, the NASA PCPlane[2], using general purpose computing platforms,

provides a simulation environment for the flight management functions and displays of advanced civil transport aircraft. It's proven to be effective in explore new display and operation concepts, but it still needs at least trained student pilot to perform each simulation run. A trajectory-centered fast-time simulation tool, the NASA TCSim[3], can simulate a variety of aircraft types in a wide region of airspace at same time. TCSim includes embedded pilot agents and generates arrival time estimations by automatically 'flying' each aircraft's trajectory and storing the time it takes to arrive at relevant points along the trajectory. However, for the specific application of TCSim, the resolution of trajectory simulation is relatively low; besides, it is not readily accessible outside the organization.

To study noise abatement approach procedures, Ho and Clarke developed a workstation based fast-time aircraft simulator using 2D point mass model formulation[4]. This simulator was improved by Ren et al for a capacity analysis study of a Modified Three Degree Decelerating Approach (MTDDA)[5]. In 2004, the fast-time simulator was redesigned to achieve 4D trajectory simulation accuracy comparable to full fidelity simulations. Yet, it was designed to be simple enough so that it can be executed in fast-time to generate large number of trajectories for different operation conditions, namely combinations of aircraft configurations, procedure design parameters, and weather conditions, in a relatively short amount of time. To this end, a careful trade-off has been made between accuracy, flexibility, simplicity, and execution speed. In order to accurately simulate aircraft behavior under various wind conditions, aircraft movement in wind condition is carefully analyzed and formulated. The simulator was developed for evaluating and down-selecting procedure design features and for analyzing separation between aircraft during execution of arrival and approach procedures. The most important parameters are altitude, thrust, distance, and time along aircraft trajectory because these parameters directly affect noise impact and spacing between aircraft. Thus, less emphasis was given to aircraft micro dynamic behavior and human-machine interactions. Should those issues become important in later stages of procedure development, researchers can move to more sophisticated simulation facilities such as the full motion simulator mentioned earlier. The resulting fast-time aircraft simulator consists of an aircraft dynamics model, Flight Management System (FMS) with Vertical Navigation (VNAV) capability, the autopilot, and the autothrottle. A pilot agent was included to manually control the extension of flap, landing gear, and speedbrakes. Procedure definition and pilot operation procedure such as the flap schedule can be given as deterministic inputs. On the other hand, individual pilot action variations, aircraft weight, and wind profile can be given as stochastic inputs. System block diagram of the fast-time aircraft simulator is shown in Fig. A-1.

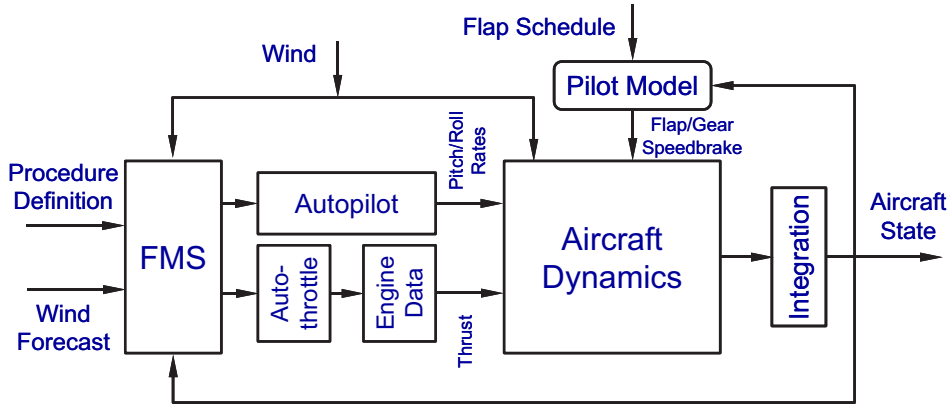

Figure A-1 Aircraft simulator block diagram.

Because the application of this fast-time simulator is focused on aircraft arrival procedures, the flat earth assumption should be sufficient in terms of accuracy. The following right-handed coordinate frame definitions are used:

North-East-Down (NED) frame. The origin of this frame is assumed at a fixed point – normally the reference point at the destination airport. The North-East plane is parallel to the Earth's surface, X – north, Y – east, Z – down. This is essentially the inertial reference frame.

Aircraft body fixed (Body) frame. This frame is fixed to the aircraft body with its origin at the nominal center of gravity of the aircraft; X – forward along aircraft longitudinal reference line, Y – starboard, Z – down.

Euler angles. These are a sequence of three rotations that define aircraft's instantaneous attitude, or the orientation of Body frame. The rotations are performed in the order of yaw ψ, pitch θ, and roll ϕ, with Body frame initially aligned with NED.

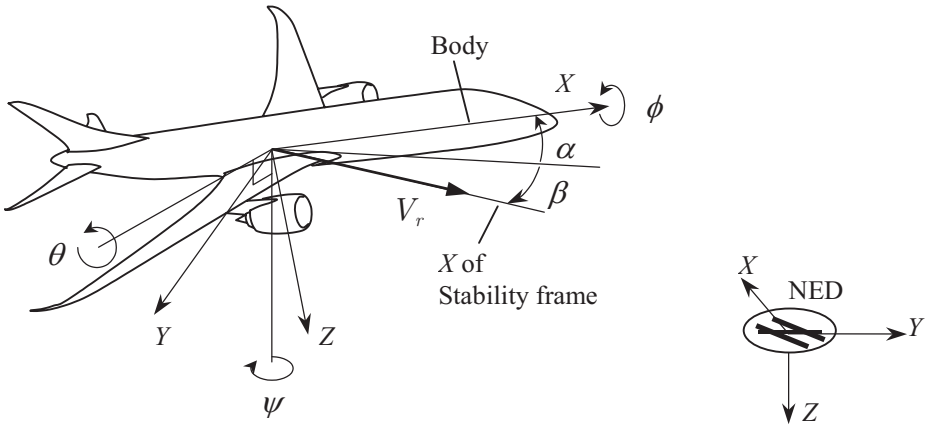

Figure A-2 The relationship between NED, Body, and Stability frames.

While the navigational computation was performed in NED frame, the aircraft dynamics computation was performed in Body frame. The transformation matrix from NED frame to Body frame can be derived as[6]

$$\mathbf{A} = \begin{bmatrix} \cos\theta\cos\psi & \cos\theta\sin\psi & -\sin\theta \\ -\cos\phi\sin\psi + \sin\phi\sin\theta\cos\psi & \cos\phi\cos\psi + \sin\phi\sin\theta\sin\psi & \sin\phi\cos\theta \\ \sin\phi\sin\psi + \cos\phi\sin\theta\cos\psi & -\sin\phi\cos\psi + \cos\phi\sin\theta\sin\psi & \cos\phi\cos\theta \end{bmatrix} \quad \text{(A-1)}$$

Stability frame. Like the Body frame, the origin of this frame is also at the nominal center of gravity of the aircraft. The stability frame can be obtained through rotating Body axis about first its Y-axis and then the new Z-axis such that the new X-axis is aligned with the aircraft velocity relative to the air mass – a widespread body of air in which the aircraft moves. This is the frame in which aerodynamic force components are calculated. The rotation from Stability frame to Body frame is aircraft side slip angle β and angle of attack α.

All computation was to be conducted under International Civil Aviation Organization (ICAO) Standard Atmosphere[7] (ISA) conditions. A set of utility functions was created to convert between Mach number, True Airspeed (TAS), Equivalent Airspeed (EAS), and Calibrated Airspeed (CAS). For aircraft with electronic speed indicator or electronic speed tape, the position error values are accounted for in the

air data computers, resulting in the pilot reading computed airspeed, or CAS[8]. Thus, whenever IAS was required CAS was used instead because the simulation was only concerned about advanced jets with FMS with electronic speed tape.

The remainder of this section is organized as follows. The next section describes the aircraft dynamics model used in the fast-time simulator. This includes the aerodynamics model and the equations of motion. Section A.3 presents an analysis of wind effects on aircraft motion. Section A.4 describes the FMS module used in this simulator. Algorithms used in the FMS to compute VNAV flight path are presented in detail. Section A.5 describes simplified autopilot and autothrottle models, and the pilot model used in this simulator. Assumptions used to simplify the autopilot and autothrottle models are discussed. Lastly, the Monte-Carlo simulation data flow, simulation accuracy, and the interfaces to external tools are described.

A.2 THE AIRCRAFT DYNAMICS MODEL

The basic procedure of aircraft simulation is to start with the aircraft dynamics model to obtain aircraft angular and translational accelerations. By integrating these accelerations, aircraft state at the next time step can be obtained. The process is shown in Fig. A-1. Starting from an initial state and iterating this process step by step, aircraft flight trajectory can be generated. This section first describes the aircraft aerodynamics model and engine model used in the fast-time simulator. It then gives the derivation of angular and translational displacement derivatives and navigation equations. The integration method is also briefly discussed.

A.2.1 External Forces

Given altitude h, true airspeed V_r, angle of attack α, and sideslip angle β, aerodynamic forces as represented by components in stability frame, namely lift L, drag D, and side force F_y, can be computed

$$L = \frac{1}{2}\rho V_r^2 S C_l \tag{A-2}$$

$$D = \frac{1}{2}\rho V_r^2 S C_d \tag{A-3}$$

$$F_y = \frac{1}{2}\rho V_r^2 S C_y \tag{A-4}$$

where ρ and S denote air density and the reference wing area respectively.

Unlike the commonly used point-mass models in which steady state equilibrium equations are used, the lift coefficient was modeled as a linear function of aircraft angle of attack. This is shown in Eq. (A-5). The instantaneous angle of attack was determined by the aircraft attitude and the wind condition. This model gives more accurate results for varying wind conditions, because the effect of varying wind on angle of attack is directly reflected in lift. It was assumed that the lift coefficient at zero angle of attack C_{l0} and the lift curve slope C_l^α were functions of the aircraft's flap/gear setting.

$$C_l = C_{l0} + C_l^\alpha \alpha \tag{A-5}$$

As shown in Eq. (A-6), the low speed drag polars were approximated as parabolic curves for the normal range of lift coefficient. The three parameters k_0, k_1, k_2 were assumed functions of aircraft's flap/gear setting. The last term in Eq. (A-6) represents the drag contribution of speedbrakes. Coefficient $C_{dSBfull}$ was used to represent drag coefficient increment when speedbrakes are fully extended; and a percentage p_{SB} was used to represent how much speedbrake was to be used. High-speed drag polars were presented as a look up table given drag coefficient as a function of lift coefficient at different Mach numbers. High-speed drag polar becomes important when descent from cruise altitude is to be simulated.

$$C_d = k_0 + k_1 C_l + k_2 C_l^2 + C_{dSBfull} p_{SB} \tag{A-6}$$

Equation (A-7) represents a generic model of the side forces coefficient as suggested by Nelson[9]. Side force was included in the model to represent the drifting acceleration behavior of a typical commercial aircraft under changing crosswind. Under stead-state conditions, the sideslip angle becomes zero, and, thus, the side force becomes zero.

$$C_y = -0.682\beta \tag{A-7}$$

Internally, engine thrust was modeled as corrected net thrust per engine under different power settings. Corrected net thrust per engine is defined[8] as net thrust per engine F_n divided by ambient pressure ratio δ, i.e. F_n/δ. Engine thrust was to be bounded by idle thrust and maximum climb thrust. Depending on the actual control mode used in a flight segment, engine thrust may be that of idle, maximum climb, or somewhere in between as determined by the autothrottle. A first order delay was used to model the engines' spool-up response. The total net thrust exerted on the aircraft was computed as

$$T = n\delta\left(F_n / \delta\right) \tag{A-8}$$

For idle power, corrected net thrust per engine and engine fuel flow were represented as a look up table given corrected thrust and fuel flow as functions of Mach number at different altitudes. For maximum climb power, only corrected net thrust per engine was represented as a look up table. At power settings other than idle, corrected engine fuel flow[8] was represented as a look up table given fuel flow as a function of corrected thrust and Mach number at different altitudes. Engine surge bleed valve schedule could also be provided to give more accurate fuel burn.

Based on the flat earth assumption, aircraft weight was assumed to only have the vertical component in NED frame with a value equal to mg, where m is the aircraft mass and g is the gravitational acceleration. The derivative of aircraft mass with respect to time was assumed to equal to the total fuel flow, but with a negative sign

$$\dot{m} = -f_f \tag{A-9}$$

In this simulator, the derivative of aircraft mass was only used to compute the instantaneous aircraft mass itself. The total fuel flow is relatively small as compared to the total aircraft mass; this is especially true during the arrival phase of flight. As such, at any given time, the aircraft mass was assumed static to simplify the computation.

A.2.2 Translational Derivatives

Applying Newton's law in the Body frame[6], the force equations yield translational derivatives of the aircraft velocity components in the *X* direction u, *Y* direction v, and *Z* direction w as follows

$$\begin{aligned} \dot{u} &= rv - qw - g\sin\theta + (T + L\sin\alpha - D\cos\alpha)/m \\ \dot{v} &= pw - ru + g\sin\phi\cos\theta + F_y/m \\ \dot{w} &= qu - pv - g\cos\phi\cos\theta + (-L\cos\alpha - D\sin\alpha)/m \end{aligned} \tag{A-10}$$

where p, q, and r denote the aircraft angular velocity components in the Body frame *X*, *Y*, and *Z* directions respectively. It was assumed that engine thrust were aligned with *X* axis in Body frame. As mentioned before, side force was included to account for side drifting acceleration due to the possible change of crosswind component along the flight path.

A.2.3 Angular Derivatives

In this simulator, aircraft attitude control is performed by an autopilot model that was assumed able to maintain certain tracking accuracy. Since autopilot has been an integral part of advanced commercial aircraft, and with modern navigation technology in place, this assumption is valid for most cases. The autopilot model provides two aircraft rotational rates as outputs, i.e. roll rate p and pitch rate q. This modeling scheme eliminated the need for aerodynamic derivatives, rotational moments, and moments of inertial momentum. Details of the autopilot are described later.

During a coordinated turn, for small flight path angles, the centrifugal force can be approximated as $F_c = L\sin\phi$. Newton's law gives $F_c = ma_c = mV_g^2/R$, where a_c denotes the centrifugal acceleration, V_g denotes the aircraft ground speed, and R denotes the radius of turn. For zero sideslip angles, the angular velocity of turn can be approximated by $V_g/R = \dot{\psi}$. Thus the derivative of aircraft yaw angle can be obtained as

$$\dot{\psi} = L\sin\phi/(mV_g) \tag{A-11}$$

Through a coordinate transformation, the *Z* component of aircraft angular velocity in the Body frame can now be obtained as

$$r = (\dot{\psi}\cos\theta - q\sin\phi)/\cos\phi \tag{A-12}$$

With all three components of aircraft angular velocity in the Body frame known, the remaining two Euler angle rates can be computed:

$$\begin{aligned} \dot{\phi} &= p + (q\sin\phi + r\cos\phi)\tan\theta \\ \dot{\theta} &= q\cos\phi - r\sin\phi \end{aligned} \tag{A-13}$$

A.2.4 Navigation Equations

The basic navigation equations define the movement of aircraft center of gravity in 3D space relative to the earth. In the NED frame, these equations were obtained by transforming the aircraft velocity components from the Body frame. They are reiterated here for the sake of clarity[6]:

$$\begin{bmatrix} \dot{X}_{NED} \\ \dot{Y}_{NED} \\ \dot{h} \end{bmatrix} = \begin{bmatrix} \dot{X}_{NED} \\ \dot{Y}_{NED} \\ -\dot{Z}_{NED} \end{bmatrix} = \begin{bmatrix} 1 & 0 & 0 \\ 0 & 1 & 0 \\ 0 & 0 & -1 \end{bmatrix} \mathbf{A}^{-1} \begin{bmatrix} u \\ v \\ w \end{bmatrix} = \begin{bmatrix} 1 & 0 & 0 \\ 0 & 1 & 0 \\ 0 & 0 & -1 \end{bmatrix} \mathbf{A}^{T} \begin{bmatrix} u \\ v \\ w \end{bmatrix} \tag{A-14}$$

The transformation matrix **A** in Eq. (A-14) is the one given by Eq. (A-1). From the components of aircraft velocity in NED frame, other properties of the aircraft movement can be obtained. By definition, the ground speed is

$$V_g = \sqrt{\dot{Y}_{NED}^2 + \dot{X}_{NED}^2} \tag{A-15}$$

Track angle

$$\lambda = \text{atan}(\dot{Y}_{NED} / \dot{X}_{NED}) \tag{A-16}$$

Flight path angle

$$\gamma = -\text{atan}(\dot{Z}_{NED} / V_g) \tag{A-17}$$

According to the above definitions, the positive sense of track angle is clockwise, the positive sense of flight path angle is climb.

A.2.5 Integration Method

With aircraft state derivatives $\dot{u}$, $\dot{v}$, $\dot{w}$, $\dot{\psi}$, $\dot{\phi}$, $\dot{\theta}$, $\dot{X}_{NED}$, $\dot{Y}_{NED}$, and $\dot{h}$ derived, aircraft state at next time step can be obtained through integration. In this simulator, the fourth-order Runge-Kutta method was used to perform the integration for its accuracy and acceptable phase lag. The integrations are performed in the frame where each state variable is defined.

A.3 THE EFFECT OF WIND

Wind is the single most important external factor that affects aircraft trajectory. In order to accurately simulate aircraft trajectory under various wind conditions, special attention must be paid to the formulation of aircraft movement when there is wind. In the following analysis, only wind components in the horizontal plane of the NED frame are considered because the vertical wind component (top shear) has a much smaller geometric scale, and its effect on the overall aircraft trajectory is limited. In this section, the effect of wind on aircraft ground speed is examined analytically first, then the computation of aircraft angle of attack and sideslip angle under wind conditions is described, and lastly the wind model used in the fast-time simulator is introduced.

A.3.1 The Effect of Wind on Aircraft Movement

Assume that aircraft is flying at a true airspeed V_r, subject to horizontal wind vector **W**, with flight path angle γ. Further assume the angle between true airspeed and the horizontal plane is γ_r. This angle represents the flight path angle relative to the air mass. The relationship between the true airspeed vector, the vertical speed vector ($\mathbf{V}_h$), the ground speed vector, and the total speed vector (**V**), as collapsed into

the vertical plane, is shown in Fig. A-3a. The relationship between speed vectors as projected in the horizontal plane is shown in Fig. A-3b, where λ_r denotes the incidental angle between the wind vector and the ground speed vector, and μ_r denotes the angle between the projection of true airspeed and the ground speed vector.

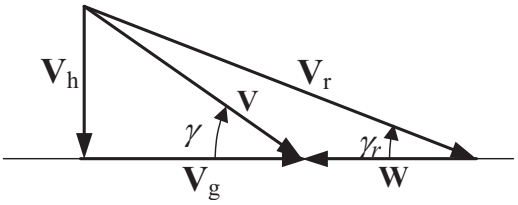

Figure A-3a Relationship between flight path angle, true airspeed, and ground speed as collapsed in the vertical plane.

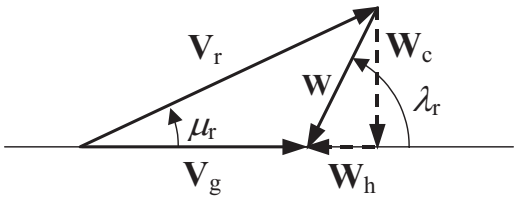

Figure A-3b Relationship between wind speed, true airspeed, and ground speed as projected to horizontal plane.

As shown in Fig. A-3a and A-3b, the general relationship can be expressed in vector form as

$$\mathbf{V} = \mathbf{V}_h + \mathbf{V}_g = \mathbf{V}_r + \mathbf{W} \tag{A-18}$$

Decomposing the wind vector into a headwind component $W_h = W\cos\lambda_r$ and a crosswind component $W_c = W\sin\lambda_r$, from Eq. (A-18), in scalar form, the following equations can be derived

$$V_g = V\cos\gamma \tag{A-19}$$

$$V_h = V_r \sin\gamma_r = V\sin\gamma \tag{A-20}$$

$$V_r^2\cos^2\gamma_r = W_c^2 + \left(V_g + W_h\right)^2 \tag{A-21}$$

Assume $0 \le |\mu_r| < \pi/2$, i.e. ground speed is positive, the following equations can be derived from Eq. (A-19), (A-20) and (A-21)

$$V_g = \sqrt{V_r^2 - V_h^2 - W_c^2} - W_h \tag{A-22}$$

$$V = \sqrt{V_r^2 - W_c^2 - W_h^2\sin^2\gamma} - W_h\cos\gamma \tag{A-23}$$

$$\sin\gamma_r = \left(V/V_r\right)\sin\gamma = \left(V_g/V_r\right)\sin\gamma/\cos\gamma \tag{A-24}$$

Equation (A-22) shows that for given vertical rate V_h and true airspeed V_r, both headwind component W_h and the crosswind component W_c affect ground speed V_g. A positive headwind component causes the ground speed to decrease, and a negative headwind component (or tailwind component) causes the ground speed to increase; while the crosswind component always causes the ground speed to decrease no matter the crosswind component comes from left or right. However, the reduction of ground speed due to the crosswind component is much smaller than that due to the headwind component, if the wind speed is relatively small. This is easily seen from the following partial derivatives

$$\partial V_g / \partial W_h = -1, \text{ independent of } W_h \tag{A-25}$$

$$\partial V_g / \partial W_c = -W_c \Big/ \sqrt{V_r^2 - V_h^2 - W_c^2} \tag{A-26}$$

For level flight $V_h = 0$, Eq. (A-22) and (A-23) reduce to Eq. (A-27); and Eq. (A-26) reduces to Eq. (A-28)

$$V_g = V = \sqrt{V_r^2 - W_c^2} - W_h = V_r - V_r\left(1 - \sqrt{1 - W_c^2 / V_r^2}\right) - W_h \tag{A-27}$$

$$\partial V_g / \partial W_c = -1 \Big/ \sqrt{V_r^2 / W_c^2 - 1}\text{, thus } \begin{cases} \partial V_g / \partial W_c < -1, & W_c / V_r > \sqrt{1/2} \\ \partial V_g / \partial W_c = -1, & W_c / V_r = \sqrt{1/2} \\ -1 < \partial V_g / \partial W_c < 0, & W_c / V_r < \sqrt{1/2} \end{cases} \tag{A-28}$$

On the right hand side of Eq. (A-27), the second term is the contribution of the crosswind component, and the third term is the contribution of the headwind component. The relationship represented by Eq. (A-27) is illustrated in Fig. A-4, for several different values of the ratio of wind speed to true airspeed (W/V_r). In Fig. A-4, the vertical axis represents the ratio of ground speed to true airspeed (V_g / V_r), the horizontal axis represents angle λ_r. As angle λ_r varies from 0 deg to 90 deg, the wind vector changes from a pure headwind to a pure crosswind; and a λ_r of 180 deg gives a pure tailwind. The effect of wind on ground speed is the highest under headwind and tailwind conditions. The effect of a pure crosswind component on ground speed is illustrated in Fig. A-5. As seen in Fig. A-4 and A-5, the effect of the crosswind component can be ignored when the crosswind component is relatively small comparing to true airspeed. However, when the crosswind component is not small, or when precise results are required, the effect of crosswind component should not be ignored. In this simulator, both headwind component and crosswind component were taken into account.

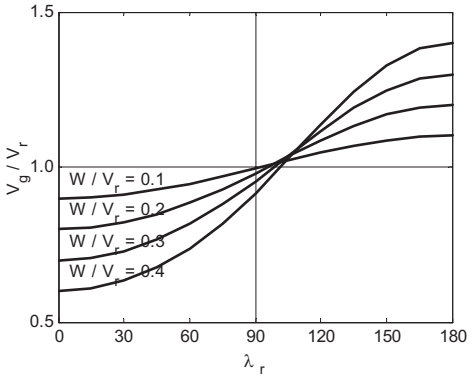

Figure A-4 The effect of wind on ground speed as wind direction varies relative to the direction of ground speed vector.

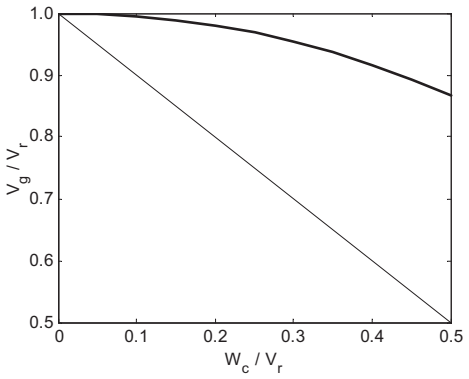

Figure A-5 The effect of a pure crosswind component on ground speed as crosswind increases relative to true airspeed.

Since aircraft control and flight operation procedures are mostly based on airspeed, the effects of wind on aircraft ground speed will affect time-to-fly, and also the evolution of spacing between consecutive

aircraft pairs. The decrease of ground speed, such as in headwind conditions, will increase time-to-fly, and cause earlier separation compression relative to zero wind condition. The increase of ground speed, such as in tailwind conditions, will reduce time-to-fly, and delay separation compression relative to zero wind condition. Uncertainties in wind forecast, and/or change of wind will transfer into uncertainties in time-to-fly and uncertainties in spacing between aircraft.

Equation (A-24) represents the effect of wind on flight path angle. Because flight path angle is small under normal flight operation conditions, $\cos\gamma \approx 1$, Eq. (A-24) can be approximated as $\sin\gamma_r \approx (V_g/V_r)\sin\gamma$. For a flight segment with fixed flight path angle γ, such as the initial constant speed segment in a Three Degree Decelerating Approach (TDDA) or MTDDA[5], the decrease in ground speed due to headwind or crosswind will result in a shallower flight path angle relative to the air mass. This in turn will require higher thrust or less speedbrake usage to maintain the same airspeed. The increase of ground speed due to tailwind will result in a steeper flight path angle relative to the air mass, which in turn will require lower thrust or more speedbrake usage to maintain the same airspeed. Both thrust and speedbrake usage have noise implications. If the engine throttle setting is fixed, such as in idle, headwind and crosswind will cause aircraft to decelerate faster, and tailwind will cause aircraft to decelerate slower. This will affect aircraft's capability to follow a specific profile.

On the other hand, for a flight segment with given flight path angle relative to the air mass γ_r, the decrease of ground speed due to headwind or crosswind will result in a steeper flight path angle. The increase of ground speed due to tailwind will result in a shallower flight path angle. For such a flight segment, the effect of wind is more complicated. Different wind conditions will result in different vertical flight paths. Not only the altitude above ground will be different, for the same airspeed profile, the longitudinal acceleration will also be different. This is because the relationship between true airspeed and calibrated airspeed will be different for different vertical profiles.

A.3.2 Aircraft Angle of Attack and Sideslip Angle

In the discussion of aerodynamic forces, to determine lift coefficient and side force coefficient, aircraft angle of attack and sideslip angle must be determined first. Assume that the aircraft is subject to horizontal wind vector **W**, with NED frame components W_N and W_E. The components of wind in Body frame can be computed through coordinate transformation

$$\begin{bmatrix} W_u \\ W_v \\ W_w \end{bmatrix} = \mathbf{A} \begin{bmatrix} W_N \\ W_E \\ 0 \end{bmatrix} \tag{A-29}$$

In Eq. (A-29) subscripts u, v, and w denote wind components in Body frame aligned with X, Y, Z directions respectively. The positive sense of the wind components is pointing to negative infinity for each direction. Aircraft speed relative to the moving air mass, true airspeed, in Body frame is thus

$$\begin{bmatrix} u_r \\ v_r \\ w_r \end{bmatrix} = \begin{bmatrix} u \\ v \\ w \end{bmatrix} + \begin{bmatrix} W_u \\ W_v \\ W_w \end{bmatrix} \tag{A-30}$$

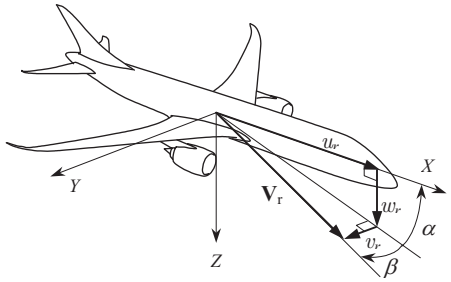

Figure A-6 Aircraft angle of attack and sideslip angle.

From the geometric relationship shown in Fig. A-6, aircraft angle of attack α and sideslip angle β can be obtained as

$$\alpha = \arctan(w_r / u_r) \tag{A-31}$$

$$\beta = \arctan \frac{v_r}{\sqrt{(u_r^2 + w_r^2)}} \tag{A-32}$$

A.3.3 The Wind Model

There are two aspects in the wind model, wind forecast and actual wind experienced by aircraft. Wind forecasts are available from a number of sources. The National Oceanic and Atmospheric Administration (NOAA) Forecast Systems Laboratory's (FSL, now the Global Systems Division of the Earth System Research Laboratory) Rapid Update Cycle, RUC40, has a horizontal resolution of 40 km and 40 vertical levels. The update rate for RUC40 is one hour. The FSL's RUC20 has a horizontal resolution of 20 km and 50 vertical levels, with improved model and algorithms[10]. Near real-time Aircraft Communications Addressing and Reporting System (ACARS) metrological reports from major US airlines are made available by NOAA for research use. ACARS data provides measurements taken by aircraft flying through the airspace, thus can be used as an alternative source of wind forecast.

Wind forecast data could be used by FMS in computing optimal speed and optimal descent path (VNAV path). According to Bulfer and Gifford[11, 12], depending on the system version, wind forecast data may be entered for each waypoint. For the Honeywell legacy FMS without the Product Improvement Package (PIP), the wind may be entered at a given flight level, and is forward propagated and backward propagated to the next waypoint if necessary. Downward propagation is linearly tapered reaching zero at the surface. For Honeywell PIP systems, wind data page provides wind entry capability for up to four altitudes. These altitudes are applied to all waypoints in the flight plan. Forward and backward propagation is done for the same flight level. Forecast winds are assumed to vary linearly between specified altitudes. Downward propagation is linearly tapered reaching zero at the surface. Descent forecast wind entry is designed for use when coming out of the jet stream. Four altitudes may be entered in the DESCENT FORECAST page. FMS uses a mixing algorithm to determine the predicted wind at points in front of the aircraft. The predicted wind is a mix of the forecast wind (entered by the pilot) and the measured wind. At the aircraft's current position, the computer uses 100% of the measured wind. During the climb and descent phase, at 5,000 ft in front of the aircraft, the FMS uses 50% of the actual wind and 50% forecast wind. At distance over 5,000 ft, the FMS uses successively less measured wind until the wind used is near 100% forecast.

In this simulator, the above-mentioned wind-mixing algorithm was implemented as part of the FMS functionality. Wind forecast data were to be provided as a separate input file allowing flexibility in the number of altitude entries to be used to accommodate different aircraft equipage. Actual wind profile was designed as another input file allowing the wind field to be defined as constant wind, or varying with time, distance, or altitude. A digital implementation of the Dryden wind turbulence model[13] was also included in the simulator. The intensity of the wind turbulence was to be defined in the wind profile, or it can be simply disabled.

A.4 THE FMS MODULE

The functionality of the FMS module is two-fold. Prior to the actual procedure run, the FMS module builds lateral flight path and vertical flight path based on entered waypoints and altitude/speed constraints. This is done according to FMS Lateral Navigation (LNAV) and VNAV logic. During the simulation run the FMS module provides guidance to the aircraft and feeds aircraft state error to the autopilot module to control the aircraft to follow the computed LNAV path and VNAV path. This section gives an overview of the basic LNAV and VNAV logic first. It then describes in detail the algorithms used for computing VNAV flight path segments.

A.4.1 LNAV Functionality

The lateral flight path is normally defined by a series of waypoints leading to the runway threshold. The location of waypoints can be given as either North-East coordinates or latitude/longitude in World Geodetic System 1984 (WGS 84). Internally, the computation is performed in North-East coordinate system. If waypoints are defined by latitude/longitude, they will be converted into the North-East coordinate system in such a way that the distance between consecutive waypoints and the angle of turn at each waypoint are preserved. Several lateral control modes are available for use during the arrival and approach phase. The most commonly used modes are LNAV path track mode (LNAVTRACK) and localizer track mode (LOC). Turn radius at each waypoint is determined based on the angle of turn and the estimated CAS at that waypoint. Before the actual simulation run, the FMS module builds a nominal flight path that consists of straight line and arc segments with corresponding control mode given at each segment.

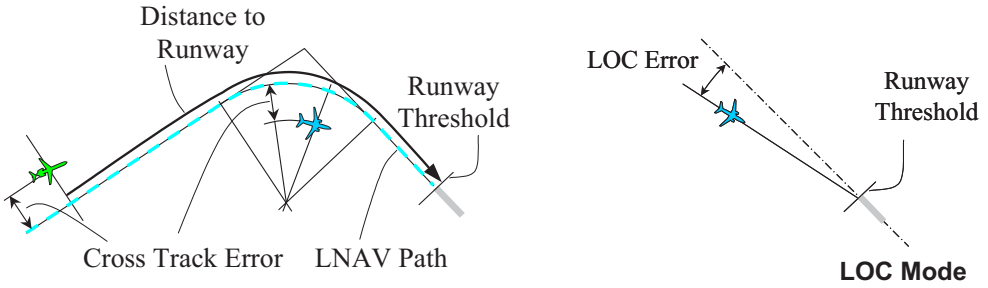

Figure A-7 Cross track error, distance to runway, and localizer tracking error.

During simulated flight, the FMS module computes an along track distance to runway threshold (distance to runway) by first projecting current aircraft position to the nominal flight path, then computing the distance of the projected intersection to the runway threshold along the nominal flight path. Distance to runway is then used as an indicator of aircraft's progress in the approach procedure. For a

LNAVTRACK segment, the cross track error, namely distance between current aircraft position and the projected intersection, is computed at the same time. This process is illustrated in Fig. A-7. Additionally, a target high level heading command is computed based on the nominal flight path track angle and wind experienced by the aircraft. Both the cross track error and the high level heading command are fed into the autopilot to control aircraft's lateral motion. For a LOC segment, normally the last segment of an approach flight path, the tracking error is defined as the angular deviation of the straight line connecting current aircraft position and runway threshold relative to extended runway centerline.

A.4.2 VNAV Functionality

The vertical flight path is defined by a series of profile parameters such as altitude, CAS/Mach, flight path angle, and engine thrust setting given at certain distances to the runway threshold. These values provide the cruise altitude, the cruise speed, the descent CAS/Mach, the vertical profile, and the Instrument Landing System (ILS) parameters should ILS be used. For VNAV descent segments, altitude and speed constraints can be given at certain waypoints on the lateral flight path to let the FMS compute an optimal descent path. When VNAV is used, altitude and speed constraints given at waypoints take precedence over the profile parameters for the same segment. The most commonly used vertical control modes in noise abatement approach and arrival procedure simulation are the VNAV flight path mode (VNAVPATH), the altitude and speed hold mode (ALTSPD_HOLD), and the ILS glide slope following mode (ILS_GS).

The FMS module builds an idle VNAV descent path from Top of Descent (T/D) to the first altitude constraint. Because there is no fixed constraint at the upper end of such a descent path, it is also referred to as unrestricted VNAV path. Below the first altitude constraint, the descent path may or may not be idle depending on the steepness of the path segments, determined by altitude constraints at waypoints. The descent path is built starting from the lowest altitude constraint through backward integration to the cruise altitude. A typical VNAV descent path is shown in Fig. A-8.

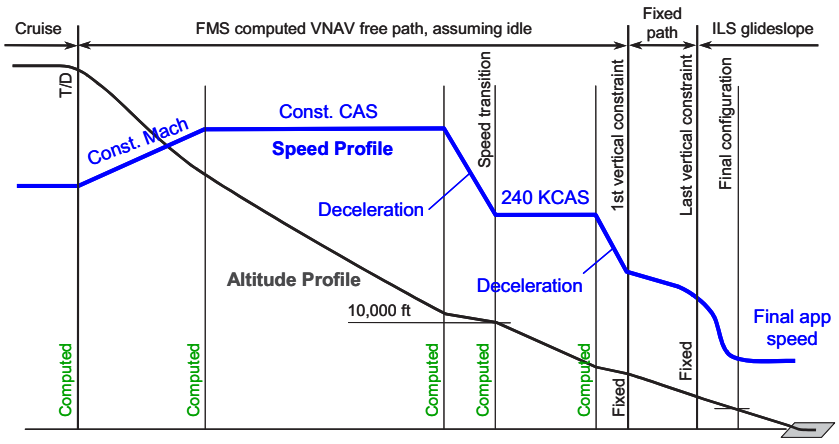

Figure A-8 Typical FMS VNAV flight path.

As shown in Fig. A-8, the unrestricted VNAV path consists of three types of idle descent segments, constant Mach, constant CAS, and deceleration segment. Fixed descent rate is assumed for the deceleration segments. Since engine power is assumed to be idle, to maintain the given CAS, Mach, or descent rate, the flight path angle at any point on the computed unrestricted VNAV path is a function of aircraft weight, wind forecast, and nominal flap/gear extension schedule. For fixed flight path segments between vertical constraints, if different speed constraints are given at the two ends of the segment, the

FMS module computes a point where an idle deceleration should start so that the aircraft would reach the speed constraint at the lower end of the segment upon arriving at that end. Before this deceleration point, the aircraft is assumed to be maintaining a speed equal to that given at the higher end of the segment. Again, the location of this deceleration point depends on the aircraft weight, wind forecast, and nominal flap/gear extension schedule. The following subsections describe in detail the algorithms used in this simulator to compute VNAV path segments.

A.4.3 Idle Constant CAS Descent and Constant Mach Descent Segments

Idle constant CAS and constant Mach descent segments are normally built starting from a known point back to a higher altitude. The known point, with known location and altitude, can either be a fixed constraint at a waypoint, or the upper endpoint of the immediate lower segment that has already been constructed. The higher end of the segment is normally defined by the cruise altitude or an altitude where speed transition occurs. In constant CAS and constant Mach descent segments, aircraft acceleration is normally not zero due to the nonlinear relationship between CAS/Mach and true airspeed, and the possible change in wind forecast along altitude.

Assume that aircraft is flying at a true airspeed V_r and flight path angle γ, subject to horizontal wind forecast vector $\mathbf{W}_F$. For the sake of simplicity, the aircraft is assumed flying straight forward; and the analysis is performed in a vertical plane parallel to ground speed. Moreover, true airspeed is treated as lying in this vertical plane too. Although due to crosswind, true airspeed and ground speed are often not in the same vertical plane, the aforementioned approximation is close enough. This is because the total acceleration will ultimately only contribute to changing the magnitude of aircraft speed and the flight path angle, based on the straight flight assumption; and that the effect of cross wind component is relatively small. Because thrust is small at idle power, it can be treated as aligned with the direction of true airspeed. Such simplified free body diagram is shown in Fig. A-9.

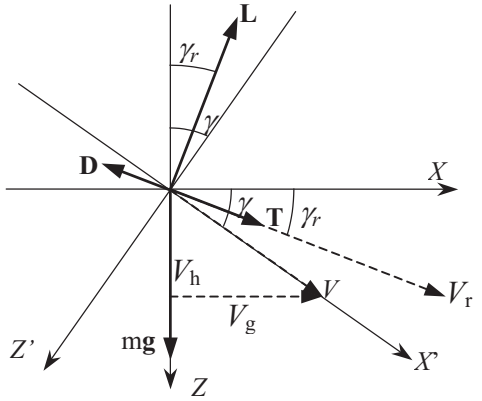

Figure A-9 Simplified free body diagram for constant CAS descent.

In Fig. A-9, special coordinate frames are used. The *X*-axis lies in the horizontal plane and points to the direction of ground speed, the *Z*-axis is perpendicular to the horizontal plane. The *Z'X'* frame is a rotation of the *ZX* frame so that the *X'*-axis aligns with the aircraft speed vector **V**. Force equations in *X*' and *Z*' directions are thus

$$(T-D)\cos(\gamma-\gamma_r)+L\sin(\gamma-\gamma_r)-mg\sin\gamma=m\frac{dV}{dt} \tag{A-33}$$

$$L\cos(\gamma-\gamma_r)+(T-D)\sin(\gamma-\gamma_r)-mg\cos\gamma=mV\frac{d\gamma}{dt} \tag{A-34}$$

Recall that drag D is determined from the drag polar, therefore it is a function of lift. At any given altitude, true airspeed V_r can be calculated directly from the given CAS or Mach; thus, it's known. Flight path angle γ and angle γ_r are related by Eq. (A-20). Thus, there are three unknowns in the force equations, i.e. aircraft speed V, flight path angle γ, and lift L. Aircraft tangential acceleration can also be expressed in the form of altitude derivative

$$\frac{dV}{dt}=\frac{dV}{dh}\frac{dh}{dt}=V_h\frac{dV}{dh}=V\sin\gamma\frac{dV}{dh} \tag{A-35}$$

Similarly,

$$\frac{d\gamma}{dt}=V\sin\gamma\frac{d\gamma}{dh} \tag{A-36}$$

From Eq. (A-23) it can be derived

$$\begin{aligned}\frac{dV}{dh}=&\frac{V_r\dfrac{dV_r}{dh}-W_{Fc}\dfrac{dW_{Fc}}{dh}-W_{Fh}\sin^2\gamma\dfrac{dW_{Fh}}{dh}-W_{Fh}^2\sin\gamma\cos\gamma\dfrac{d\gamma}{dh}}{\sqrt{V_r^2-W_{Fc}^2-W_{Fh}^2\sin^2\gamma}}\\&-\cos\gamma\frac{dW_{Fh}}{dh}+W_{Fh}\sin\gamma\frac{d\gamma}{dh}\end{aligned} \tag{A-37}$$

In Eq. (A-37), W_{Fh} and W_{Fc} are the headwind and crosswind components of FMS wind forecast that is known. Plug Eq. (A-35) and (A-36) into Eq. (A-33) and (A-34) respectively, plus Eq. (A-37), there are now three independent equations. The three unknowns can now be solved through backward integration to the higher end altitude. With aircraft speed V and flight path angle γ known for each integration step, a flight path segment can be constructed.

A.4.4 Fixed Descent Rate Deceleration

Deceleration segments are normally built starting from a known point back to a point where a higher CAS is reached. The descent rate used would assure a shallower descent path to allow effective deceleration without adding additional drag. Again, assume that the aircraft is flying straight forward; and the true airspeed is treated as lying in the vertical plane parallel to ground speed; and the thrust is treated as aligned with the direction of true airspeed. The simplified free body diagram is shown in Fig. A-10.

This free body diagram is the same as Fig. A-9 except that force equations are now derived in the *ZX* frame shown. For fixed descent rate segments, vertical acceleration is zero. The force equations are thus

$$L\cos\gamma_r+(T-D)\sin\gamma_r-mg=0 \tag{A-38}$$

$$-L\sin\gamma_r+(T-D)\cos\gamma_r=m\frac{dV_g}{dt} \tag{A-39}$$

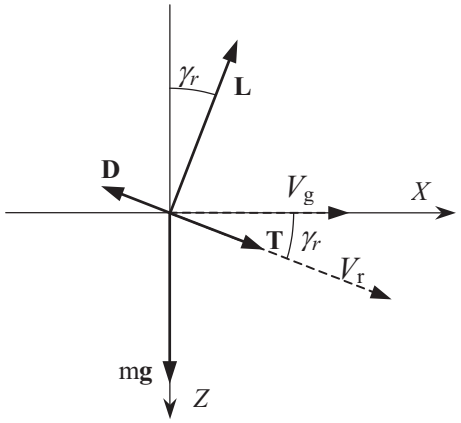

Figure A-10 Simplified free body diagram for fixed flight path angle descent.

There are three unknowns in the force equations, i.e. ground speed V_g, angle γ_r, and lift L. From Eq. (A-20) and (A-21), an additional equation can be obtained

$$\left[W_{Fc}^2 + \left(V_g + W_{Fh}\right)^2\right]\tan^2\gamma_r = V_h^2 \tag{A-40}$$

There are now three independent equations. The three unknowns can be solved through backward integration to the point where the desired CAS is reached. With ground speed V_g known for each integration step, and the given vertical rate V_h, a deceleration segment can be constructed.

A.4.5 Fixed Flight Path Angle Descent

Fixed flight path angle descent segments are normally segments with the both ends fixed. If speed constraints at the two ends are the same, no further computation is needed. The aircraft simply follow the path and maintain the constant speed. If speed constraints at the two ends are different, an idle deceleration point needs to be computed. Following the same assumptions as in the previous subsection, the same simplified free body diagram shown in Fig. A-9 can be used. Since the flight path angle is fixed, force equations in *X*' and *Y*' directions are

$$(T - D)\cos(\gamma - \gamma_r) + L\sin(\gamma - \gamma_r) - mg\sin\gamma = m\frac{dV}{dt} \tag{A-41}$$

$$L\cos(\gamma - \gamma_r) + (T - D)\sin(\gamma - \gamma_r) - mg\cos\gamma = 0 \tag{A-42}$$

Equation (A-41) is exactly the same as Eq. (A-33). It is repeated here for clarity. Rewrite Eq. (A-23) by substituting wind components with FMS wind forecast components

$$V = \sqrt{V_r^2 - W_{Fc}^2 - W_{Fh}^2\sin^2\gamma} - W_{Fh}\cos\gamma \tag{A-43}$$

Plug Eq. (A-24) into Eq. (A-41), there are now three unknowns, i.e. aircraft speed V, true airspeed V_r, and lift L. The above three independent equations can be solved through backward integration from the lower end of the fixed flight path angle segment up to the point where the speed given at the higher end of the segment is reached. This is the deceleration sub segment. From that point on up to the higher end of

the fixed flight path angle segment is a constant CAS sub segment. The difference between this constant CAS sub segment and the idle constant CAS segment mentioned earlier is that thrust may be needed to maintain the speed.

A.5 AIRCRAFT CONTROL

During approach, pilot assumes the responsibility to control the extension of flap and landing gear as aircraft decelerates and approaches to the airport. The pilot may also use speedbrakes when additional drag is needed to slowdown the aircraft to follow procedure speed profile. In this simulator, a pilot model is included to perform these tasks. Although some noise abatement approach procedures can be manually performed, advanced procedures are assumed being performed with autopilot and autothrottle engaged. As mentioned earlier, in developing this simulator, focus was given to aircraft trajectories rather than micro dynamic behavior. It was further assumed that on advanced civil transport aircraft, autopilot and autothrottle are able to maintain certain tracking accuracy. Thus, control surfaces and aircraft rotational dynamics were modeled as a single controller element, there by eliminated the need of using aerodynamic derivatives, rotational moments, and moments of inertial momentum. This greatly simplified the simulator while maintaining certain simulation accuracy. The autopilot model consists a lateral control module and a longitudinal control module. The functionality of the autothrottle was included in the longitudinal control module.

A.5.1 The Pilot Model

The pilot model performs the extension of flap and landing gear according to a predefined customizable flap schedule. The initiation of each flap extension could be individually defined either as at a given speed (a fixed number or as an additive to the reference speed), at a certain distance to runway, or at a given altitude. Speedbrake usage could be defined as keeping the aircraft speed within a certain range, such as 5 kts, from the target speed. Two different speed range values can be defined, one for altitude above 10,000 ft, and the other for altitude below 10,000 ft.

A random pilot response delay was incorporated into the pilot model to represent pilot action uncertainties. This is the time between a cue, say reaching the speed to initiate a flap extension, and the actual initiation of the flap extension. Aside from the pilot delay, flap and landing gear control and actuation system needs a certain amount of time to extend to the next position. The flap and gear extension times were modeled after performance data of each aircraft type. Since under normal operation conditions the variation in extension time for a given flap or gear configuration is relatively small, the extension times were modeled as deterministic values. Because of the existence of the extension time, it could happen that when the cue for the next flap or gear extension arrives the system is still in transition to the target position of the current extension. In this case, the new extension would not be initiated by the system until the current extension is completed. Flap and landing gear extension time was also modeled in the FMS in computing the VNAV flight path.

Speedbrakes were to be pulled out when aircraft speed exceeds the given upper range; and they were to be retracted when the aircraft speed fells back to the target speed. Random pilot response delay was also modeled in operating speedbrakes. In computing the VNAV flight path, the FMS assumes no speedbrake usage.

A.5.2 Lateral Control Autopilot Module

The lateral control autopilot module relies on the FMS LNAV guidance functionality to provide control commands. There are several different lateral control modes. Taking LNAVTRACK mode as an example, the FMS module feeds two parameters to the lateral control autopilot module, namely the high level heading command and the cross track error. The object of the lateral control autopilot module is to track the heading command and minimize the cross track error. The block diagram of the LNAVTRACK control mode is shown in Fig. A-11.

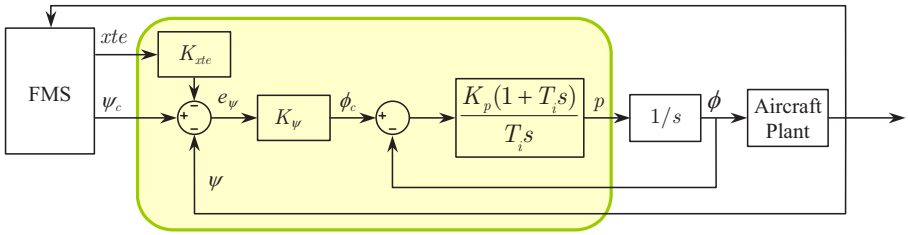

Figure A-11 Lateral control autopilot.

As shown in Fig. A-11, at first, a quickened heading error e_ψ is derived from the heading command ψ_c, actual heading ψ, and cross track error xtc. The quickened heading error is then fed into a proportional controller to yield the banking command ϕ_c, which is limited to the maximum banking angle (the limiter is not shown). The banking command is then passed through a proportional-plus-integral controller[14] to yield aircraft roll rate. The proportional-plus-integral controller was used to approximate the overall effect of the roll control, the actuator/aileron system, and the aircraft roll dynamics. This greatly simplified the modeling effort. On the other hand, the integration from roll rate to bank angle and the integration process from bank angle to heading change were preserved yielding relatively accurate results. Other control modes in the lateral control pilot module were modeled in similar fashion.

A.5.3 Longitudinal Control Autopilot Module

The longitudinal control autopilot module includes two separate functions, autothrottle and pitch control. The following longitudinal control modes were modeled

ALTSPD_HOLD Altitude and speed hold mode. Autothrottle and pitch control work together to maintain constant altitude and constant CAS.

SPDFPA_HOLD Speed and flight path angle hold mode. Autothrottle and pitch control work together to maintain constant CAS and follows a fixed flight path angle.

IDLFPA_HOLD Idle and flight path angle hold mode. Throttle is set to idle; pitch control maintains a fixed flight path angle. If this mode is used in a decelerating segment, the autopilot will be switched to SPDFPA_HOLD mode once the target speed is reached.

PWRFPA_HOLD Throttle and flight path angle hold mode. This mode is useful for flying a geometric low noise segment in that the required thrust may be estimated in advance and the throttle is fixed to provide the required thrust to avoid thrust spikes. If this mode is used in a decelerating segment, the autopilot will be switched to SPDFPA_HOLD mode once the target speed is reached.

VNAVIDESCM	VNAV idle descent with constant Mach. Throttle is set to idle, pitch control follows FMS computed VNAV path. If aircraft speed falls beyond a certain range below the target Mach, thrust will be added to maintain the target Mach.
VNAVIDESCV	VNAV idle descent with constant CAS. Throttle is set to idle, pitch control follows FMS computed VNAV path. If aircraft speed falls beyond a certain range below the target CAS, thrust will be added to maintain the target CAS.
VNAVSDESC	VNAV constant speed descent. Autothrottle and pitch control work together to maintain constant CAS and follows FMS computed VNAV path.
VNAVDECEL	VNAV deceleration. Throttle is set to idle, pitch control follows FMS computed VNAV deceleration path. For the speed transition at 10,000 ft, if aircraft CAS is still higher than the target speed, i.e. 250 kts, when aircraft reached 10,000 ft, aircraft will level off to decelerate to the target speed.
ILS_CPTR	ILS Glideslope capture mode.
ILS_GS	ILS Glideslope mode.

The block diagram of the autothrottle model is shown in Fig. A-12. The object of the autothrottle is to maintain the CAS command $V_{c,c}$ provided by the FMS model. A proportional-plus-integral controller was used to generate thrust command T_c from the quickened speed error e_v. Engine response time was modeled as a first order delay; this delay was included in the aircraft plant shown in the block diagram.

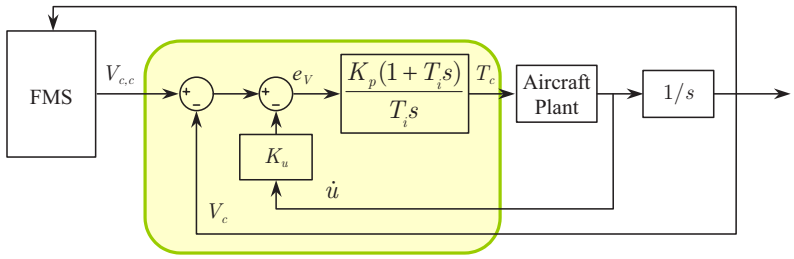

Figure A-12 Autothrottle.

The longitudinal autopilot model was designed to follow the vertical guidance command from the FMS model. In most of the vertical control modes listed above, this vertical guidance command is provided in the form of altitude command h_c. The block diagram of the longitudinal autopilot is shown in Fig. A-13. The outer loops yield a pitch command θ_c, which is then passed through a prepositional-plus-integral controller to yield aircraft pitch rate. Similar to the lateral autopilot, to simplify the modeling effort, the proportional-plus-integral controller was used to approximate the overall effect of the pitch control, the actuator/elevator system, and aircraft pitch dynamics.

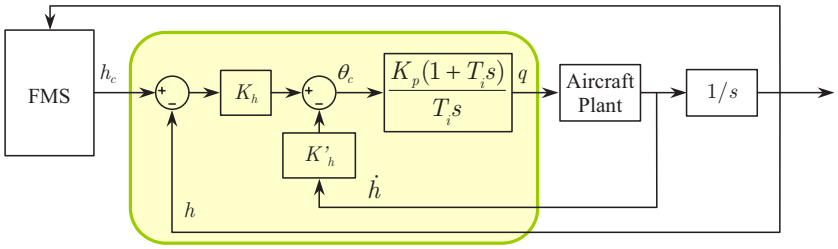

Figure A-13 Longitudinal control autopilot.

A.6 THE APPLICATION OF THE AIRCRAFT SIMULATOR

The simulator was designed to allow fast and easy testing of different procedure designs with customized pilot operation procedures and under different operating conditions. It can be applied to down-selecting procedure design parameters or evaluating existing procedure designs. Since the simulation can be executed numerous times in batch mode, it is especially useful for Monte-Carlo simulation to explore aircraft trajectory variations under uncertainty conditions. This section describes the simulation data flow and how the simulation results can be fed into external programs for noise and emissions evaluation.

A.6.1 Simulation Data Flow

Currently, five aircraft types have been modeled in the fast-time simulator. They include Airbus A319 and Boeing 737-300, 757-200, 767-300, and 747-400. The simulation data flow is illustrated in Fig. A-14. The first step is to prepare the lateral flight path and vertical profile parameters as described in Section A.4. Pilot operation procedures, as defined in the flap schedule for a given aircraft type, can be customized for the specific procedure to be tested. Wind forecast can also be provided. In Fig. A-14, the three elements to the left of the simulator core define procedure operating conditions, namely the randomness in pilot response delay, the randomness in aircraft landing weight, and uncertainties in wind. If the purpose of the simulation is to evaluate the trajectory of aircraft performing a procedure under nominal conditions, the mean pilot response delay, normal aircraft landing weight, and a fixed wind field model can be used. If the procedure is designed to relying on FMS to compute a VNAV path, wind forecast may also be provided to simulate the effect of FMS wind forecast.

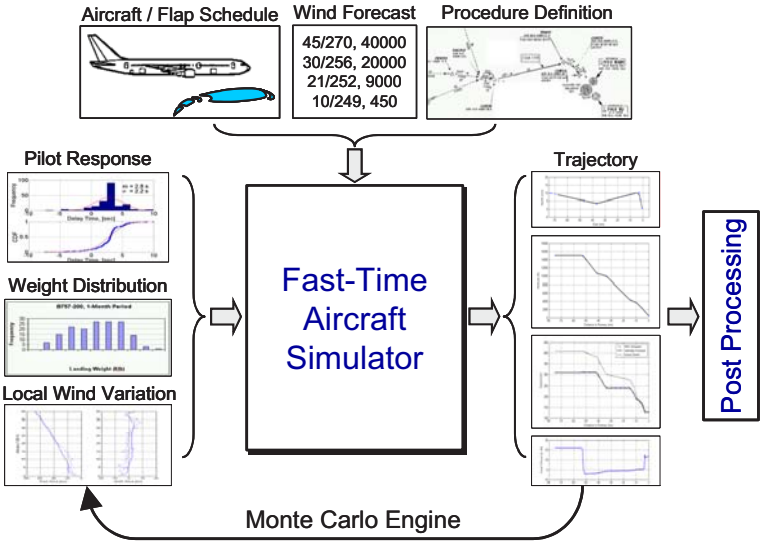

Figure A-14 Monte Carlo Simulation data flow diagram.

If the purpose of the simulation is to analyze aircraft trajectory variations under varying operation conditions, random pilot response time model based on human-in-the-loop experiment or flight test data, random aircraft weight depicting data collected from airline operations, and a varying wind model developed based on historical wind data can be used. With these three uncertainty contributors modeled, a full Monte-Carlo simulation can be formed. For each single run of the Monte-Carlo simulation, pilot response time for each flap extension, aircraft landing weight, and the wind profile would be randomly

generated by the respective models to form a unique set of operating conditions. The output of each single simulation run would be a unique sample of aircraft trajectories for the specific procedure. Through a large number of simulation runs, an ensemble of aircraft trajectories can be obtained to represent the range of trajectory variations what would occur in the real world.

The simulation output is a time history of aircraft position, altitude, distance, speed, engine thrust, fan speed, fuel flow, weight, Euler angles, along with flap/gear position and speedbrake usage. The FMS generated lateral and vertical path parameters are also logged. A sample of simulated trajectories is shown in Fig. A-15. This was a simulated Continuous Descent Approach (CDA) to Louisville International Airport (KSDF) runway 17R by B757-200. The upper left graph is the ground track. The lower left graph is the vertical profile vs. distance to runway with two shallower VNAV deceleration segments shown. The upper right graph is the speed profile vs. distance to runway, with both CAS and ground speed shown. The deceleration from 310 kts to 240 kts corresponds to the deceleration segment at 10,000 ft shown in the vertical profile. The deceleration from 240 kts to 180 kts corresponds to the deceleration segment at 3,800 ft shown in the vertical profile. The lower right graph is the total thrust. It is seen that in this procedure, thrust stayed in idle from top of descent until final approach speed was reached.

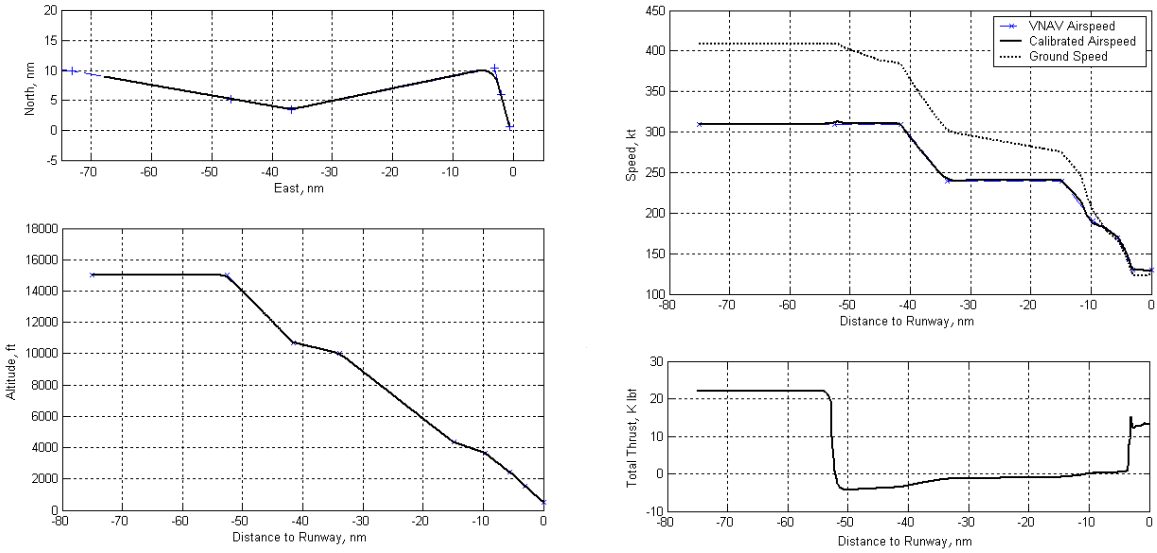

Figure A-15 Simulated B757-200 trajectory.

Figure A-16 shows the range of trajectory variations from Monte-Carlo simulation of the same CDA procedure performed by B757-200. The horizontal axis is distance to runway; the vertical axis is the time since aircraft passed the metering point that is about 53.4 nm from runway. Time-distance-trajectory graph is a common tool used in traffic flow study[15]. Figure A-16 was obtained through aligning all simulated trajectories at the metering point. In the simulation, all three major uncertainty contributors, pilot response time, aircraft weight, and wind variations were simulated. It is seen from the figure that at around 8.2 nm from runway, where glide slope capture occurs, aircraft position could varying within a range of 1.5 nm for the same flight time. With simulated trajectory variations, capacity and separation analysis can be performed.

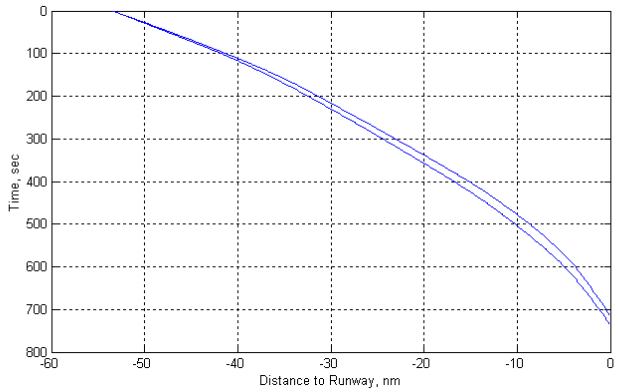

Figure A-16 Simulated B757-200 trajectory variation.

A.6.2 Simulation Accuracy

Components of the aircraft simulator were carefully formulated and developed to assure simulation accuracy. Aircraft performance engineering data provided by manufactures were used to model aircraft dynamics and engine performance. Since actual performance depends on many internal and external factors and it could vary aircraft by aircraft, aircraft performance engineering data provided by manufactures reflect average performance of the same aircraft type. The aircraft simulator would thus reflect average performance of the aircraft type being modeled. A direct method to verify simulation accuracy is to compare simulation results with actual flight test data. To do this, the simulator was configured to simulate the same procedure used in flight test. To closely depict the flight test conditions, wind profile and flap extension extracted from flight test data were used in the simulation. Aircraft landing weight was also set as the same as the test aircraft. Since the simulation was done under Standard Atmosphere conditions, for comparison purpose pressure altitude in the flight test data was corrected to reflect actual altitude above mean sea level. One of such comparisons, between simulation results and flight test data from a CDA to KSDF 17R, performed by a B757-200 in early September 2004, is shown in Fig. A-17. On the left hand side is the comparison of the altitude profiles, on the right hand side is the comparison of the CAS profiles. It is seen that both the simulated altitude and CAS profiles closely depicted the flight test profiles. It is also seen that in the simulated profile, the transition from cruise to descent was rudimental. However, for simulating arrival and approach procedures, this should not pose a

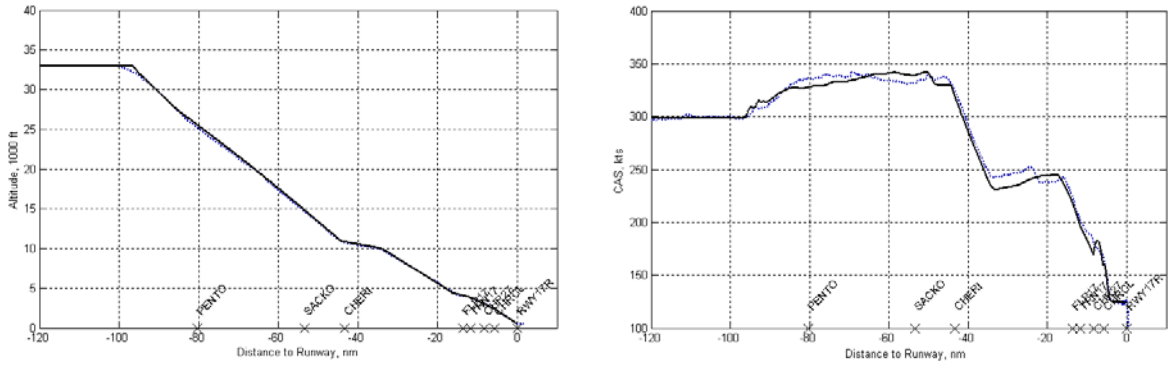

Figure A-17 Comparison between simulated (solid curve) and flight test (dotted curve) trajectory.

significant problem, because only the part of the trajectory close to the airport is concerned.

A.6.3 Interfaces to External Tools

The simulator was developed to interface with two external tools, the Federal Aviation Administration (FAA) Integrated Noise Model (INM) and the Boeing Method 2 (BM2) fuel flow emissions estimation methodology. INM is the widely used standard tool for determining the predicted noise impact in the vicinity of airports. The current version INM 6.1 was released in April 2003[16]. To evaluate noise impact, aircraft trajectories need to be imported to INM as profile points files containing aircraft type, operation type (arrival, departure, or overflight), distance to runway, altitude, true airspeed, corrected net thrust per engine, and operation mode (arrival or departure). INM input files are in dBase IV format. INM users frequently use commercially available spreadsheet or database management programs to manually port trajectory data into dBase IV file format by inserting data points into INM input file templates. The manual process is tedious and error can occur when file format is accidentally changed. A tool was created to automatically convert the simulation output files in text format into INM profile points files in dBase IV format. This greatly simplifies the process for evaluate noise impact from simulated trajectories. Figure A-18 shows the INM noise contour based on the simulated aircraft trajectory shown in Fig. A-15.

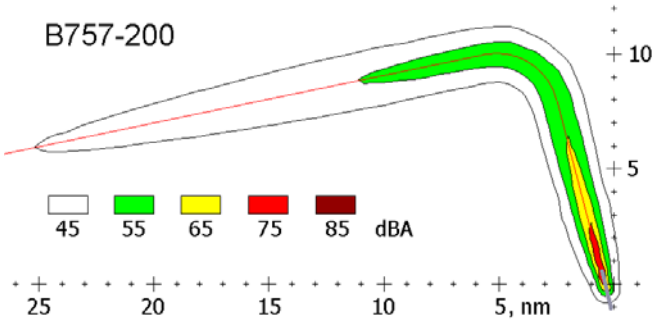

Figure A-18 INM noise contour from simulated trajectory.

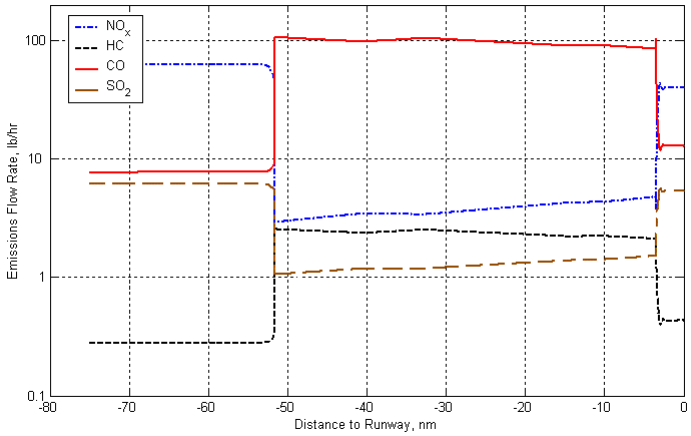

Figure A-19 Emission flow rates from simulated trajectory.

BM2 is an empirical method to estimate aircraft emissions using installed engine fuel flow. BM2 uses engine emissions indices in the ICAO Engine Exhaust Emissions Data Bank[17] and takes into account ambient temperature, pressure, humidity, and aircraft Mach number[18]. BM2 has been adopted by FAA and ICAO since its introduction. To evaluate aircraft emissions from simulated aircraft trajectories, a revised BM2[19] was implemented. This implementation calculates at each trajectory data point the flow rate of the following emission species, NOx, HC, CO, CO2, H2O, and SO2. The output is a time history of flow rate of these emission species. Emissions flow rate from BM2 for the simulated B757-200 trajectory is shown in Fig. A-19.

A.7 SUMMARY

The development and preliminary application of the workstation based fast-time aircraft simulator has been presented. The fast-time simulator provides 4D trajectory simulation accuracy comparable to full fidelity simulations but is simple enough to allow fast execution. Although the simulator was initially developed for simulating noise abatement approach and arrival procedures, with slight enhancements, it can also be used to simulate departure procedures and cruise flight segments. The fast-time aircraft simulator provides a tool for evaluating and down-selecting design features and a platform for the fast-time Monte-Carlo simulation study of flight operation procedures.

REFERENCES

[1] Elmer, K., Wat, J., Gershzohn, G., Shivashankara, B., Clarke, J. P., Ho, N., Tobias, L., and Lambert, D., "A Study of Noise Abatement Procedures Using Ames B747-400 Flight Simulator," *8th AIAA/CEAS Aeroacoustics Conference*, Breckenridge, CO, Jun. 17-19, 2002.

[2] Palmer, M. T., Abbott, T. S., and Williams, D. H., "Development of Workstation-Based Flight Management Simulation Capabilities within Nasa Langley's Flight Dynamics and Control Division," *9th International Symposium on Aviation Psychology*, Columbus, OH, Apr. 28-May 1, 1997.

[3] Callantine, T. and Palmer, E., "Fast-Time Simulation Studies of Terminal-Area Spacing and Merging Concepts," *22nd Digital Avionics Systems Conference*, Indianapolis, IN, Oct. 12-16, 2003.

[4] Ho, N.T., and Clarke, J.-P., "Mitigating Operational Aircraft Noise Impact by Leveraging on Automation Capability," *1st AIAA Aircraft Technology, Implementation, and Operations Forum*, AIAA-2001-5239, Los Angeles, CA, Oct. 16-18, 2001.

[5] Ren, L., Clarke, J.-P., and Ho, N. T., "Achieving Low Approach Noise without Sacrificing Capacity," *22nd Digital Avionics Systems Conference*, Indianapolis, IN, Oct. 2003.

[6] Stevens, B. L. and Lewis, F. L., *Aircraft Control and Simulation*, John Wiley & Sons, Inc., New York, 1992.

[7] *Manual of The ICAO Standard Atmosphere: Extended to 80 Kilometers (262,500 feet)*, 3rd ed., Doc 748813, International Civil Aviation Organization, Montreal, Quebec, Canada, 1993

[8] *Jet Transport Performance Methods*, 7th ed., Boeing Document No. D6-1420, Boeing Flight Operations Engineering, 1989.

[9] Nelson , R. C., *Flight Stability and Automatic Control*, McGraw Hill, Inc., New York, 1989.

[10] Benjamin, S. G., Brown, J. M., Brundage, K. J., Dévényi, D., Grell, G. A., Kim, D., Schwartz, B. E., Smirnova, T. G., Smith, T. L., Weygandt, S. S. and Manikin, G. S., "RUC20 - The 20-km version of the Rapid Update Cycle," *NWS Technical Procedures Bulletin No. 490*. Apr. 2002.

[11] Bulfer, B. and Gifford, S., *FMC User's Guide – B757, B767, B747, NON PIP/PIP*, Bill Bulfer and Skeet Gifford, Kingwood, TX, 1996.

[12] Bulfer, B., *737 FMC User's Guide*, Leading Edge Libraries, Kingwood, TX, 1997.

[13] MIL-HDBK-1797, *Flying Qualities of Piloted Aircraft*, Department of Defense Handbook, December 19, 1997.

[14] Ogata, K., *Modern Control Engineering*, 3rd ed., Prentice Hall, Upper Saddle River, New Jersey, 1997.

[15] Leutzbach, W., "Modelling of Traffic Flow," *Advanced Technologies for Air Traffic Flow Management, Proceedings of an International Seminar Organized by Deutsche Forschungsanstalt für Luft und Raumfahrt (DLR), Bonn, Germany, Apr. 1994*, edited by H. Winter and H.-G. Nüßer, Lecture Notes in Control and Information Sciences 198, Springer-Verlag, New York, 1994, pp. 30-42.

[16] Olmstead, J. R., Fleming, G. G., Gulding, J. M., Roof, C. J., Gerbi, P. J., and Rapoza,A. S., "Integrated Noise Model (INM) Version 6.0 Technical Manual," Report No. FAA-AEE-02-01, Federal Aviation Administration, Washington, D.C., Jan. 2002.

[17] "ICAO Engine Exhaust Emissions DataBank," 1st ed, ICAO, Doc 9646- AN/943, 1995.

[18] Baughcum, S. L., Tritz, T. G., Henderson, S. C. and Pickett, D. C. "Scheduled Civil Aircraft Emission Inventories for 1992: Database Development and Analysis," NASA CR-1996-4700, NASA Langley Research Center, Apr. 1996, Appendix D, Boeing Method 2

[19] "Guidance on the Use of LTO Emissions Certification Data for the Assessment of Operational Impacts," Committee on Aviation Environmental Protection (CAEP) 6th Meeting, Montreal, Quebec, Canada, Feb. 2004.